Cardiff University
School of Chemistry

The Synthesis and Evaluation of Novel Soluble Lytic Transglycosylase Inhibitors

A thesis submitted to Cardiff University for the degree of Doctor of Philosophy

By

Aysha Belgasem Abdosalam Mezoughi

2019

Abstract

Lytic transglycosylases (LTs) present an attractive target of antibiotics due to their unique function in bacterial cell growth and division. They act on peptidoglycan (PG) by creating spaces via non-hydrolytic reactions to facilitate insertion of cell-envelop spanning structures that the cell requires for PG biosynthesis and recycling. In addition to that, these enzymes are involved in pivotal cell events including control of β-lactamases expression (enzymes that confer resistance to β-lactam antibiotics) by formation of the 1,6-anhydromuramic acid product. The most common compound used to inhibit LTs is Bulgecin.

In this study, sixteen novel dihydroxylated amidine inhibitors were derived from 2-deoxy-D-ribose (eight free bases and eight hydrochloride salts) and four free bases were synthesised starting from 2-deoxy-L-ribose. Molecular docking was performed on the first five designed amidines from 2-deoxy-D-ribose and their analogues from 2-deoxy-L-ribose. The synthetic route employed involved sugar oxidation and azide reduction followed by ring opening and closure and transformation of lactam to amidine as key steps. However, a number of difficulties were faced this synthetic route in some reactions and purification. Synthesis of trihydroxylated amidines failed in the conversion step of lactam to thiolactam.

In order to evaluate the synthesised inhibitors, membrane-bound soluble lytic transglycosylase (Slt35) was expressed, purified and its activity was optimised. The amidines were tested their activity against Slt35 revealing that most compounds derived from 2-deoxy-D-ribose exhibited inhibition toward Slt35 activity at high micromolar level whereas analogues derived from 2-deoxy-L-ribose were all inactive except one. In general, free base amidines are more potent than hydrochloride salts.

Crystallisation of the best inhibitor generated in this study with Slt35 would be useful to investigate its interactions and improve its potency as antibacterial agent as well as testing the activity of all active compounds against bacteria.

Dedication

This thesis is dedicated to the great and supportive people in my life, to my father and the spirit of my mother.

To my dear brother (Almabrouk) and my uncle (Mohammed)

To my sisters and brothers.

To my dear husband (Saladein)

To the light that lightens my life, my awesome son Mohammed.

Acknowledgments

My thanks go first and foremost to Allah who helped and guided me until I reached this stage in my life.

I would like to express my gratitude to my supervisor, Dr Joel Loveridge for giving me the opportunity to work in this research and for his support, guidance and advice throughout my PhD course and for proofreading this thesis. I would also like to thank Prof. Rudolf Allemann. I am very grateful to both Dr Enas Behiry and Dr Alan Scott for their time and excellent support during my work in the biochemistry lab. I would also like to thank Dr Robert Mart and all people in the Allemann group for their support. My thanks to Dr Benson Kariuki for X-ray diffraction analysis and all technical staff in the school of chemistry for their continued help. I would also like to offer my thanks to people in PGR office, namely Prof Simon Pope, the director of PGR, Moira Northam and George Summers for their help and support.

Many thanks to Dr Richard Sessions (Bristol University, School of Chemistry) for his assistance in the molecular docking. I would also like to thank Libyan Ministry of Higher Education and Scientific Research and Tripoli University for funding. Thanks go to all people who taught me since I started my scientific journey, people who supported me and all my friends.

I have to express my thanks to my parents for their love and support throughout my life, without them I would not be able to achieve my dream. I would say great thanks to you, and may Allah bless my mother with Heaven. A huge thanks to my best brother, Dr Almabrouk Mezoughi and my best uncle Mohammed Sultan for their profound support during my life, I thank them deeply. A big thanks also go to my sisters and brothers for excellent and continued support and help, I would not be where I am today without you.

A special thanks go to my dear husband for his support, encouragement, understanding and patience, I could not have even begun or achieved this without you. Finally, I owe much of this degree to my wonderful son Mohammed for being there for me throughout the doctorate programme, I could not have done it without you. Thank you my love Mohammed your inspiration pushed me forward.

Table of Contents

List of Figures

List of Schemes

List of Tables

Abbreviations

A	Adenosine
Ac_2O	Acetic anhydride
APS	Ammonium persulfate
Å	Angstrom
AMP	Adenosine monophosphate
ATP	Adenosine triphosphate
Boc	t-Butoxycarbonyl
Bn	Benzyl
CD	Circular dichroism
COSY	Homonuclear correlation spectroscopy
CV	Column volume
DCM	Dichloromethane
DEPT	Distortionless enhancement by polarisation transfer
DNA	Deoxyribose nucleic acid
DMF	*N*,*N*-Dimethylformamide
EI	Electron ionisation
eq.	Equivalent
ES	Electrospray ionisation
G	Guanosine
HEPES	2-[4-Hydroxyethyl]piperazin-1-yl]ethanesulfonic acid
HPLC	High pressure / performance liquid chromatography
HRMS	High resolution mass spectrometry
HSQC	Heteronuclear single-quantum correlation spectroscopy
IC_{50}	Half maximal inhibitory concentration
IPTG	Isopropyl β-D-1-thiogalactopyranoside
I_f	Fluorescence intensity
K_d	Disassociation constant
LB	Luria-Bertani growth media
MeCN	Acetonitrile
MeOH	Methanol

Mlt	Membrane-bound lytic transglycosylase
m.p	Melting point
MRSA	Methicilin-resistant *Staphylococcus aureus*
MW	Molecular weight
NAG	*N*-acetylglucosamine
NAM	*N*-acetylmuramic acid
NMR	Nuclear magnetic resonance
SDS	Sodium dodecyl sulfate
SDS-PAGE	Sodium dodecyl sulfate – polyacrylamide gel electrophoresis
Slt	Soluble lytic transglycosylase
TBDMSCl	tert-Butyldimethylsilyl chloride
TEMED	*N,N,N',N'*-Tetramethylenediamine
TFA	Trifluoroacetic acid
THF	Tetrahydrofuran
TMSCl	Chlorotrimethylsilane
Tris	Tris(hydroxymethyl)aminomethane
Ts	Tosyl

1 Introduction

1.1 Antibiotics

Preface

Microbial infection is an emerging global threat to human health. To overcome this crisis, medical substances called antibiotics, which have the ability to kill or inhibit microbial activity, have been introduced. Alexander Fleming discovered penicillin from the fungus *Penicillium notatum* in 1928. In the 20th century, more than 100 antimicrobial compounds have been discovered as well. These discoveries had profound impact on human health by preventing and treating serious infectious diseases. However, the overuse and misuse of antibiotics led to microbial resistance by adapting defence against these drugs. Recently, much more attention has been given to the rise of antibiotic resistance.[1,2]

1.1.1 Antibiotic Classification and Resistance

Antibiotics can be classified based on their chemical structure and mode of action that generally include inhibition of cell wall synthesis, cell wall integrity, protein synthesis and nucleic acid synthesis[2] (Figure 1-1).

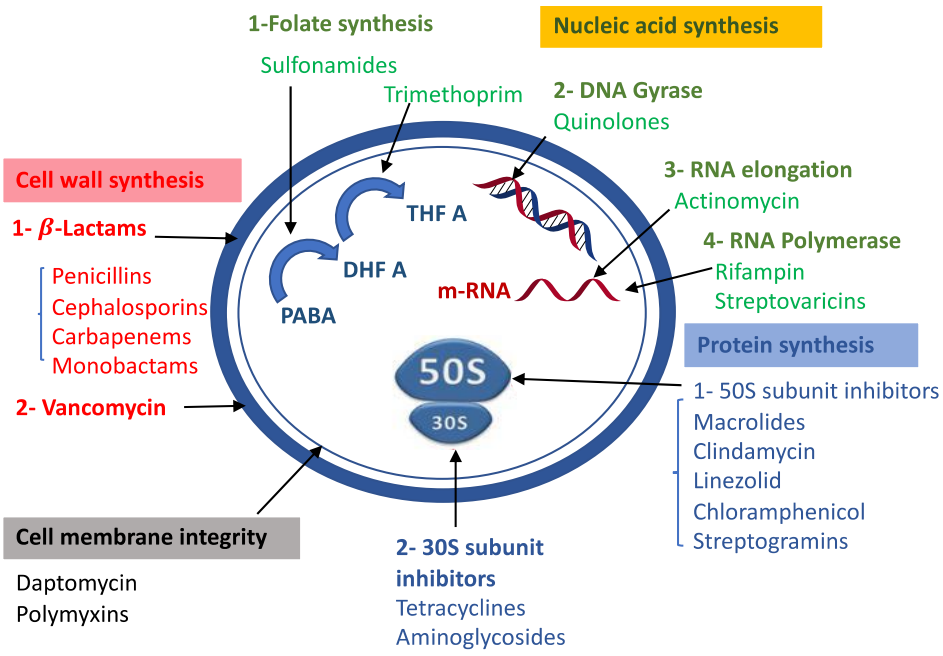

Figure 1-1: *Mechanism of action of antibiotics (this figure was inspired by http//www.orthobullets.com/basic-science/9059/antibiotic-classification-and-mechanism and ref.* ***3****).*

Inhibition of Cell wall synthesis

A series of enzymatic reactions occur in the cytoplasm of bacteria during bacterial cell wall biosynthesis. This process can be inhibited by one of the following antibiotics.

β-lactam antibiotics

Penicillin-binding proteins (PBPs), enzymes responsible for peptidoglycan cross-link synthesis are excellent targets of β-lactam antibiotics. These are the oldest and largest type of antibiotics; they consist of a four membered β-lactam ring typically fused to a second, five- or six-membered ring. Binding of these compounds to one of PBPs lead to prevention of cross-link formation, consequently, cell autolysis and death. The commonly used β-lactam antibiotics are: Penicillins (**1**),[4] carbapenems (**2**),[5] cephalosporins (**3**),[6] and monobactams (**4**)[7] (Figure 1-2).

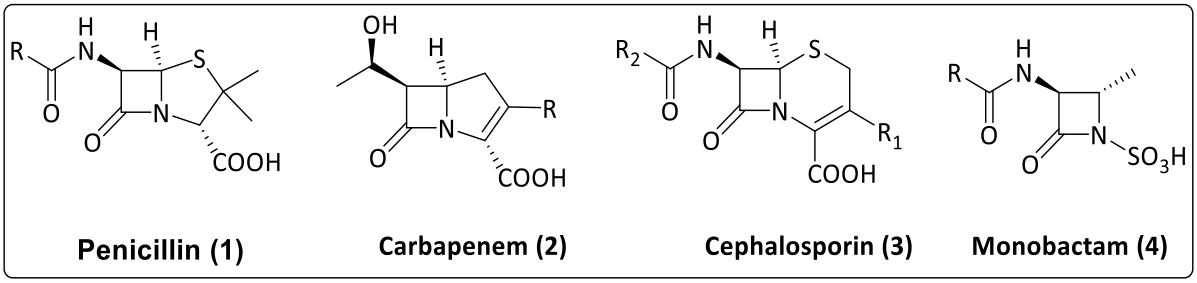

Figure 1-2: *Structure of different β-lactam antibiotic classes.*

Resistant bacteria deactivate β-lactam antibiotics by producing β-lactamases that hydrolyse the β-lactam core. These enzymes have the potential to deactivate all β-lactam groups.[8]

Vancomycin

Vancomycin is a glycopeptide antibiotic that inhibits cell wall biosynthesis by forming a complex with the terminal D-alanine-D-alanine of the pentapeptide precursor N-acetyl-muramyl-L-Ala-D-γ-Glu-L-Lys-D-Ala-D-Ala thus preventing transpeptidase from catalysing formation of cross-links.[9] Resistance to vancomycin occurs by producing D-alanine-D-lactate (strains VanA, -B, -D and –M) or D-alanine-D-serine (strains VanC, -E, -G, -L and –N) in resistant bacteria instead of D-alanine-D-alanine.[10]

Inhibition of cell membrane integrity

Bacterial cell membrane can be damaged by nonribosomal lipopeptide antibiotics such as daptomycin, an acidic lipopeptide Ca^{2+} dependent antibiotic. This molecule disrupts cell membrane integrity by making pores in the cell membrane and thus causing leakage of solute

when it binds to Ca^{2+} ion through its acidic side chains.[11, 12] Another lipopeptide antibiotic affects only Gram-negative pathogens bacteria is polymyxin, which binds to lipopolysaccharide in bacterial outer membrane leading to disintegration of bacterial membrane.[11,13]

Protein synthesis inhibition

Protein synthesis in bacteria can be inhibited at all steps, initiation, elongation and termination, by antibiotics. The ribosomal subunits 30S and 50S are the functional targets of these inhibitors, which may bind to the 50S subunit site, interrupting the access of aminoacyl-tRNAs to the ribosome (chloramphenicol (**5**), streptogramins, linezolid (**6**) and other oxazolidinones, clindamycin and macrolides), or to the 16S ribosomal RNA within the 30S subunit leading to translation inhibition (tetracyclines (**7**) and aminoglycosides).[11,15-18]

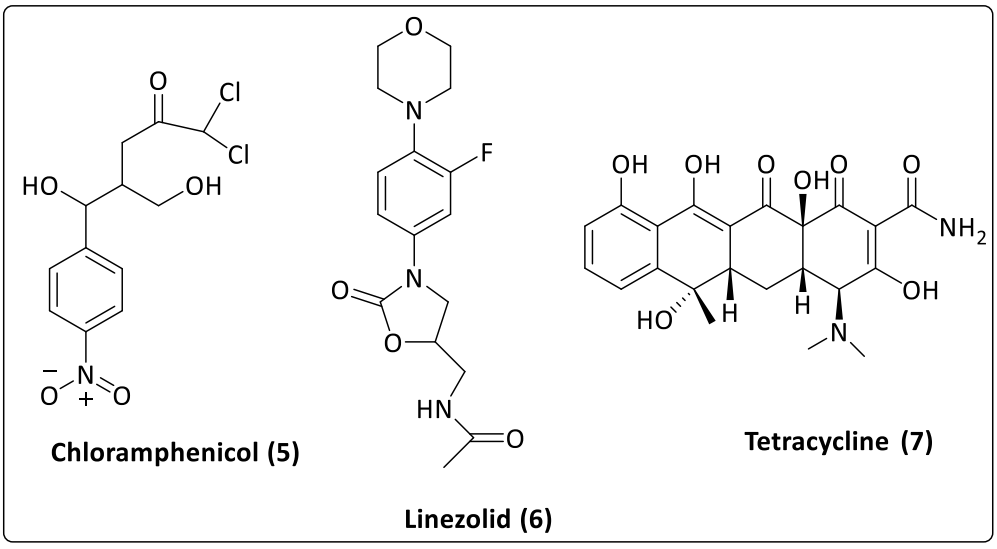

Figure 1-3: *Different classes of antibiotics involved in protein synthesis inhibition.*

Another way to inhibit protein synthesis is the interfering of tRNA with puromycin and mupirocin antibiotics. Mupirocin is an effective polyketide antibiotic widely used in the clinic to control the MRSA infections by inhibiting bacterial isoleucyl-tRNA synthetase, which leads to blocking of protein synthesis.[18,19]Puromycin binds to rRNA, which is essential for tRNA binding during protein synthesis.[20]

Nucleic acid synthesis inhibition

Synthesis of bacterial nucleic acid can be inhibited by various antibiotics in different ways: inhibition of DNA gyrase, folate synthesis, and RNA polymerase (Figure 1.4). Bacterial DNA gyrase and topoisomerase IV are enzymes involved in DNA replication and transcription by

relieving the strain of the supercoiled DNA, these enzymes are targets for fluoroquinolone antibiotics.[21] Actinomycin is responsible for the inhibition of RNA synthesis in both prokaryotic and eukaryotic by its interaction with DNA and thereby disrupting the transcription process.[22] Dihydrofolate reductase and dihydropteroate synthase, enzymes involved in dihydrofolate biosynthesis in bacteria, are also targets for antibiotics. The effective inhibitors against these enzymes are trimethoprim (**8**) and sulfamethoxazole (**9**) respectively, but resistance to these drugs by mutations to the coding genes have been characterised in many pathogens.[23]

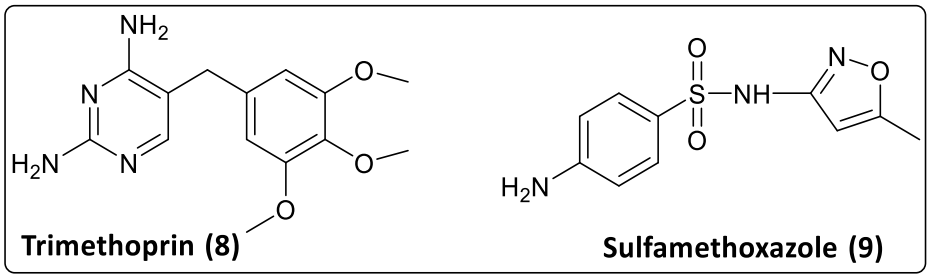

Figure 1-4: *Different classes of antibiotics involved in nucleic acid synthesis inhibition.*

The natural product antibiotic rifamycin produced by *Amycolatopsis mediterranei* blocks DNA transcription by inhibiting RNA polymerases in most pathogens, such as mycobacteria, Gram-positive cocci, *Clostridium difficile* and some selective Gram-negative pathogens *Neisseria meningitides, N. gonorrhoeae,* and *Hemophilus influenza.*[11,24] Streptovaricin and its degradation compounds (streptovadienal C, prestreptovarone and streptoval F) were found to inhibit RNA-directed DNA polymerases of Raucher leukemia virus.[25]

1.1.2 Mechanism of antibiotic resistance

The widespread use of antibiotics led to the emergence of antibiotic resistance, which impedes bacterial disease treatment. Awareness of this problem as a result of misuse of antibiotics was noted since penicillin has been discovered by Fleming.[26] Bacteria use different ways to protect themselves from drug effects (Figure 1-5).[11,27]

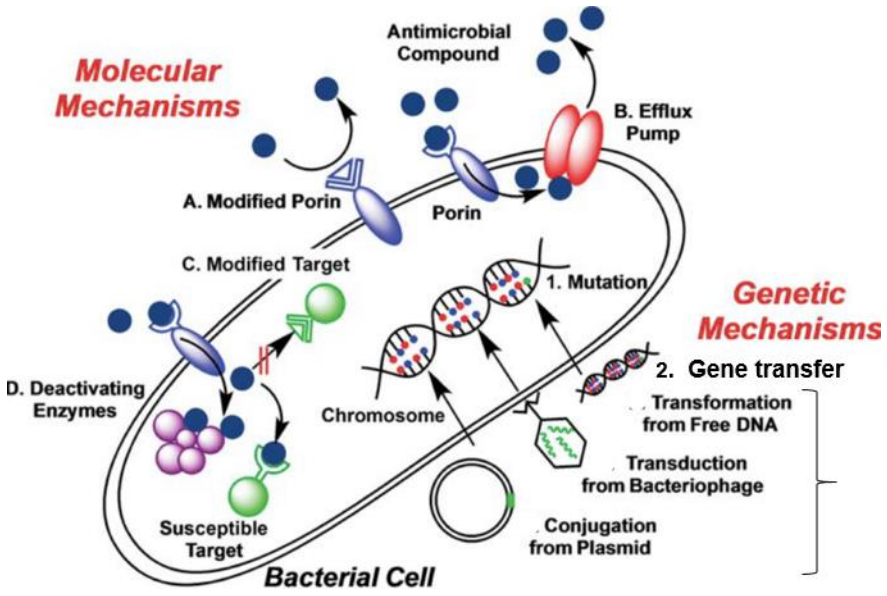

Figure 1-5: *Schematic of antibiotic resistance mechanism in bacteria (this figure reproduced from ref.* ***11****).*

Genetic mechanisms

Two major genetic strategies can be used by bacteria in order to neutralize antibiotics and their activity, gene mutation and horizontal gene transfer (HGT). Mutational resistance includes modifications of defence systems in susceptible bacteria by altering their drug-influencing genes leading to change of the antibiotic action and consequently cell survival in the presence of antibiotics. Generally, this mutation can occur via various mechanisms including: modifications of antibiotic targets, decrease of cell permeability by alteration of cell wall to prevent drugs from reaching their targets, increase the efflux pump activity to extrude the drug out the cell and alteration of the cell-adaptive regulatory system.

Acquisition of external genetic material (horizontal evolution) between strains of the same or different species, which includes transformation (incorporation of naked DNA), transduction (phage mediated), and conjugation (bacterial sex where both donor and recipient can acquire a copy of the transferred plasmid), can lead to gain of entirely new functions of benefit to the bacterium.[28-30] Conjugation is a crucial resistance mechanism often used by pathogens bacteria in hospital. An example for this mechanism is β-lactamase gene in *Haemophilus influenzae* that is carried on conjugative plasmid, which can be transferred to *gonococci* and subsequently to *Neisseria*. Transformation is less important mechanism for HGT, but it is used by *Pneumococci* and *Neisseria* to deactivate penicillin.[31]

Molecular mechanisms

There are four main bacterial resistance mechanism including: modification of the antibiotic molecule, decrease antibiotic penetration and efflux, changes in target site and global-adaptation. A successful strategy for bacterial resistance is deactivating antibiotics by producing enzymes able to add specific chemical moieties to the drug molecules or destroy it. Chemical alteration reactions include: acetylation, phosphorylation and adenylation. For example, deactivation of aminoglycosides antibiotics by aminoglycosides modifying enzymes that react covalently with hydroxyl or amino groups of the 2-deoxystreptamine core or the sugar unit of the drug molecule. The three modification pathways are used for this process by three modifying enzymes include: **i)** *O*-acetyltransferase (AACs) that transfers acetyl group from acetyl coenzyme A to NH_2 group of the antibiotic, **ii)** *O*-nucleotidyltransferase (ANTs), transfers an AMP group from ATP to the OH group of the drug molecule and **iii)** phosphotransferase (APHs) that transfers phosphate group to OH group of aminoglycoside.[32] An example of modification by antibiotic destruction is β-lactam antibiotics by β-lactamases, which hydrolyse β-lactam ring via nucleophilic attack of hydroxyl group in Ser residue on carbonyl of the amide group.[11]

Active pumping efflux is the major route of bacterial resistance against most antibiotic classes, which expels the antimicrobial from the cell. This mechanism leads to the export of antibiotic drugs before they reach their target inside the cell. For instance, antibiotics that inhibit protein synthesis in the cytoplasm must enter through the cell membrane into the cytoplasm and accumulate at high concentrations. There are five intrinsic membrane protein families of efflux pumps have been reported, major facilitator (MFS), small multidrug resistance (SMR), multidrug and toxin exclusion (MATE), resistance-nodulation-division (RND), and ATP-binding cassette (ABC) proteins. Single-protein efflux pumps are used in gram-positive bacteria while gram-negative bacteria need three protein pumps to eject the antibiotic across two membranes.[33] Efflux provides a wide range of resistance to antibiotics, including β-lactam, chloramphenicol, trimethoprim, tetracycline, and fluoroquinolones.[34]

Influx is the second transport system within the bacterial membrane used by gram-negative organisms to regulate antibiotic entry. This system is controlled by porins, water-filled diffusion channels, which are classified to monomeric or trimeric based on their structure. Alteration of porins affects the antimicrobial uptake especially for hydrophilic antibiotics that

are used by these channels to cross the outer membrane Tetracyclines, some fluoroquinolones and β-lactams fall into this category. Bacteria modify porins to decrease the uptake of β-lactams using one of the following strategies: an exchange of the type of expressed porin, alteration of porin level and mutation of porin properties.

In general, bacteria usually use multiple pathways for sufficient antibacterial resistance. For instance, fluoroquinolone resistance can be achieved via three routes: i) mutation of the DNA gyrase encoding gene, ii) activation of efflux pumps, iii) alteration of fluoroquinolone target site by protection with protein. However, in few cases bacteria use a single step mutation, such as resistance of rifampin (*E. coli* and *Staphylococcus aureus)*, streptomycin, sulphonamides and trimethoprim.[31,32] Another important example is deactivation of β-lactams by bacteria via several mechanisms including: i) producing enzymes known as β-lactamases that have the ability to hydrolyse β-lactam ring in Gram-negative bacteria, ii) mutations in the active site of PBPs to prevent drug binding in Gram-positive organisms, iii) modifications of cell wall to prevent drug entry.[11]

1.2 Peptidoglycan structure and architecture

The main component of the bacterial cell wall is peptidoglycan (PG). This is a heteropolymer consisting of glycan strands and peptide chains forming a continuous, mesh-like layer called the sacculus which surrounds the bacterial cell to confer strength, support and shape to the cell. Glycan strands are composed of repeating *N*-acetylglucosamine (NAG) and *N*-acetylmuramic acid (NAM) residues linked together by β-1,4 glycosidic bonds.[35,36] These strands are linked together via linkage between peptide stems attached to the lactyl groups of NAM residues (Figure 1-6).[37]

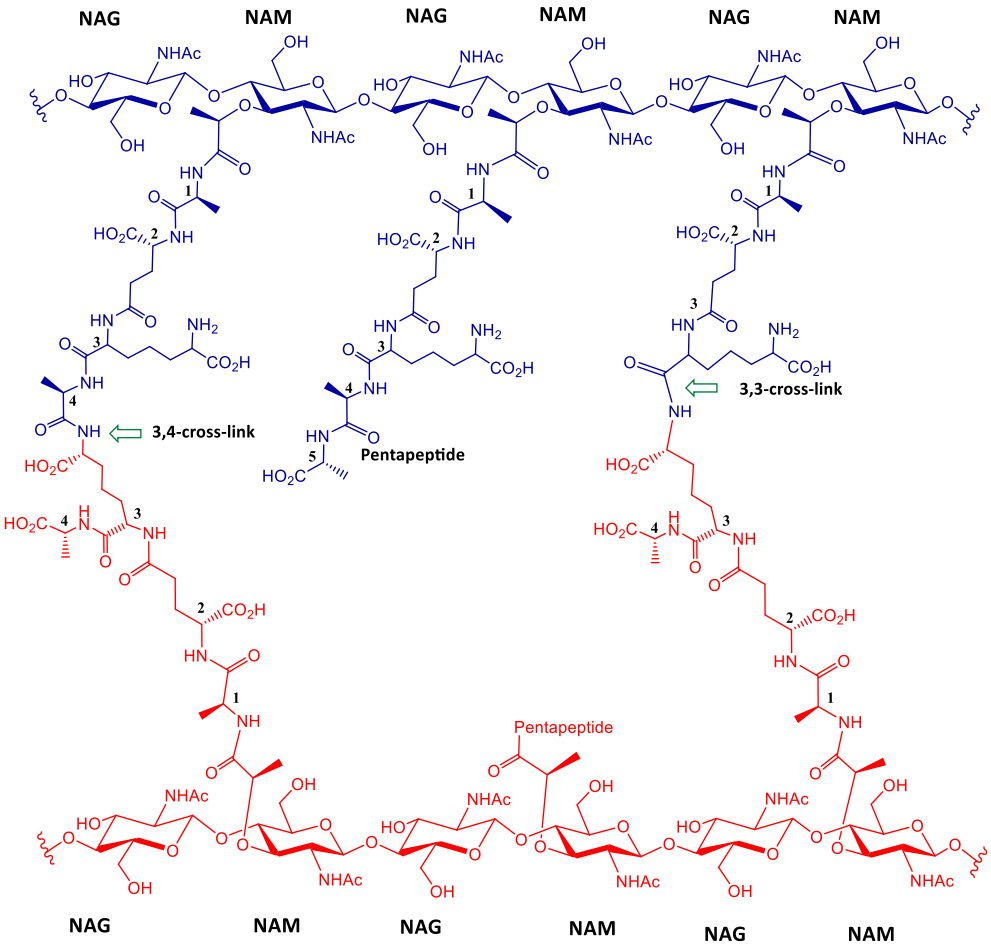

Figure 1-6: *Chemical structure of cross-linked bacterial peptidoglycan of P. aeruginosa. The donor strand is blue while the acceptor is in red. Different types of cross-link are shown by green arrows. The glycan chains consist of alternating N-acetylmuramic acid (NAM) and N-acetylglucosamine (NAG) residues connected via β-1,4-glycosidic bonds (this figure was adapted from ref.* ***37****).*

Generally, this basic structure of PG is conserved in all known bacterial species with some variation in the strands. These variations include modifications to the glycan strands, such as *N*-deacetylation, *N*-glycosylation and *O*-acetylation. The glycan strand in Gram-negative bacteria ends with 1,6-anhydromuropeptide whereas Gram-positive (e.g. *Staphylococcus aureus)* do not contain this reducing end except *Bacillus subtilis* that contains 0.4% of this modified end.[38] Moreover, the peptide stem in PG can vary according to the enzymes responsible for its biosynthesis.[37]

1.3 Peptidoglycan biosynthesis

Peptidoglycan plays a critical role in maintaining cell integrity, it represents an important target of chemotherapeutic agents like antibiotics. The dynamic process of peptidoglycan biosynthesis occurs in three different stages:

1.3.1 Synthesis of nucleotide precursors

The initial cytoplasmic stage includes four steps:[39] **1)** synthesis of the activated nucleotide UDP-*N*-acetylglucosamine, **2)** synthesis of UDP-*N*-acetylmuramic acid, **3)** formation of UDP-NAM-pentapeptide from UDP-NAG via six steps, **4)** synthesis of D-glutamic acid and dipeptide D-alanyl-D-alanine.[40] The first step needs four different enzymes namely; glucosamine-6-phosphate synthase (GlmS), phosphoglucosamine mutase (GlmM), glucosamine-1-phosphate acetyltransferase and *N*-acetylglucosamine-1-phosphate uridyltransferase.[41,42] The second stage requires two enzymes, MurA which catalyses formation of UDP-NAG-enolpyruvate from phosphoenolpyruvate (PEP)[43,44] followed by MurB which catalyses an NADPH-dependent reduction.[45] The assembly step is catalysed by four essential Mur ligases (MurC, D, E and F). In most cases the peptide stem is composed of L-alanine-D-glutamic acid-diaminoacid-D-alanine-D-alanine. MurC adds the first amino acid in the stem, and MurD adds the second. The third amino acid, added by MurE, is generally *meso*-diaminopimelic acid (*m*-DAP) in gram-negative bacteria and *Bacilli*, and Lys in gram-positive bacteria, although in some species it may be L-ornithine, LL-DAP, L-diaminobutyric acid, L-homoserine and *meso*-lanthionine. Dipeptide D-Ala-D-Ala is added in position four and five in the peptide stem by ligase MurF. In vancomycin resistant strains, position five is replaced with D-serine or D-lactate.[46]

1.3.2 Formation and translocation of lipid II

After UDP-NAM-pentapeptide is generated in the cytoplasmic space, it is joined to membrane-bound C_{55}-P carrier lipid through the integral membrane protein MarY to form lipid I which is then glycosaminylated with UDP-NAG by MurG to form lipid II (Figure 1-7).[47,48] Modifications in lipid II in gram-positive species can occur at positions two and three of the peptide stem by amidation of glutamate to iso-glutamine or acetylation of the ε-amino group of lysine for the attachment of a peptide bridge, both are required for PG cross-linking in *Streptococcus*

pneumonia and *Staphylococcus aureus*. Following this, lipid II is transferred cross the cytoplasmic membrane to outer membrane to start the next stage of PG biosynthesis.[49-51]

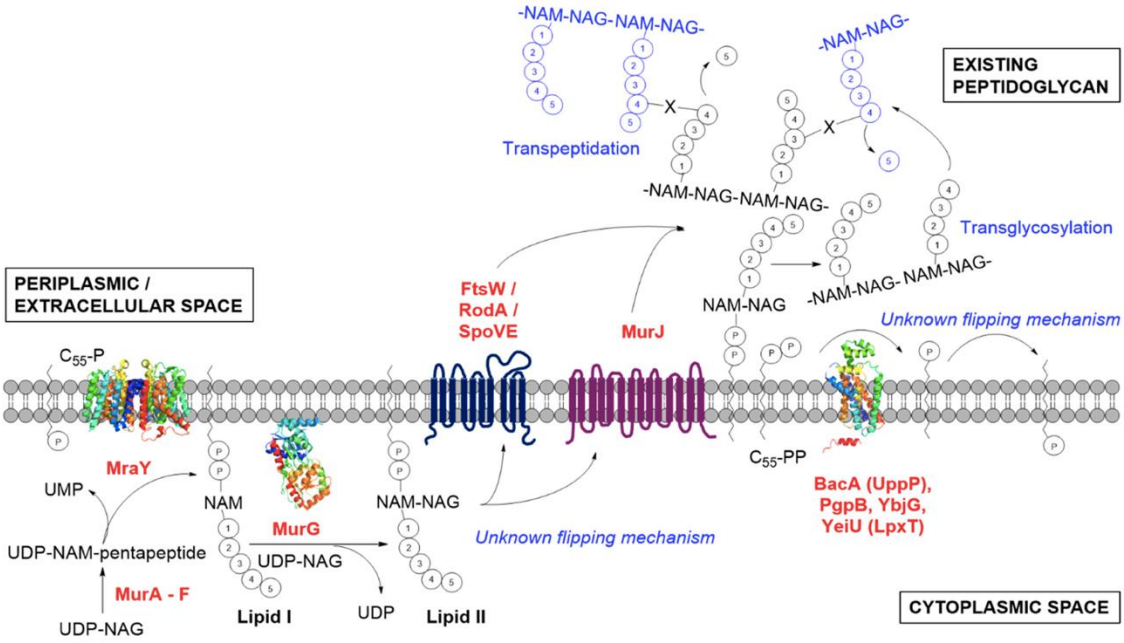

Figure 1-7: *PG biosynthesis in bacteria: formation and translation of lipid II (reproduced from reference 47).*

Two flippases are responsible for lipid II translocation, FtsW and MurJ. The first enzyme FtsW belongs to the SEDS (shape, elongation, division and sporulation) family. During cell division, it is localised to the septum and interacts with two PBPs (PBP1B and PBP3).[52,53] The second enzyme, MurJ, a member of the MOP (multidrug / oligosaccharide-lipid / polysaccharide) exporter superfamily, is essential in *E. coli* as cells depleted of MurJ leads to PG biosynthesis failure and accumulation of PG lipid and nucleotide precursors which eventually results in cell lysis.[54-56]

1.3.3 Transglycosylation and transpeptidation

In this stage, lipid II is polymerised by the cross-linking of nascent strands in the presence of mono and bi-functional PBPs. Energy from phosphodiester-NAM bond and D-alanyl-D-alanine bond of lipid II is needed in this stage in order to derive the transglycosylation and transpeptidation reactions respectively.[57,58] Bacteria have two different classes of PBPs, high molecular mass (HMM), which are responsible for polymerisation and insertion into the pre-existing sacculus, and low molecular mass (LMM), involved in cell separation and PG recycling. According to the activity of PBPs within the C-terminal they are divided into class A and B. Transpeptidase can be inhibited by β-lactams and glycopeptides.[59]

1.4 Peptidoglycan cleaving enzymes

Peptidoglycan has a number of metabolic activities that require cleavage of the saccules. For example, *E. coli* turns over about 50% of its sacculus per generation.[60] The recycled muropeptides from the sacculus are reutilised by the PG-recycling pathway and may be used as a signal of β-lactamase expression. The degradation and remodelling activities of the sacculus are catalysed by different hydrolases including: glycosidases, amidases and peptidases (endopeptidases and carboxypeptidases).[61,62] Glycosidases cleave glycan backbone include: β-*N*-acetylglucosamidase, which cleaves the glycosidic bond between neighbouring NAG units, *N*-acetylmuramidase, which hydrolyses the β-1,4-glycosidic bond between *N*-acetylmuramic acid (NAM) and *N*-acetylglucosamine (NAG) (lysozyme and lytic transglycosylase). Amidases consist of *N*-acetylmuramyl-L-alanine amidases which are responsible for cleaving the amide bond between NAM in the glycan strand and L-alanine residue within peptide stem. On the other hand, peptidases include endopeptidases which cleave the amide bond between two amino acids in peptide chain, and carboxypeptidases which hydrolyse the terminal amide bond in the peptide stem. Lytic transglycosylases are glycosidases, specifically muramidases, but they are not hydrolases. Instead they cleave the glycosidic bond in PG backbone between NAG and NAM with concomitant formation of a 1,6-anhydromuramoyl product.[63]

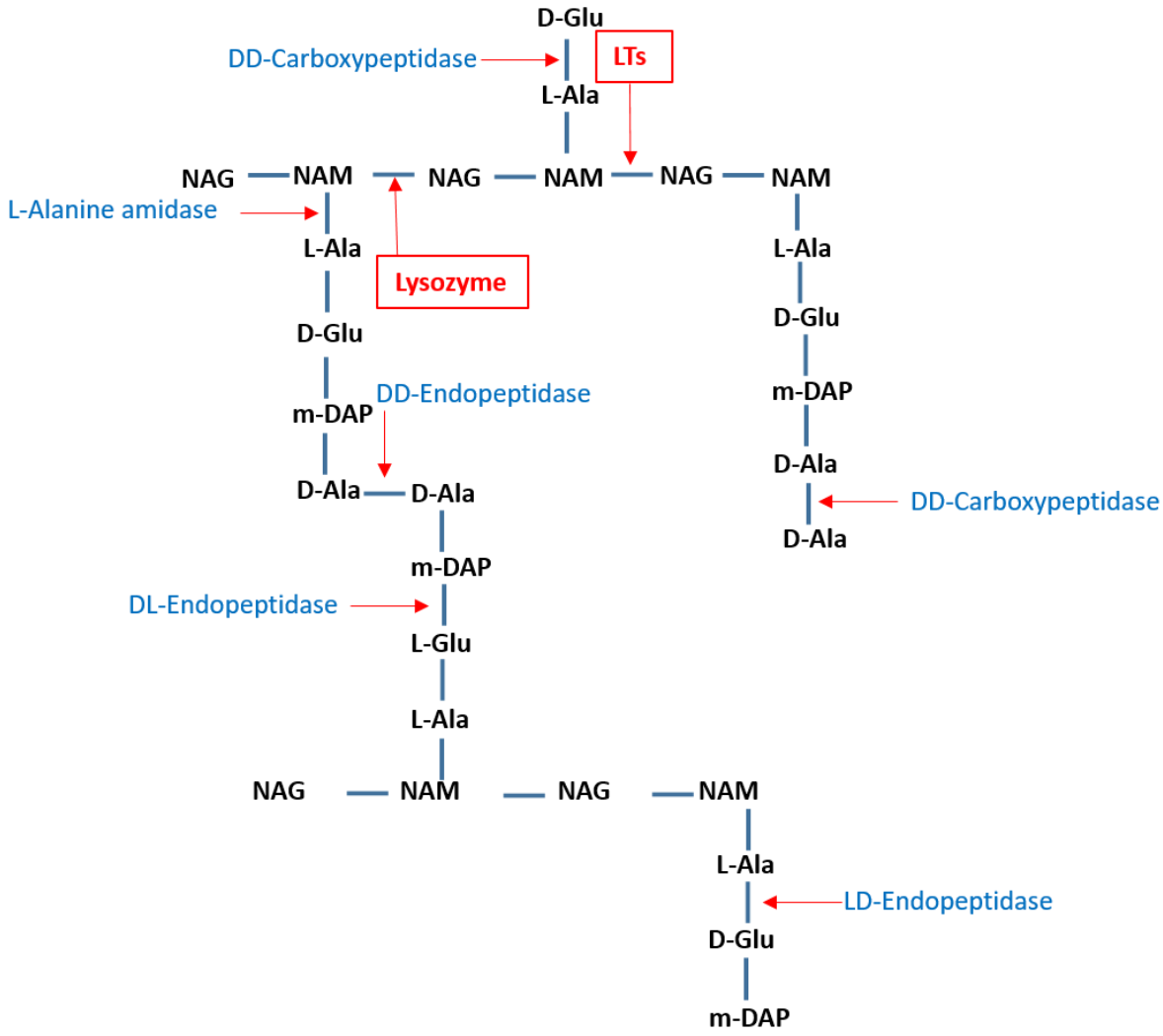

Figure 1-8: *PG-cleaving enzymes with the different cleaving sites. The PG structure shown represents the E. coli sacculus. The different PG hydrolyses are indicated in blue, each enzyme is capable to cleave at specific bonds within the sacculus. LTs and lysozyme cleavage sites are indicated in red.*

1.4.1 *N*-Acetylglucosaminidases

These enzymes are widespread in nature and are involved in PG hydrolysis by cleaving the glycosidic bond between NAG and NAM within the PG backbone producing a reducing NAG product (Figure 1-9). They include seven different glycoside hydrolases (GH) families based on their secondary structure, GH3, GH18, GH20, GH56, GH73, GH84 and GH85. Family GH73 involved in PG daughter separation during cell division. Five phylogenetic clusters harbouring characteristic sequence motifs have been identified. The acidic catalytic residue in their catalytic mechanism has been identified as glutamic acid while aspartate residue acts as a base.[64,65]

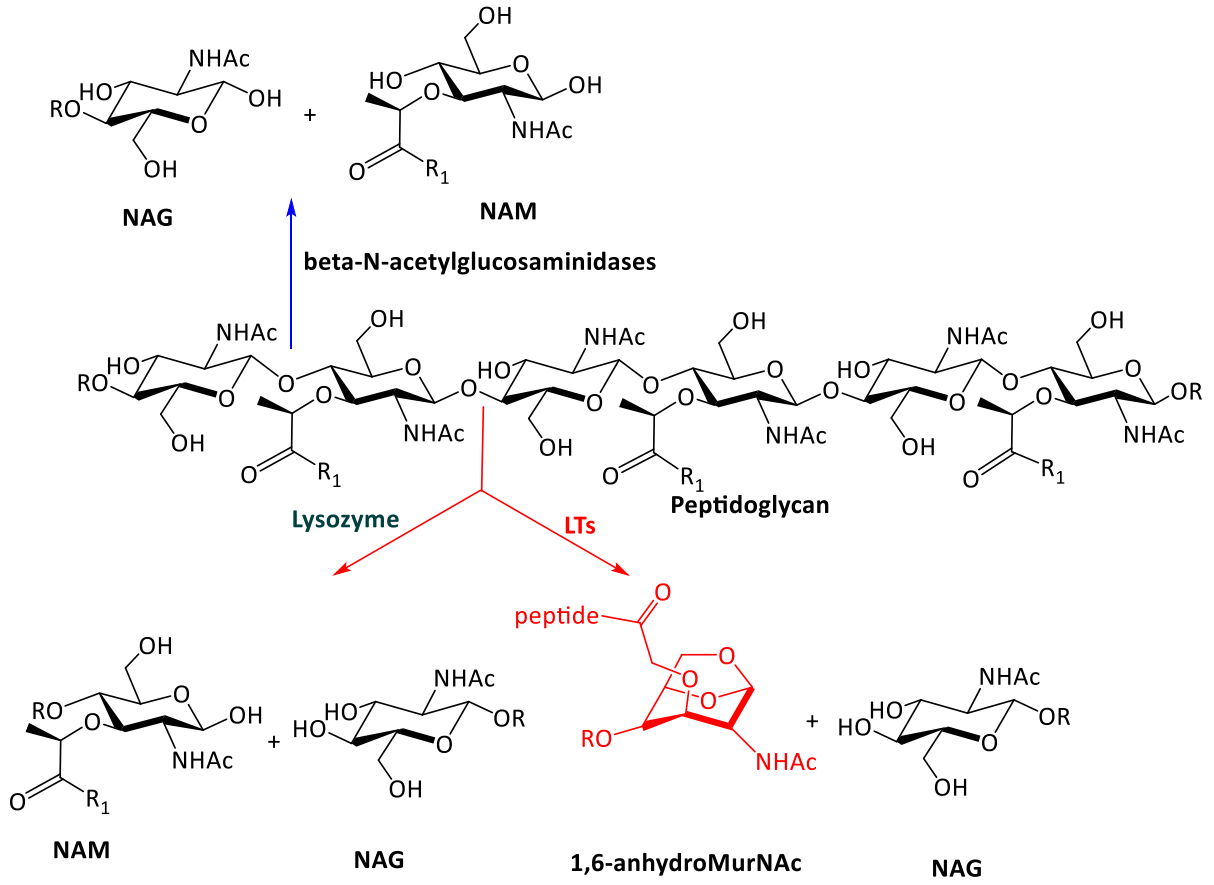

Figure 1-9: *Glycolytic cleavage of bacterial peptidoglycan by autolysis enzymes. The β-N-acetylglucosaminidases hydrolyse the β-1,4-linkage between NAG and NAM residues in PG, while the muralytic enzymes muramidases and LTs cleave non-hydrolytically between NAM and NAG residues.*

Hydrolysis of glycosidic bonds catalysed by most GH can occur via either inversion or retention of anomeric configuration as following:[66-69]

Inverting glycosidases

A single-displacement reaction takes place through protonation of the glycosidic oxygen by the acidic catalytic residue in the active site followed by basic attack via an Asp residue (general base) located on the active site cleft by an average distance of 10.5 Å. This basic attack to abstract a proton from water molecule generates a hydroxide ion which attacks the anomeric carbon of the NAG residue leading to bond cleavage and a product with an inverted anomeric stereochemistry.

Retaining glycosidases

Double-displacement reactions are involved in this mechanism. In the first reaction, and as with the single displacement mechanism, the carboxyl group of one of the catalytic residues serves as a general acid catalyst, protonating the glycosidic oxygen concomitant with cleavage

of the bond, followed by nucleophilic attack on the anomeric centre of the intermediate oxocarbenium ion by the second catalytic residue, producing the non-reducing end product and leading to covalent attachment of the remaining substrate. In the second reaction, the catalytic residue serves as a base, abstracting a proton from a water molecule and producing hydroxide ion which attacks the covalent adduct leading to hydrolysis of the covalent bond and release of the resulting sugar product with retention of the anomeric configuration.

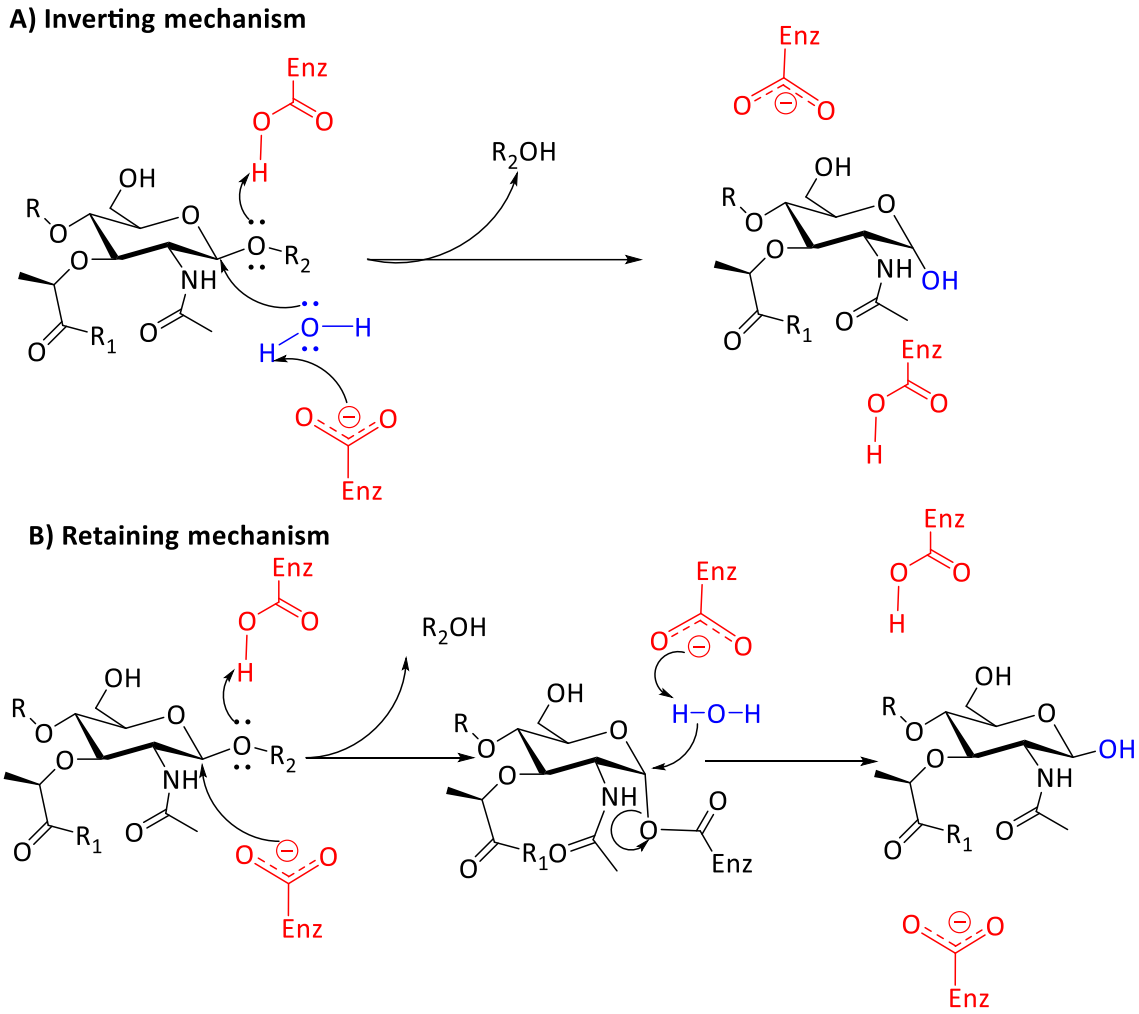

Figure 1-10: *Hydrolytic mechanism of glycosidases on bacterial peptidoglycan. R, R_1, and R_2 denote GlcNAc, MurNAc, and stem peptides respectively.*

Glycosidase inhibitors

NagZ (*β-N*-acetylglycosaminidase) is a family 3 *β*-glycosaminidase located in the bacterial cytoplasm. It is involved in PG recycling by catalysing the first reaction in the cytoplasm, the cleavage of a non-reducing NAG residue from NAG-1,6-anhydroNAM-peptides using a double-displacement mechanism, resulting in 1,6-anhydroNAM-peptides. These are important in *β*-

lactamase induction by activating the AmpR.[70,71] Therefore, inhibition of this enzyme can block the generation of AmpC inducer and thereby preventing the expression of β-lactamase. Due to this crucial function, many efforts have been directed towards the synthesis of small molecules that can inhibit the enzymatic activity of NagZ. Several compounds have been synthesised and evaluated as potent inhibitors against NagZ such as PUGNAG (*N*-acetylglucosamino-1,5-lactone *O*-(phenylcarbamoyl)-(Z)-oxime **(10)**, NHNAc DNJ (2-acetamido-2-deoxynojirimycin **(11)** and azepane **(12)** (Figure 1-11).[72-75]

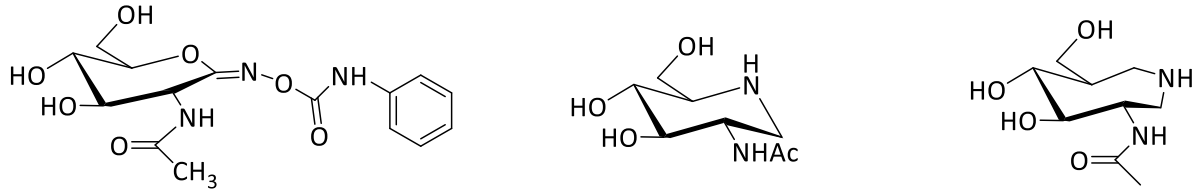

10
PUGNAc

11
NHNAcDNJ

12
Azepane

Figure 1-11: *Chemical structure of some known NagZ inhibitors (10-12).*

1.4.2 Muramidases (lysozyme)

Lysozymes are lytic enzymes that hydrolyse the glycosidic bond between NAM and NAG within its natural substrate bacterial peptidoglycan, resulting in terminal reducing NAM residues. The most common types of lysozyme are c-type (chicken type e.g. hen egg white lysozyme, HEWL), g-type (goose egg white lysozyme, GEWL) and i-type (invertebrate type e.g. *Tapes japonica* lysozyme). It has been reported that these enzymes are produced by vertebrate, invertebrate, phages, fungi and bacteria. They have biological roles as key enzymes in defence systems, for example they are used by higher organisms and plants as a first defence against pathogenic bacteria. According to the crystal structure of lysozyme, the enzyme consists of two domains separated by a deep substrate-binding cleft containing the active site. One domain is a small β-sheet while the other domain is alpha-helix rich with N- and C-terminal segments and a loop links between the two domains. Although the lysozyme types have different sequence and they are variable in length, they share similar fold.[76]

Reaction mechanism

The lysozyme active site consists of six subsites (A-F or -4 to +2) which can bind up to six consecutive sugars. The glycosidic bond in this configuration is cleaved between NAM at subsite D (-1), and NAG at E (+1) through a double displacement reaction using two catalytic

residues, Glu35 as an acid and Asp52 as a base. Two different mechanisms were proposed for HEWL catalytic reaction; path A (by Koshland) and path B (by Phillips) (Figure 1-12). The first step in path A, the basic residue Asp52 attacks via its carboxylate group at the glycosidic bond producing the glycosyl intermediate with configuration inversion. Following this, the acidic residue Glu35 protonates the glycosidic oxygen to facilitate bond cleavage. Secondly, a water molecule attacks from the opposite face (β-face) to remove the enzyme carboxylate leading to the hydrolysed product with retained stereochemistry. In path B, the substrate binds to the enzyme cleft in a distorted conformation followed by protonation of the glycosidic oxygen by Glu35 residue producing oxocarbenium ion intermediate which is stabilised by Asp52. In the next step, Aps52 was suggested to attack at the anomeric centre of the oxocarbenium ion to shield the α-face which is then intercepted by a water molecule from the β-face producing the hydrolysed product. Hydroxyl groups at C6 of murmoyl residues are necessary for substrate binding with the amino acids in the long groove of HEWL. Consequently, bacteria such as *Staphylococcus aureus* deactivate HEWL activity by modifying their glycan backbone via *O*-acetylation of C6-NAM to prevent the binding with lysozyme (HEWL).[77,78]

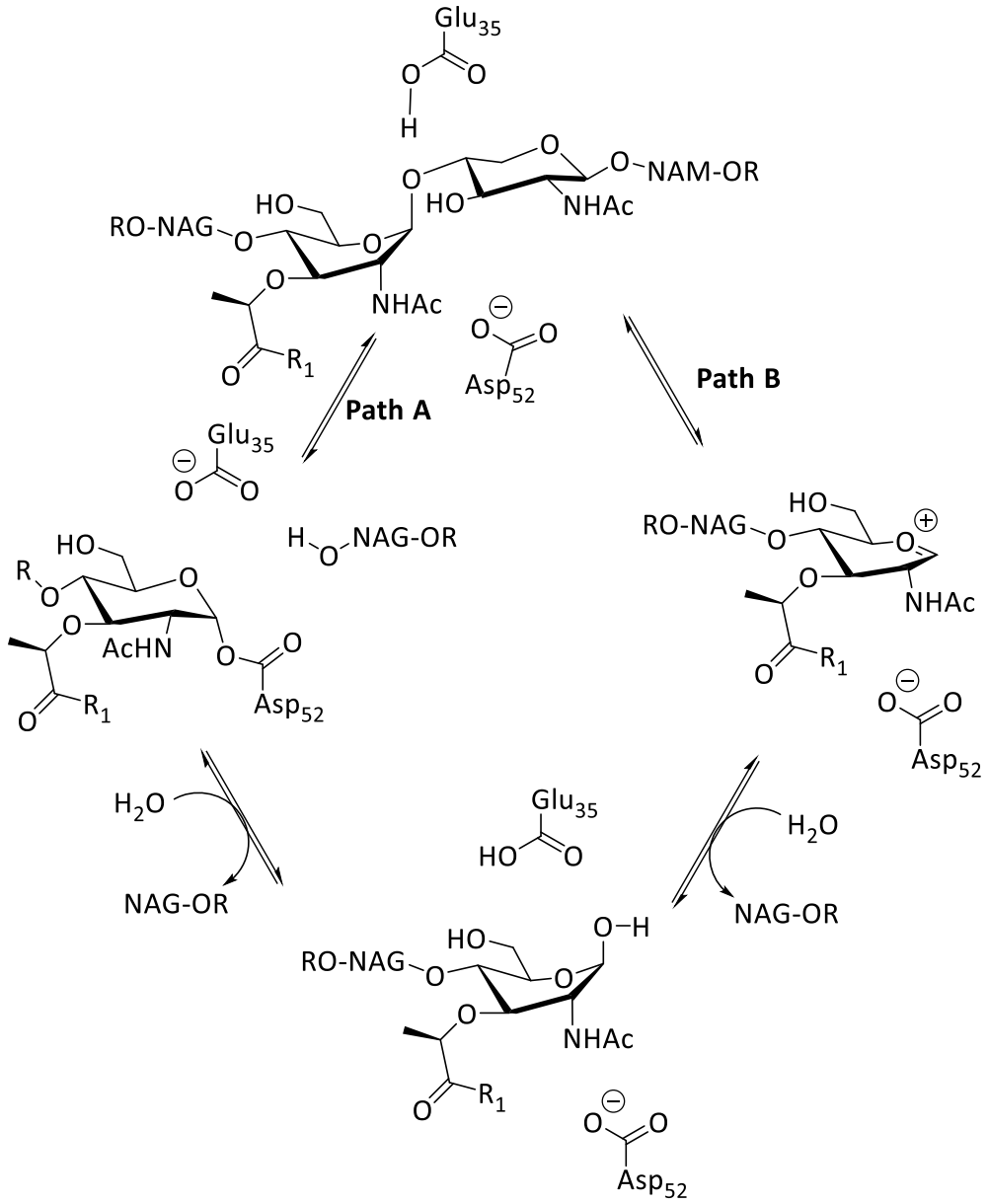

Figure 1-12: *The proposed catalytic mechanism for lysozyme (HEWL) on the bacterial peptidoglycan.*[77]

Lysozyme inhibition

As mentioned above, due to the important role of lysozyme as an effective antibacterial agent, some bacteria have found methods to protect their cell wall from lytic activity of lysozyme c-type by *N*-deacetylation or *O*-acetylation modifications to their peptidoglycan. Additionally, gram-negative bacteria produce proteinaceous inhibitors to defend themselves from lysozymes actions, such as Ivyc (inhibitor of vertebrate lysozyme), which inhibits vertebrate c-type lysozyme.[79,80] Crystal structures of Ivyc and Ivyp1 in complex with HEWL have been studied, Ivyc forms a homodimer with two dimers of HEWL and human lysozyme (HL), whereas Ivyp1 is a monomer (Figure 1-13). The crystal structure indicated that the His62 in the active

site of Ivy interacts with the catalytic acid/base Glu35 and the catalytic nucleophile Asp52 residues in the catalytic domain of HEWL via hydrogen bonds causing a reduction in the lysozyme activity. In contrast, Ivyp2 that lacks the His62 does not inhibit lysozyme activity.

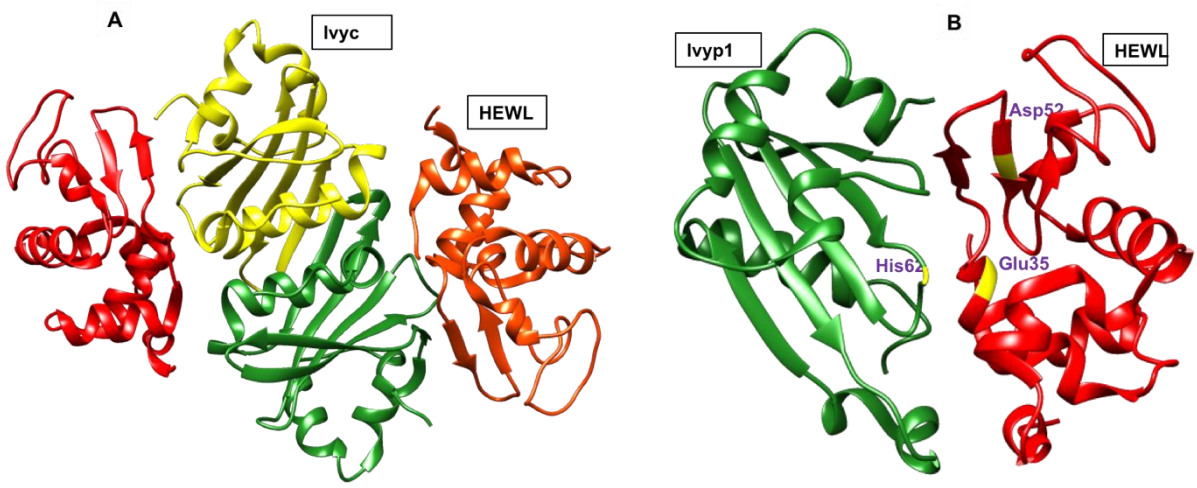

Figure 1-13: *Cartoon representation of the crystal structure of Ivy-HEWL complex. A) The dimer form of Ivyc interacting with two molecules of HEWL (PDB 1GPQ). B) The monomer of Ivyp1 in complex with HEWL showing the His62 residue in the loop of Ivyp1 and the two catalytic residues in the HEWL active site.*

More recently, PliC (periplasmic inhibitor of c-type human lysozyme) and MliC (membrane-bound lysozyme inhibitor) have been found in many Gram-negative bactria. Crystal structures of MliC from *P. aeruginosa* complexed with HEWL[81] and MliC from *Brucella abortus* in complex with human lysozyme (HL)[82] have been reported. The comparison between both structures revealed that the MliC is more specific inhibitor for HL than HEWL. Moreover, 4-*O*-β-tri-*N*-acetylchitotriosylmoranoline (**13**), a transition state analogue, has been synthesised from the reaction of lysozyme (HEWL) with tetra-*N*-acetylchitotetraose and moranoline was tested for its effect on the lysozyme activity using different techniques including X-ray crystallography. This compound exhibited good inhibition of wild type HEWL activity.[83] Recently, a planar cationic phenothiazinium dye 3,7-diamino-5-phenothiazinium acetate (thionine acetate (**14**)) has been investigated for its effect on lysozyme activity by studying its binding using synchronous fluorescence and circular dichroism.[84]

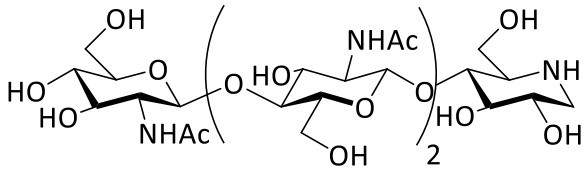

13

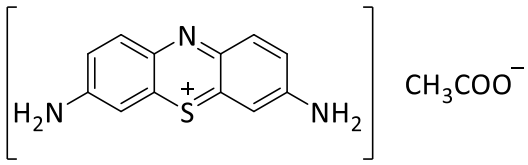

14

Figure 1-14: *Chemical structure of some known lysozyme inhibitors.*

1.4.3 Lytic transglycosylases

Lytic transglycosylases (LTs) are peptidoglycan degrading enzymes found within the periplasmic space of Gram-negative bacteria as soluble or membrane-bound proteins (Slt or Mlt). They play critical roles during cell growth and division by insertion of envelop-spanning structures such as secretion system into the cell by cleaving β-1,4-glycosidic bond between NAM and NAG residues within bacterial peptidoglycan, like lysozymes (e.g. hen egg white lysozyme, HEWL). In contrast to lysozymes, these enzymes are not hydrolytic but instead form 1,6-anhydro-*N*-acetylmuramyl residue.[85] *E. coli* produces nine known LTs (MltA, MltB, MltC, MltD, MltE, MltF, MltG, RlpA and Slt70). However, the pathogenic *Pseudomonas aeruginosa* produces eleven LTs, Mlts (MltA, MltB, MltD, MltF, MltF2 and MltG) including the rare lipoprotein A (RlpA) and four isozymes of MltB (Slt, SltB1, SltB2, and SltB3).[86]

LTs produced by *E. coli* are generally exoenzymes (cleavage at the terminus) and release disaccharide-peptide from the reducing or non-reducing ends of PG chains, except for MltF and MltE which are endolytic enzymes (cleavage in the middle of the PG).[87,88]

Classification of LTs

LTs were classified by Blackburn and Clarke into four distinct families based on sequence similarity and consensus motifs and more recently extended to six families (Figure 1-15). [89,90] The archetypes of these families are based on seven known LTs from *E. coli* (Slt70, MltA-MltF), MltB from *P. aeruginosa* and endolysins from lmda-bacteriophage.[89,91] Family 1 is a

superfamily of five subfamilies (A-E). All five subfamilies possess some limited sequence similar to the goose-type lysozyme. Six known LTs from *E. coli* are included in this family: Slt70 (1A), MltC (1B), MltD (1D), MltE (1C), MltF (1E), and more recent SltF (1F), which is encoded in flagellated α-proteobateria, has been included. This subfamily contains four consensus motifs, which have been divided into two subsets featured by including extra catalytic residue either Ser or Thr beside the Glu catalytic residue.[92] The LTs that possess sequence identical to MltA from *E. coli* are classified within family 2. In contrast to other families, two aspartates are involved in the catalytic mechanism of this family. Family 3 includes known LTs that have identity similar to MltB from both *E. coli* and *P. aeruginosa.* Family 4 consists of bacteriophage enzymes. The recent two families 5 and 6 include MltG from *E. coli* and RlpA from *Pseudomonas aeruginosa* respectively.[93]

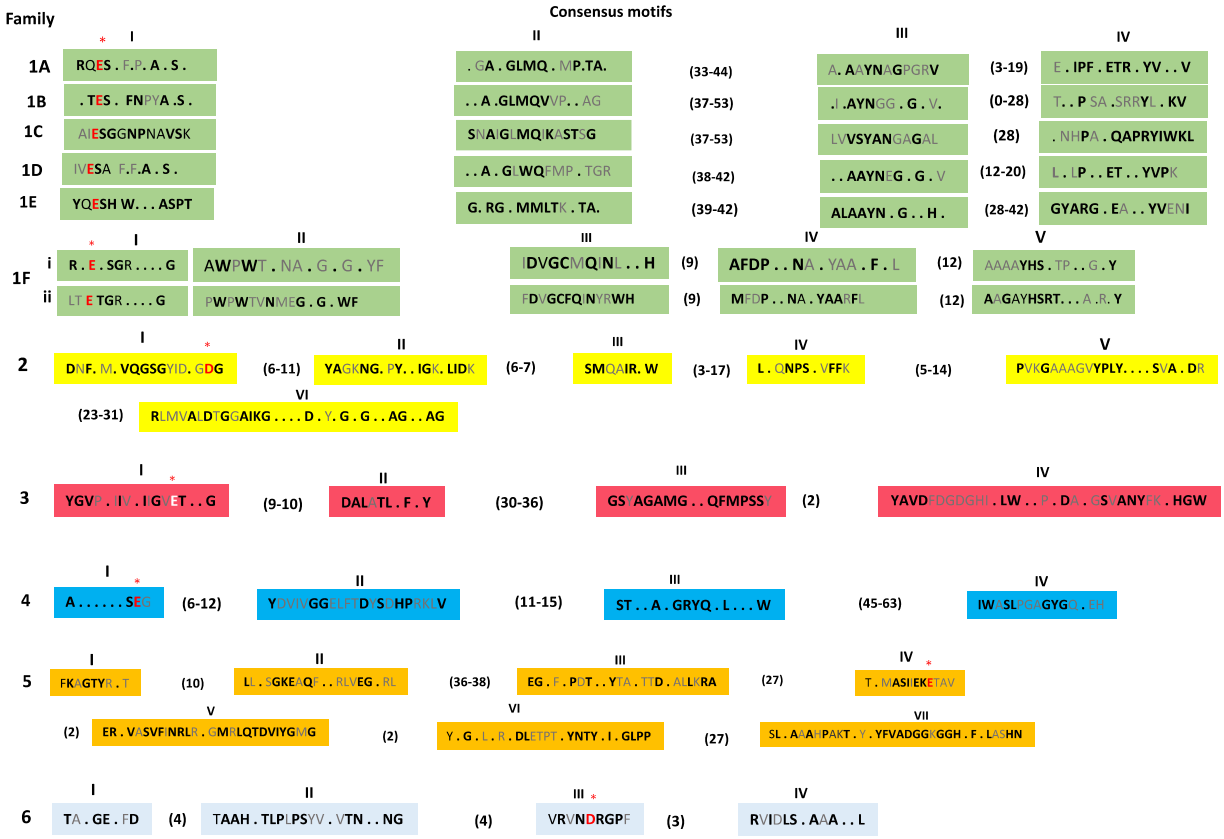

Figure 1-15: *Family archetype organisation of LTs in E. coli. Residues in bold (labelled by roman numerals) exist in greater than 80% of the sequences of the individual families, while residues coloured in red and labelled with asterisks represent the catalytic acid/base residues. The numbers indicate the number of residues between the motifs.*[90]

Three-dimensional structures

Crystal structures of eleven LTs representing families from different species have been determined by X-ray crystallography. Six different structures of LTs from *E. coli* have been solved: Slt70 (1A),[94] MltC (1B),[88] MltE (1C),[95] MltA (2),[96,97] Slt35 (3),[98] MltG (5). Three enzymes from *P. aeruginosa* have had their structures identified: MltF (1E), SltB1 (3),[99] and SltB3 (3),[100] along with MltA from *Neisseria gonorhoeae* (2) and bacteriophage $\phi\lambda$ LT (4).[101] The catalytic active site cleft in families 1, 3, 4 and 5 are α-helix rich similar to g-type lysozyme fold, while family 2 is a double-Ψ-β-barrel structure (Figure 1-16).

Overall, these enzymes lack similarity in their amino acid sequences and tertiary structures between all members.

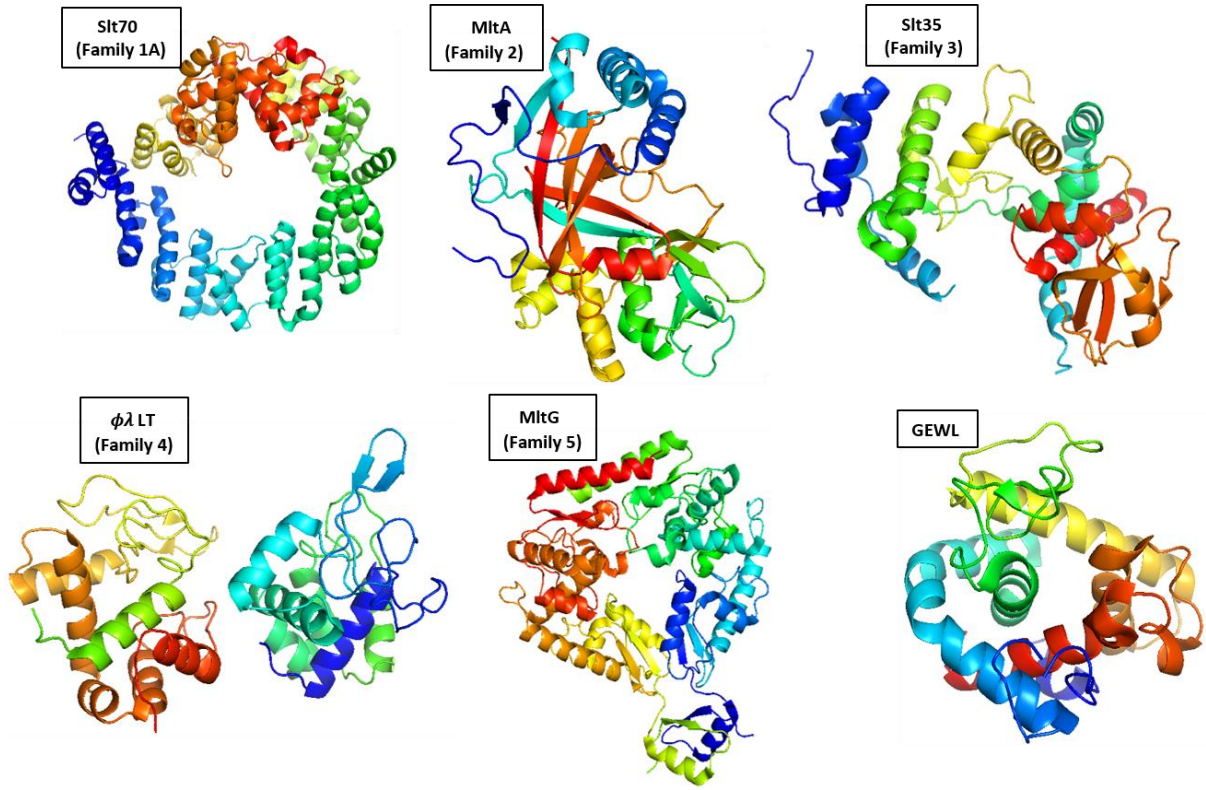

Figure 1-16: *Cartoon representations of crystal structures of three LTs that resemble g-type lysozyme fold. Slt70 (E. coli, PDB 1QTE), MltA (E. coli, PDB 2GAE), Slt35 (E. coli, PDB 1QUS), $\phi\lambda$ LT (E. coli phage lambda, 1D9U), MltG (E. coli, PDB 2R1F, GEWL (Salmo salar, PDB 3MGW).*

Mechanism of action

LTs are autolysins enzymes which catalyse the cleavage of the PG backbone to allow insertion of new PG material (e.g. DNA and proteins) into the cell wall during cell growth, most of them are exolytic enzymes. In principle, the active site of these enzymes can be divided into saccharide binding subsites –i to +j which refer to various numbers from enzyme to enzyme. When PG binds to the active site it straddles these subsites before the lytic reaction takes place.[100] For example, Slt70 is divided into six subsites labelled -4 to +2. NAG residues of the glycan strand can bind at -4, -2 and +1 sites while NAM residues bind at -3, -1 and +1 sites.[94] On the other hand, Slt35 from *E. coli* has four binding subsites labelled -2 to +2, that are located in a deep groove where a NAG residue was found to be accommodated. It has been reported that the catalytic residue of LTs is often a Glu residue located in the centre of the active site between subsites (-1 and +1) and which functions as a general acid.[102]

Based on the crystal structure of Slt70 complexed with bulgecin,[103] a reaction mechanism of LTs has been proposed. The mechanism starts by protonation of the glycosidic oxygen by the catalytic residue Glu478 as a general acid, resulting in bond cleavage and formation of an oxocarbonium ion intermediate, which is promoted by steric distortion of the low-energy chair conformation leading to a higher energy half-chair conformation. Next step, intramolecular nucleophilic attack at C-1 of the oxocarbenium by the hydroxyl group on C-6 of the NAM ion, causes the glycosidic ring to adopt a boat conformation. In the last step, Glu478 abstracts a proton from O-6 in the product and the structure changed into a more stable chair conformation producing 1,6-muramoyl product.

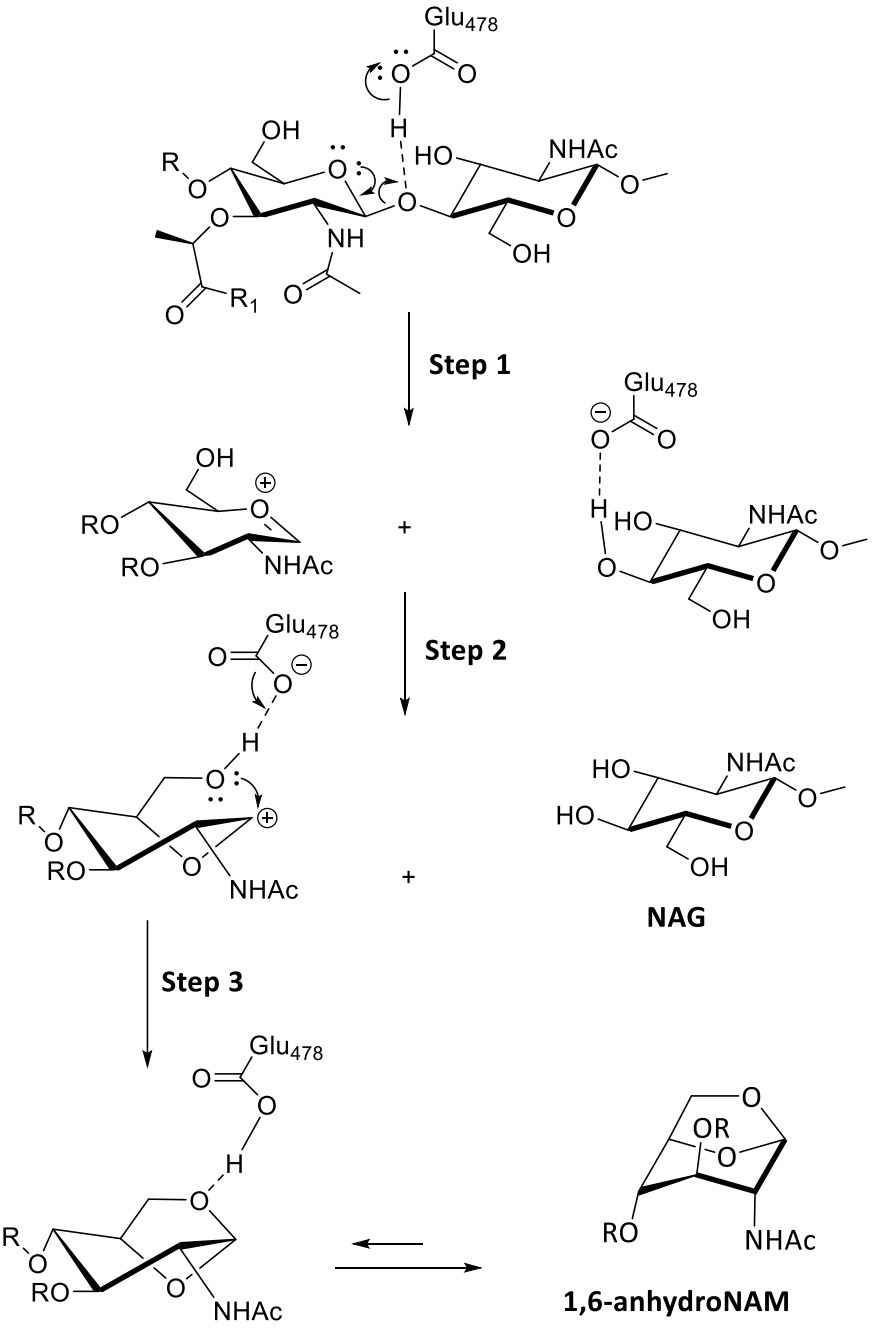

Figure 1-17: *Proposed reaction mechanism catalysed by Slt70 on the bacterial peptidoglycan.*[103]

On the other hand, Clarke et al.[85,102] suggested a mechanism based on the effect of NAG-thiazoline on the enzymatic activity of MltB from *P. aeruginosa.* The first step is similar to the mechanism mentioned above, protonation of glycosidic oxygen by the catalytic residue Glu162 residue followed by cleavage of the glycosidic bond and then formation of oxocarbenium intermediate. Due to the lack of the basic catalytic residue which in lysozyme serves as a nucleophile, LTs stabilise the transient oxocarbenium ion through the formation of

an oxazolinium intermediate which involves the *N*-acetyl group of the muramoyl residue at subsite -1. In the second step, the catalytic residue Glu162 acts as a general base to abstract a proton from the oxazolinium species producing 1,6-anhydromuramic acid product.

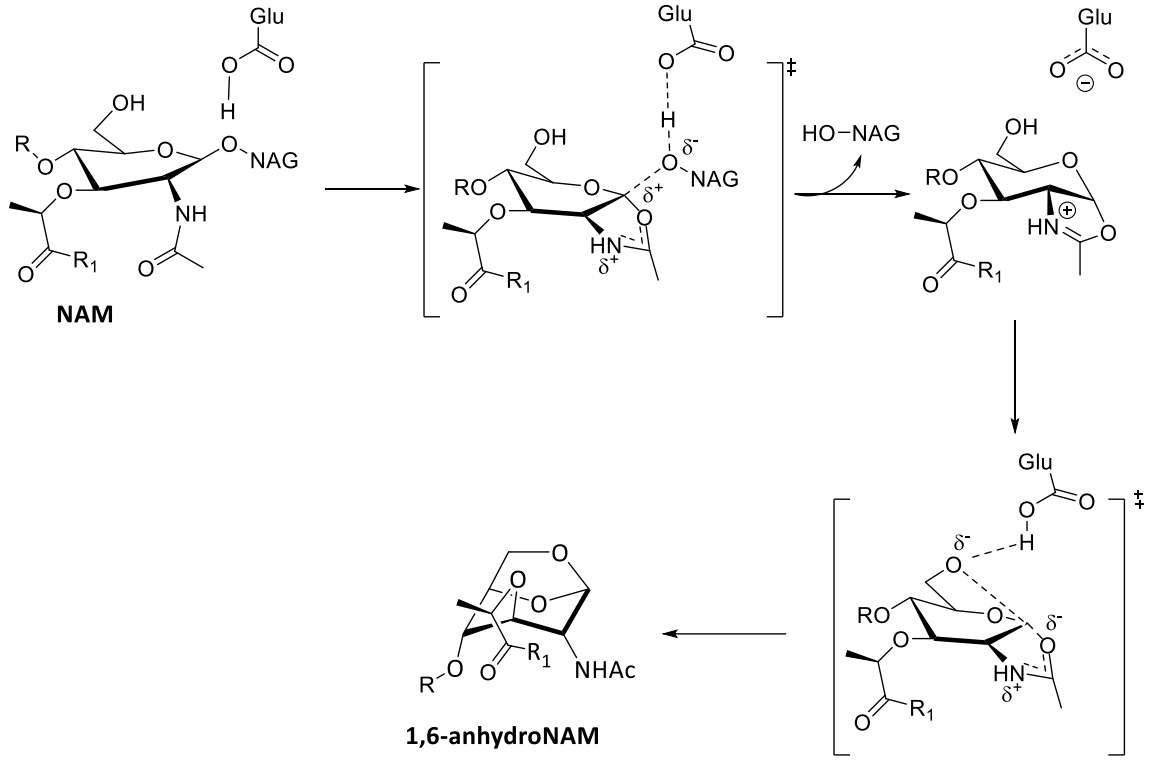

Figure 1-18: *Mechanisms Proposed by Clarke of the catalytic reaction on PG catalysed by LTs.*[85]

Biological activity

As mentioned above, LTs are lytic enzymes involved in cell wall degradation and remodelling. The catalytic sites of these enzymes resemble the lysozyme (goose type lysozyme) active site with the catalytic residue Glu. However, LTs lack the Asp residue as a general base as in lysozyme. They are mostly present in Gram-negative bacteria and also in some Gram-positive bacteria. They play critical roles during cell growth and division by making pores within the cell wall to insert different materials, they contribute to cell wall biosynthesis and PG recycling by association with multi-protein complexes involved in PG synthesis (e.g. MltG from *E. coli)* [104] and release of daughter cells (e.g. RlpA from *P. aeruginosa)*.[93] In addition, the product from their lytic reaction, 1,6-anhydromuramyl tripeptide, is considered to be a signal to control β-lactamase expression. Recently, SleB from *B. anthracis* was used as a spore cortex degrading agent.[105] Based on the total formation of muropeptides for each enzyme reaction, the enzyme activity is as follows: MltA > MltB > MltC >> Slt70 > MltE > MltD > MltF.[87]

Regulation of lytic transglycosylase activity

As LT overexpression can cause bacterial cell death, the activity of these enzymes must be controlled. Three mechanisms at the enzyme level can be used to regulate the activity of LTs enzymes: substrate modification, complex formation via association with the membrane, and allosteric regulation.

Substrate modification

Various modifications on the PG strand can be made, including *O*-acetylation of the C-6 hydroxyl group of NAM and *N*-deacetylation of NAG. Many bacterial species use this modification depending on their age, strain, and environmental conditions. *Enterococcus faecalis* increases *O*-acetylation of their PG to about 10-40% in the stationary phase, compared to about 10-16% in viable but non culturable phase. Gram-positive bacteria, such as *S. aureus, Streptococcus pneumonia, E. faecalis, Lactococcus lactis* and *Staphylococcus* produce *O*-acetyltransferase (OatA) involved in acetyl transfer to acceptor sites on PG.[97] Moreover, bacteria that modify their PG by *O*-acetylation produce *O*-acetyl PG esterases, which deacetylate this blocking group when required. It has been proposed that LT activity could be blocked by inhibition of *O*-acetyl PG esterase.[106-108]

Multi-enzyme complexes

It has been proposed by Höltje that the LTs are controlled by their incorporation into multi-enzyme complexes involved in murein biosynthesis machinery in the periplasmic space. In this way, the LTs can only reach their murein substrate when they interact with other PG synthases. LTs involved in PG biosynthesis are complexed with PBPs and other murein machinery enzymes, such as the endolytic MltG in *E. coli* that is involved in releasing newly synthesised non-crosslinked strand, formed a complex with PBP1b to terminate the elongation of the nascent polymer.[104, 109, 110]

Allosteric inhibition

The enzymatic activity of LTs can be controlled via their binding with molecules at allosteric sites. For example, a large conformational change in MltF from *P. aeruginosa* has been observed when its *N*-terminal ABC-transporter-like regulatory domain is associated with PG-derived muropeptides. This change occurs over the entire protein structure in order to open the active site for occupancy by its substrate and subsequent catalysis. The effector molecule, which is a tetrapeptide, is presumed to be released by AmpDh3-amidase from the sacculus.[111]

Soluble lytic transglycosylases

As mentioned above, most LTs are membrane-bound proteins except Slt70 and Slt35. Both enzymes have a similar catalytic domain fold with a comparable substrate-binding groove.

Slt70

This is a soluble lytic transglycosylase found in the periplasmic space. During bacterial growth and division, it plays an important role in peptidoglycan metabolism by starting degradation at the *N*-acetylglucosamine end of the glycan strand. The crystal structure reveals a protein built up of three distinct domains (U, L and C domain) as a large ring-shaped α-superhelix. The catalytic C-domain shows structural homology to the fold of goose-type lysozyme, however, there is no similarity in amino acid sequence between those two enzymes.[94] The active site is found in a deep groove, which divides into six saccharide biding sites (labelled -4 to +2) where the NAG unit on glycan strand can bind at -4, -2 and +1 and the NAM binds at -3, -1, and +2. The catalytic residue Glu478 is located at site -1 in the active site and functions as a general acid in the lytic reaction of Slt70 where it cleaves at β-1,4-glycosidic bond between NAM and NAG residues.[102] According to the crystal structure of Slt70 complexed with 1,6-anhydromuropeptide, the muropeptide is bound at sites +1 and +2 in the active site. This enzyme is inhibited by the glycopeptide bulgecin, which showed a strong inhibition to Slt70 catalytic activity. The crystal structure of Slt70 in complex with bulgecin has been solved (Figure 1-19).[94] The inhibitor is bound to the catalytic residue Glu478 by hydrogen bonds to the hydroxymethylproline unit. Additionally, interactions between the Glu583 and NH group in the acetamido group have been observed. These interactions suggest that this inhibitor mimics the oxocarbonium ion intermediate in the catalytic reaction mechanism. Despite the inhibitory activity shown by bulgecin towards most lytic transglycosylase enzymes, it is considered a specific inhibitor for Slt70.[103]

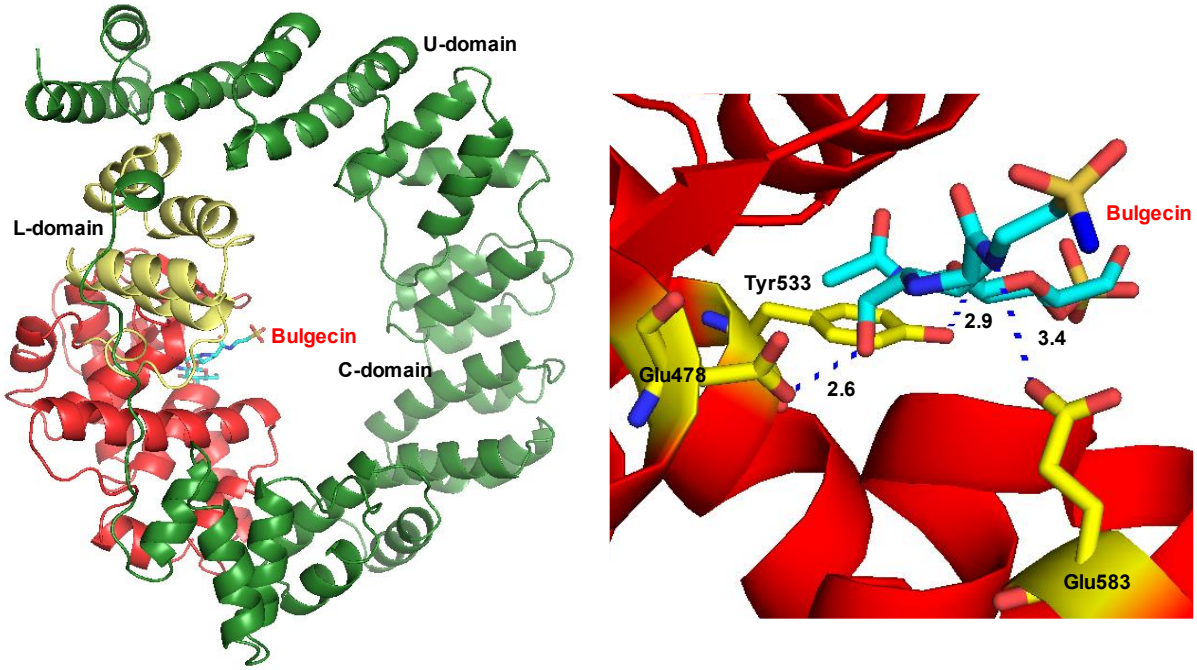

Figure 1-19: *Cartoon representation of soluble lytic transglycosylase (Slt70) complexed with bulgecin. A) The overall structure of Slt70 consisting of three domains, U-domain (residues 1-361), linker domain (L-domain, residues 380-448), and C-terminal domain (residues 449-618).*[93] *B) The interactions between the catalytic residue (Glu478) and other important residues (Tyr533 and Glu583) with the bonding distances (in Å) in the enzyme active site.*

Slt35

This is a fully active soluble proteolytic fragment of membrane-bound lytic transglycosylase MltB, belonging to family 3 in *E. coli*. It has been successfully cloned using T7 promoter system and overexpressed then purified in large scale.[112] It consists of three domains namely; α, β and core domains (Figure 1-20).[98] The core domain, between the β-domain and α-domain, resembles the catalytic domain of Slt70 and goose-type lysozyme fold. Four sugar-binding sites (labelled -2 to +2) have been identified within the active site with the catalytic residue Glu162 located in a deep groove, which occupies the carbohydrate-binding subsite -2 where a NAG residue binds.

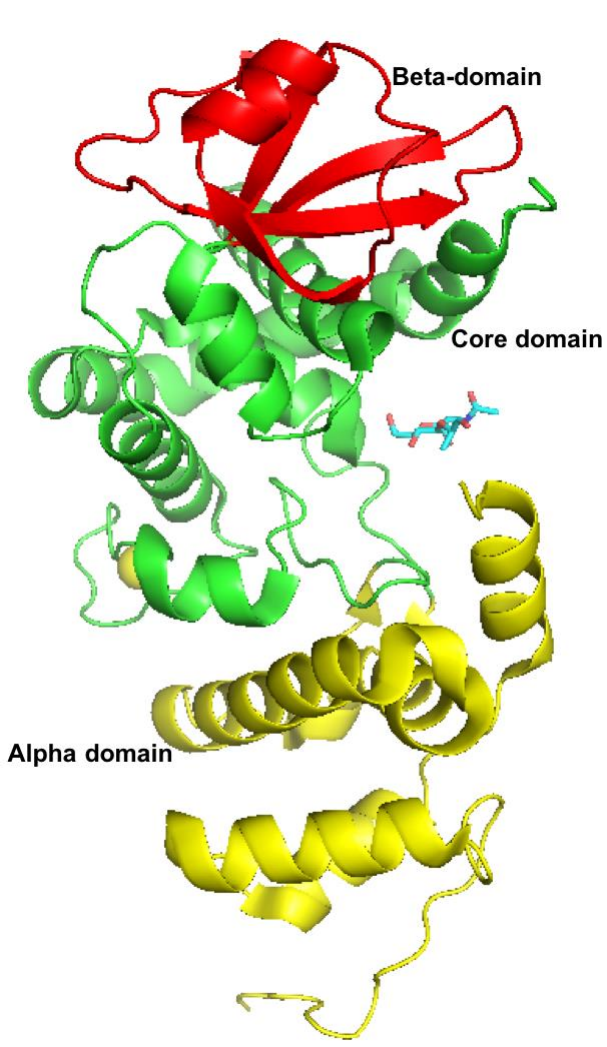

Figure 1-20: *Cartoon representation of soluble lytic transglycosylase Slt35 in complex with GlcNAc. The three domains are shown in different colours, beta-domain in red, core-domain (the catalytic domain) in green, and alpha-domain in yellow.*

EF-hand in Slt35

The EF-hand fold is composed of two α-helices linked together through an intrathecal loop forming the finger (helix E) and the thumb (helix F) of a right hand. The loop contains an EF-hand consensus sequence that coordinates a single calcium ion.[113] Typical coordinating functional groups are the carbonyls of the peptide bond or negatively charged side chains such as carboxylates of aspartate or glutamate or hydroxyl groups such as in threonine.[114] In Slt35 from *E. coli,* an EF-hand calcium-binding site is located about 20 Å from Glu162, in which α-helices H10 (residues 228-234) and H11 (residues 249-262) and residues 237-251 comprise the metal ion-binding loop.[115] The residues within the peptide sequences that coordinate the metal ion are; Asp237, Asp241, Asp251, Ser239 and His243 (Figure 1-21).

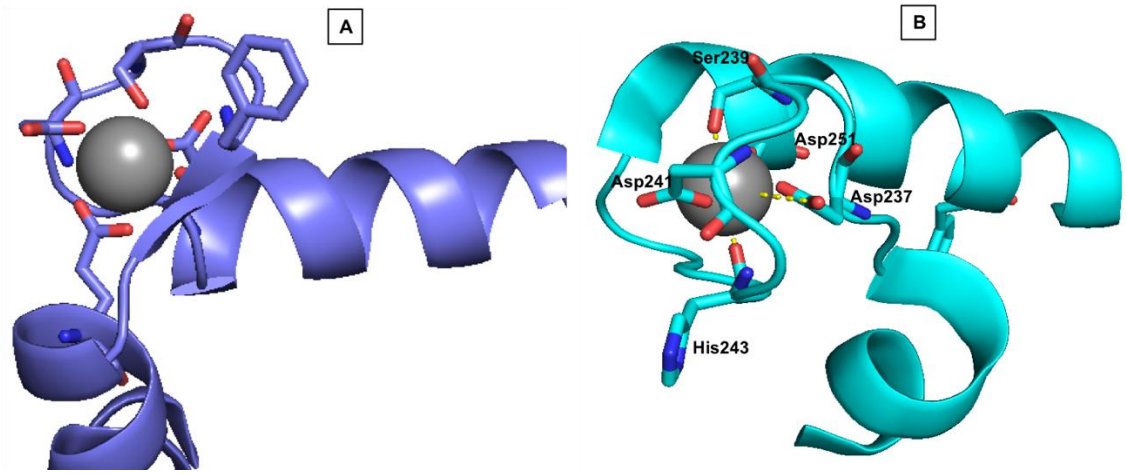

Figure 1-21: *Cartoon representations of* ***A)*** *the EF-hand in carp parvalbumin with the helices perpendicular and interconnected through the calcium binding loop (PDB code 5CPV).*[104] ***B)*** *the EF-hand in Slt35 from E. coli. Binding residues are labelled and* Ca^{+2} *is shown as a grey sphere.*

Despite the similarity between the metal ion-binding sites in Slt35 and the EF-hand calcium-binding sites, some differences have been noticed. **1)** EF-hands normally contain 12 residues while Slt35 has 15. **2)** The metal ion usually coordinates to seven oxygen ligands, whereas it was coordinated by only six in Slt35. **3)** The ligands adopt a distorted octahedral configuration around the metal ion in Slt35 instead of the typical pentagonal bipyramid as normal in EF-hands.[98] Although the function of the EF-hand is not clear in Slt35, its thermostability is significantly increased in the presence of Ca^{+2} ion compared with Na^{+} ion.[115]

To investigate the contributions of other amino acid residues located in the active site to the catalytic mechanism of this enzyme, it has been crystallised in complex with three different ligands (Figure 1-22): two PG fragments (murodipeptides) and bulgecin A. The murodipeptide A (murodipeptide NAG-NAM-L-Ala-D-Glu) binds at subsites -2 and -1 with its NAG and NAM residues respectively, whereas murodipeptide B (disaccharide $(NAG)_2$) interacts at subsites +1 and +2. Bulgecin A bound at the -2 subsite with its NAG residue while the hydroxyproline unit interacted with active site at subsite -1. Accordingly, important interactions have been observed, which revealed that in addition to the known catalytic residue Glu162, Ser216 and Asn339 may play an important role in the catalytic mechanism (Figure 1-22A).[116] The catalytic residue Glu162 has been confirmed as an important amino acid in the enzyme mechanism through its replacement by Ala and/or Asp, which resulted in inactive enzyme.[117] Additionally, it has been reported that two Arg residues (Arg187 and Arg188) located in the active site play an important role in the enzyme activity. This result was supported by mutation of these residues by Ala and Glu100 by Ala as well. Following this, the activity of these variants was

tested and indicated that the double replacement of Arg187 and Arg188 resulted in completely inactive enzyme, whereas the Glu100Ala variant did not show any effect on the activity (Figure 1-22B). The lytic activity of this enzyme requires the peptide side chain be attached to PG, as shown by kinetic studies of MltB from *E. coli.*[118,119]

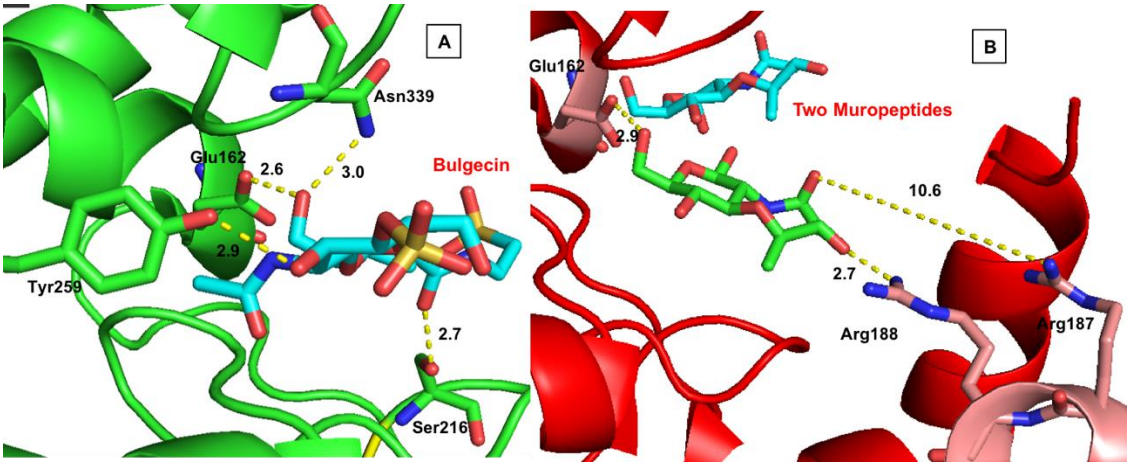

Figure 1-22: *Cartoon representations of Slt35-substrate complexes.* ***A)*** *The Slt35-bulgecin complex, showing the interactions of the bulgecin with Glu162, Asn339, Tyr259 and Ser216 in the active site.* ***B)*** *The Slt35-murodipeptide complex showing the interactions with Glu162, Arg187 and Arg188 in the catalytic domain.*

Implications of LTs in pathobiology

The widely used β-lactam antibiotics are analogues of the terminal D-alanyl-D-alanine of the stem peptide in PG in the bacterial cell wall. They inhibit PG biosynthesis by attachment to the most important enzymes (PBPs), specifically transpeptidases (TP),[120] that are responsible for cross-link synthesis.[121] The general mechanism of action of β-lactam antibiotics is binding to the catalytic serine residue in the TP causing inhibition of these enzymes, thereby leading to murein degradation and then cell death. Unfortunately, bacteria have found different mechanisms to resist this class of antibiotics by mutations to the active site of PBPs to prevent its binding to the drug, modification of the cell wall in order to prevent drug insertion, or by producing enzymes known as β-lactamases, which hydrolyse the β-lactam four-membered ring resulting in inactive drugs. After the lactamase was induced by resistant bacteria, it enters the periplasmic space to attack the β-lactam antibiotics before they can bind to their target PBPs in the cytoplasmic membrane.[27]

The expression of β-lactamases is linked to LTs activity as they produce anhydromuropeptides during PG recycling (Figure 1-23).[37] After these PG-recycling metabolites are transported into the cytoplasm through the AmpG permease, they are cleaved by NagZ followed by binding to the transcriptional activator AmpR to induce AmpC β-lactamases. When AmpD (*N*-acetyl-

muramyl-L-alanine amidase) is active, the peptide stem is removed, preventing the transcription of the *ampC* gene, instead leading to recycling of the anhydromuropeptides.[122] The recycling products are *N*-acetylglucosamine (NAG), anhydro-*N*-acetylmuramic acid (anhNAM), D-alanine, and the murein tripeptide. Following this, the resulting murein tripeptide is ligated to UDP-*N*-acetylmuramic acid by murein peptide ligase (MpI) to return to the biosynthetic pathway for the murein synthesis.[123] It has been observed that the overproduction of MltB increased the induction of β-lactamases, whereas inhibition of Slt70 by bulgecin restrained *ampC* expression. Therefore, the potency of penicillins and cephalosporins can be enhanced by combining them with specific LTs inhibitors.[124]

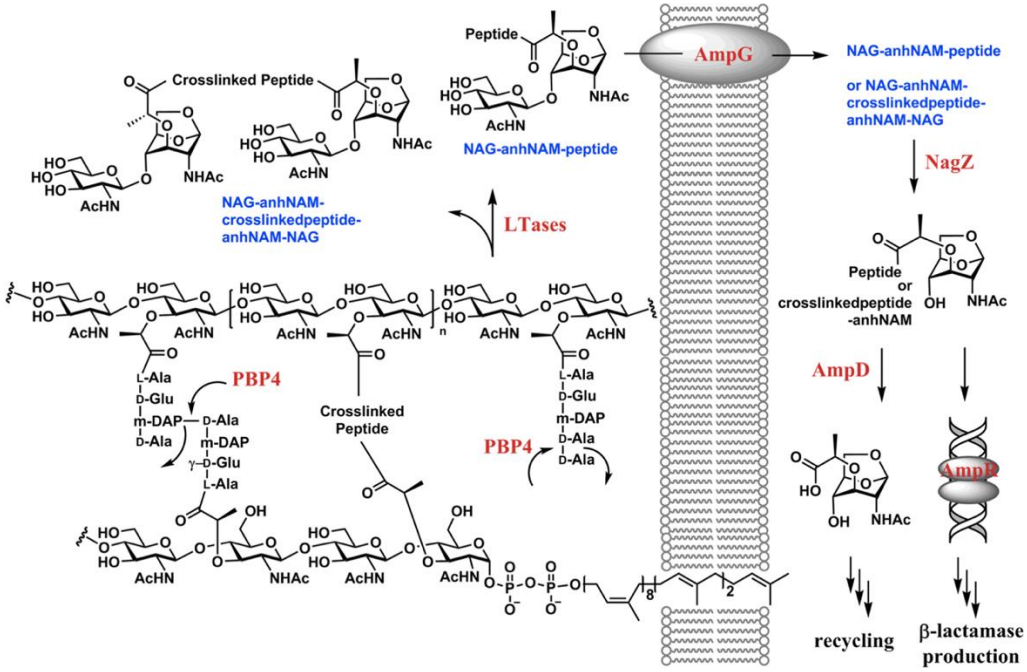

Figure 1-23: *Degradation events of the cell wall in Gram-negative bacteria. The initial step is catalysed by LTs in the periplasmic space, followed by the insertion of the degraded fragment into the cytoplasm to start the degradation by NagZ. The final product contributes to β-lactamase induction.*[37]

The over-dependence on β-lactams as antibacterial agents led to the rise of drug resistant strains. Therefore, LTs are suitable targets for structure-based design of novel antibiotics are LTs, due to their unique function within the bacterial cell wall and their contributions to β-lactamase induction.

Lytic transglycosylases inhibition

Lytic transglycosylases are of pharmaceutical interest, providing an attractive target for structure-based design of novel antibiotics. Despite the lack of the inhibitors for LTs, some efforts have been directed towards the discovery of effective inhibitors against these enzymes. The most common compounds used to inhibit LTs are the naturally occurring glycopeptides (bulgecins A-C) **(15a-c)** produced in *Pseudomonas acidophilia* (recently reassigned as *Paraburkholderia acidophila*) (Figure 1-24)[125,126] and *Pseudomonas mesoacidophila*. Bulgecin has been used in combination with β-lactams as a strategy to improve the efficacy of these antibiotics against resistant bacteria by forming bulges.[127-129] Indeed, the susceptibility of different species (*H. pylori, E. coli, P. aeruginosa, A. baumannii,* and recently *N. meningitidis* and *N. gonorrhoeae*) to β-lactams has been enhanced by this strategy.[130] A β-hexosaminidase inhibitor, NAG-thiazoline **(16)**, a structural analogue of a proposed intermediate in the LT catalytic mechanism, was also used to inhibit MltB activity.[117] Despite the weak affinity of NAG-thiazoline toward MltB, it caused changes in the cellular morphology and cell surface in the growing cells of *E. coli.*[131] Clarke *et al*. reported inhibition of MltB from *P. aeruginosa* by proteinaceous, vertebrate lysozyme inhibitor Ivy (Ivyp1 and Ivyp2). These proteins were suggested to regulate the autolytic activity of LTs in Gram-negative bacteria that are unable to *O*-acetylate their PG. However, no crystal structure has been reported to analyse the interactions between these inhibitors and MltB that cause the reduction in the enzyme activity on the peptidoglycan substrate of *M. luteus.*[132]

Mobashery *et al.*[133] synthesized four piperidine iminosaccharide derivatives **(17a-d)** as oxocarbenium-mimicking inhibitors for NagZ in *P. aeruginosa* and MltB (Slt35) in *E. coli.* The ability of these compounds to bind MltB was evaluated by using the intrinsic fluorescence of tryptophan and/or tyrosine. However, the affinity of these sugars toward MltB was weak.

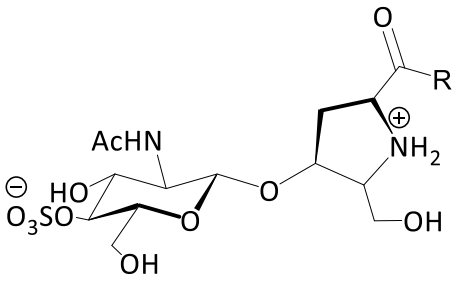

Bulgecin A-C 15 a-c

Bulgecin A: R= $NHCH_2CH_2SO_3^{\ominus}$

Bulgecin B: R= $NHCH_2CH_2COO^{\ominus}$

Bulgecin C: R= OH

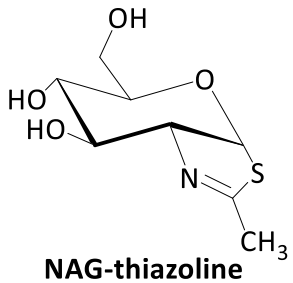

NAG-thiazoline 16

K_d = 1.36 ± 0.077 mM

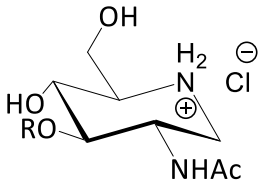

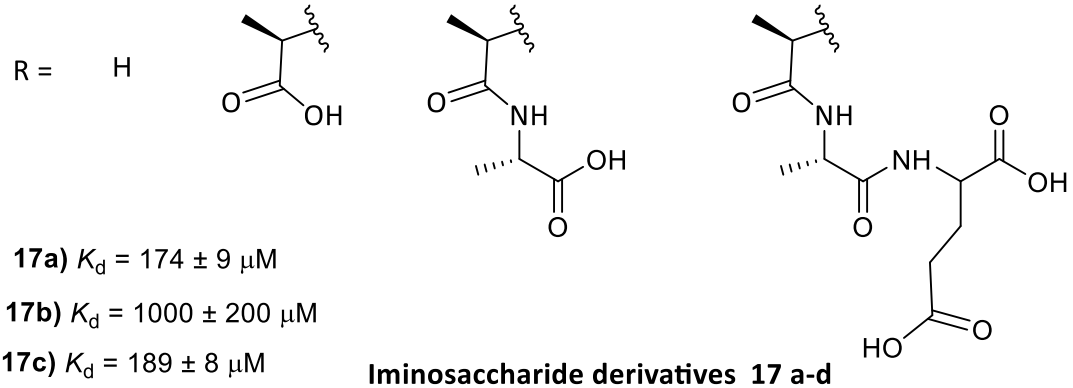

17a) K_d = 174 ± 9 μM

17b) K_d = 1000 ± 200 μM

17c) K_d = 189 ± 8 μM

17d) K_d = 1010 ± 20 μM

Iminosaccharide derivatives 17 a-d

Figure 1-24: *Some known inhibitors for Slt35.*

Inhibiting the autolytic LTs represents a promising area of research for the development of novel therapeutics.

1.5 Aim of work

The spread of antibiotic-resistant bacterial pathogens has increased the focus towards finding potential novel antibiotic targets. The key point of searching for new antibiotic targets is the cell wall due to its unique chemical structure and metabolism. Different antibiotics target enzymes that act on various stages of PG metabolism: for example, fosfomycin targets PG synthetase, β-lactams prevent glycan cross-linking and both moenomycin and vancomycin inhibit transglycosylase. LTs are assumed to be a promising target as they are critical to the bacterial cell growth, division by facilitating the insertion of protein complex and PG precursors as well as PG remodeling.

The aim of this work was to find suitable inhibitors for the soluble lytic transglycosylase (Slt35) because it has been successfully overexpressed and purified. Our strategy was first to make the known inhibitor (NAG-thiazoline) and study its interactions with the enzyme via crystallography, and to develop this compound. The second plan was to design new compounds and study their interactions with the enzyme by molecular docking. The most promising leads would then be synthesized and tested for Slt35 inhibition. Due to the lack of LT inhibitors, the initial design of new inhibitors was based on mimicking the oxocarbenium ion intermediate in the enzyme catalytic mechanism. The most active compounds that mimic this intermediate and that have been successfully synthesised before are the amidine derivatives which have been used as inhibitors of glycosidases.

2 Design and synthesis of potential lytic transglycosylase inhibitors

2.1 Introduction

As discussed in chapter 1, the emergence of bacterial resistance to most antibiotics has led to great concern regarding the treatment of bacterial infections, thus the generation of new antibiotics has become essential. Lytic transglycosylases present an attractive new target for development of broad-spectrum antibiotics due to their important role in bacterial processes including cell growth and division.[134] Bulgecin, an *O*-sulfated glycopeptide, was used as an inhibitor for all lytic transglycosylases.[129] A structural analogue of the oxazolinium intermediate of the LT catalytic reaction **(18)**, the β-hexosaminidase inhibitor NAG-thiazoline **(16)** [135-141] (Figure 2-1), was used to inhibit Slt35. However, it has low affinity for this enzyme.[117, 131]

Figure 2-1: *Structure of the proposed oxazoline reaction intermediate of LTs* ***(18)*** *and NAG-thiazoline* ***(16)****.*

Amidine analogues of D-glucose (sp^2-based structures) adopt a half-chair conformation that resembles a putative transition state for the LT-catalysed reaction[142] (Figure 2-2). These compounds were found to be strong inhibitors of β-glycosidase activity. Mobashery et al., reported a series of piperidine iminosaccharides and evaluated them against Slt35 as mentioned early in this thesis (Chapter 1, Section 1.4.3).

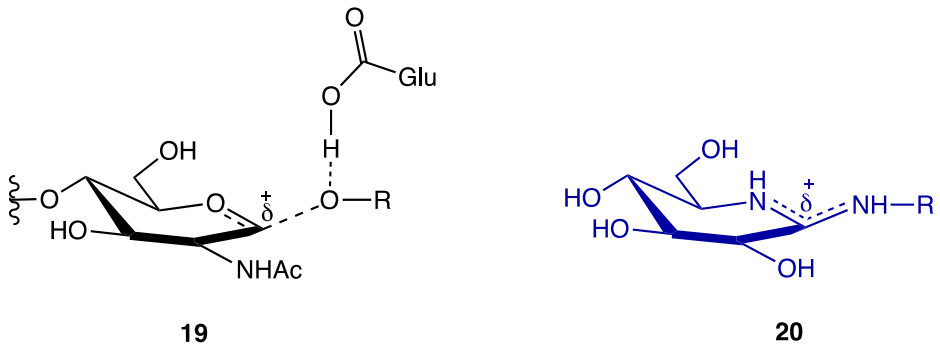

Figure 2-2: (19)*; Transition state of the acetal cleavage step of the LT catalysed reaction.* ***(20)****; Conformation of amidine.*

Generally, amidines **(21a,b)** are nitrogen analogues of carboxylic acids and esters **(22)**. Their properties are a combination of an azomethine-like C=N double bond and an amide-like C-N single bond with partial double bond character (Figure 2-3).[143] The amidinium group (N-C-N) could be included in cyclic or acyclic systems. They are strong bases (conjugate acid pK_a ~12). Their basicity is measured by their pK_a values, which depends on the type of substitution at the amino and imino nitrogen. The basicity of amidines is stronger than the corresponding amines but it is less than guanidines.[144]

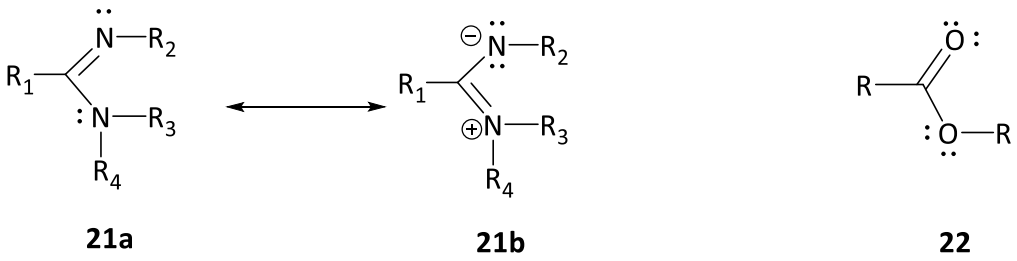

Figure 2-3: *General structure of amidine group.*

In acidic medium, the imino nitrogen becomes protonated, affording a symmetrical amidinium ion which is stabilised by resonance like the isoelectronic carboxylate ion (Figure 2-4).

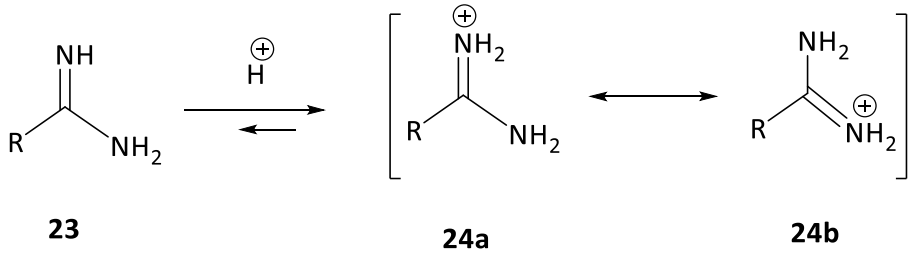

Figure 2-4: *The resonance structures of amidine in acidic medium.*

2.1.1 Literature syntheses of sugar-based amidine derivatives

Ganem *et al*. reported the first synthesis of amidine analogues of D-glucose[142,145] starting from nojirimycin bisulfite adduct **(25)** (Scheme 2-1). The first step was basic hydrolysis of nojirimycin bisulfite to produce nojirimycin **(26)** which was then oxidized to lactam **(27)** by treatment with iodine and potassium iodide in sodium hydroxide. The next step was protection as the corresponding O-trimethylsilyl derivative **(28)** by using trimethylsilylchloride, followed by treatment with Lawesson's reagent to produce thionolactam **(29)**. The protecting groups were hydrolysed during the reaction. The thionolactam was then reacted with different amines to afford the desired amidine derivatives **(30)**.

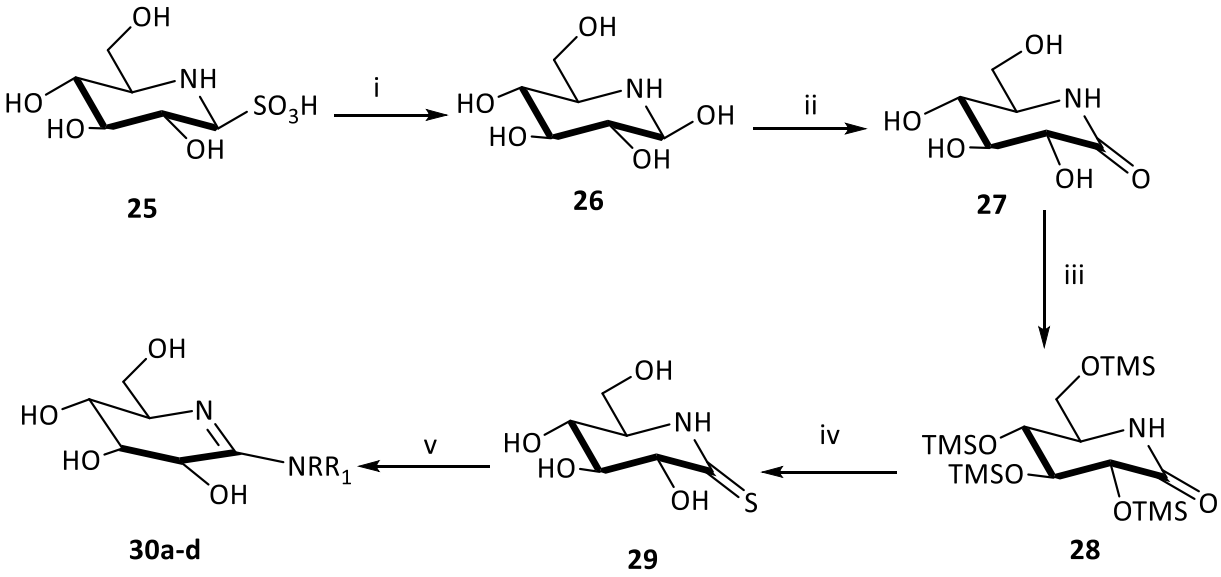

30a); R= R_1= H, **30b)**; R=R_1= Me,
30c); R= H, R_1= NH_2, **30d)**; R= H, R_1= OH

Scheme 2-1: *Synthetic route to the first glucoamidine derivatives. (i) Dowex 1X2-200 resin (OH^-). (ii) I_2/KI, NaOH. (iii) TMSCl/$(TMS)_2$NH, dry pyridine. (iv) Lawesson's reagent, benzene. (v) RRNH, MeOH.*

More recently, commercially available gluconolactone **(31)** has been used as starting material for amidine synthesis (Scheme 2-2).[146-150] After four steps, the fully benzylated lactam **(32)** was prepared, which was treated with Lawesson's reagent to produce glucothionolactam **(33)**. The next step was activation of the thionolactam by triethyloxonium tetrafluoroborate (Meerwein's reagent) followed by reaction with different amines giving benzylated glucoamidine derivatives **(34)**. The protecting groups were removed by hydrogenation.

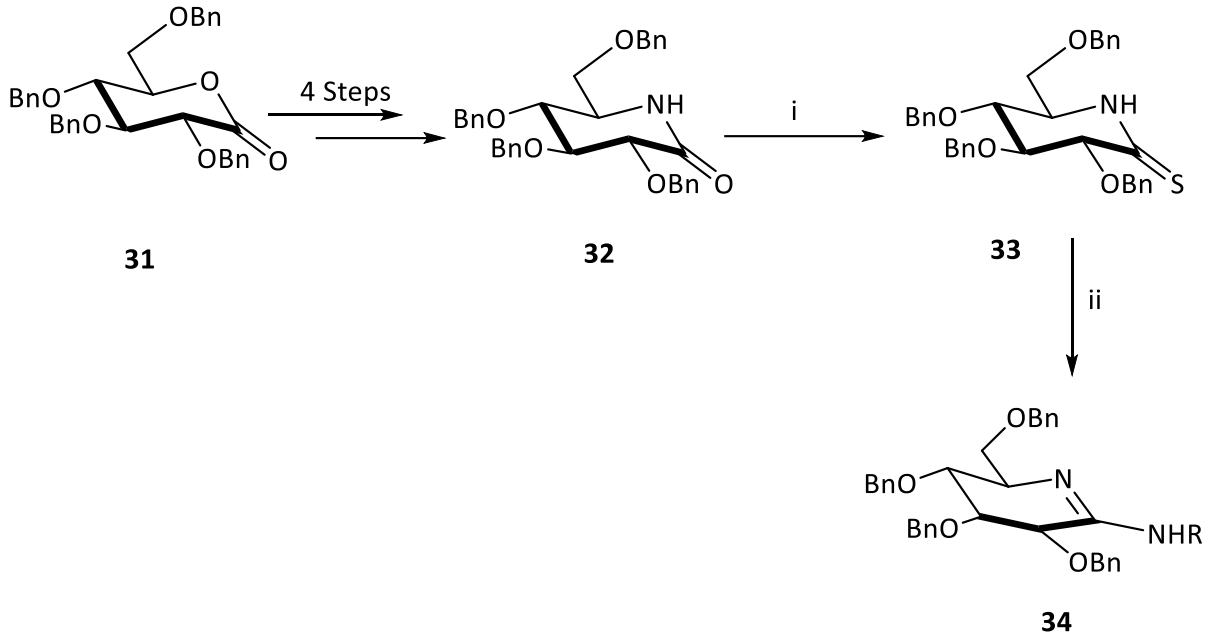

Scheme 2-2: *Synthesis of glucoamidine derivatives from benzylated gluconolactone. (i) Lawesson's reagent, benzene. (ii)* $Et_3O^+BF_4^-$, CH_2Cl_2, 0 °C, 2 h; RNH_2, *ambient temperature, 36 h.*

2.2 Design of potential inhibitors

In this study, the first target was synthesis of NAG-thiazoline **(16)**. The second target was producing a series of different sugar based amidine derivatives (Figure 2-5) based on the structure of the transition state of enzyme mechanism (Figure 2-2).

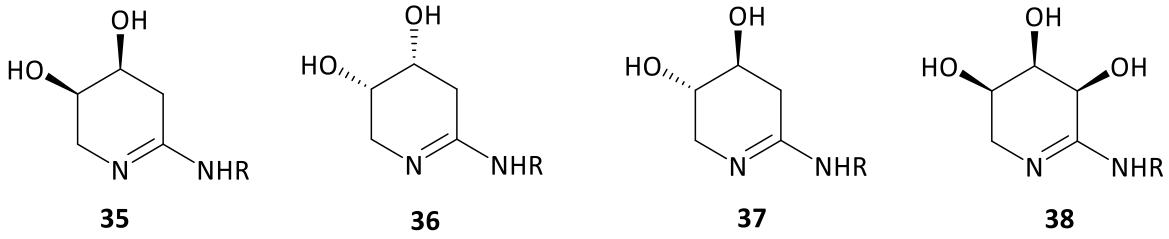

Figure 2-5: *Structures of amidine target compounds.*

Once prepared, they would be tested as inhibitors of the soluble fragment of membrane-bound lytic transglycosylase Slt35.

2.2.1 Design of amidine-based inhibitors

Different amidine analogues were designed in order to mimic the flattened conformation of the transition state of the acetal cleavage step of the LT catalysed reaction (Figure 2-6). The design was based on a six membered cyclic amidine that contains hydroxyl groups attached

to the ring (Figure 2.6). Different groups were selected to be attached to the amidinium group for instance: hydroxyl group **(35a)** linear alkyl **(35b)**, cyclic alkyl **(35c)**, and aromatic ring **(35d** and **35e)**. These were chosen to present different functional groups. After these compounds were designed, they were docked with Slt35.

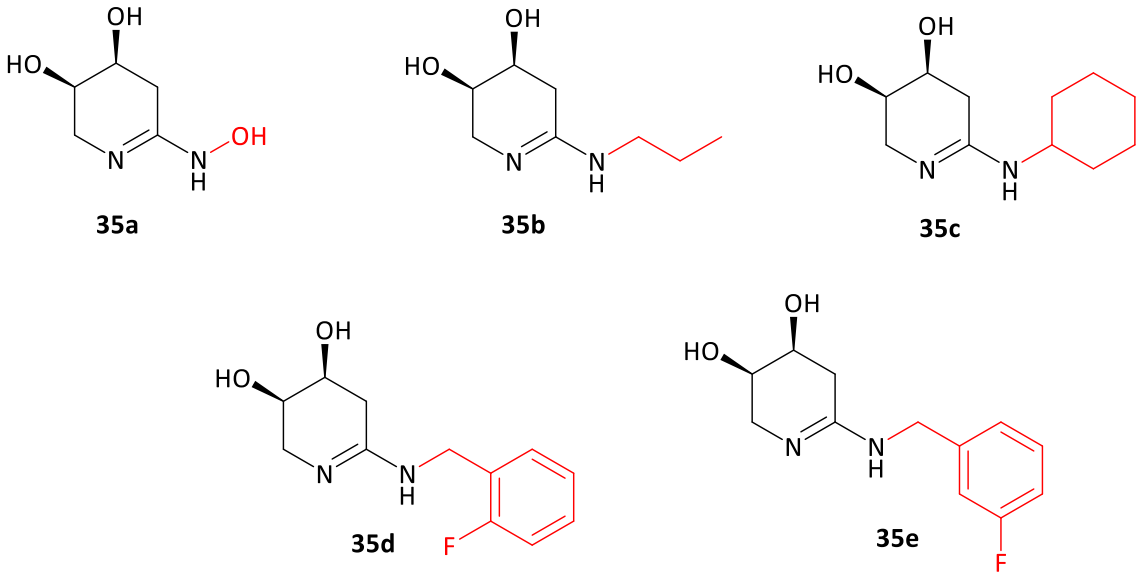

Figure 2-6: *Structure of selected designed amidine-based inhibitors.*

2.2.2 Molecular docking of amidine-based potential inhibitors.

Molecular docking is a computational method used to predict the binding mode of two molecules. It is frequently used for determination of binding mode and affinities in biology and pharmaceutics such as drug design.[151] Different software is used in docking purposes for instance MolDock, Gold, Maestro, Pymol and BUDE. Docking in this study was performed by our collaborator (Richard Session) using BUDE. Eight amidine analogues have been designed and docked to analyse their binding mode with Slt35 (PDB 1D0L).[116] Before the synthesis of amidines was conducted, structures of five different amidine derivatives **(35a-e)** derived from 2-deoxy-D-ribose were designed and then docked. All designed compounds were predicted to exhibit interactions with the catalytic residue Glu162 in the active site of the enzyme before docking was run because they mimic the transition state of the LTs enzymatic reaction (Figure 2-2). According to the computational modelling results (Figure 2-7), there are interactions between Glu162 and the amidinium group in all these inhibitors with predicted distance in the range 1.9 to 2.9 Å except compound **35d**, which lacks any interaction to Glu162 but binds to Ser230 through a hydroxyl group on the amidine six-membered ring and other interaction

between fluoride and Asn339 residue. Modelling results in the first generation set predicted that compound **35b** has two salt bridge interactions with Glu162 through the positive charge in the two nitrogen atoms of the amidinium group (Figure 2-7A) and hydrogen bonds between 4-OH and Ser230 whereas compound **35a** bound to the catalytic residue by hydrogen bonds via the hydroxyl group attached to the amidinium group, but there was no interaction to the amidinium group itself (Figure 2-7G). Interestingly, compound **35e** interacted with Asn339 through its fluorine atom on position 3' (Figure 2-7H), which might support the interactions with HO- on Tyr259 and Ser230 via two hydroxyl groups in the amidine six-membered ring as well as the interaction with the amidinium group. The fluorine on position 2' in compound **35d** did not show any interaction and the molecule interacted just with Ser230 (Figure 2-7E). However, compound **35c** showed one salt bridge interaction with the amidinium group. Hydrophobic interactions are also presented in the docking models: Ala220 residue is predicted to interact with the side chain through the methyl group in (**35b-e)** whereas **35a** did not show any interaction. More hydrophobic interactions were observed in compound **35b**, **35c** and **35e** between methylene groups in the amidine six-membered ring and Tyr259, Tyr338, Asn339, and Phe226 residues, and compound **35d** has the same interactions except Phe226. In contrast, in compound **35a** these hydrophobic interactions were with Tyr259 and possibly Phe226.

A second set of three enantiomers that have pseudo axial hydroxyl groups on the amidine six-membered ring **(36a-c)** were designed and then docked. Unfortunately, the conformations of these compounds in the enzyme active site were changed and there was no interaction with the amino acid residues except weak salt bridge interaction in case of compound **36a** (Figures 2-7B, 2-7D and 2-7F).

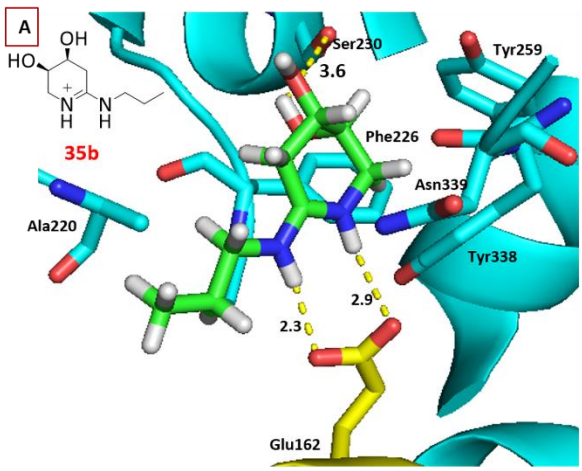
A
35b
Ser230
3.6
Tyr259
Phe226
Asn339
Ala220
Tyr338
2.9
2.3
Glu162

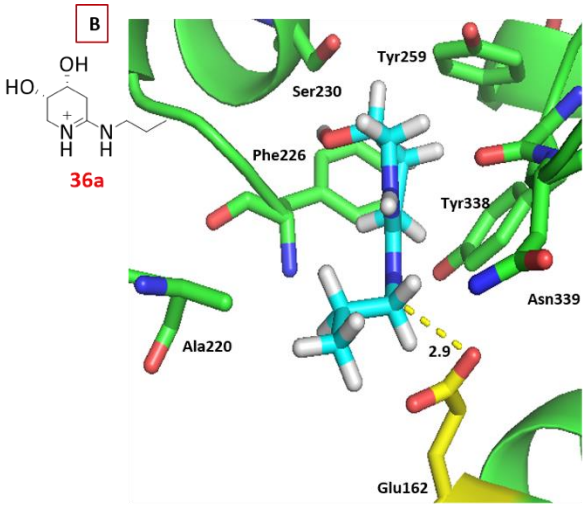
B
36a
Tyr259
Ser230
Phe226
Tyr338
Asn339
Ala220
2.9
Glu162

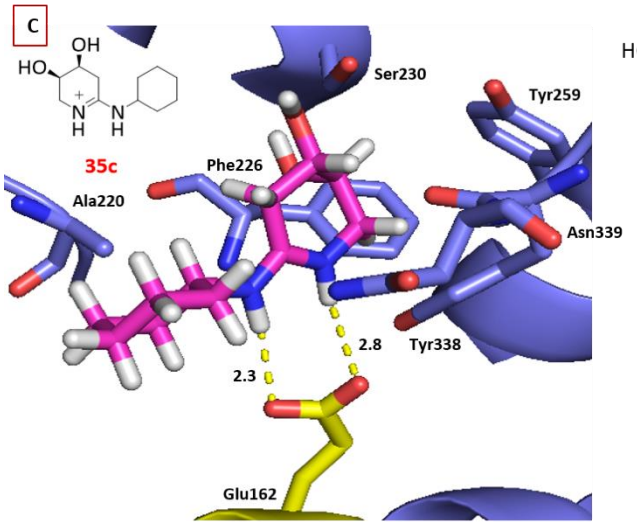
C
35c
Ser230
Tyr259
Phe226
Ala220
Asn339
2.8
Tyr338
2.3
Glu162

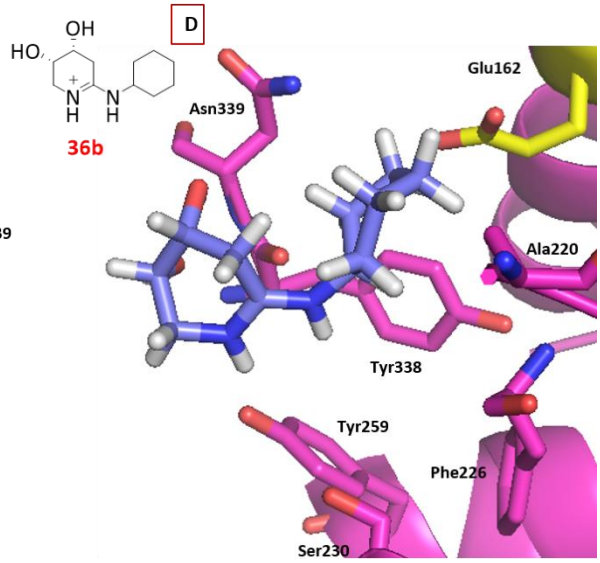
D
36b
Glu162
Asn339
Ala220
Tyr338
Tyr259
Phe226
Ser230

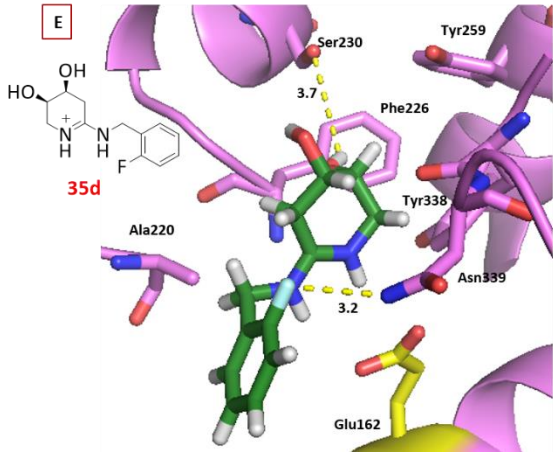
E
35d
Ser230
Tyr259
3.7
Phe226
Tyr338
Ala220
Asn339
3.2
Glu162

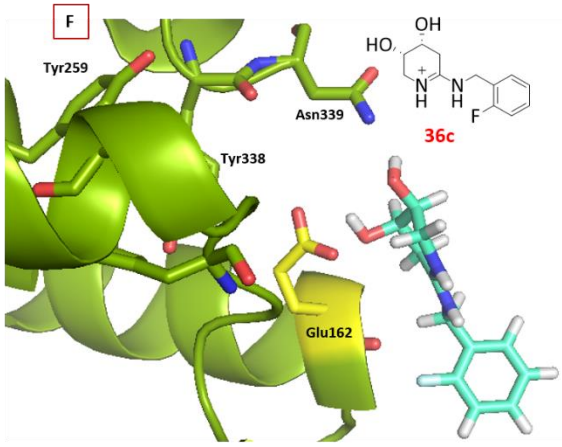
F
Tyr259
Asn339
36c
Tyr338
Glu162

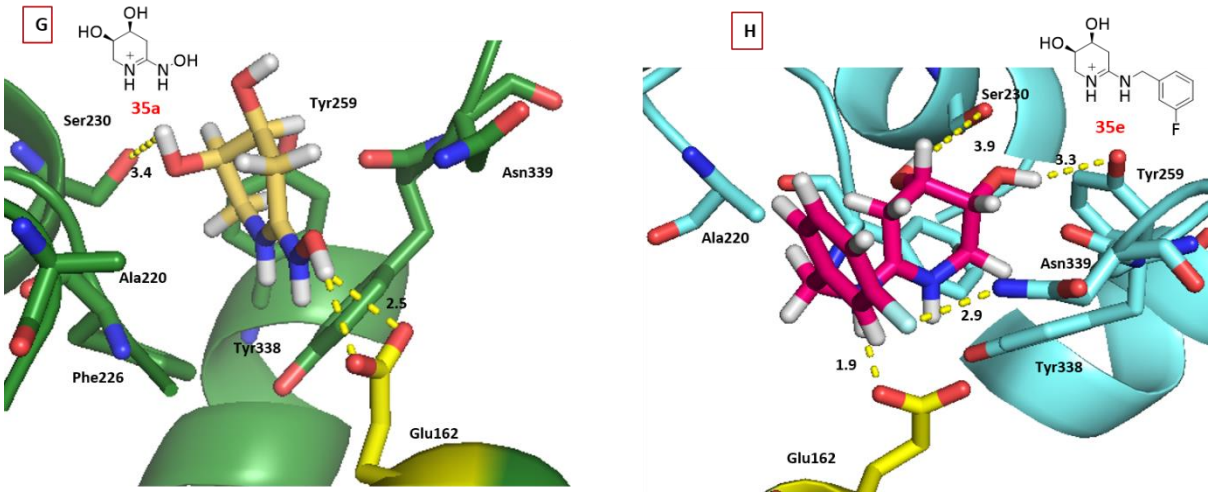

Figure 2-7: *Binding site of Slt35 (PDB 1D0L) showing docked ligands (electrostatic surface view)**. (A) 35b, (B) 36a, (C) 35c, (D) 36b, (E) 35d, (F) 36c, (G) 35a and (H) 35e**. Atom colours of amino acid residues and inhibitors in all figures as follows: blue-nitrogen, red-oxygen and white-hydrogen. Carbon back bone of amino acids residues and inhibitors has different colours as shown in figures. The predicted salt bridge and hydrogen bonds interactions are shown as yellow dashes with distances in Å.*

The retrosynthetic analysis of the amidine target molecules was based on the reaction of lactams as key intermediates (Scheme 2-3). Disconnection of the amidine **(35** or **36)** suggested dihydroxylactam (**39** or **42**) as an intermediate, the synthesis of which has been reported by Scarpi *et al*.[152] It can be further disconnected to azidolactone **(40** or **43)**, which is itself obtained from 2-deoxy-D-ribose or 2-deoxy-L-ribose **(41** or **44)**. The azide can be synthesised from 2-deoxyribose **(41** or **44)** through three steps: sugar oxidation, tosylation[153-157] and then reaction with sodium azide, activating the primary hydroxyl group to a good leaving group, followed by replacement by the azide group. Conversion of the azide to the lactam requires reduction of the azide group to an amino group, which then can attack at the carbonyl lactone leading to C-O bond breakage accompanied by ring expansion.[157-160] Finally, the lactam intermediate can be transformed into amidine as reported in literature[146-149] by conversion of the amide carbonyl to a thioamide, which then can be replaced by an amine group after activation to a thioester. Therefore, despite most previous synthesis of amidine sugar-based structures starting from hexoses, synthesis in this study started from pentoses.

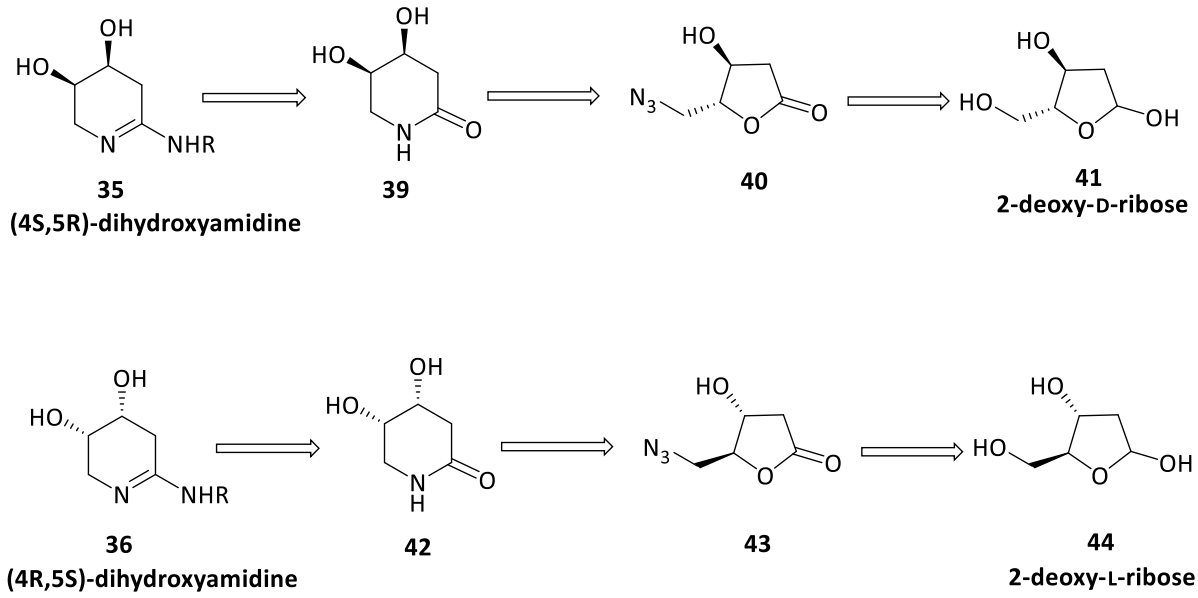

Scheme 2-3: *Retrosynthetic analysis of dihydroxyamidine derivatives.*

Trihydroxylactam **(38)** can be prepared using the same route (Scheme 2-4) but an extra step is required which is a protection of secondary hydroxyl groups before the tosylation can be done. Other protection steps might be needed to transform the trihydroxylactam into amidine.

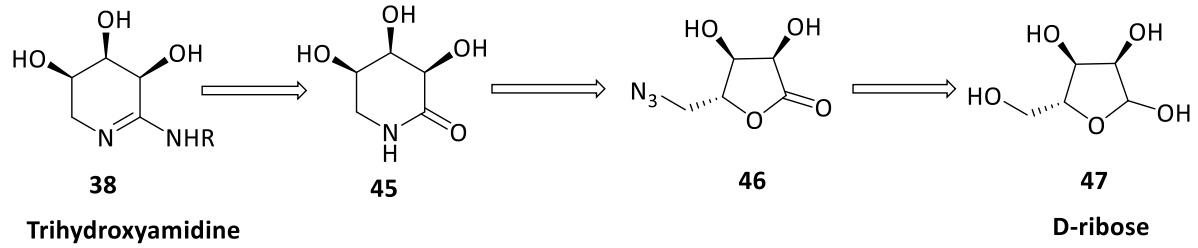

Scheme 2-4: *Retrosynthetic analysis of trihydroxyamidine derivatives.*

The possible route to prepare amidine **(37)** was by stereoinversion of secondary hydroxyl group in azide **(40)** by activation of secondary hydroxyl group followed by nucleophilic displacement (Scheme 2-5).

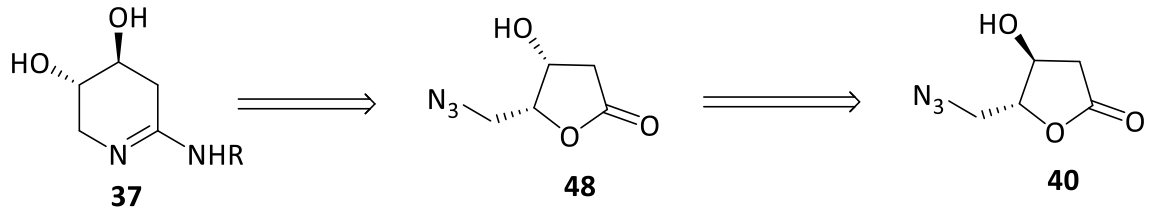

Scheme 2-5: *Retrosynthetic analysis of (4R,5R)-dihydroxyamidine derivatives.*

2.3 Synthesis of potential inhibitors

The first synthesis conducted in this study was that of NAG-thiazoline **(16)**, following the literature methodology.[138] Next was the synthesis of designed amidine inhibitors after their docking studies were completed. Preparation of lactam was the first route in this synthesis following the previously reported procedure.[152] Once the lactam was prepared, transformation to amidine could be done using reported glucoamidine methods.[146-149]

2.3.1 Synthesis of NAG-thiazoline

Three steps were performed as previously reported by Knapp *et al.*[138] in order to synthesise NAG-thiazoline (Scheme 2-6). In the first step, all hydroxyl groups in *N*-acetylglucosamine **(49)** were protected. This method was described by Horton,[161] where the hydroxyl groups were protected by acetylation using acetic anhydride in pyridine to produce a fully acetylated glucosamine **(50)** as white crystals in 70% yield. In the second step, the product from the first step was reacted with Lawesson's reagent in order to form the thiazoline ring. The result was unexpected; instead of producing peracetylated NAG-thiazoline **(51)**, thioamide **(52)** was formed. The reaction was repeated four times using different conditions but at all times cyclisation was unsuccessful (Table 2-1).

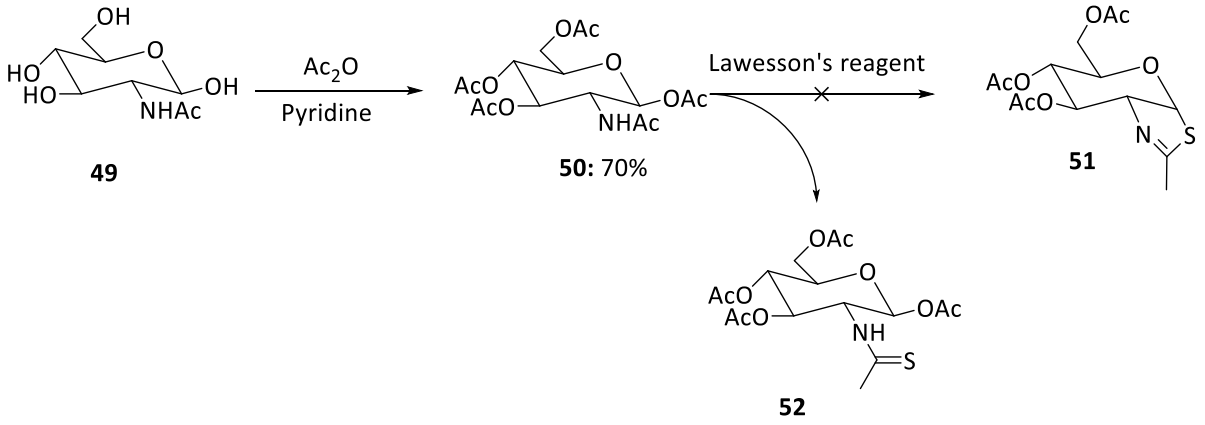

49 **50:** 70% **51** **52**

Scheme 2-6: *Schematic synthesis of NAG-thiazoline.*

Solvent	Temperature / °C	Time	Yield of **52** (%)
Dry toluene	80	1.5 h	61
Dry toluene	80	overnight	82
Dry pyridine	100	4 h	44
Dry THF	66	overnight	77

Table 2-1: *Different conditions of cyclisation reaction of compound* ***52.***

2.3.2 Synthesis of non-carbohydrate-based amidine potential inhibitors

The amidine formation methodology was tested on a non-carbohydrate based molecule. Treatment of commercially available lactam **(53)** with Lawesson's reagent in THF for 24 hours afforded thiolactam **(54)**. The resulting thiolactam was then activated with Merwein's salt as the thioethyl product followed by treatment with propylamine to produce amidine **(55)** in 87% yield (Scheme 2-7).

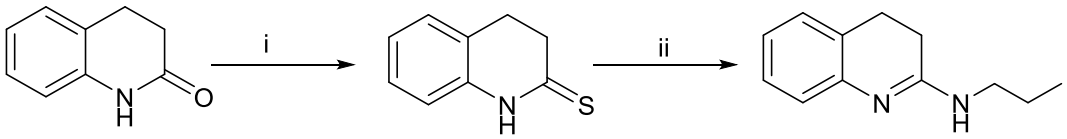

53 **54:** 91% **55:** 87%

Scheme 2-7: Synthesis of non-carbohydrate-based amidine. i- Lawesson's reagent, THF. ii- (1) $[C_2H_5]_3O^+BF_4^-$, DCM, (2) propylamine.

2.3.3 Synthesis of dihydroxy amidine derivatives

The first generation of amidine was dihydroxy amidine derivatives, which were prepared from 2-deoxy-D-ribose **(41)** (Scheme 2-8) using four synthetic steps to produce the corresponding lactams. These lactams were then protected followed by conversion to thiolactams. Alkylation of the sulfur atom in the thiolactam to the iminothioethyl ether was required as prior reaction before the reaction with amine. The acetonide lactam produced free-base amidines, while TBS-lactam gave amidine salts after deprotection step. The second generation of amidine inhibitors derived from 2-deoxy-L-ribose **(44)** were produced by the same route but only an acetonide protection group was used to protect the lactam intermediate.

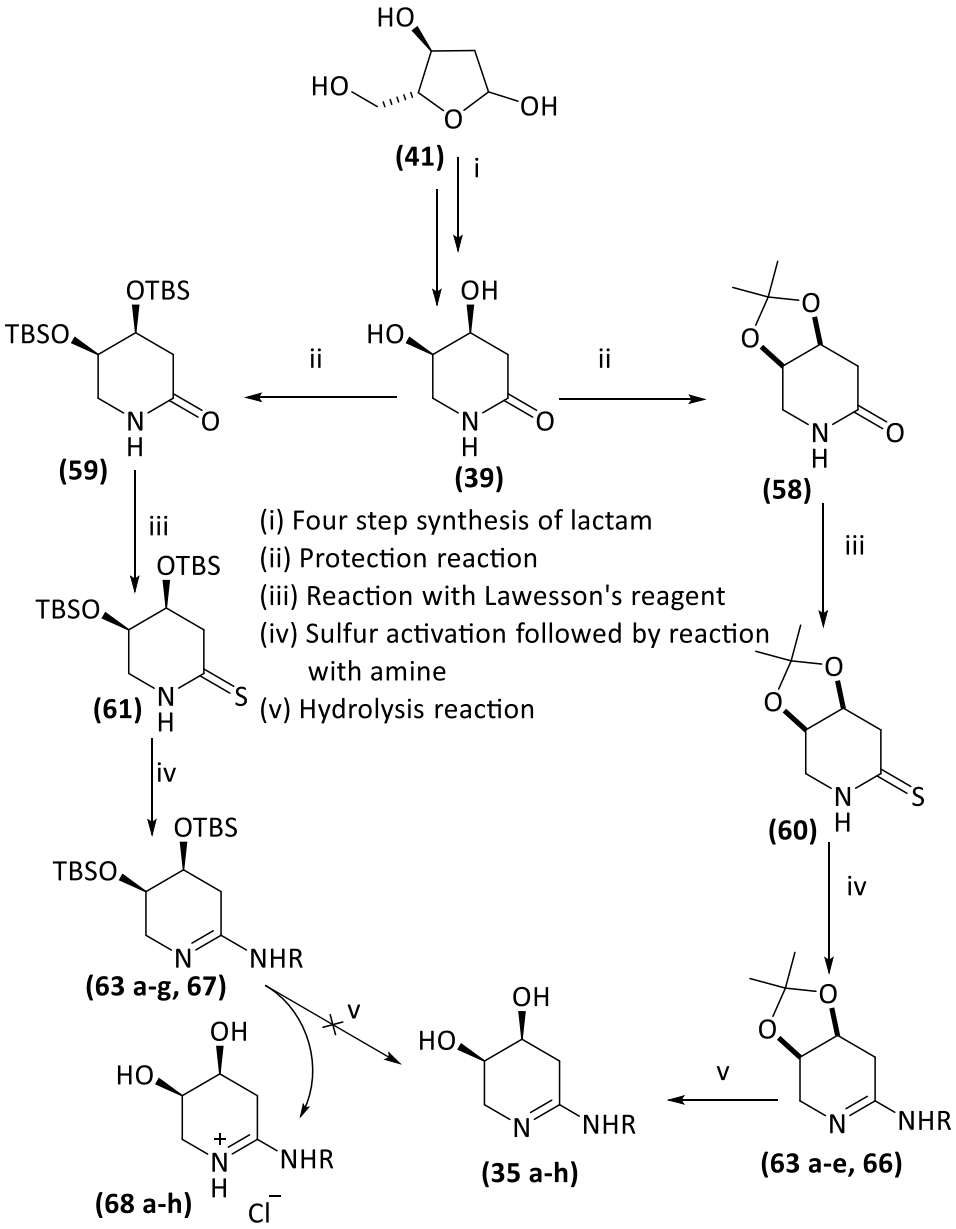

Scheme 2-8: *Synthetic route of dihydroxyamidine.*

The intermediate lactam can be obtained from the conversion of azide **(40)** via ring opening and closing.[157-160] The azide can be synthesised from 2-deoxy-D-ribose **(41)** through three steps: sugar oxidation, tosylation[153-156] and then reaction with sodium azide.

Synthesis of (4S,5R)-4,5-dihydroxy lactam

The procedures of Scarpi *et al*.[152] were applied with minor modifications, such as increasing reaction time (Scheme 2-9). 2-Deoxy-D-ribose **(41)** was treated with bromine in water for five days to produce lactone **(56)**. The primary hydroxyl group was activated as its p-toluenesulfonate (tosyl) ester **(57)** by treatment with tosyl chloride in pyridine and

transformed to the azide by treatment with sodium azide in acetonitrile to yield 5-azido-D-ribonolactone **(40)**. The azide product was then converted quantitively into lactam **(39)** by hydrogenation.

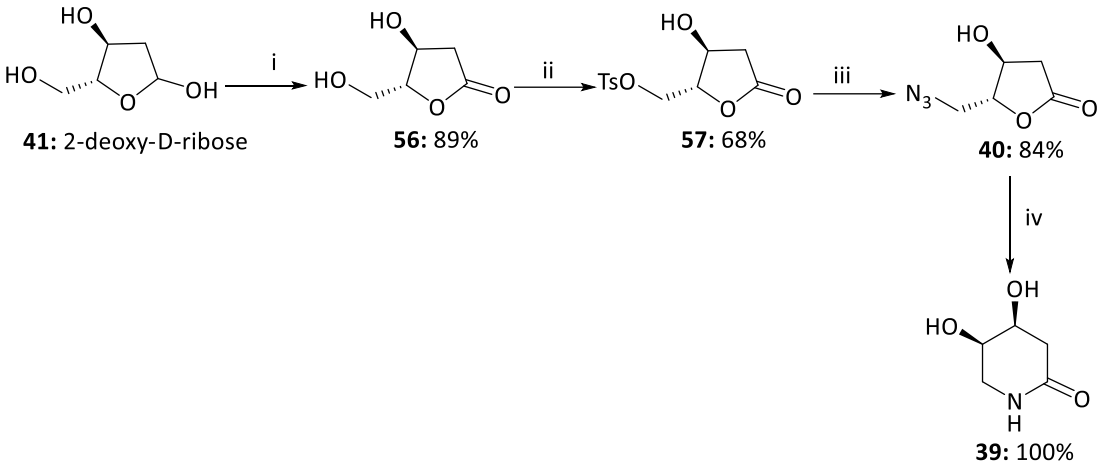

Scheme 2-9: *The synthetic route of (4S,5R)-dihydroxylactam. (i) Br_2/H_2O, r.t. (ii) tosyl chloride, pyridine. (iii) NaN_3, 15-crown-5, CH_3CN. (iv) $Pd(OH)_2$-C, MeOH, H_2.*

Protection of lactam

The two hydroxyl groups of the key lactam **(39)** were protected as the acetonide **(58)**[152,162,163] by treatment with 2,2-dimethoxypropane in dry methanol with a catalytic amount of p-toluenesulfonic acid. However, when this acetonide was used for the synthesis of the thiolactam and subsequently the amidine, some weaknesses were observed such as poor yields and difficulty in purification. Consequently, tert-butyldimethylsilyl chloride was used as protecting group[164-167] instead (Scheme 2-10), forming the protected lactam **(59)** in 62% yield.

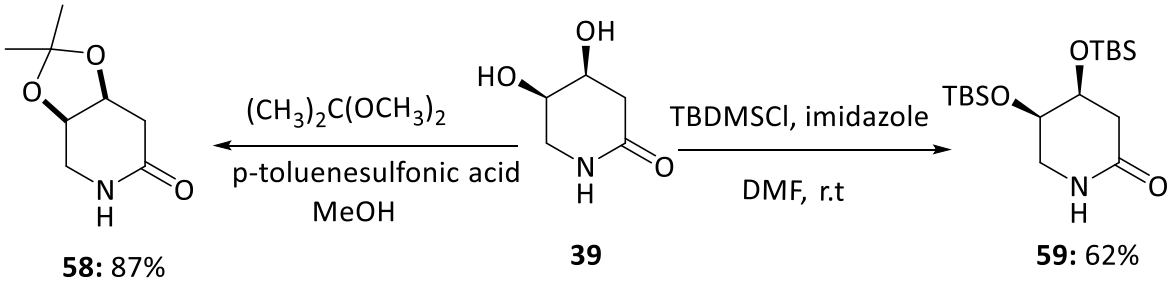

Scheme 2-10: *Protection reactions of (4S,5R)-dihydroxylactam.*

Conversion of lactam to thiolactam

The lactam carbonyl was activated as the thionolactam by using Lawesson's reagent[168-173] (Scheme 2-11). The yield of the product from protected lactam with TBDMS **(61)** was much higher than that from the acetonide lactam **(60)**.

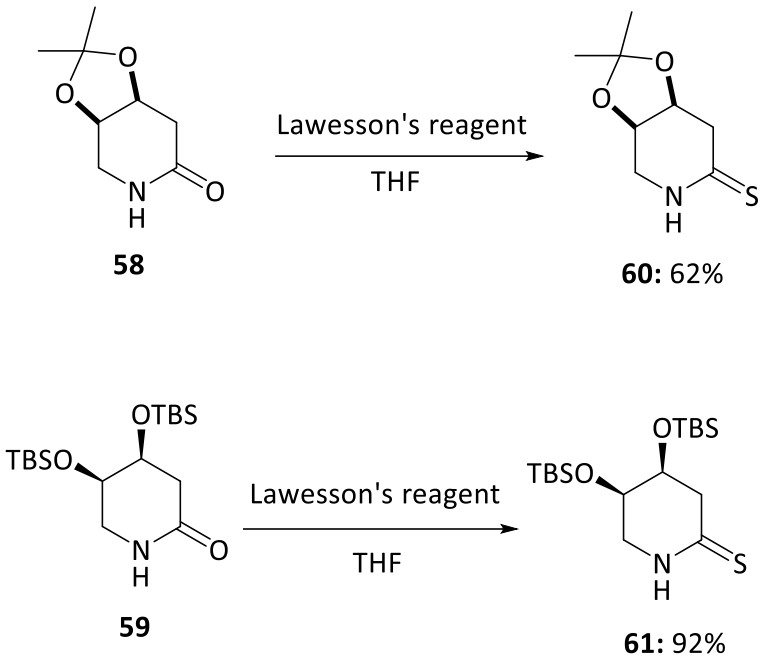

Scheme 2-11: *Conversion reaction of (4S,5R)-dihydroxylactam to (4S,5R)-dihydroxythionolactam..*

Amidine synthesis

Amidines were prepared over two steps starting with activation of the sulfur atom in thiolactam **(60** or **61)** by Meerwein's salt in cold dichloromethane as a solvent yielding the iminothioethyl ether **(62** or **64)** as an intermediate. The activated intermediate was not isolated from the solution and the next step was performed immediately in the reaction mixture without further purification. Different amines (namely, substituted benzylamines, aliphatic linear amines and aliphatic cyclic amines) were then added individually to the reaction mixture in different experiments to produce different protected amidine derivatives. Reaction of acetonide thiolactam with linear aliphatic amines including propylamine and hexylamine yielded the unprotected amidine **(35a** and **35f)**, whereas reaction of the same thiolactam with other amines produced protected amidines **(63 b-e)** (Scheme 2-12,Table 2-2).

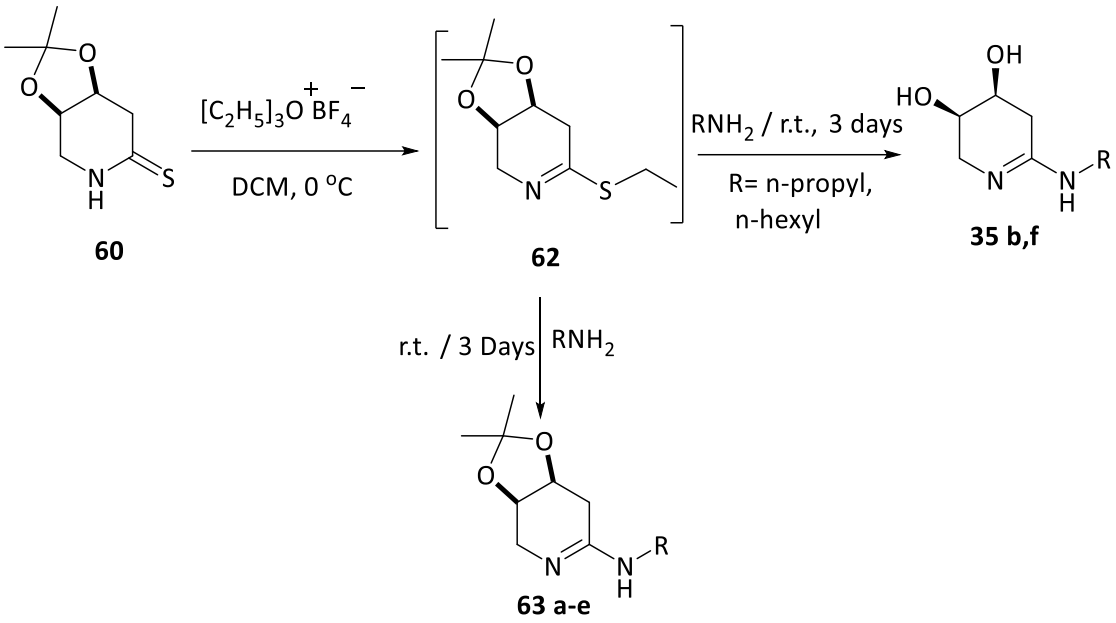

R= cyclohexyl, 2-fluorobenzyl, 3-fluorobenzyl, 2-hydroxybenzyl, morpholinoethyl

Scheme 2-12: *Synthesis of (4S,5R)-dihydroxyamidine.*

Comp. no.	R	%	Comp. no.	R	%
35b	$-CH_2CH_2CH_3$	68	**63c**	$3\text{-F-}CH_2C_6H_4$	15
35f	$-CH_2(CH_2)_4CH_3$	27	**63d**	$2\text{-OH-}CH_2C_6H_4$	30
63a	$-C_6H_{11}$	49	**63e**	$-(CH_2)_2N(CH_2)_4O$	25
63b	$2\text{-F-}CH_2C_6H_4$	49			

Table 2-2: *(4S,5R)-Dihydroxyamidine derivatives derived from acetonide intermediate.*

Activation of TBS-protected thiolactam **(61)** with Lawesson's reagent and subsequent reaction with different amines provided additional protected amidine derivatives **(65a-g)** (Scheme 2-13, Table 2-3).

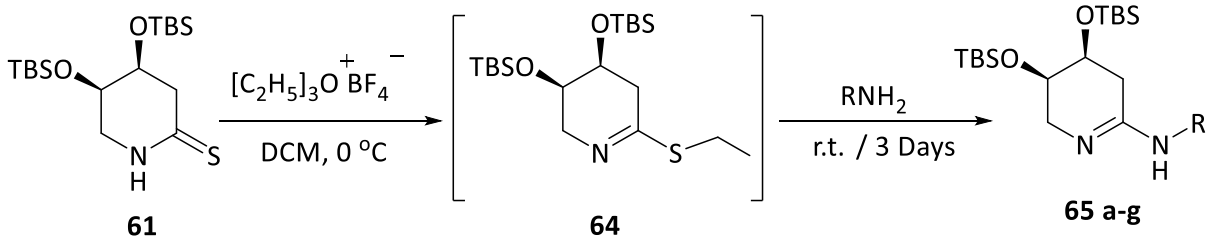

R= n-propyl, cyclohexyl, N-Boc-1,2-diaminoethan, 2-fluorobenzyl, 3-fluorobenzyl, morpholinoethyl, 2-piperazinoethyl, $(CH_2)CH(OTBS)CH_2(OTBS)$

Scheme 2-13: *Synthesis of (4S,5R)-dihydroxyamidine.*

Comp. no.	R	%	Comp. no.	R	%
65a	$-CH_2CH_2CH_3$	86	**65e**	$3\text{-F-}CH_2C_6H_4$	52
65b	$-C_6H_{11}$	93	**65f**	$-(CH_2)_2N(CH_2)_4O$	98
65c	$-CH_2CH_2NHBoc$	79	**65g**	$-(CH_2)_2N(CH_2)_4NH$	52
65d	$2\text{-F-}CH_2C_6H_4$	73	**65h**	$-CH_2CH(OTBS)CH_2(OTBS)$	23

Table 2-3: *(4S,5R)-Dihydroxyamidine derivatives derived from thionolactam protected by TBS group.*

Hydroximolactam was prepared from the reaction of acetonide thionolactam **(60)** with hydroxylamine in the presence of sodium bicarbonate and methanol as a solvent (Scheme 2-14).[174-176]

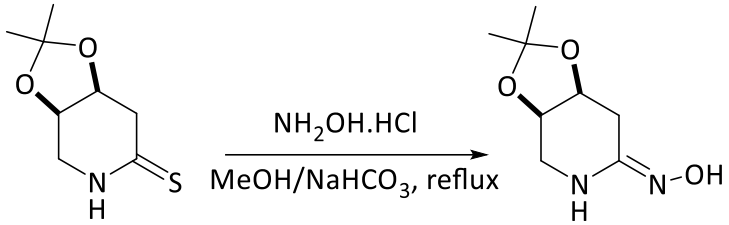

60 **66:** 27%

Scheme 2-14: *Condensation reaction of acetonide thionolactam with hydroxyl amine.*

Condensation of TBS-protected thionolactam **(61)** with hydroxylamine hydrochloride *via* the same reaction produced the desired hydroximolactam **(67)** (Scheme 2-15).

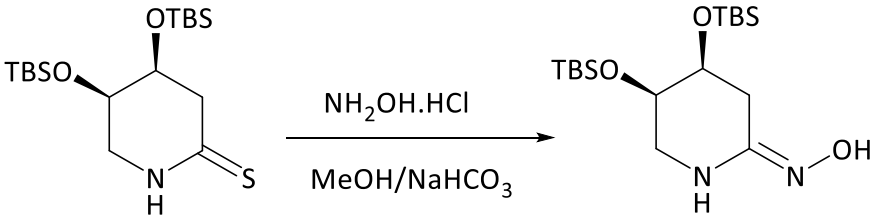

61 **67:** 100%

Scheme 2-15: *Condensation reaction of TBDMS thionolactam protected with hydroxyl amine hydrochloride.*

Hydrolysis of the protecting groups.

The final step of amidine synthesis was a deprotection reaction. Protected amidine derivatives can be deprotected by treatment with HCl affording the amidine derivatives themselves.[152] Compounds **(63a-e** and **66)** derived from acetonide thionolactam were deprotected by stirring in 2N HCl for five hours at room temperature, producing free bases amidine derivatives **(35a** and **35c-g)** (Scheme 2-16, Figure 2-8).

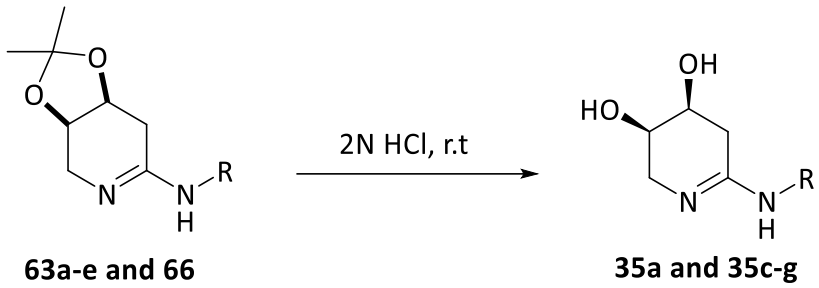

Scheme 2-16: *Deprotection reaction of protected amidine derivatives.*

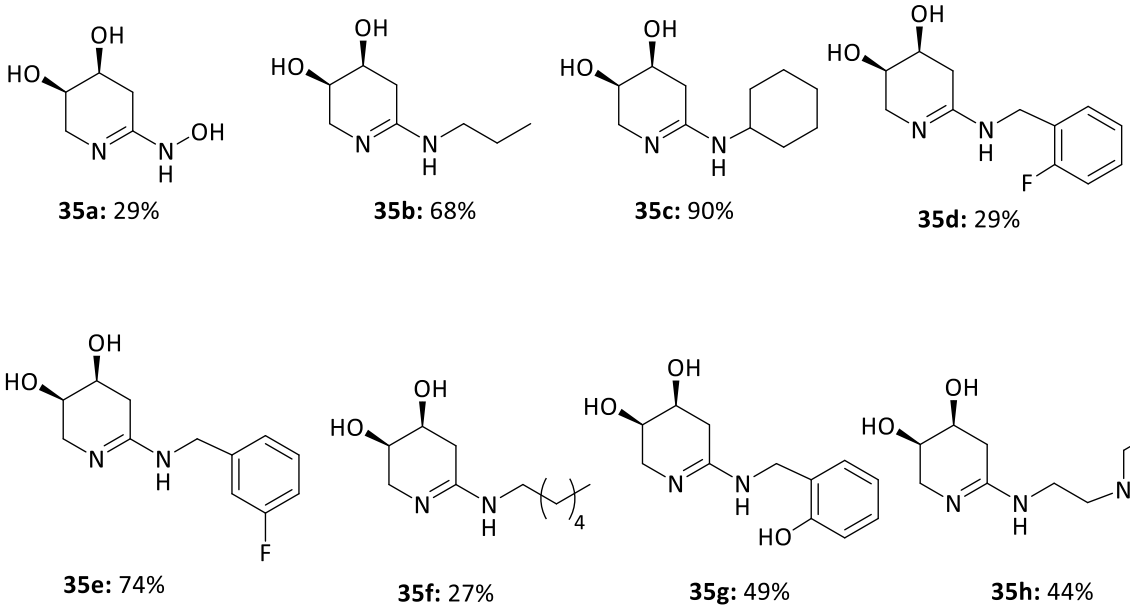

Figure 2-8: *Synthesised (4S,5R)-4,5-dihydroxyamidine derivatives.*

However, deprotection of the TBS group **(65a-g** and **67)** was carried out by refluxing in 2 N HCl after it was dissolved in 10 % methanol overnight affording amidine hydrochloride salts **(68a-h)** (Scheme 2-17, Figure 2-9).

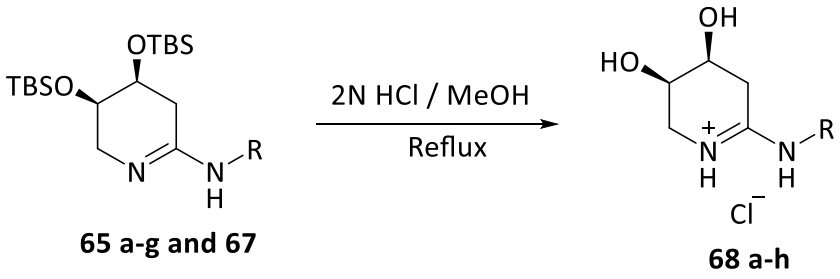

Scheme 2-17: *Deprotection reaction of protected amidine derivatives.*

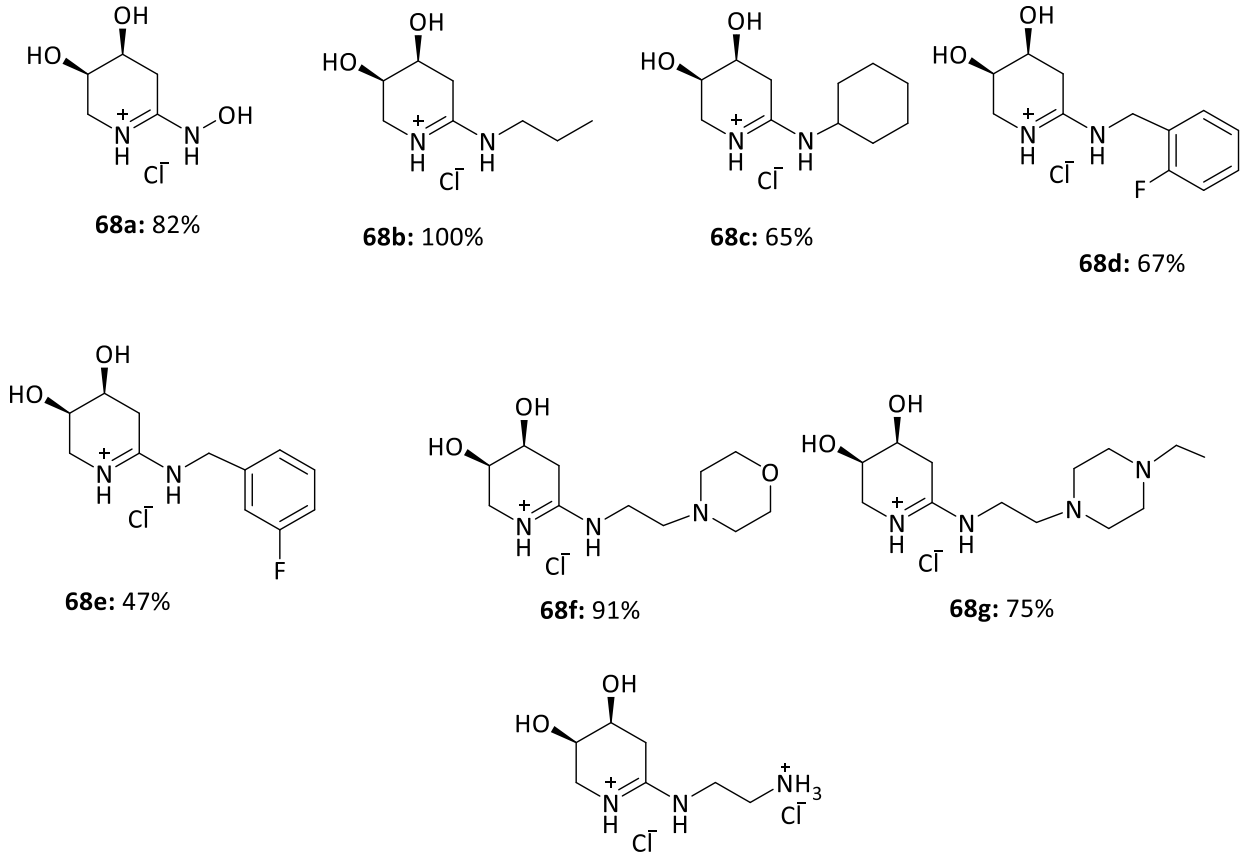

68a: 82%

68b: 100%

68c: 65%

68d: 67%

68e: 47%

68f: 91%

68g: 75%

68h: 71%

Figure 2-9: *Synthesised (4S,5R)-4,5-dihydroxyamidine hydrochloride derivatives*

Compound **(68a)** was crystallised by dissolving in methanol and a few drops of dichloromethane, which was then left to evaporate slowly. The resulting crystal was then used for X-ray crystallography (Figure 2-10), which demonstrated that the structure of amidines derived from the TBS-protected intermediate are hydrochloride salts. However, amidines produced from the acetonide intermediate are free bases. This result was obtained after the evaluation of all inhibitors against enzyme activity (Chapter 4), where compounds derived from the acetonide and deprotected by acid hydrolysis at room temperature were more active than that derived from TBS intermediate and deprotected by acid hydrolysis under reflux conditions in the presence of methanol.

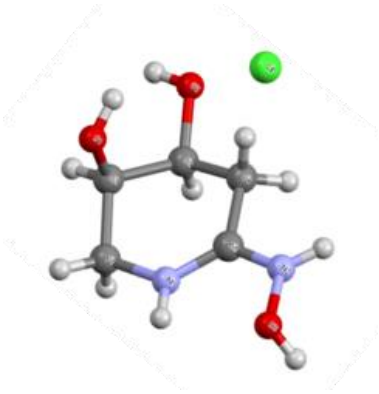

Figure 2-10: *X-Ray crystallography of amidine* ***(68a).*** *Atoms colours as follow: grey-carbon, red-oxygen, white-hydrogen, purple-nitrogen, green-chloride.*

Protection of 3-aminopropan-1,2-diol

The two hydroxyl groups in the 3-aminopropan-1,2-diol **(69)** must be protected before they can be added to the reaction mixture of iminothioethyl ether and Meerwein's salt (Scheme 2-13). Therefore, they were protected as OTBS groups **(70)** (Scheme 2-18).

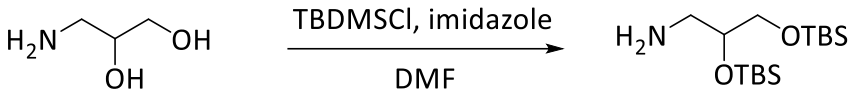

69 **70:** 47%

Scheme 2-18: *Protection reaction of amino-1,2-diol.*

Synthesis of (4R,5S)-4,5-dihydroxy lactam

In order to synthesise amidine enantiomers **(36)**, the same route described in section 2.2.5 above was applied to 2-deoxy-L-ribose **(44)** which was treated with bromine in water for five days followed by activation of primary hydroxyl group as tosylate **(71)** by using tosyl chloride.[152] The resulting tosylate **(72)** was then treated with sodium azide in acetonitrile for five days to produce azide product **(43)**. Hydrogenation of azide by hydrogen atmosphere over pallidum hydroxide on activated carbon in methanol led to the enantiopure lactam **(42)**. Lactam was then protected as acetonide **(73)** followed by transformation to thionolactam **(74)** after treatment with Lawesson's reagent (Scheme 2-19).

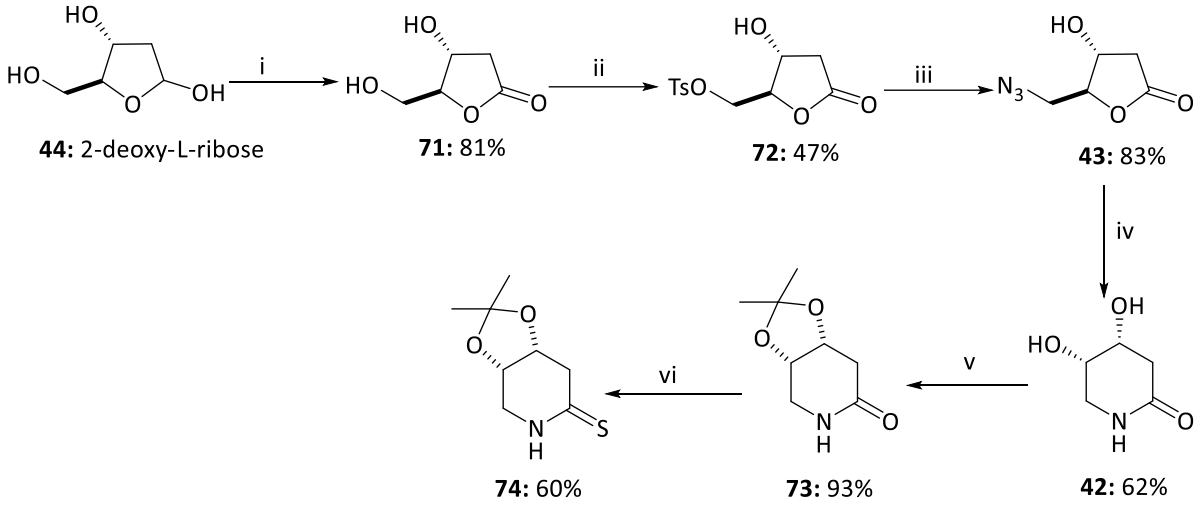

Scheme 2-19: *The synthetic route of (4R,5S)-dihydroxylactam. (i) Br_2/H_2O, r.t. 5 days (ii) p-Toluenesulfonyl chloride, pyridine. -15 °C 2 h. and then 0 °C 5 h. (iii) NaN_3, 15-crown-5, CH_3CN, 5 days (iv) $Pd(OH)_2$-C, MeOH, H_2, O/N (v) 2,2-dimethoxypropane, p-TsOH, MeOH, 55 °C, 7 h. (vi) Lawesson's reagent, THF, r,t. 2 days.*

The sulfur atom was then activated by alkylation with Meerwein's reagent followed by addition of different amines (propyl amine, cyclohexyl amine, 2-fluorobenzyl amine and 4-(2-aminoethyl)morpholine). In case of propylamine the product was unprotected whereas with other amines the resulting amidines were protected, which required deprotection by acid hydrolysis at r.t as with previous amidine analogues producing free base amidine analogues (Scheme 2-20, Table 2-4).

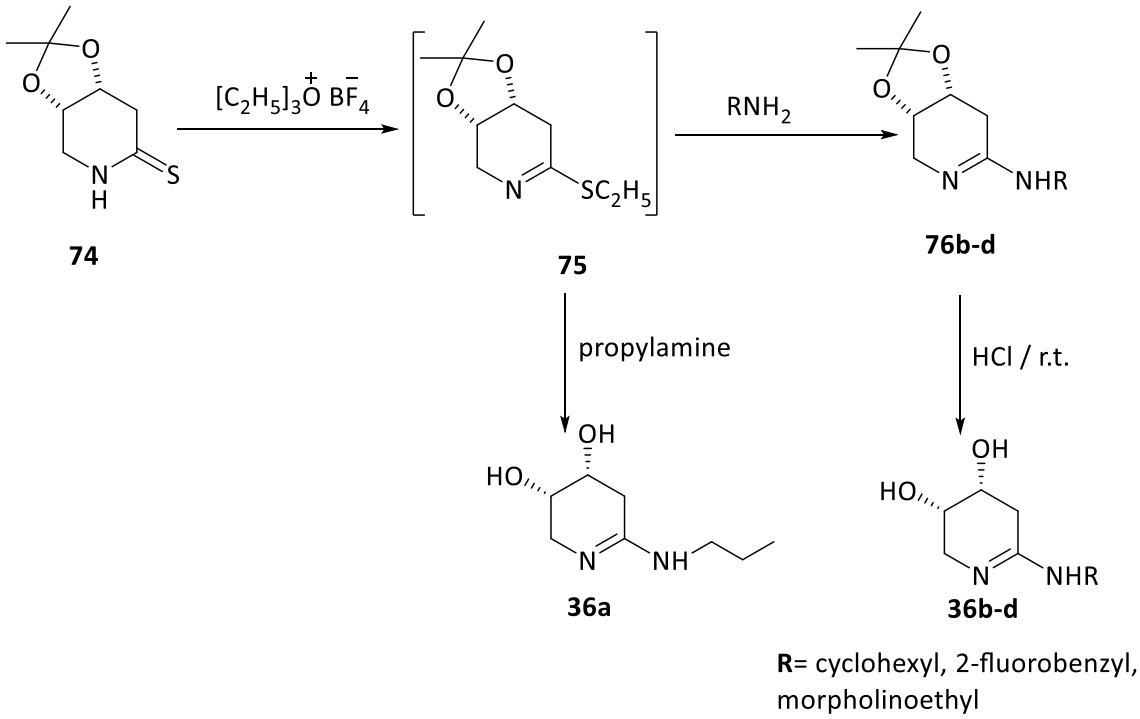

Scheme 2-20: *Synthesis of (4R,5S)-dihydroxyamidine derivatives.*

Comp. no.	R	%
76b	$-C_6H_{11}$	23
76c	$2\text{-}F\text{-}CH_2C_6H_4$	18
76d	$-(CH_2)_2N(CH_2)_4O$	12

Table 2-4: *(4S,5R)-Dihydroxyamidine derivatives.*

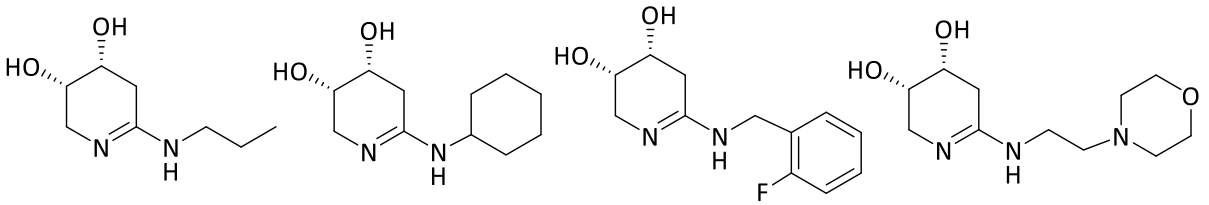

36a: 39% **36b:** 61% **36c:** 68% **36d:** 47%

Figure 2-11: *Synthesised (4R,5S)-4,5-dihydroxyamidine analogues.*

2.3.4 Synthesis of trihydroxamidine from D-ribose

Starting from D-ribose **(47)**, a five step synthesis was used to prepare partially protected trihydroxylactam **(79)** (Scheme 2-21). The first step was oxidation of sugar to lactone **(77)** by using bromine in water followed by protection of two secondary hydroxyl groups as acetonide **(78)**[177]. The primary hydroxyl group was then activated by reaction with tosyl chloride **(79),**[178] which was replaced by azide **(80)** after treatment with sodium azide. Hydrogenation of the azide product afforded the desired lactam **(81)** via ring opening and then ring closing.

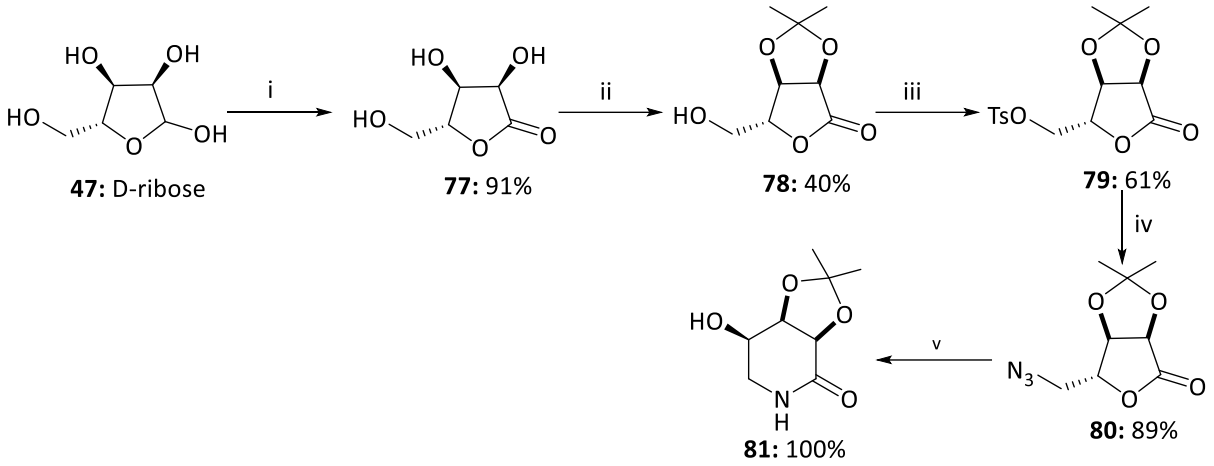

Scheme 2-21: *Synthesis pathway of trihydroxylactam. (i) Br_2/H_2O, r.t. (ii) acetone, H_2SO_4 (cat.). (iii) TsCl, Et_3N, DCM (iv) NaN_3, 15-crown-5, CH_3CN. (v) $Pd(OH)_2$-C, MeOH, H_2..*

However, attempts to continue the synthesis in the same manner as that used previously (Scheme 2-8) were unsuccessful (Scheme 2-22).

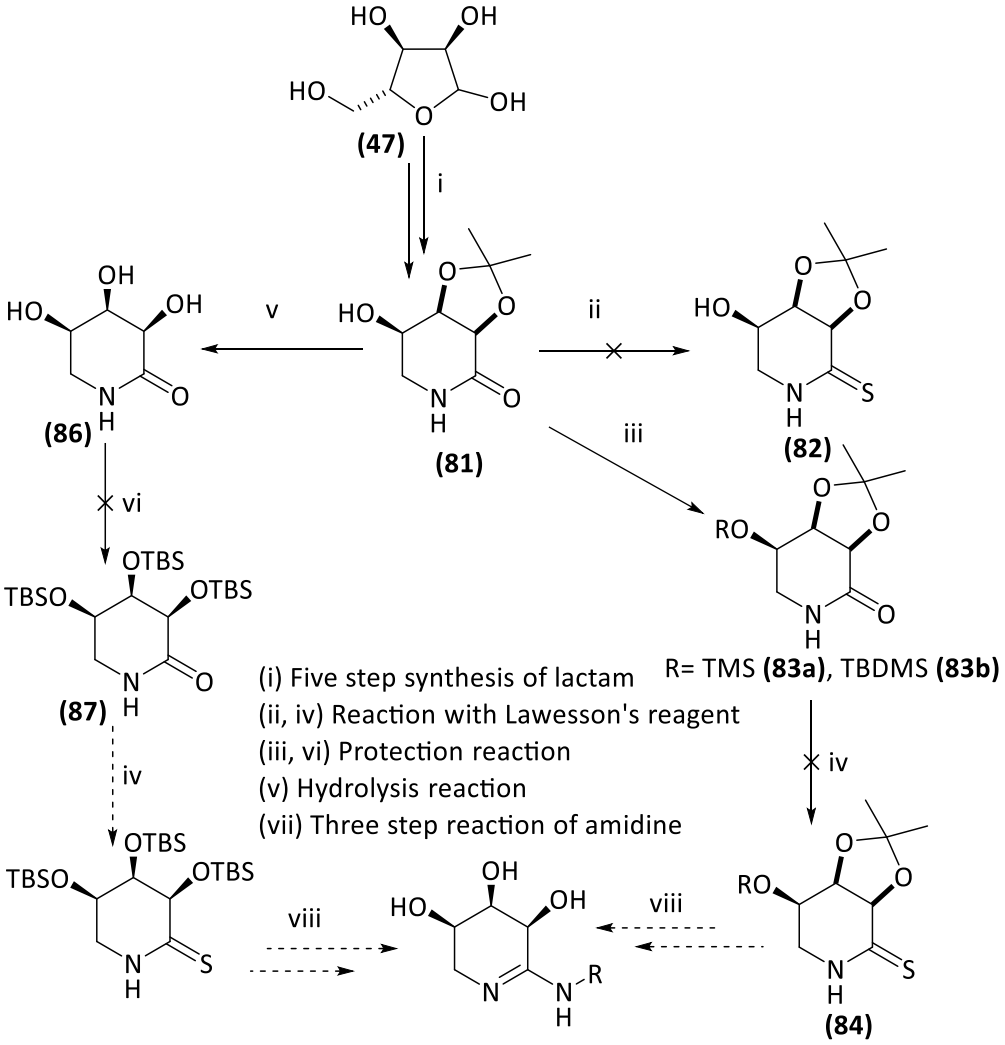

Scheme 2-22: *Synthetic route of trihydroxyamidine.*

An attempt to prepare thionolactam **(82)** by treatment of partially protected lactam **(81)** with Lawesson's reagent met with failure. The possible reason for this is the presence of the unprotected hydroxyl group. Subsequently, this hydroxyl group was protected by using two different protecting groups: trimethylsilyl[179] and tert-butyldimethylsilyl.[164-167] Although the lactam became fully protected **(83a and 83b)**, transformation to the thiolactam **(84)** again failed by giving the start material instead of the desired product. Acetylation of the free hydroxyl group in partially protected trihydroxylactam has been performed by the reaction of lactam with acetic anhydride[180] but the cyclic amino group in the lactam ring was acetylated as well **(85)**, therefore, the next reaction would not be possible in this case (Scheme 2-23).

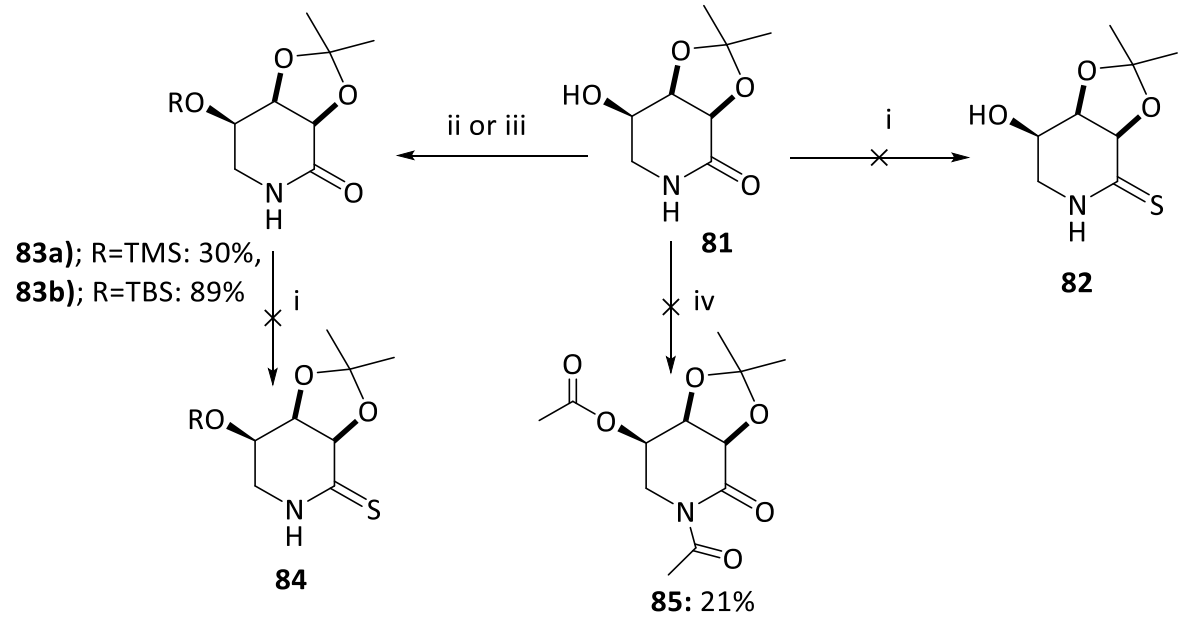

Scheme 2-23: *Reactions of partial protected trihydroxylactam. i) Lawesson's reagent / THF. ii) TMSCl, Et_3N / DCM. iii) TBDMSCl, imidazole/DMF. iv) Ac_2O, pyridine/ DCM.*

A proposed reason for this failure to produce the thiolactam was ring strain created by the acetal group, which can potentially affect the reactivity of the amide carbonyl. Consequently, the acetonide was removed through treatment with 2 N hydrochloric acid for five hours (Scheme 2-24) to produce unprotected trihydroxylactam **(86)**. This lactam was then reacted with tert-butyldimethylsilyl chloride (TBDMSCl) in the presence of imidazole in DMF in order to protect the three hydroxyl groups. Unfortunately, hydroxyl group in position three in the ring was formylated instead of protection by TBS group **(87)**.

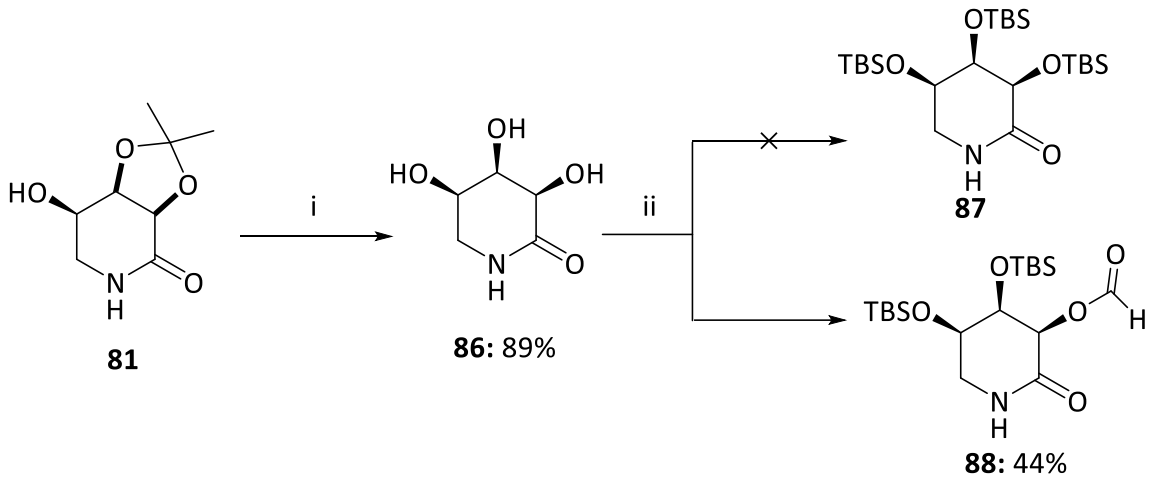

Scheme 2-24: *Reactions of partial protected trihydroxylactam. i) 2 N HCl. ii) TBDMSCl, imidazole / DCM.*

The reason for producing this product was illustrated in the proposed reaction mechanism in Scheme 2-25.[181] However, the formyl group position has not been confirmed in this study.

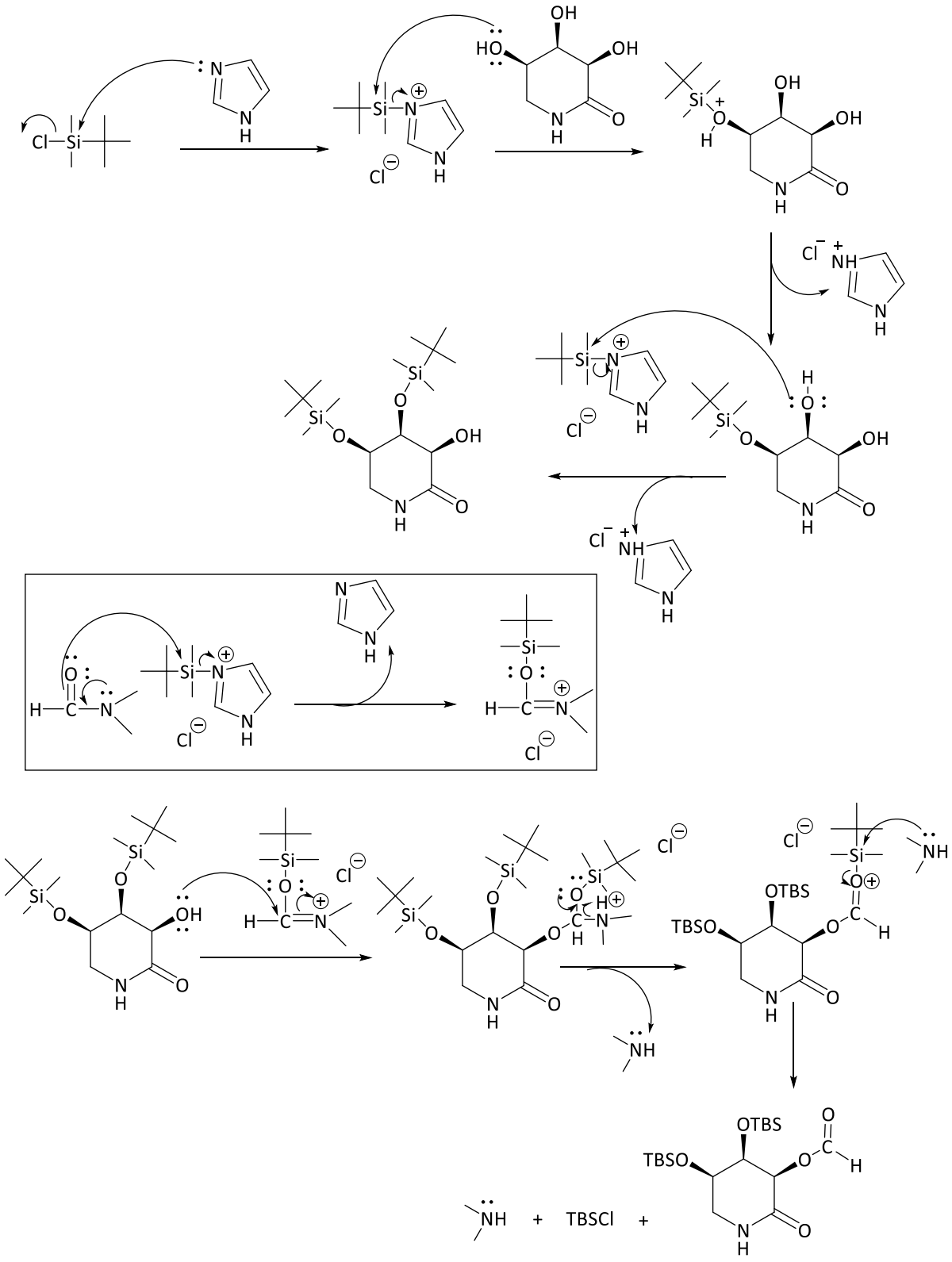

Scheme 2-25: *The proposed mechanism of protection reaction of trihydroxy lactam using TBDMSCl.*

2.3.5 Stereoinversion of (4S,5R)-5-(azidomethyl)-4-hydroxydihydrofuran-2(3*H*)-one (40) to (4R,5R)-5-(azidomethyl)-4-hydroxydihydrofuran-2(3*H*)-one (89).

Stereoinversion of the secondary hydroxyl group in azide **(41)** was attempted following a one-pot procedure that has been applied before on sugar derivative.[182] Unfortunately, an elimination reaction instead occurred, to produce the unsaturated azide **(89)**, rather than stereoinversion (Scheme 2-26).

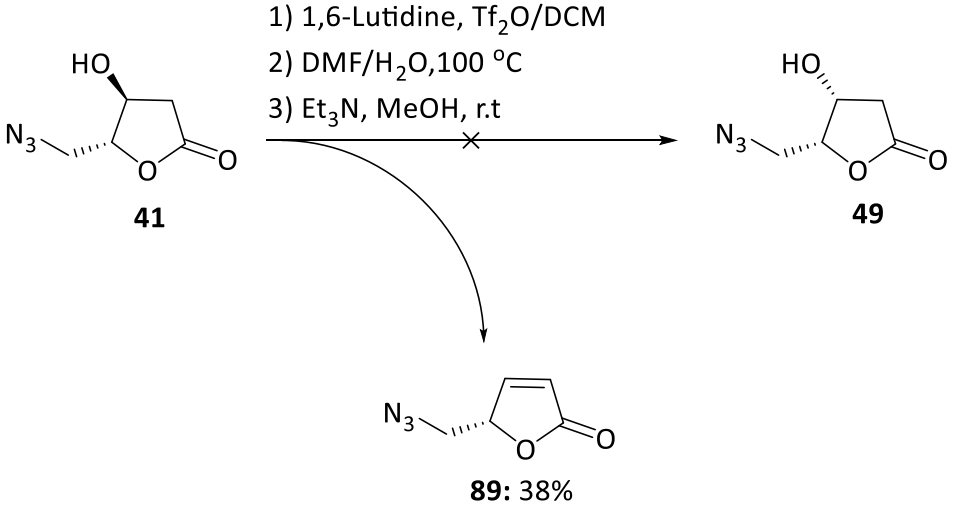

Scheme 2-26: *Attempted stereoinversion reaction of (4S,5R)-azidolactone.*

2.3.6 Synthesis of glucoamidine

An attempt to generate gluconoamidines **(91)**, which are known glycosidase inhibitors,[147-150] was made starting from commercially available benzylated gluconolactone **(31)** as previously reported[146] but this synthesis has not been completed (Scheme 2-27).

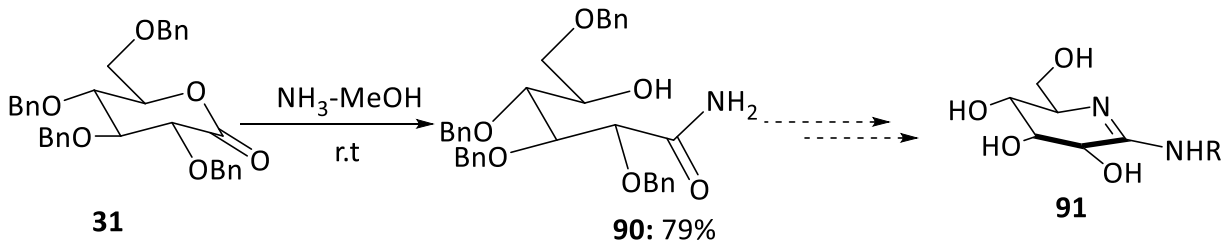

Scheme 2-27: *Synthetic route of gluconoamidine derivatives.*

2.4 Conclusion

A number of different amidine-based potential inhibitors have been synthesised in this work. These were designed based on the structure of the oxocarbenium ion intermediate that is generated in the catalytic mechanism of the LTs. Next, molecular docking of the first generation set **(35a-e)** was run and the results suggested that they should form appropriate interactions with Slt35. A nine step synthesis was followed to form (4S,5R)-dihydroxyamidine derivatives starting from 2-deoxy-D-ribose, with difficulties faced for some reactions, for example the low yield and difficult purification of acetonide thiolactam, as well as trouble with the reaction with Meerwein's reagent and the purification of amidine products. The second generation of compounds was developed from the first set through changes to the orientation of the two hydroxyl groups in amidine ring from (4S,5R) to (4R,5S)-dihydroxyamidine derivatives **(36a-d).** Four new amidine derivatives were designed as analogues of compounds **(35a-e)** and then synthesised starting from 2-deoxy-L-ribose by the same route showed in Scheme 2.8. Docking for the three (4R,5S) compounds **(36a-c)** has been performed and then compared to the first five (4S,5R)-dihydroxyamidine derivatives to analyse the difference between their interactions to the enzyme pocket (Section 2.2.2).

Synthesis of further compounds by adding a hydroxyl group to the amidine ring by starting from D-ribose to prepare (3R,4R,5R)-trihydroxyamidine derivatives was attempted following the synthetic route in Scheme 2.22. Although partially protected trihydroxylactam was prepared, conversion of this to the thiolactam in order to make amidine derivatives failed. Different attempts were made to achieve the synthesis of trihydroxyamidine derivatives, but they were unsuccessful. Similarly, an attempt to improve the effectiveness of amidine derivatives inhibitory in this study by inversion of stereochemistry of hydroxyl group in position 4 in amidine ring from R- to S- to produce the enantiomer (4S,5S)-dihydroxyamidine, but this reaction failed again due to the competing elimination reaction.

Additional amidine derivatives derived from 2-deoxy-D-ribose were successfully synthesised by making changes on the propyl group in amine moiety. Activity of all compounds synthesised is reported in Chapter 4.

3 Development of protein purification and activity assay

3.1 Introduction

The study of proteins has become an essential part of molecular biology to understand life at the molecular level. The recombinant protein can be produced by cloning the gene of interest into an expression vector. This vector will be transformed into a host cell, usually *E. coli* because it has a fast growth rate with inexpensive media and growth conditions and can easily achieve a high culture density. Protein production is induced following inoculation in large quantities of media. Protein needs to be soluble and in an active form, before it can be used for any purpose.[183]

One of the common problems that can affect biological protein function is protein folding. To estimate protein aggregation and stability, circular dichroism spectroscopy is a valuable tool for that by assessing the changes in protein secondary structure. When the light emitted from the circular polarised light source hits a chiral molecule within a sample it changes in orientation. The change in orientation of the polarised light at each wavelength provides information about the protein's secondary structure elements. Negative peaks at 220 nm and 208 nm and a positive peak between 192 in a CD spectrum are indicative of α-helices. If the protein structure contains a lot of β-sheet a negative peak is observed at 216 nm with two positive peaks at 200 nm (Figure 3-1).[184-186]

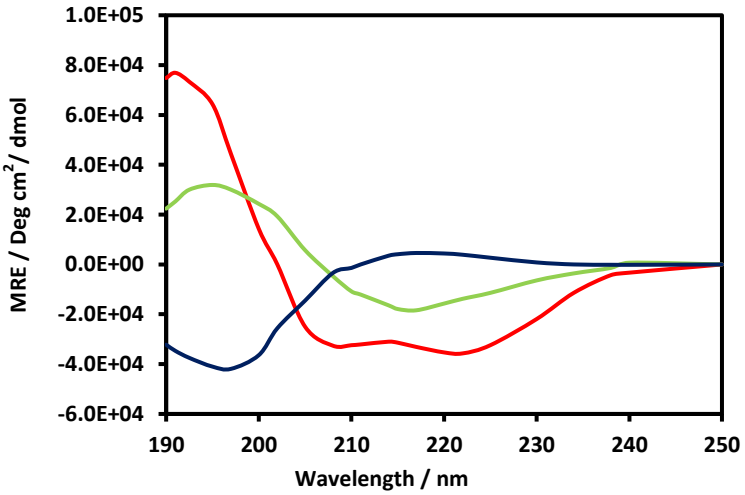

Figure 3-1: *CD spectra of ideal protein structures consisting of α-helical (red curve), β-sheet (green curve) and random (blue curve) conformation[4].*

Protein purification can be achieved by different protocols including: separation by size of protein using a column containing a porous gel (size exclusion), by protein charge by binding to a column containing charged resin followed by washing by series of solutions increasing gradually in salt concentration (ion exchange), and affinity chromatography where the resin contains a particular substance that the protein binds to, for example nickel affinity where histidine residues are added to the C or N terminus of the protein. However, there are some problems that might be faced during protein purification, so optimisation of this method is needed in order to gain highly pure protein.

A suitable assay must be found and optimised in order to determine the enzyme activity. For this purpose, there are different types of assays that can be used. The enzyme used in this study is lytic transglycosylase, one of the enzymes that are involved in PG metabolism. Since the substrate of these enzymes is an insoluble polymer, it is extremely challenging to evaluate their activity. In previous studies, different assays have been used to determine the activity of these enzymes, for example zymography, turbidometry, and HPLC-based assay.[187-189]

3.2 Plasmid transformation and gene expression

A gene encoding the membrane bound soluble lytic transglycosylase slt35 with an N-terminal His-tag for purification was purchased in a pET28a expression vector between the two restriction sites *Nde*I and *Xho*I (Figure 3-2). This was transformed into XL1-blue or DH5α *E. coli* cloning strain to allow easy propagation. Following this, the DNA was purified and then digested with *Nde*I and *Xho*I restriction enzymes to check the insertion of slt35 gene (Figure 3-3). Sequencing of the DNA plasmid was performed to confirm the nucleotide identity (Figure 3-4).

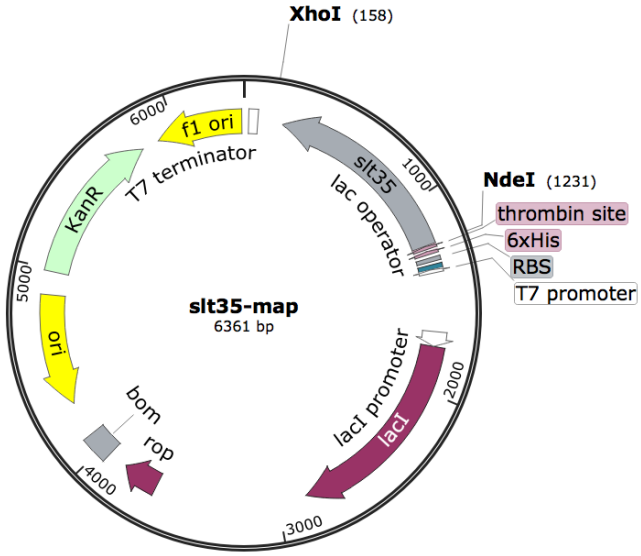

Figure 3-2: *Plasmid map of pET28a vector with slt35 gene. The unique restriction sites are noted on the map.*

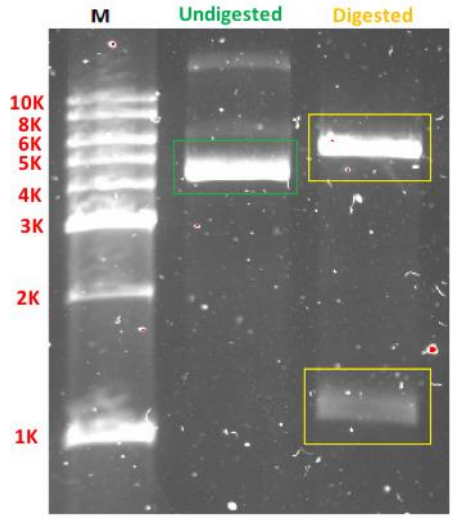

Figure 3-3: *Agarose gel electrophoresis of the products resulting from digestion of the pET28a vector containing the slt35 gene with NdeI and XhoI. M: molecular weight marker.*

Figure 3-4: *DNA sequence of the slt35 gene inserted into the pET28a expression vector.*

A gene expression test was carried out in *E. coli* BL21(DE3) competent cells for protein production. The resulting cells were inoculated into LB medium supplemented with kanamycin sulfate (50 μg ml^{-1}) and incubated at 37 °C until the optical density reached 0.6-0.8 at 600 nm. To determine the optimum temperature for gene expression, induction with IPTG was performed at different temperatures. Samples were collected from the cultures and analysed by sodium dodecyl sulfate polyacrylamide gel electrophoresis (SDS-PAGE). According to the SDS-PAGE, protein expression was successful at all temperatures (Figure 3-5). However, protein production was conducted at 18 °C overnight, where the protein is high in quantity and more stable.

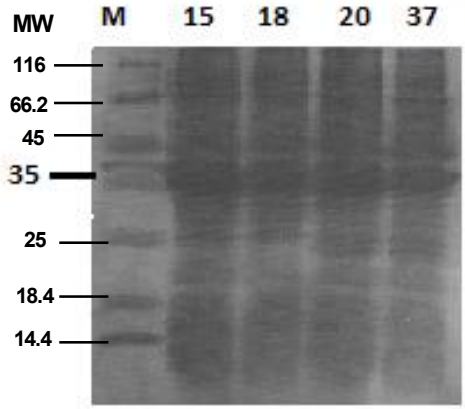

Figure 3-5: *SDS-PAGE of small scale expression experiments of Slt35 at different temperatures. Protein expression was conducted at different temperatures (15, 18, 20 and 37 °C) in order to assess the best expression temperature.*

3.3 Protein purification

3.3.1 Initial trials

Purification of protein was trialled using different buffers. The first buffer was 20 mM HEPES pH 7 containing 500 mM NaCl and 10% glycerol.[133] Initial purification of the clarified cellular lysate was performed using Ni-NTA resin to capture His-tagged Slt35. The column was washed with purification buffer and then the protein was eluted using a gradient of 0-500 mM imidazole in the same buffer (Figure 3-6).

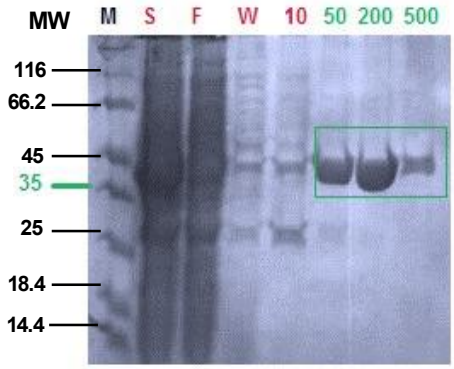

Figure 3-6: *SDS-PAGE of His-tagged Slt35 purified by nickel affinity chromatography using 20 mM HEPES pH 7.0 containing 500 mM NaCl and 10% glycerol. M= marker, S= supernatant, F= flowthrough, W= wash, 10, 50, 200, and 500 = imidazole concentrations in mM for elution.*

Fractions containing pure protein were combined and dialysed overnight against the dialysis buffer A (Chapter 6, section 6.2.1). Precipitation of protein was observed after dialysis; therefore, Triton 100-X was added to the purification buffer as a detergent in order to stop protein precipitation, but it was unsuccessful. The same HEPES buffer was adjusted at different pH (6.0 and 8.0) and used for protein purification but protein precipitation continued. One of the reasons for this precipitation could be misfolding of protein secondary structure. Consequently, circular dichroism was used to characterise protein structure and determine whether the protein has been folded properly.

3.3.2 Circular dichroism (CD)

CD spectra of Slt35 in 10 mM Tris-HCl (pH 7.0) containing 250 mM NaF were measured at intervals over nineteen days. Strong signals were observed in the CD spectrum at 208, 228 and 230 nm indicating that the protein structure was predominantly α-helical (Figure 3-7). This result is consistent with the published crystal structure which revealed a helical structure.[98] It also demonstrates that the protein secondary structure does not alter significantly over nineteen days. Circular dichroism was also run in phosphate buffer at two different pH values 7.0 and 8.0 containing 250 mM NaF. The results were the same as in Tris-HCl buffer, but the focus was on the Tris buffer because it has been chosen as purification and enzyme assay buffer, not phosphate buffer because it was subsequently found (section 5.2.1) that calcium chloride promoted enzyme activity and calcium phosphate is insoluble.

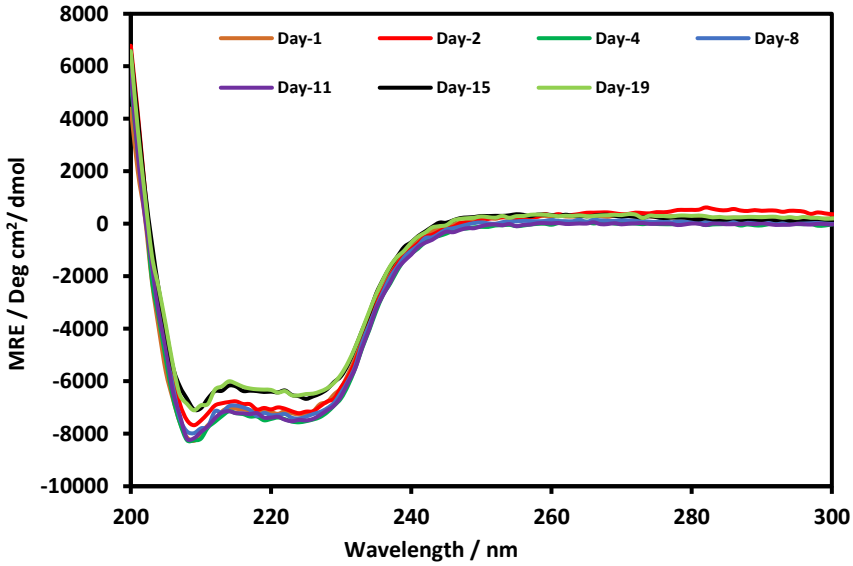

Figure 3-7: *CD spectra of Slt35 in Tris-HCl pH 7.0 containing 250 mM NaF at different times after purification.*

The melting temperature of the protein was determined from the loss of signal at 220 nm (Figure 3-8). Slt35 was found to melt at 51.6 ± 0.05 ° C, similar to the published melting temperature (48 °C in the absence of salt, 53.5 °C in the presence of 100 mM NaCl, and 55.5 °C in the presence of 1 mM $CaCl_2$).[115]

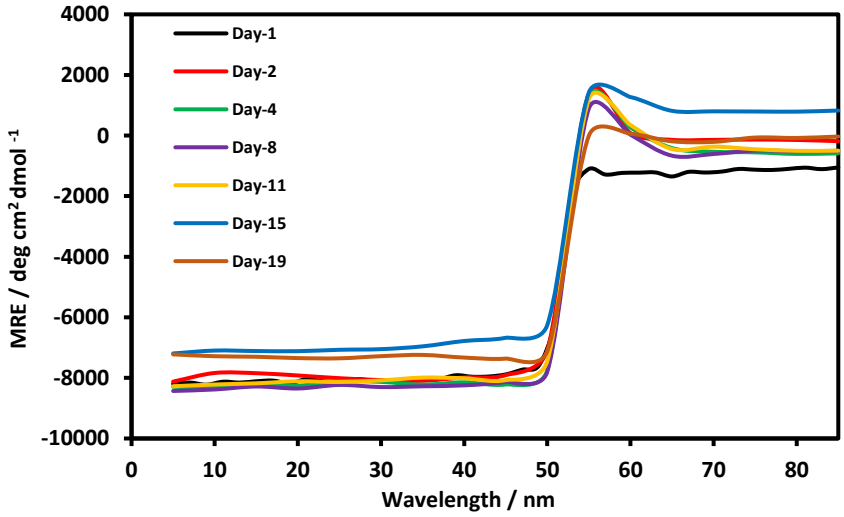

Figure 3-8: *CD temperature ramp of Slt35 in Tris-HCl pH 7.0 at 220 nm on different days.*

3.3.3 Final purification method

50 mM Tris-HCl pH 7.0 was the second buffer used for protein purification where the protein was stable according to CD results. At the beginning this buffer was supplemented with 500 mM NaCl and 10% glycerol but the protein still precipitated. Consequently, 0.05% Tween-20 was added to the purification buffer. After this, the protein became more stable and no precipitate was observed after purification. Accordingly, 50 mM Tris-HCl pH 7.0 supplemented with 500 mM, 10% glycerol and 0.05% Tween-20 was used as protein purification buffer for the remainder of this work. The protein was initially purified by nickel affinity chromatography, eluting with imidazole (Figure 3-9).

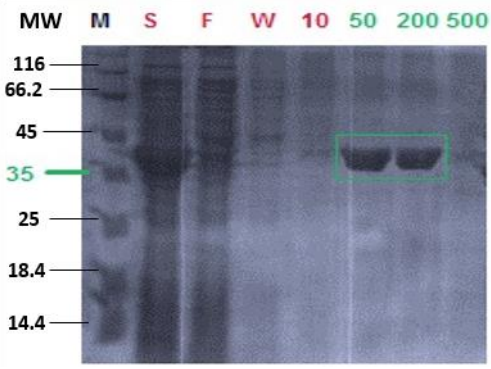

Figure 3-9: *SDS-PAGE analysis of His-tagged Slt35 purified by nickel affinity chromatography using 50 mM Tris-HCl pH 7.0 containing 500 mM NaCl, 10% glycerol and 0.05% Tween-20. M= Marker, S= supernatant, F= flowthrough, W= wash, 10, 50, 200, and 500 = imidazole concentrations in mM for protein elution.*

Fractions that contained pure protein were combined, dialysed overnight against 50 mM Tris-HCl pH 7.0 supplemented with 500 mM NaCl, 10% glycerol and 0.05% Tween-20, then concentrated and further purified by size exclusion chromatography (SEC) using Superdex 200 resin in 50 mM Tris-HCl buffer, pH 7.0, containing 500 mM NaCl and 0.05% Tween-20 (Figure 3-10).

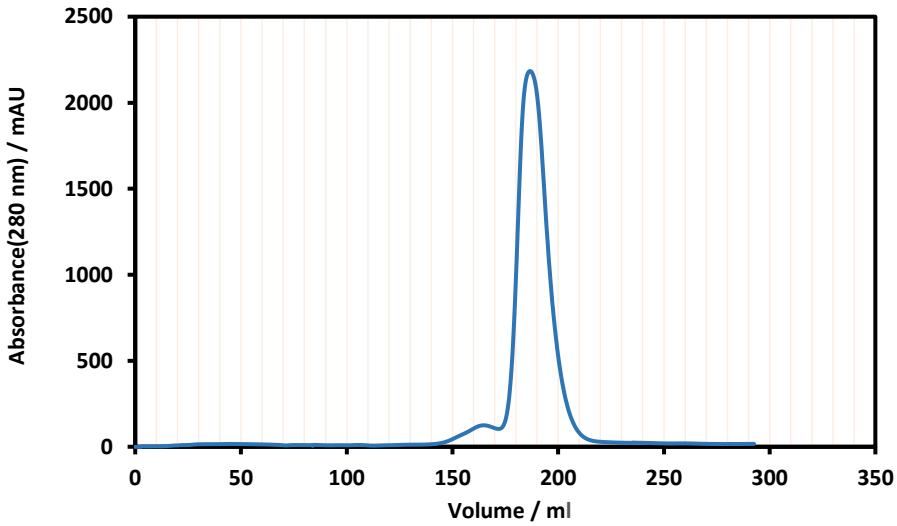

Figure 3-10: *The chromatogram from the purification of Slt35 by size exclusion chromatography on Superdex 200 resin in 50 mM Tris-HCl buffer, pH 7.0, containing 500 mM NaCl and 0.05% Tween-20.*

SDS-PAGE indicated that the major peak from size exclusion chromatography had the correct mass for Slt35 and was almost completely pure. (Figure 3-11).

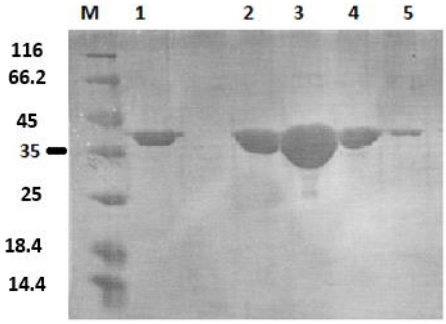

Figure 3-11: *SDS-PAGE analysis of Slt35 purified by size exclusion chromatography in 50 mM Tris-HCl buffer, pH 7.0, containing 500 mM NaCl and 0.05% Tween-20, with M=marker, 1,2,3,4 and 5 pure protein fractions.*

3.3.4 Mass spectrometry

To determine the exact mass of protein, ESI-TOF time of flight mass spectrometry was used. Two major species were observed with deconvoluted masses 40009.00 and 40187.00 (Figure 3-12). These differ from each other by 177.22 g/mol which could be accounted by the removal of the N-terminal formylmethionine. This is a common bacterial modification.[190] These masses come close to the values deduced from the gene sequence. However, the mass 40009.00 g/mol differs from the gene sequence mass (39962.03 g/mol) by 46.97 g/mol and the mass 40187.00 g/mol differs from the gene sequence mass (40139.25 g/mol) by 47.75 g/mol. A possible explanation is the presence of formic acid (46.03 g/mol) adducts on the protein

surface, caused by the presence of this compound in the chromatography solvents, although the mass does not match exactly. To confirm the accuracy of the mass obtained, a second sample of protein was analysed by mass spectrometry. The same masses were observed.

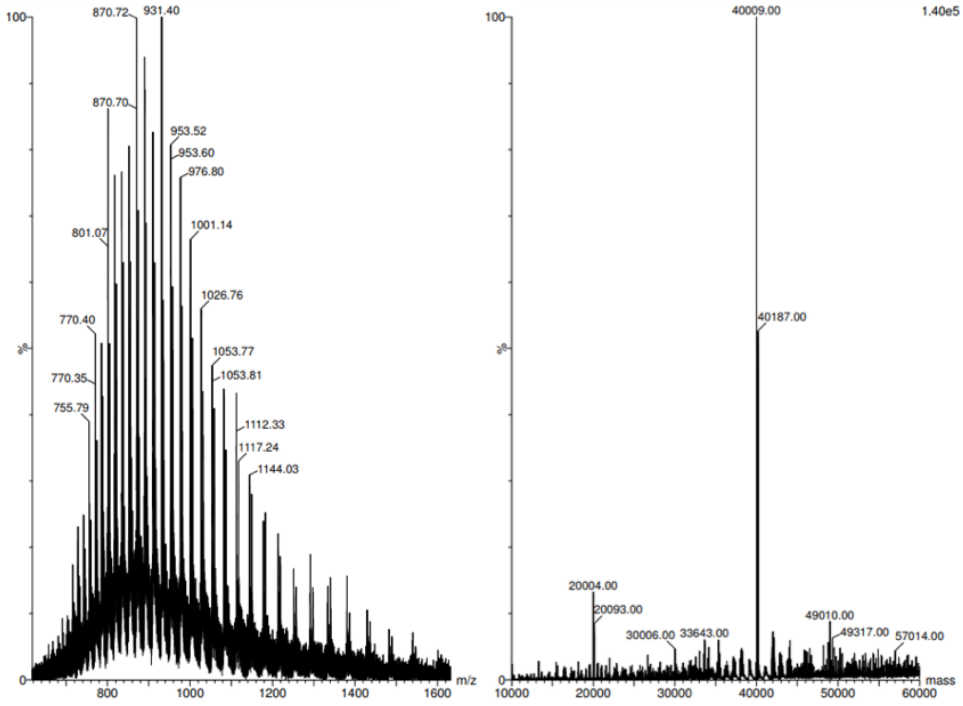

Figure 3-12: *Raw (left) and deconvoluted (right) mass spectra of purified Slt35.*

3.4 Enzyme activity

HPLC-based methods for determining lytic transglycosylase activity have previously been investigated in our research group, without success. Two assays were used to investigate the catalytic activity of purified Slt35 in this study: glycoside hydrolysis and turbidimetric assays.

3.4.1 Glycoside hydrolysis assay

Generally, lytic transglycosylase activity cannot be detected by a direct spectrophotometric assay, due to the lack of a suitable chromophore in their substrate. However, many other carbohydrate-cleaving enzymes are typically assayed using p-nitrophenol acetals[191] (Figure 3-13). This assay is spectrophotometric but uses a substrate analogue rather than true substrate. Although such assays do not appear to have been applied to lytic transglycosylases previously, they were investigated here in the hope of finding a simple method for assaying activity.

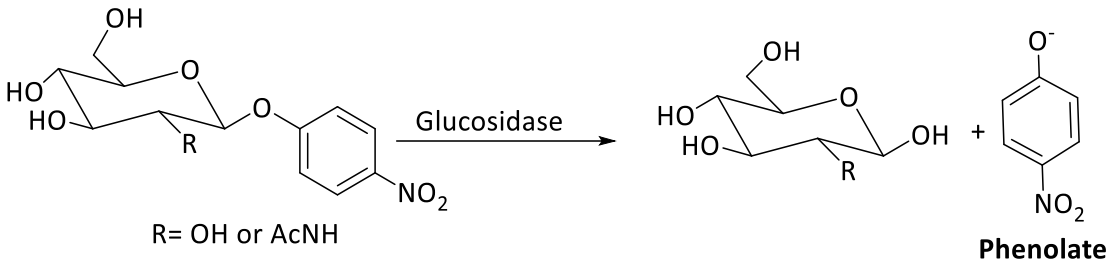

Figure 3-13: *Enzymatic hydrolysis of p-nitrophenylglucopyranoside derivatives by glycosidases.*

The assay was attempted using *p*-nitrophenyl-D-glucopyranoside (pNPG) or p-nitrophenyl-*N*-acetyl-D-glucosamine in 100 mM sodium acetate buffer pH 4.5 or 25 mM Tris-maleate pH 5.8 supplemented with 10 mM $CaCl_2$ or 100 mM NaCl. Different concentrations of substrate were used, and the reaction mixture was incubated at different temperatures for different times. The reaction was quenched by adding Na_2CO_3 (1 M) and the absorption was read at 405 nm in a plate reader. There was no change in the colour of the reaction mixture and no absorption has been detected. This shows that the p-nitrophenol acetals were not cleaved by the lytic transglycosylase.

3.4.2 Turbidimetric assay

Turbidimetry is the process that measure the decrease of light transmitted intensity by the effect of particles suspended in solvent. It is widely used to determine the activity of enzymes that act upon insoluble substrates, such as lysozyme and bacteriolytic enzymes,[192] although due to the random hydrolysis of substrate by these enzymes it is not possible to express the rate in molar terms. The turbidimetric assay of Hash[193] was used to determine lytic activity of lysozyme and Slt35 by monitoring the time course of PG solubilisation when the enzyme is added to the reaction mixture. Clarke *et al.* performed this assay in sodium phosphate buffer to determine activity of the same enzymes.[132] Here, the assay was performed using whole cells of *Micrococcus lysodeikticus* in different buffers at different pH to investigate enzyme activity of lysozyme and Slt35. Lysozyme was active in most cases while Slt35 was not (Figure 3-14). The possible reason for that could be the effect of imidazole, which might remain in the protein solution after dialysis.

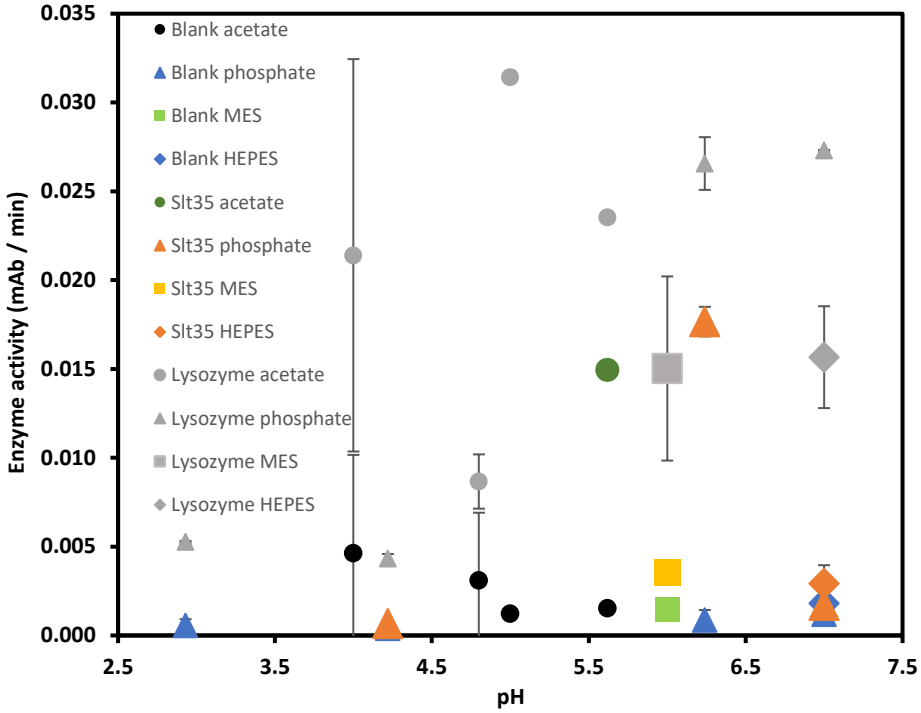

Figure 3-14: *Enzyme activity of Slt35 in comparison with lysozyme in different buffers at different pH.*

To avoid effects from imidazole on enzyme activity, purification of protein was performed as previously reported in 50 mM phosphate buffer pH 7.0 supplemented with 500 mM NaCl, 10% glycerol and 0.05% Tween-20. The bound protein was eluted from the column by decreasing pH ranging from 6.5 to 4.0 (Figure 3-15).[188]

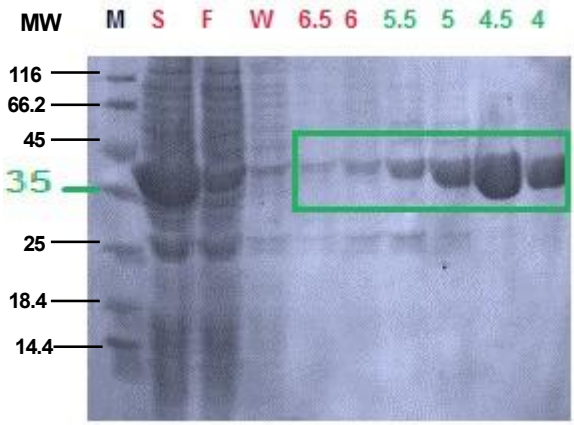

Figure 3-15: *SDS-PAGE analysis of His-tagged Slt35 purified by nickel affinity chromatography using phosphate buffer pH 7.0 containing 500 mM NaCl, 10% glycerol and 0.05% Tween-20. M=marker, S=supernatant, F= flowthrough, W= wash, (6.5, 6.0, 5.5, 5.0, 4.5 and 4.0) are different pH from phosphate buffer.*

Fractions 5.5 and 4.5 were concentrated individually and their activity tested on the same day by the same turbidometry assay using 10 mM sodium acetate buffer pH 5.5 containing 100 mM NaCl. Lysozyme was tested as a control, which was active but Slt35 in both fractions did

not shown any activity. In this case, the acidic pH of enzyme stock solutions may have influenced activity. Subsequently, buffer exchange was performed following purification in order to remove the imidazole from protein solution by using a Superdex 25 G column. Protein was purified by 50 mM Tris-HCl buffer at pH 7.0 supplemented with 500 mM NaCl, 10% glycerol and 0.05% Tween-20 followed by elution with imidazole. Pure protein fractions that have 50 and 200 mM imidazole were combined immediately, concentrated and then subjected to size exclusion chromatography. Fractions that contained protein were collected and analysed by SDS-PAGE (Figure 3-16).

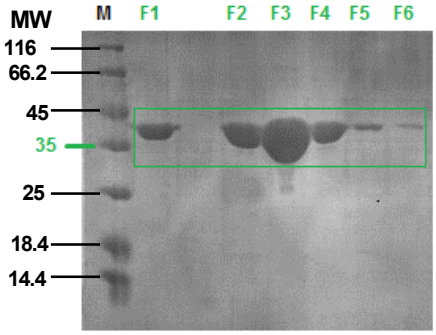

Figure 3-16: *SDS-PAGE analysis of Slt35 fractions from size exclusion chromatography. M= Marker, F1,F2,F3,F4,F5 and F6 are protein fractions.*

Enzyme activity of pure protein was tested with the same turbidometry assay under the same conditions that were used above. No activity, however, was detected in the buffer-exchanged enzyme sample. In another attempt to achieve favourable conditions for enzyme activity, the concentration of substrate was increased, adjusting the OD of the cell suspension to between 0.8 and 2.5 at 600 nm. Three different buffers were used: 20 mM sodium acetate supplemented with 100 mM NaCl, 25 mM potassium phosphate contained 100 mM potassium chloride and 25 mM Tris-maleate contained 100 mM NaCl (Table 3-1). It can be seen from Figure 3-17 that there is a decrease in the absorption of cell suspension by adding the enzyme. However, this change was within a very short time (20 s) especially in case of acetate and phosphate buffer. More reliable results were in the case of Tris-maleate buffer where the initial rate of the enzyme activity continued for 60 s, but the decrease of turbidity was not high enough (Figure 3-17).

Purification buffer	Assay buffer	Protein activity
50 mM Phosphate + 500 mM NaCl + 10% glycerol + 0.05% Tween-20.	10 mM Sodium acetate + 100 mM NaCl pH 5.5	No activity was observed
50 mM Tris-HCl + 500 mM NaCl + 10% glycerol + 0.05% Tween-20 followed by (SEC) with the same buffer.	As above	As above
50 mM Tris-HCl + 500 mM NaCl + 10% glycerol + 0.05% Tween-20.	20 mM Sodium acetate + 100 mM NaCl, pH5.5, $OD_{substrate}$ = 0.8	Very weak activity was observed
As above	The same buffer, $OD_{substrate}$ = 2.0	Weak activity was observed
As above	The same buffer, $OD_{substrate}$ = 2.4	Weak activity was observed
As above	25 mM Potassium phosphate + 100 mM KCl, pH 5.5, $OD_{substrate}$ = 0.8	No activity was observed
As above	The same buffer, $OD_{substrate}$ = 2.0	Weak activity was observed
As above	The same buffer, $OD_{substrate}$ = 2.4	Protein was active
As above	25 mM Tris-maleate + 100 mM NaCl, pH 5.5, $OD_{substrate}$ = 0.8	Weak activity was observed
As above	The same buffer, $OD_{substrate}$ = 2.0	Protein was more active
As above	The same buffer, $OD_{substrate}$ = 2.4	As above

Table 3-1: *Enzyme activity of Slt35 in different buffers.*

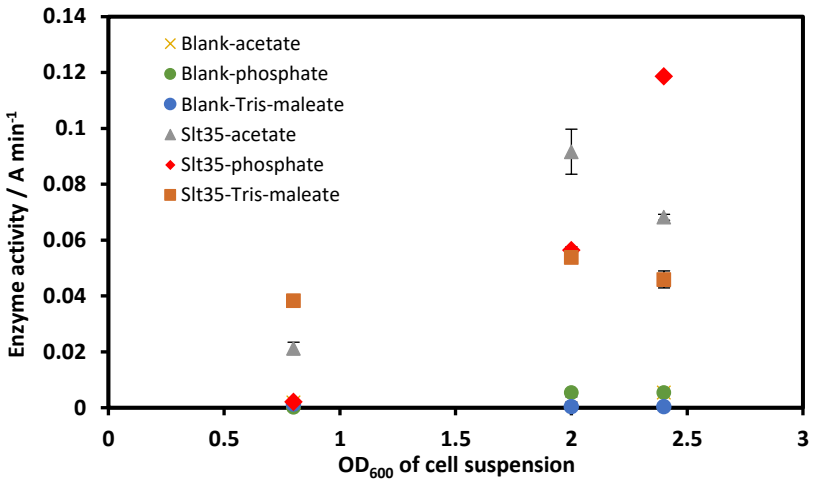

Figure 3-17: *Enzymatic activity of Slt35 in different buffers.*

To improve the buffer conditions of enzyme activity of Slt35, different factors have been tested including; salt effect, optimum pH and substrate concentration. Tris-maleate buffer was chosen as an assay buffer in this study because it is the suitable buffer that would operate at the desired pH.

Effects of salts on enzyme activity

Since protein stability and function can be affected by supplemented buffer salt, the effect of various monovalent (NaCl and KCl) and divalent ($MgCl_2$ and $CaCl_2$) salts on enzyme activity was determined. Different concentrations of these salts were prepared (1, 10, 25, 50 and 100 mM) in 25 mM Tris-maleate buffer pH 5.8 to test their effect on Slt35 activity and the enzymatic activity was evaluated by turbidometric assay. The maximum activity of Slt35 was observed in 10 mM $CaCl_2$, with $MgCl_2$ giving only slightly lower activity. In monovalent salts the enzyme activity was lower (Figure 3-18) and was not so greatly affected by concentration. Although sodium chloride was used in protein purification buffer and protein storage buffer, the lowest activity of enzyme was in the buffer that was supplemented with sodium chloride.

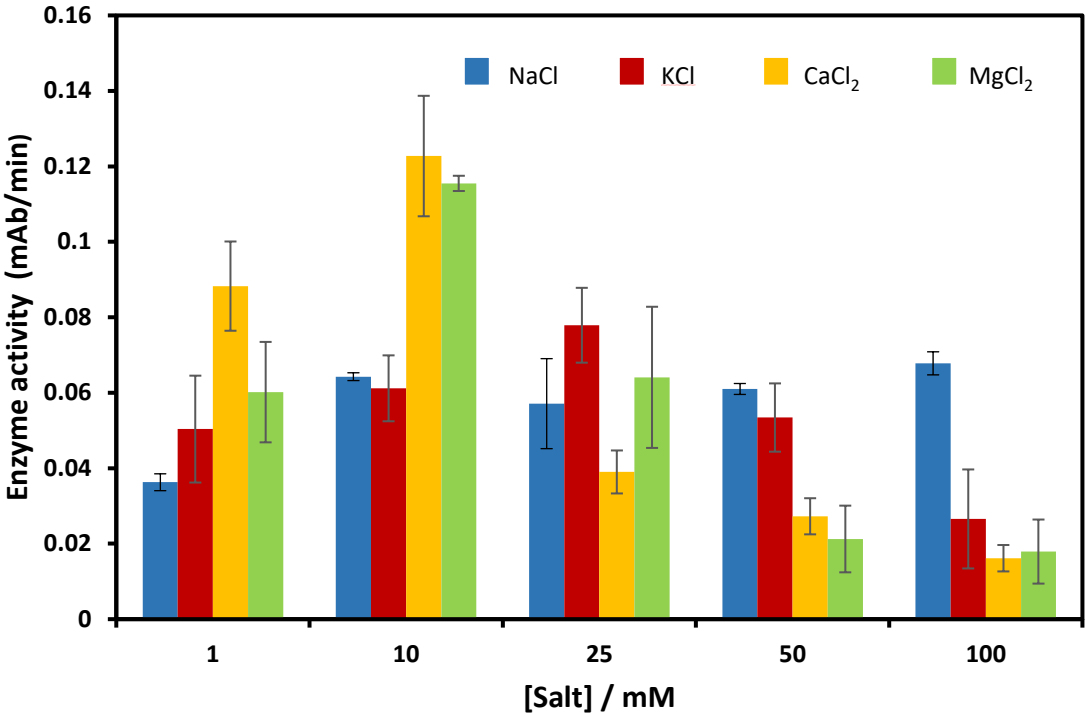

Figure 3-18: *The effect of salt concentration on Slt35 activity in 25 mM Tris-maleate buffer, pH 5.8.*

According to these results, it can be concluded that Slt35 activity was influenced by divalent cations especially calcium ion rather than monovalent. This affinity of enzyme could be due to the EF-hand calcium binding site in the helix-loop-helix region in Slt35 (Figure 3-19). In previous study, the thermostability of Slt35 increased when it was bound to calcium ions. This led to suggestion that the EF-hand site of Slt35 plays an important role in protein stability. However, the functional role of EF-hand calcium binding site in the catalytic mechanism of Slt35 has not been established.[115]

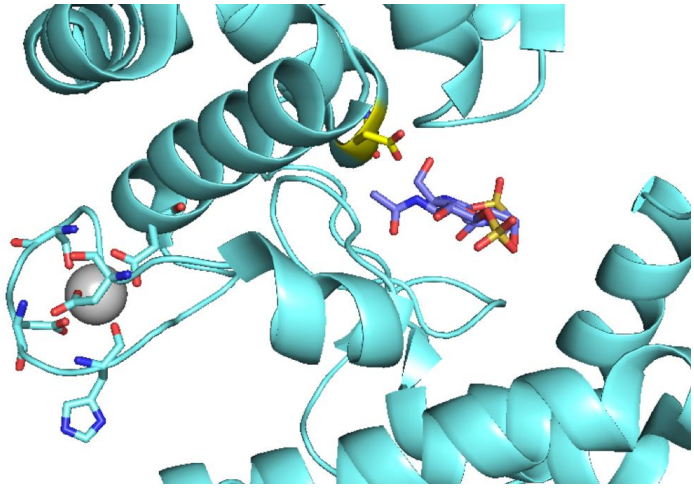

Figure 3-19: *Cartoon representation of the metal ion-binding site in Slt35[7]. The calcium ion (grey) is bound to six protein oxygen atoms in the loop that connects between α helices. The average Ca-O distance is 2.4 Å. The active-site Glu162 residue is shown in yellow and the bulgecin inhibitor in purple.*

Optimal pH

The dependence of Slt35 and lysozyme activity on pH was assessed by using turbidometric assay. A wide pH range of 25 mM Tris-maleate buffer supplemented with 10 mM $CaCl_2$ was prepared for Slt35. The maximum enzyme activity of Slt35 was found to be at pH 5.8 (Figure 3-20A). The suggested mechanism for Slt35 requires the Glu162 to be protonated. The side-chain pK_a of free glutamate is 4.5, suggesting that Glu162 has its pK_a value perturbed to a higher value by its local environment, as seen in many other enzymes.[194] The loss of activity at lower pH is then likely to be due to unfavourable protonation of a different residue, with a pK_a below 6. Unlike Slt35, lysozyme activity did not show big change over the pH range 5.0-8.0. A slight decrease of enzyme activity was observed at pH 4.0, 4.5 and 8.2 (Figure 3-20B).

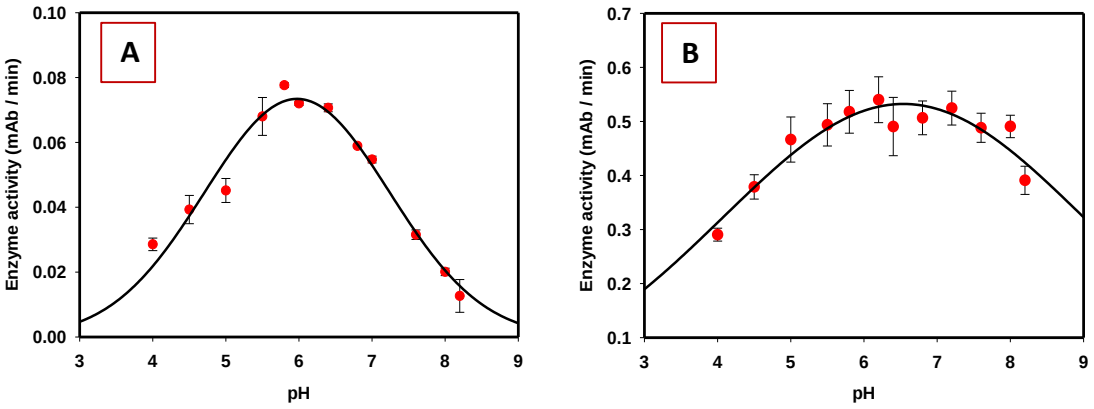

Figure 3-20: ***A:*** *Effect of pH on the activity of Slt35 in 25 mM Tris-maleate buffer containing 10 Mm $CaCl_2$.* ***B:*** *Effect of pH on the activity of lysozyme in 25 mM Tris-maleate buffer containing 100 mM KCl.*

Substrate concentration

In order to determine the substrate concentration where enzyme has the optimal activity, a series of various substrate concentrations were used (0.05-1.0 mg/ml). These concentrations were chosen based on the concentrations that used in previous studies (0.4-0.6 mg/ml)[132] with concentrations above and below these reported concentrations. Substrate concentration was measured in mg/ml because the molar concentration of the substrate cannot be determined due to its unknown molecular weight. The same turbidometry assay of Hash was conducted with the same buffer and pH conditions that determined above. It can be seen from Figure 3-21 A that the maximum activity of Slt35 was at substrate concentrations between 0.3 and 0.6 mg/ml and then declined to about zero by increasing the concentration due to the substrate inhibition.[195] The optimal lysozyme activity was observed at substrate concentrations above 0.6 mg/ml (Figure 3-21 B). Unlike Slt35, lysozyme activity reached the saturation after 0.6 mg/ml and was not inhibited by the increase of substrate concentration.

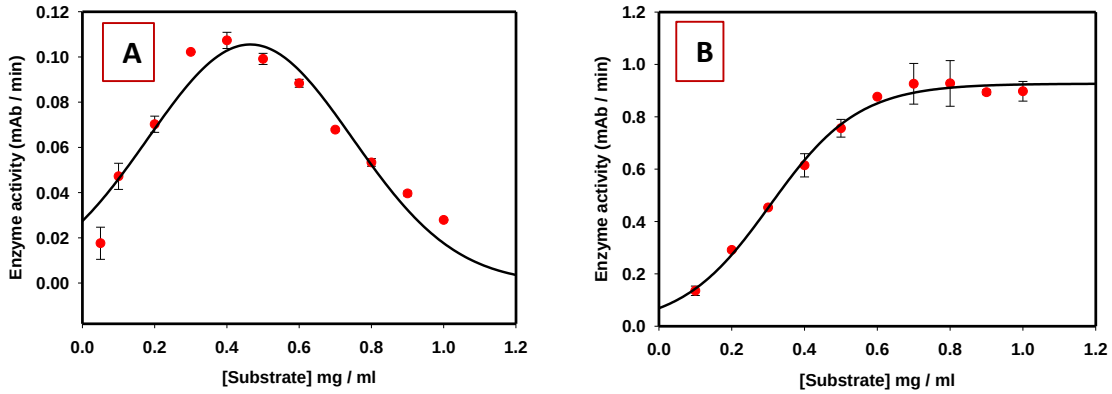

Figure 3-21: ***A:*** *Effect of substrate concentration on Slt35 activity in 25 mM Tris-maleate buffer, pH 5.8, supplemented with 10 mM $CaCl_2$.* ***B:*** *Effect of substrate concentration on lysozyme activity in 25 mM Tris-maleate buffer, pH 5.8, supplemented with 100 mM KCl.*

Final assay conditions

Following optimization of the assay conditions as described above, the final assay buffer used to determine Slt35 activity was 25 mM Tris-maleate at pH 5.8, containing 10 mM $CaCl_2$. For lysozyme assay, 25 mM Tris-maleate pH 6.0 supplemented with 100 mM NaCl was used. Whole cells were suspended in assay buffer and incubated at 37 ^{o}C before adding the purified enzyme. The decrease in turbidity was determined at 600 nm for 1 min. The initial rate of Slt35 was calculated over the first 40 s of the assay, while for lysozyme it was determined over the entire 60 s.

3.5 Enzyme inhibition

Inhibition of Slt35 and lysozyme activity was measured by using the same turbidometry method. Whole cells were suspended in assay buffer and incubated at 37 ^{o}C before adding the enzyme. Negative control experiments were conducted without inhibitor present in the reaction mixture. Thionine acetate (Figure 3-22), a known lysozyme inhibitor,[12] was used as a positive control. The effect of this inhibitor on lysozyme fluorescence has been measured but its IC_{50} has not been determined. Inhibition tests were performed by preincubating the enzyme with different concentrations of the potential inhibitors at 37 ^{o}C or r.t. Although these temperatures have been previously used for the incubation of the same enzymes,[118,119,132] in this study they lost about half of their activity during the incubation at these temperatures. Therefore, their activity was no longer affected by increasing the concentration of inhibitors.

To find the suitable temperature for inhibition assays, both Slt35 and lysozyme were incubated at different temperatures for 10 minutes before they were added to the mixture of substrate and buffer. It can be seen from Figure 3.23 that Slt35 lost its activity gradually as temperature was increased. The maximum lytic activity of Slt35 was recorded when the enzyme was incubated below 15 ^{o}C, while the enzyme lost about half of its activity at 25-40 ^{o}C, and at 50 ^{o}C the enzyme precipitated, in line with the melting temperature of 51.6 ºC measured (Section 3.2). However, increasing the temperature did not show any effect on lysozyme activity.

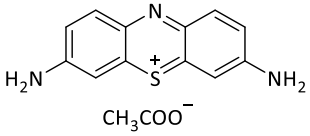

Thionine acetate

Figure 3-22: *Structure of thionine acetate.*

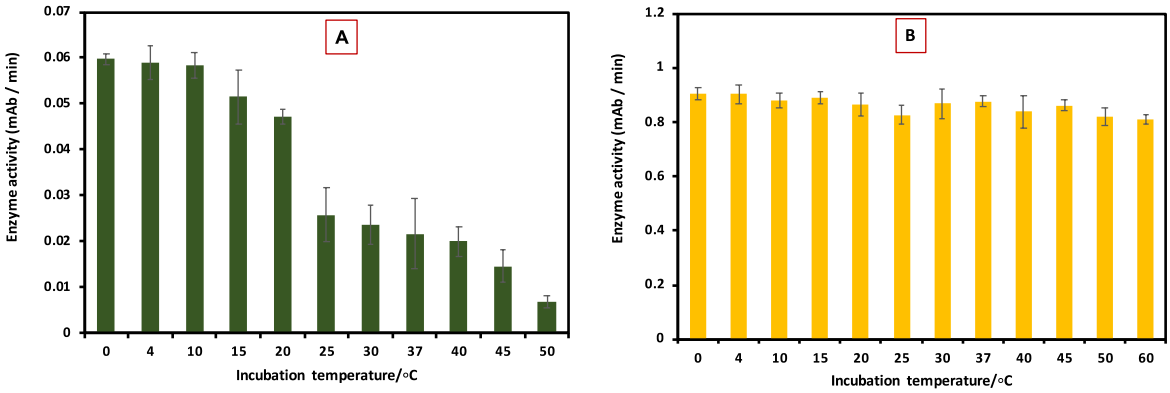

Figure 3-23: *Effect of temperature on Slt35 and lysozyme activity.* ***A:*** *Slt35 was incubated for 10 min at different temperatures before it was added to the substrate in 25 mM Tris-maleate buffer pH 5.8 containing 10 mM $CaCl_2$. B: Lysozyme was incubated at the same temperatures for 10 min before it was added to the substrate in 25 mM Tris-maleate buffer pH 6.0 containing 100 mM NaCl.*

Following these experiments, Slt35 was incubated with the inhibitor at 0 °C for 10 min before it was added to the mixture of the substrate and buffer while lysozyme was incubated at r.t. Thionine acetate was tested for inhibition of both lysozyme and Slt35. Turbidometry assay was used to determine IC_{50} values for each inhibitor in the same assay conditions that have been optimised above. By increasing the concentration of inhibitor, the rate of lytic reaction of both enzymes was decreased. Results are plotted as percent inhibition, by normalising between the rate in the absence of inhibitor (0% inhibition) and the rate in the absence of enzyme (100% inhibition). The concentration of inhibitor that was required to reduce the rate of enzymatic reaction by half was recorded as the IC_{50} value of each enzyme (Figure 3-24). The IC_{50} of lysozyme was found to be 89.3 ± 3 µM, while the IC_{50} of Slt35 was not observed.

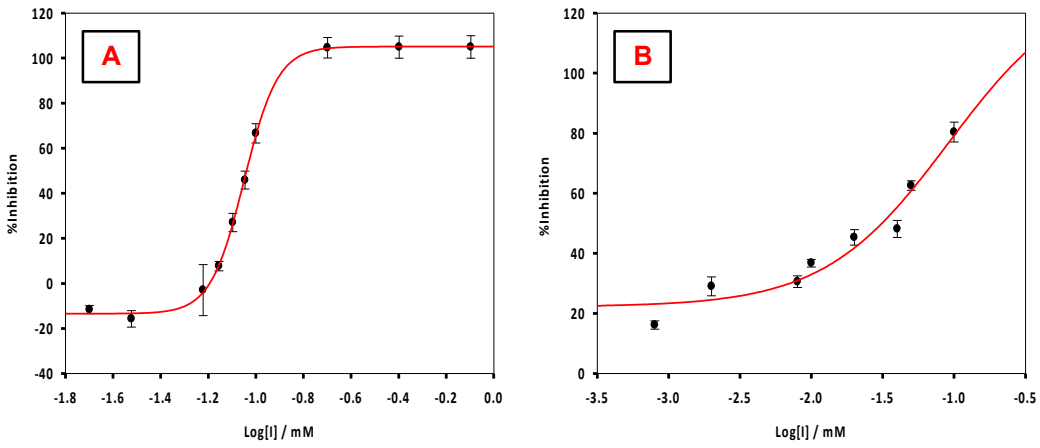

Figure 3-24: *Effect of thionine acetate on the enzymatic activity of lysozyme (A) and Slt35 (B)***.** Complete inhibition of Slt35 activity was not observed.

3.6 Conclusion

Although Slt35 has been previously expressed and purified, the solubility and stability of the protein was initially very poor. To optimise protein purification and gain soluble active protein, different conditions including those involved in expression, purification and storage were adjusted. Initially, protein production was performed at low temperature using a recently transformed colony. To the lysis, purification and dialysis buffers was added a mild non-ionic detergent Tween-20 to improve protein solubility by breaking protein non-specific binding. The enzyme was stable within nineteen days as CD results showed, subsequent it is stored in the dialysis buffer at 4 ^{o}C.

The dependence of enzyme activity on different factors, including salt concentration, pH, substrate concentration and temperature were examined in order to determine the optimal assay conditions for the kinetic analysis of enzyme. Different salts with different concentrations were used to test the effect of the type and strength of metal on the enzyme function. The pH profile was generated to determine the optimal pH of the enzyme activity. The lytic activity of Slt35 was very sensitive to the slight changes of pH while lysozyme activity was less affected. Substrate concentration affects the rate of enzyme activity; therefore, it has been tested for both enzymes. As discussed above in this chapter, Slt35 was inhibited by increasing the substrate concentration over 0.6 mg/ml whereas lysozyme reached the saturation curve at 0.5 mg/ml. The effect of temperature on the enzyme activity was observed when the inhibition of Slt35 by thionine acetate was conducted by incubation of the mixture of enzyme and inhibitor at 37 ^{o}C. Therefore, the incubation was tested at different temperatures and the higher activity of enzyme was found when the enzyme was incubated at 0 ^{o}C while lysozyme was not affected by the change of the temperature.

4 Biological Evaluation of Inhibitors

4.1 Introduction

Enzymes are proteins that catalyse biochemical reactions involved in cellular life. They show a selectivity toward a particular substrate or group of substrates in a single chemical reaction.[196] The rate of catalysed enzymatic reactions is typically faster than that of spontaneous reactions by 10^6 to 10^{12} times.[197] They bind to the substrate through a region of their tertiary structure called the active site, which is normally a cleft or cavity with an array of amino acids sidechains. The substrate is bound to the enzyme by different binding types, e.g. electrostatic interactions, hydrogen bonding, van der Waals forces, and hydrophobic interactions. Following binding with substrate, formation of an enzyme-substrate complex occurs, and then product transformation via a transition state complex.[198]

Enzymes are susceptible to inhibition by molecules that affect the rate of enzymatic reactions. Usually, these molecules are relatively small with molecular weight no more than 500 Da, they normally have polarizable groups, a number of specifically oriented heteroatoms and hydrogen bond donors.[199] Hence, enzyme inhibition presents an attractive target for new drug therapy, they also used in cells to regulate the enzyme activity. There are two different classes of inhibitors: **1)** reversible inhibitors include three types: competitive, uncompetitive and non-competitive. **2)** irreversible inhibitors.

4.2 Evaluation of inhibitors

Kinetic studies of Slt35 and lysozyme were conducted by monitoring the decrease in turbidity of *Micrococcus lysodeikticus* cell suspension. Inhibition potency is represented by the IC_{50}, the concentration of inhibitor required to reduce the enzyme activity by 50%. The IC_{50} values were determined by using the turbidometric assay that was performed to investigate enzyme activity as discussed in Chapter 3. The first experiment was conducted in the absence of inhibitors and then repeated by using various concentrations of each inhibitor separately.

4.2.1 Evaluation of some known glycosidase inhibitors

Iminosugars are polyhydroxylated alkaloids that have the ability to inhibit glucosidases, enzymes involved in carbohydrate metabolism. Generally, iminosugars present potential candidates for the treatment of a broad range of diseases, including type II diabetes, cancer, lysosomal storage disorder and viral infection. These biological activities may be due to their capacity to mimic the conformation of the glycosyloxocarbenium ion-like transition state in the enzymatic glycoside hydrolysis reaction. 1-deoxynojirimycin **(92)**, a D-glucose analogue, is the best known iminosugar that might have the ability to bind lytic transglycosylases by simulating the charge of the corresponding glycosyl cation of the enzymatic reaction transition state of glycoside hydrolase.[200] For this reason, it was tested against Slt35 activity. The NAG-thiazoline derivative thiamet G **(93)** is a potent inhibitor of β-acetylglucosaminidases.[139] Because synthesis of NAG-thiazoline, a structural analogue of the oxazolium intermediate of the LT catalytic reaction, failed (Chapter 2), thiamet G was tested for inhibition of Slt35 activity due to the similarity in their structures. Miglitol (Glyset) **(94)** is currently used as a drug for treatment of type II diabetes[201] and castanospermine **(95)** has been reported as a potent inhibitor of β-glucosidases.[202] These two inhibitors were also tested for inhibition of Slt35 activity.

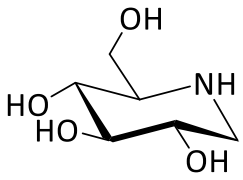

1-Deoxynojirimycin (92)

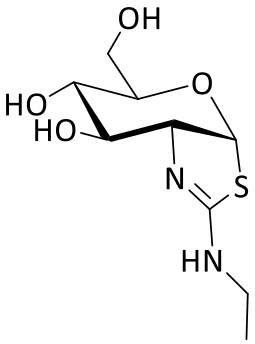

Thiamet G (93)

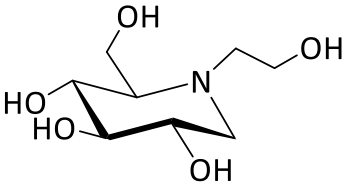

Miglitol (94)

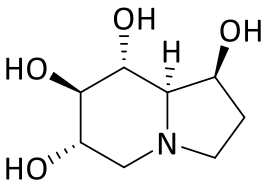

Castanospermine (95)

Figure 4-1: *Structure of some known glycosidase inhibitors.*

Unfortunately, all of these compounds were inactive toward this enzyme even at high concentrations (up to 10 mM) (Figure 4.2). All these inhibitors were also assessed against lysozyme activity, but they did not display any inhibition at concentrations up to 10 mM.

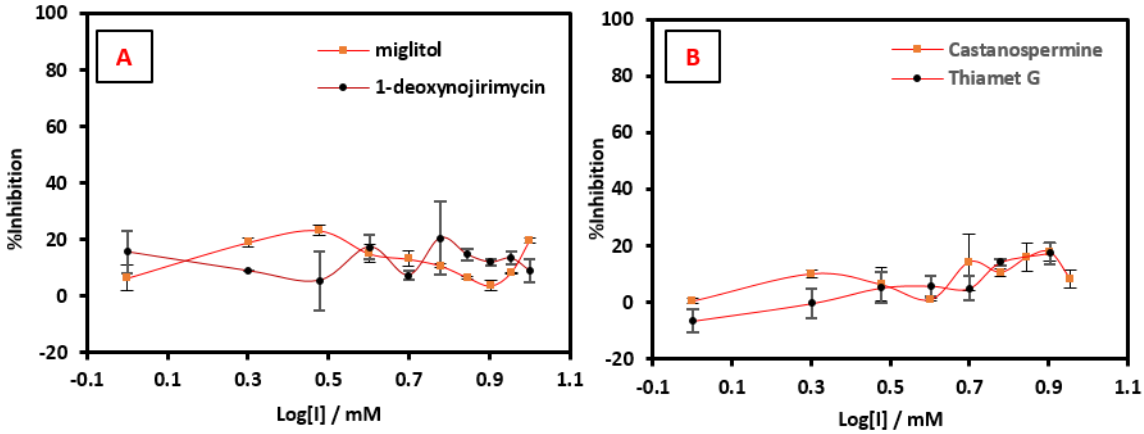

Figure 4-2: *Effect of some known glycosidase inhibitors on enzymatic reaction catalysed by Slt35.*

This weak inhibition observed from these compounds could be explained by the small size of these compounds compared to bulgecin (Figure 4-3), therefore, they lack the possibility of interacting with sufficient amino acid residues in the enzyme active site.

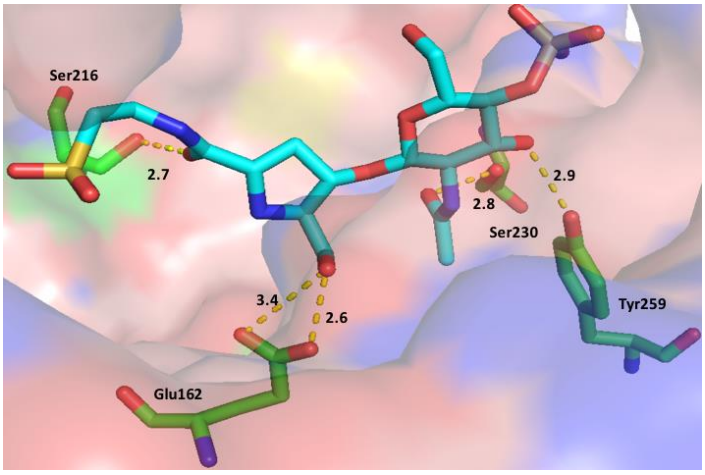

Figure 4-3: *Surface representative of Slt35 active site bound with Bulgecin A showing the binding mode between Bulgecin and the most important residue in the enzyme active site.*

4.2.2 Evaluation of synthesised inhibitors against Slt35

After the target molecules were synthesised, they were assessed against Slt35 and some of them against lysozyme (**35b-d**). In general, there was no significant inhibition from these compounds against lysozyme activity at the concentrations used. Both compounds **35b** and **35d** started to inhibit lysozyme activity at 5 mM while compound **35c** started to inhibit at 1 mM (Figure 4-4) and since the amount available was insufficient to use at higher concentrations than 1 mM, the IC_{50} of this inhibitor was not measured. However, most of the compounds displayed inhibition in the high micromolar range against Slt35. The inhibitory activity of **35a-e** and **35g** was first evaluated against Slt35 (Figure 4-5).

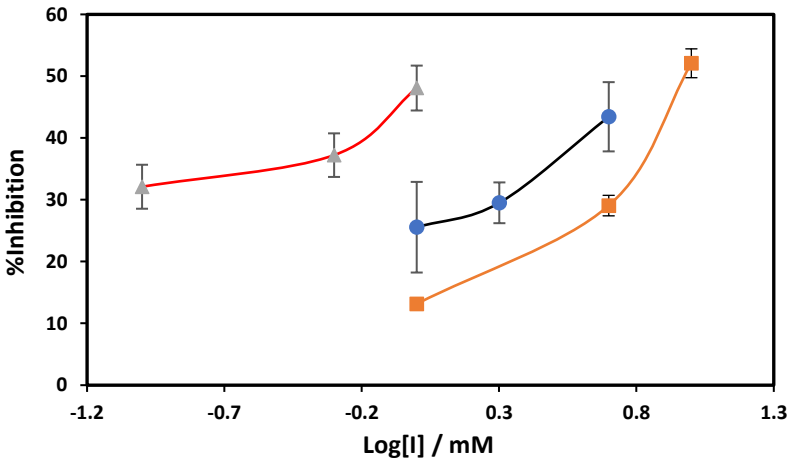

Figure 4-4: *Effect of some synthesised amidine derivatives on enzymatic activity of lysozyme. Amidine with side chain; propyl* ***(35b, brown)****, cyclohexyl* ***(35c, red)*** *and 2-fluorobenzyl* ***(35d, black)****.*

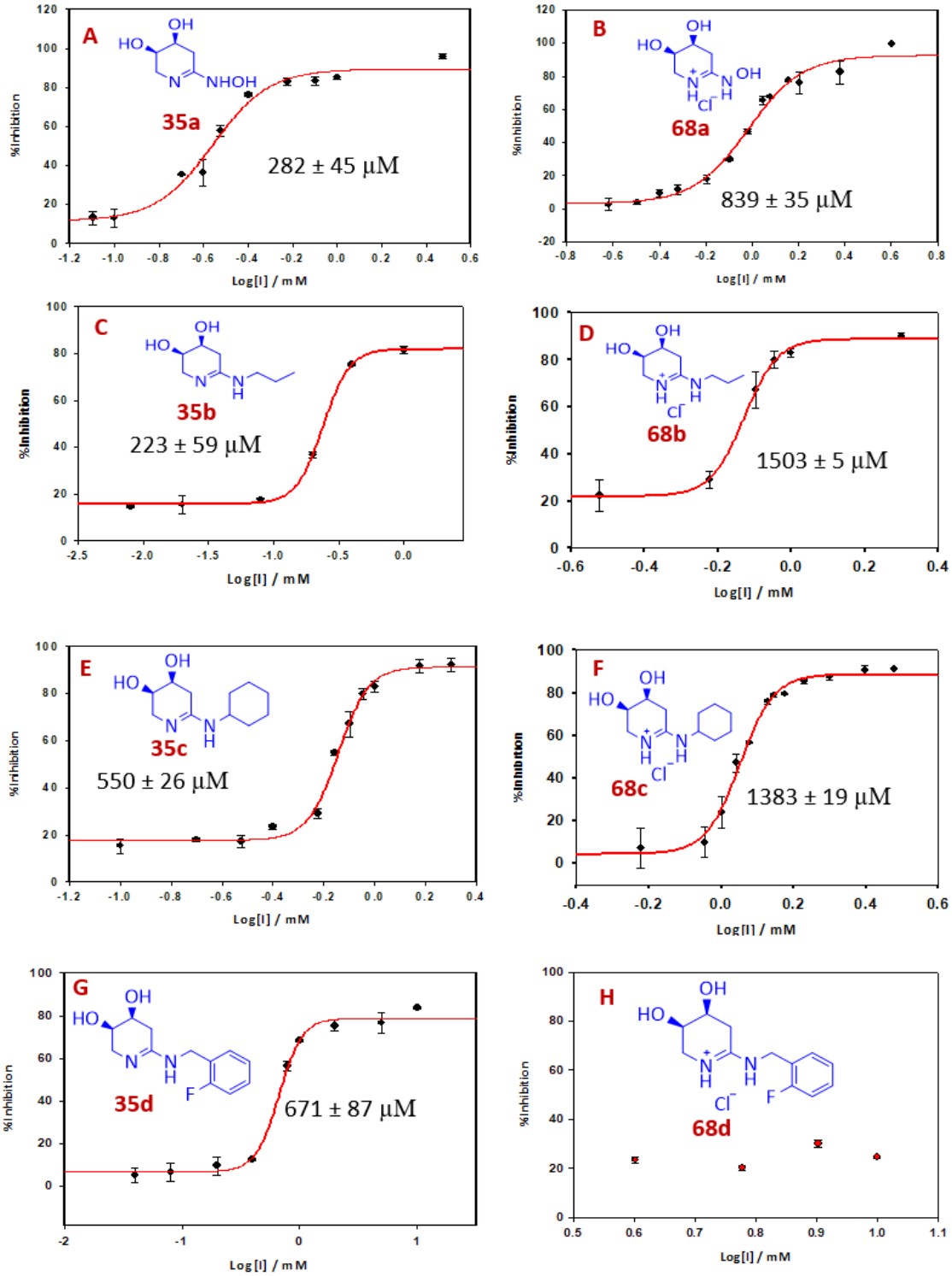
A
35a
282 ± 45 µM
B
68a
839 ± 35 µM
C
35b
223 ± 59 µM
D
68b
1503 ± 5 µM
E
35c
550 ± 26 µM
F
68c
1383 ± 19 µM
G
35d
671 ± 87 µM
H
68d
%Inhibition
Log[I] / mM

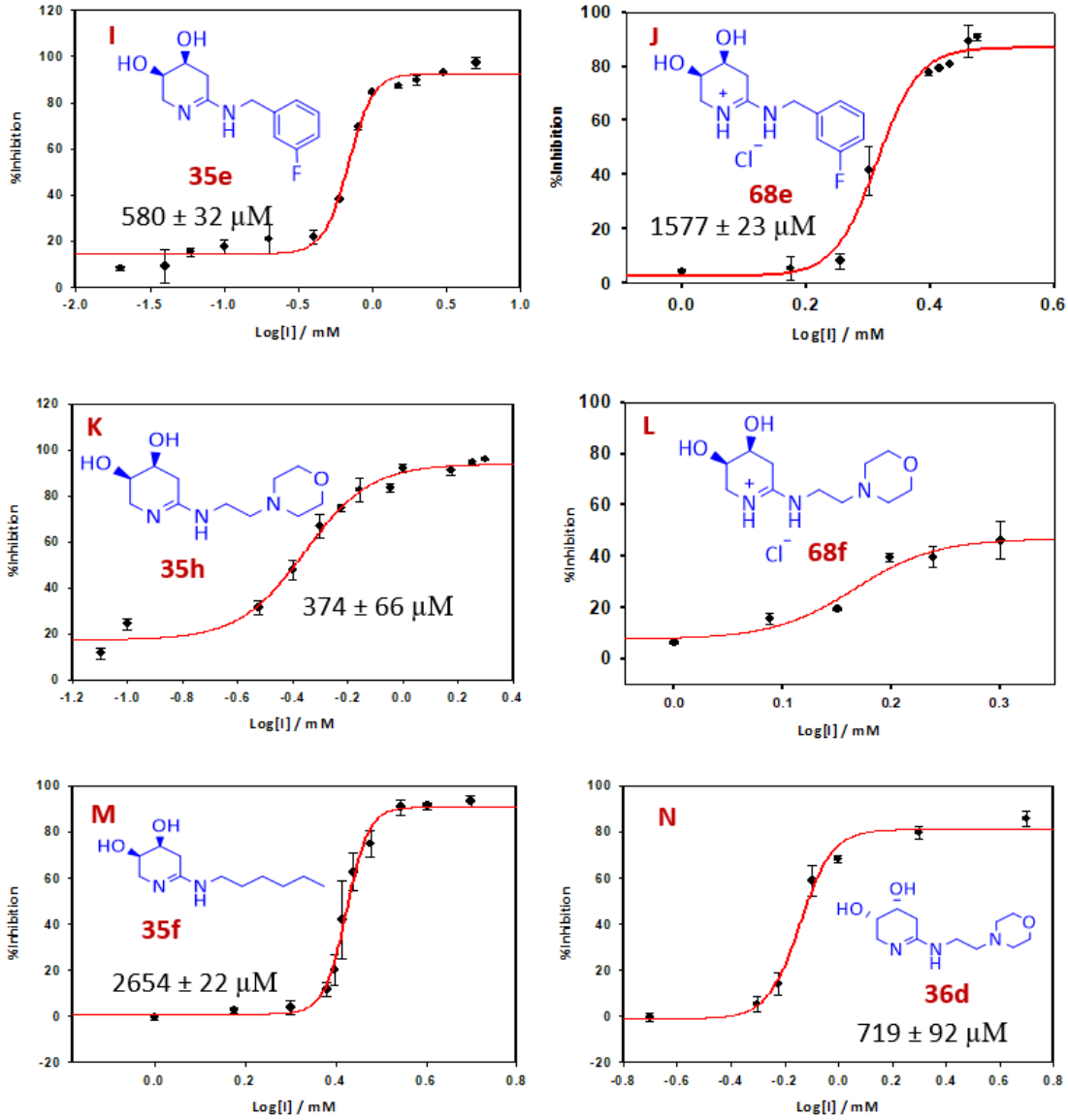

Figure 4-5: *IC_{50} curves of amidine derivatives against Slt35 activity using Micrococcus lysodeikticus cells as a substrate. IC_{50} values are indicated on each panel.* ***A); (35a)****: Free base amidine with hydroxyl group, compound concentrations range 0-3 mM.* ***B); (68a)****: Amidine salt with hydroxyl group, compound concentrations range 0-5 mM.* ***C); (35b):*** *Free base amidine with n-propyl side chain, compound concentrations range 0-0.8 mM.* ***D); (68b)****: Amidine salt with n-propyl side chain, compound concentrations range 0-2 mM.* ***E); (35c)****: Free base amidine with cyclohexyl side chain, compound concentrations range 0-2 mM.* ***F); (68c)****: Amidine salt with cyclohexyl side chain, compound concentrations range 0-3 mM.* ***G); (35d)****: Free base amidine with 2-fluorobenzyl side chain, compound concentrations range 0-5 mM.* ***H); (68d)****: Amidine salt with 2-fluorobenzyl side chain.* ***I); (35e)****: Free base amidine with 3-fluorobenzyl side chain, compound concentrations range 0-3 mM.* ***J); (68e)****: Amidine salt with 3-fluorobenzyl side chain, compound concentrations range 0-3 mM.* ***K); (35h)****: Free base amidine with ethyl morpholine side chain, compound concentrations range 0-2 mM.* ***L); (68f)****: Amidine salt with ethyl morpholine side chain.* ***M); (35f)****: Free base amidine with hexyl side chain, compound concentrations range 0-5 mM.* ***N); (36d)****: Amidine salt with ethyl morpholine side chain, compound concentrations range 0-5 mM.*

The results showed that the amidine **35b** with a linear side chain consisting of three carbons gave the lowest IC_{50} value while no IC_{50} could be detected for **35g**. The inhibitory effect of the salts of most compounds was also determined. In general, the inhibitory efficiency of amidine chloride derivatives is less than that for amidine derivatives themselves.

Replacement of the propyl group by a hydroxyl group in amidoxime **35a** resulted in weaker inhibition (IC_{50} 282 ± 45 μM) (Figure 4-5 A) than that for the parent compound **35b** (IC_{50} 223 ± 59 μM) (Figure 4-5 C). This decrease in the inhibition ability of this compound may be due to the interaction of the catalytic residue Glu162 with NH-OH instead of the amidine group, as predicted by docking software (Section 2.2.2). However, the salt form of amidoxime **68a** displayed inhibitory efficiency (IC_{50} 839 ± 35 μM) (Figure 4-5 B) higher than that determined of the salt form of amidine with propyl group **68b** (IC_{50} 1503 ± 5 μM) (Figure 4-5 D), which is consistent with the predicted interaction with the catalytic residue.

Amidine with aglycon consisting of a 6-membered cyclic amine attached directly to the amidine group **35c** and its salt form **68c** were found to be inhibit Slt35 activity with IC_{50} 550 ± 26 μM and 1383 ± 19 μM respectively (Figure 4.5 E and F). The reduction in the inhibition efficacy is attributed to steric constraints for the large cyclohexyl substituent. A similar decrease of the inhibition ability is apparent when comparing the effect of inhibitors with *N*-benzyl aglycons substituted with fluoride on *ortho* **35d** (671 ± 87 μM) or *meta* **35e** (579.5 ± 32 μM) position (Figure 4-5G and 4-5I) respectively. Although the molecular docking predicted more interactions between compound **35e** and the amino acid residues in the enzyme active site than that with compound **35d**, the IC_{50} of **35d** is slightly higher than **35e**. Generally, in comparison between *ortho* and *meta* substituent, *meta*-fluorobenzylamidine has inhibition ability slightly higher than that for *ortho*-fluorobenzylamidine. With this observation in hand and the molecular docking prediction, there is a hydrogen bonding between fluoride in the meta position and NH_2 group on the side chain of residue Asn339 (Chapter 2, Figure 2-7H). On the other hand, salt form of *meta*-fluorobenzylamidine **68e** showed an inhibition against the enzyme activity of Slt35 (1577 ± 23 μM) (Figure 4-5 J) while salt form of *ortho*-fluorobenzylamidine **68d** did not show any inhibition up to 8 mM (Figure 4-5 H).

To support the hydrophobic effect of the amidine moiety in compound **35b**, compounds **35f** and **35h** with hexyl and morpholine groups respectively were synthesised, and their ability to inhibit enzyme activity was compared to the parent compound **35b**. The increase of chain length of the hexyl group in compound **35f** strongly lowered the inhibition ability (IC_{50} 2654 ±

22 µM) (Figure 4-5 M) compared to the parent inhibitor (IC_{50} 223 ± 59 µM)**,** which is attributed to steric constraints of the hexyl chain in the active site. Replacement of a methyl group in the propyl side chain in compound **35b** by morpholine group **35h** led to reduction of inhibitory potency giving (IC_{50} 374 ± 66 µM) (Figure 4-5 K) but it is higher than that for **35f**. This observation indicates that might be the endo-cyclic oxygen in the morpholine ring side chain bounded to the amino acid residues in the enzyme pocket by H-bonding. Meanwhile, its inhibition potency is still smaller than that of the parent compound **35b**, which can be illustrated by a steric constraint of the morpholine ring in the active site.

In contrast, the inhibitor with a hydroxyl group on the *ortho* position **35g** did not display any inhibition against Slt35 activity (Figure 4-6) and lysozyme.

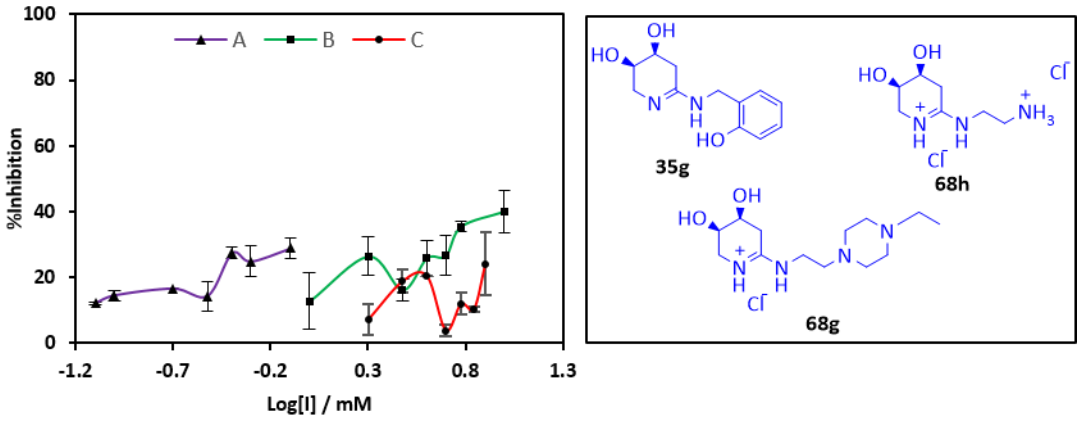

Figure 4-6: *Effect of some amidine derivatives on enzymatic hydrolysis of Slt35.* ***A****: Free base amidine with 2-hydroxybenzyl side chain* ***(35g)****.* ***B****: Amidine salt with ethyl amino side chain* ***(68h)****.* ***C****: Amidine salt with ethyl piperazine side chain* ***(68g)****.*

Amidine derivatives with ethyl amino and ethyl piperazine substituents (compounds **68h** and **68g** respectively) are also not active against Slt35 activity up to 8 mM (Figure 4.6). This behaviour of compound **68h** is probably due to the effect of the charge on the terminal amino group of the side chain. Obviously, compound **68g** contains steric constraints due to the large size of the alkylated piperazine ring, which might cause a change in molecular conformation inside the enzyme pocket.

Compounds derived from 2-deoxy-L-ribose **36a-c** were evaluated against Slt35 activity but displayed very weak inhibition after 8 mM concentration (Figure 4-7). Indeed, this decrease of the inhibition ability of these analogues could be due to the change of the orientation of (HO-3 and HO-4) in the amidine six-membered ring that caused change of the confirmation of

these compounds in the active site as predicted by docking (Chapter 2). According to the molecular docking prediction, there is a hydrogen bonding between the catalytic Glu162 in the active site and nitrogen atom in the amidinium group of compound **36a** but the conformation of propyl side chain is changed, subsequently the hydrophobic interaction with the amino acid residues were weak. Although the conformation of compound **36c** was completely changed in the active site pocket, the evaluation of this inhibitor indicated that it started to affect the enzyme activity after 8 mM as well. In contrast, compound **36b** with cyclohexyl side chain did not show any inhibition against Slt35 activity, this observation is consistent with the molecular docking prediction where the catalytic residue was far away from the molecule.

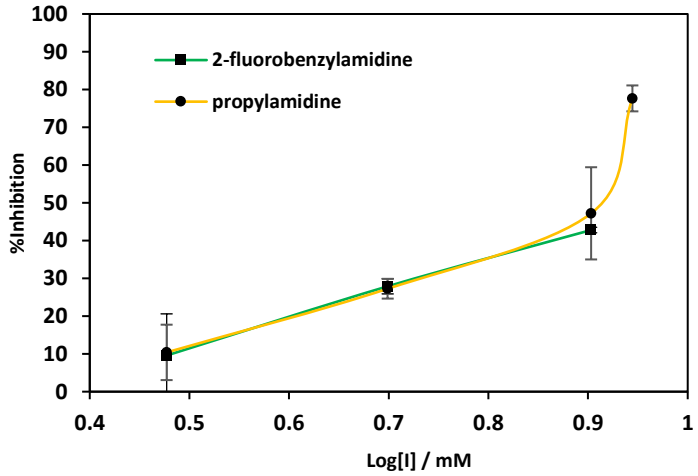

Figure 4-7: *Effect of some amidine derivatives derived from 2-deoxy-L-ribose on enzymatic hydrolysis of Slt35. Amidine with 2-fluorobenzyl side chain* ***(36c)*** *(green line). Amidine with propyl side chain* ***(36a)*** *(yellow line).*

Interestingly, compound **36d** showed inhibition ability against Slt35 (719 ± 92 μM) (Figure 4-5N) weaker than its enantiomer **35h** but better than other molecules that have the same orientation of the two hydroxyl groups on the amidine ring. The different affinity of this compound might be attributed to the presence of morpholine group which probably changed the structural conformation of this inhibitor, consequently enhanced the binding with amino acid residues in the enzyme active site. The difference between the two enantiomers **35h** and **36d** may be rationalised by the different orientation of both hydroxyl groups (OH-3 and OH-4) on the amidine ring, which led to insufficient interaction of hydroxyl groups in the active

site and change the structural conformation of the inhibitor as predicted by docking (Chapter 2) with compounds having the same amidine ring.

On the other hand, amidines derived from non-sugar- based starting material **55** did not show any inhibition toward both Slt35 and lysozyme activities.

The inhibition data of all synthesised free bases amidine derivatives in comparison with the corresponding salts of most of them are summarised in Figure **4-8** and Table 4-1. Although both the free base and the salt amidine derivatives would predominately exist in the ionized state at assay buffer pH (5.8), IC_{50} values of salts are much higher than that for free bases amidines, as mentioned above. The lower activity of the salts may be due to the presence of inorganic salts in the salt samples; this could be clarified by elemental microanalysis. The lowest IC_{50} among the free amidines was for the compound with a propyl substituent side chain **35b** while for the salts it was amidoxime **68a.**

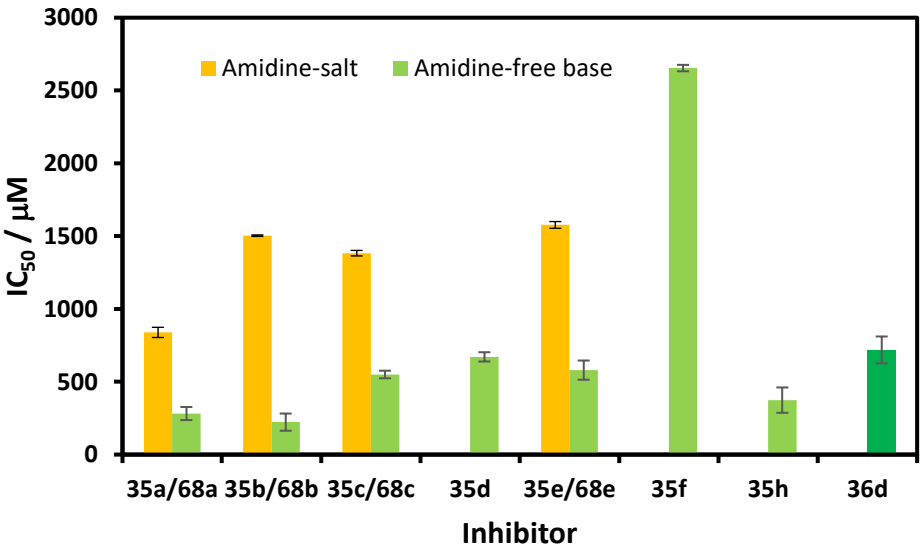

Figure 4-8: *Differences in the inhibition potency of synthesised amidine derivatives. Green bars represent free base amidine inhibitors* ***(35a-f)*** *whereas yellow bars represent amidine salts* ***(68b, 68c, 68e and 68a)****.* ***36b/68b****: propyl side chain.* ***35a/68a****: hydroxyl group.* ***35c/68c****: Cyclohexyl side chain.* ***35e/68e****: 3-Fluorobenzyl side chain.* ***35h****: Ethyl morpholine side chain.* ***35d****: 2-Fluorobenzyl side chain.* ***35f****: Hexyl side chain.* ***36d****: Enantiomer of* ***35h****.*

The simulated docking of some synthesised amidine compounds by BUDE software had predicted that compounds (**35a-e**) bind to the catalytic residue in the enzyme active site Glu162, while the enantiomers (**36a-c**) did not show any binding with this residue except (**36a)** which showed weak binding through a single hydrogen bond (Section 2.2.2). In general, the predicted binding energies of all docked amidine compounds are not very high and are not very different overall (Table 4-1). However, the trend of the predicted energy (E_{score}) values is

not consistent with the assay results. This can be attributed to the low accuracy of the software used, the results of which can only be used as a guide rather than firm evidence.

Compound (free base)	MolDock Score (kcal / mol)	IC_{50} (μM)	Compound (salt)	IC_{50} (μM)
35a	-55.00	282 ± 45	**68a**	839 ± 35
35b	-65.54	223 ± 59	**68b**	1503 ± 5
35c	-70.46	550 ± 26	**68c**	1383 ± 19
35d	-71.19	671 ± 87	**68d**	ND
35e	-73.41	580 ± 32	**68e**	1577 ± 23
35f	-----	2654 ± 22	**68f**	ND
36g	-----	ND	-----	-----
35h	-----	374 ± 66	-----	-----
36a	-66.33	ND	-----	-----
36b	-70.52	ND	-----	-----
36c	-70.54	ND	-----	-----
36d	-----	719 ± 92	-----	-----

Table 4-1: *The IC_{50} values (μM) of all amidine derivatives for the inhibition of Slt35 and calculated energies of some docked amidine free bases. Reported IC_{50} values are mean ± standard deviation from two or three biological replicates, each with three technical replicates. ND: no inhibition detected.*

4.2.3 Evaluation of binding of inhibitors with enzymes

The extinction of the intrinsic fluorescence of protein was used to determine binding of inhibitors to Slt35 and lysozyme by titration with increasing concentration of each compound. Lysozyme contains six tryptophan residues (Trp28, Trp62, Trp63, Trp108, Trp111 and Trp123) (Figure 4.9B); Trp62 and Trp108 are located at the active site.[203] It has been reported that Trp62 and Trp108 are the most important residues that contribute to lysozyme fluorescence while residues 28, 63, 111 and 123 make small contributions.[204] Slt35 contains eight tryptophan (Trp247, Trp165, Trp134, Trp265, Trp114, Trp326, Trp349 and Trp145) and sixteen tyrosine residues. Most of tryptophan residues in Slt35 are located on the loop close to the active site (Figure 4-9A) while tyrosine residues (Tyr117, Tyr191, Tyr259, Tyr338 and Tyr344)

are lined in the active site groove.[133] If these fluorophores interacted with small molecule, the emission intensity of the enzyme will decrease. The emission spectra of intrinsic fluorescence were recorded in the range from 300 to 450 nm. The maximum emission of both enzymes was observed at 344 nm with slight shifts to lower wavelengths.

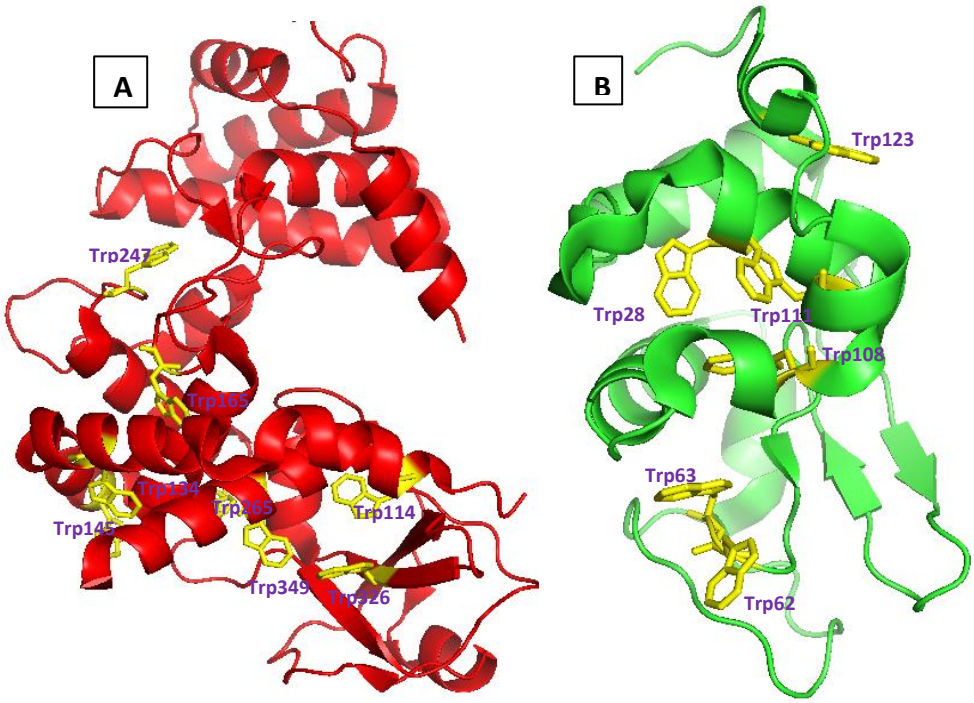

Figure 4-9: *Cartoon representative of three-dimensional structure of hydrolase enzymes. A; Slt35 structure with eight tryptophan residues (PDB 1QUS).[115] B; Lysozyme structure with six tryptophan residues (PDB 2VB1).[205]*

To study the binding of both enzymes to the inhibitors, commercially available thionine acetate (TH) was initially used. Fluorescence quenching by thionine acetate has been reported for lysozyme[74] but not Slt35. This inhibitor showed saturable binding to the enzyme active site of both enzymes (Figure 4-10C and 4-10D; K_d(Slt35)= 17.1 ± 1 µM, K_d(lys)= 18.6 ± 1.2 µM).

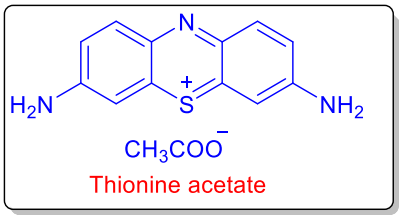

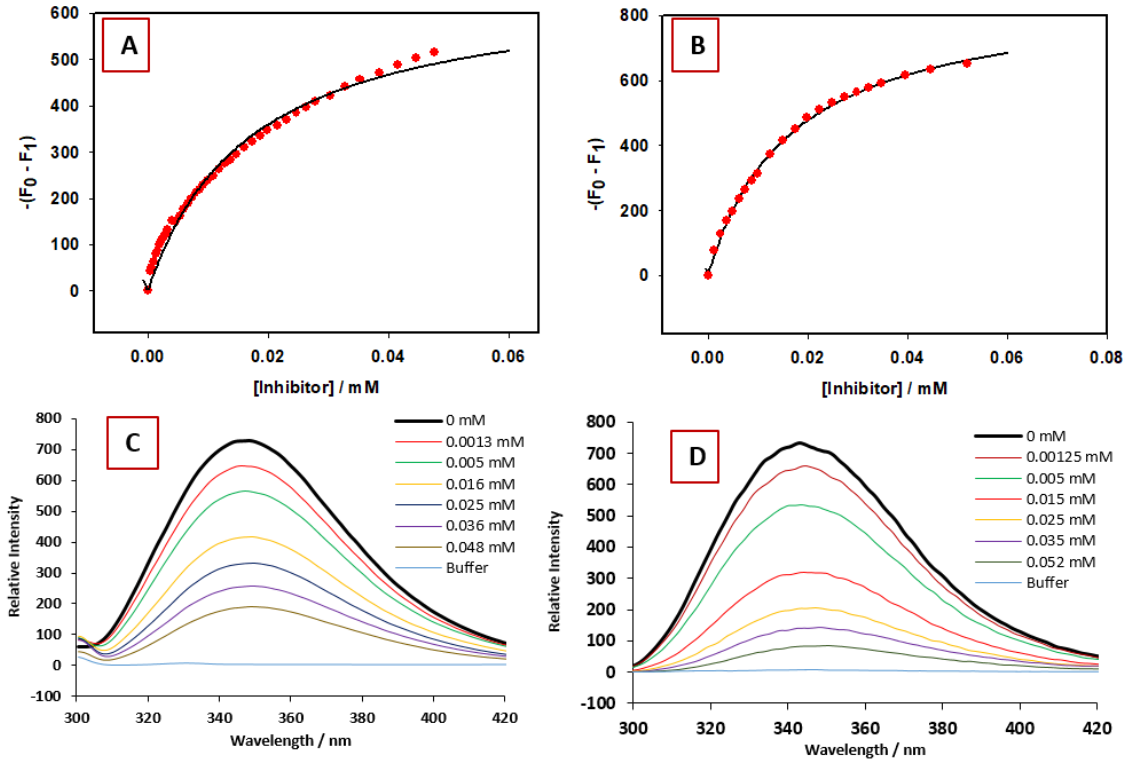

Figure 4-10: *Fluorimetric titration of thionine acetate* ***(14)*** *complexed to lysozyme or Slt35:* ***A****: Change in the intensity of fluorescence TH-lysozyme.* ***B****: Change in the intensity of fluorescence TH-Slt35.* ***C****: The intrinsic emission of Trp residues for lysozyme. A 2.3 µM concentration of lysozyme was titrated with maximum concentration 0.048 mM TH.* ***D****: The intrinsic emission of Trp residues for Slt35. A 3.0 µM concentration of Slt35 was titrated with maximum concentration 0.052 mM TH.*

The inhibition ability of this compound against both enzymes were measured by determining the IC_{50} (Chapter 3). The IC_{50} against lysozyme was 89.3 ± 3 µM while no inhibition was detected for Slt35. The observation of binding but not inhibition of Slt35 by thionine acetate could be attributed to the interaction of the ligand with the β-domain of the enzyme, which contains most of the tryptophan residues, rather than the active site.

Binding affinities of some synthesised amidine salts (**68a, 68b** and **68c**) to Slt35 were determined. The interactions of these inhibitors with Slt35 were very weak comparing to thionine acetate. Generally, the possible reason for this big difference could be due to the hydrophobic and π-stacking interactions between tryptophan residues in Slt35 and thionine acetate, which contains three aromatic rings.

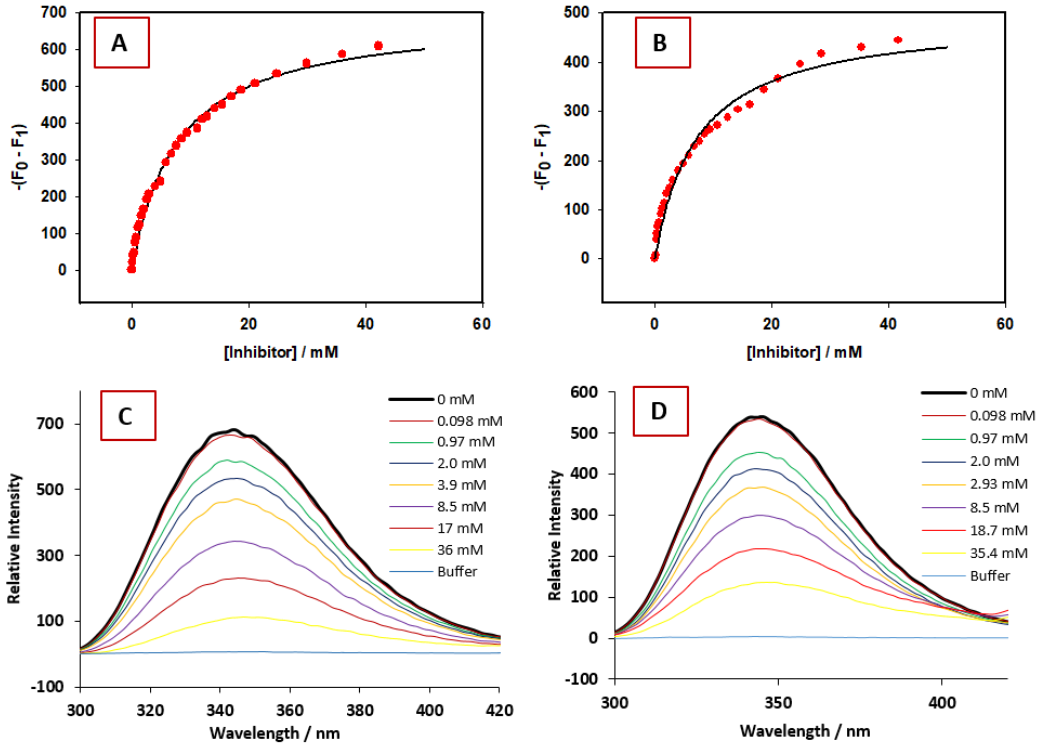

Figure 4-11: *Fluorimetric titration of amidine salts **68h** and **68a** complexed to Slt35: **A**: Change in the intensity of fluorescence of **68a-Slt35** at 280 nm. **B**: Change in the intensity of fluorescence **68b-Slt35**. **C**: The intrinsic emission of Trp residues for Slt35. A 3.0 µM concentration of Slt35 was titrated with maximum concentration 36 mM compound **68a**. **D**: The intrinsic emission of Trp residues for Slt35. A 3.0 µM concentration of Slt35 was titrated with maximum concentration 35.4 mM compound **68b**.*

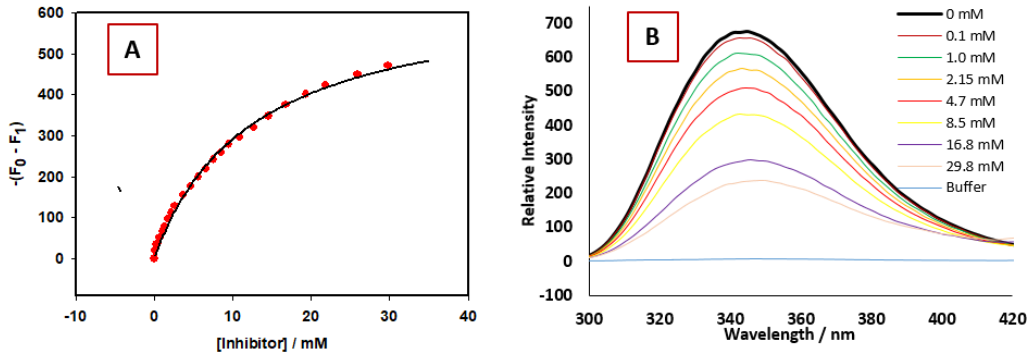

Figure 4-12: *Fluorimetric titration of amidine salt **68b** complexed to Slt35: **A**: Change in the intensity of fluorescence of **68c-Slt35** at 280 nm. **B**: The intrinsic emission of Trp residues for Slt35. A 3.0 µM concentration of Slt35 was titrated with maximum concentration 29.8 mM compound **68c**.*

The effect of the three chosen amidine salts on the Slt35 emission was similar at high mM concentration (Table 4-2).

Comp. no.	K_d / mM (Slt35)	K_d / mM (lysozyme)
68a	8.4 ± 0.7	------
68b	9.0 ± 1.8	------
68c	10.5 ± 1.6	------
TH	0.0171 ± 0.0010	0.0186 ± 0.0012

Table 4-2: *K_d values of Slt35 complexed to some amidine salts and thionine acetate and lysozyme complexed to thionine acetate. Reported values are mean ± standard deviation from two (in case of amidine salts) or three (in case of thionine acetate) biological replicates, each with three technical replicates.*

Based on the structure and the lowest IC_{50} value of the amidine inhibitors in this study, compound **35b** was chosen as a general basis for the development of new inhibitors (Figure 4-13). By taking the side chain and replacing the terminal methyl group by a polar group like hydroxyl, carboxyl or amino group, a hydrogen bonding interactions between this group and Gln225 and/or Ser216 residues in the enzyme pocket may be formed. Extension of the hydroxyl groups in positions 3- and 4- in the amidine six-membered ring could improve the interactions between the inhibitor and Ser230 and/or Tyr259 residues in the active site. Moreover, incorporation of bulky and polar groups in positions 2- and 5- in the six-membered ring instead of hydrogen may enhance the binding of the inhibitor to the amino acid residue.

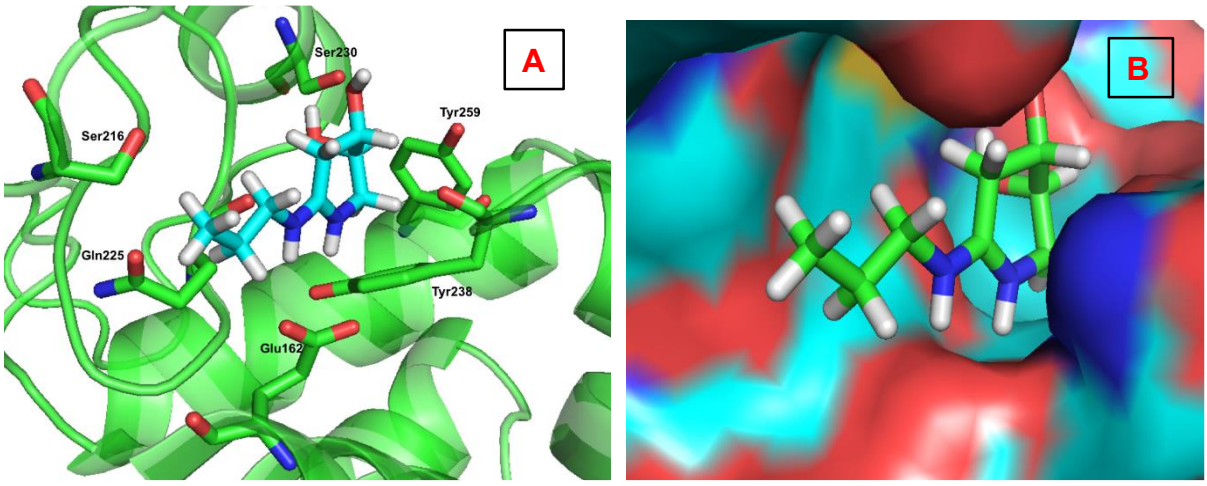

Figure 4-13: *Computational binding mode of amidine derivative with propyl side chain **35b** in the Slt35 active site. **A**: Cartoon representative showing the amino acid residues in the active site located close to the ligand. **B**: Representative surface of the binding site.*

According to Figure 4-13B, incorporation of any hydrophobic group in the ring or side chain will not be useful to improve the inhibition ability of the new designed inhibitors. This speculation is supported by looking at the IC_{50} of the inhibitor with a hexyl side chain **35f** compared to that with a propyl group, **35b**. Some of these improvements have been performed in this study such as compound **65a** with two hydroxyl groups in 2 and 3 in the propyl side chain but deprotection of this molecule has not been performed. Another suggested development is gluconoamidine, its synthesis has been started but not completed.

4.3 Conclusion

Initially, some known glycosidase sugar-based inhibitors and thionine acetate were evaluated against Slt35 and lysozyme activities. All glycosidase inhibitors were inactive toward both enzymes while thionine acetate showed an inhibition against the activity of these enzymes. Compounds that were produced in this study were evaluated against Slt35 and IC_{50} curves were generated for most of them except those did not show any inhibition activity. In general, the inhibition activity of synthesised amidine derivatives was poor. Amidine derivatives produced from the starting material 2-deoxy-L-ribose were inactive against enzyme activity except that with a morpholine moiety, which exhibits inhibition at high micromolar concentration. This observation was consistent with the molecular docking predictions discussed in Chapter 2. The most potent inhibitor amongst the synthesised amidine derivatives derived from 2-deoxy-D-ribose in this work was the compound with propyl side chain **35b**. Most inhibitors were investigated in two forms, free base and hydrochloride salt form and their inhibition against Slt35 activity was compared. Generally, hydrochloride salts displayed less activity toward the enzyme and some salts did not show any inhibition even at high concentrations (i.e. **68h**, **68d** and **68g**). The binding of thionine acetate to both lysozyme and Slt35 was stronger than that of amidine salts (**68a**, **68b** and **68c**).

5 Conclusions and future directions

5.1 Conclusions

The research presented in this thesis includes design, organic synthesis and subsequent evaluation of new soluble lytic transglycosylase (Slt35) inhibitors. The first plan was synthesis of the known β-hexosaminidase inhibitor NAG-thiazoline. Although it has low affinity towards Slt35 (K_d = 1.36 ± 0.077 mM),[117] its interaction has not been studied. Therefore, our direction was to crystallise this compound with Slt35, investigate their interactions and then improve the chemical structure of this compound. Unfortunately, this synthesis failed, despite many attempts.

The bulk of the work therefore focused on the design, organic synthesis and evaluation of potential novel inhibitors based on the structure of the oxocarbenium ion intermediate in the enzyme catalytic mechanism. Five different amidine derivatives derived from 2-deoxy-D-ribose were first designed and docked using BUDE. The interactions between these compounds and the catalytic residue Glu162 in the active site were analysed. Accordingly, it was predicted that there would be important H-bonding interactions between the catalytic residue in the Slt35 active site Glu162 and the two nitrogen atoms in the amidine group in all five synthesised amidine derivatives. The amidine with an n-propyl side chain displayed more interactions with Ser230, which might increase the binding affinity of the enzyme for the inhibitor. With these promising results, synthesis of the first six amidine compounds was performed. However, we encountered some difficulties, including low yield of the thiolactam and amidine, and purification of amidine compounds. The poor yield could be attributed to the effect of the acetonide protecting group in the six-membered ring of thiolactam and amidine respectively.

Prior to the evaluation of these compounds, the expression, purification and activity assay of Slt35 were optimised. Following this, evaluation of some known inhibitors for lysozyme (e.g. thionine acetate) and glycosidase inhibitors (e.g. 1-deoxynojirimycin, Thiamet G, castanospermine and miglitol) was performed using a turbidimetry assay. Next, the efficacy of the first six designed amidines towards Slt35 was assessed. Glycosidase inhibitors were inactive against Slt35, whereas amidine compounds exhibited inhibition against Slt35 at low

micromolar level with the lowest value for the amidine with an n-propyl side chain. Meanwhile, thionine acetate inhibited the activity of Slt35 at micromolar concentrations, lower than those of the amidines. On the other hand, three amidine derivatives were tested against lysozyme activity but no inhibition was observed.

A second generation of amidine-based compounds was designed based on the change of the orientation of two hydroxyl groups in the amidine ring to improve the interactions with the Ser230 residue, which might play an important role in the ligand binding as the inhibitor that displayed the lowest IC_{50} possesses interaction with Ser230 unlike other inhibitors. Newly designed analogues were derived from 2-deoxy-L-ribose with the same three amine moieties (propyl, cyclohexyl, 2-fluorobenzyl) and ethyl morpholine. Evaluation of these molecules against Slt35 revealed that they did not exhibit any inhibition, except the amidine with ethyl morpholine side chain, which inhibited the enzyme at high micromolar concentration. Docking of the second-generation molecules was performed and compared to the first generation. The position of these compounds inside the enzyme active site pocket was changed due to the different orientations of the amidine ring hydroxyl groups.

Another strategy was based on the modification of the propyl side chain of the best first-generation inhibitor. Two new inhibitors were synthesised, either replacing the terminal methyl group by morpholine or increasing the length of the chain by three more carbons. The amidine with an ethyl morpholine side chain showed potency towards Slt35 slightly less than the propyl amidine, whereas hexyl amidine displayed significantly worse inhibition than all first generation inhibitors. Moreover, a series of hydrochloride salts from amidine derivatives with the same side chain moieties of the previous free bases were produced. However, the effectiveness of inhibition by all these salts is much weaker than that of their corresponding free bases. Further modification was planned to dihydroxy amidine by stereoconversion of hydroxyl group in position three of amidine six-membered ring, but it was unsuccessful.

Additional attempts to improve the interactions of the first series of synthesised amidines investigated addition of a hydroxyl group in position 2 in the six-membered ring of the amidine. Synthesis of these analogues followed a route similar to that used for the first generation compounds, but starting from D-ribose. Unfortunately, the synthesis failed at the

conversion of lactam to thiolactam step despite different attempts, which could be attributed to the strain of five-membered ring of acetonide group that affects the reactivity of carbonyl amide.

5.2 Future directions

Although these compounds showed poor activity towards Slt35, they provided the groundwork towards the design of effective inhibitors for LTs based on the amidinium group. This would be an important step in the development of antibiotic agents that target such enzymes. The first next step will be testing them against bacteria to investigate their activity as antibacterial agents. Further modifications can be made to the best inhibitor that possesses a propyl side chain by studying the crystal structure of this inhibitor bound to Slt35. Moreover, evaluation of the all synthesised amidines in this study against other LTs is required, especially Slt70 which resemble Slt35 in their active sites.

Some possible modifications to compound **(35b)** have been made, such as a dihydroxy propyl side chain (Figure 5-1). This compound may exhibit good interactions with the enzyme active site through the two hydroxyl groups in the side chain. Deprotection of this compound can be performed and then tested against Slt35 activity.

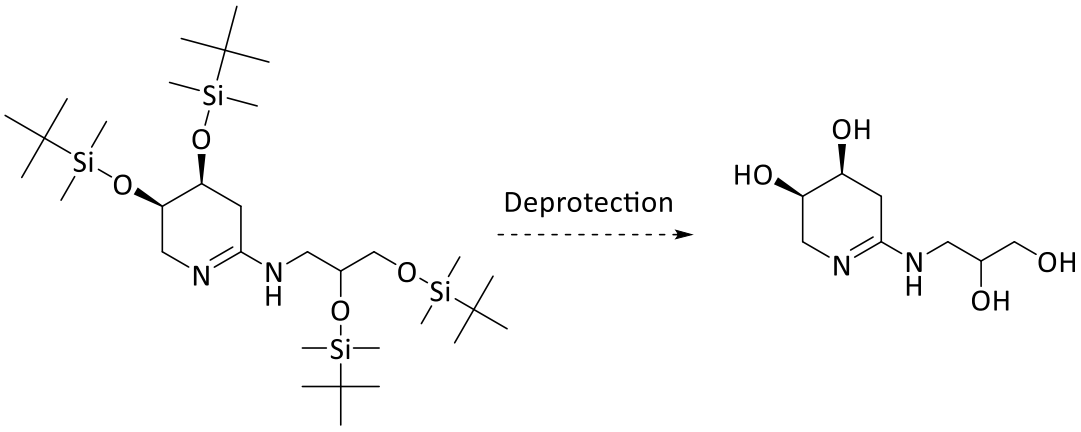

Figure 5-1: *Deprotection of compound* ***(65h).***

In addition, an attempt to synthesise the intermediate (4R,5R)-dihydroxy lactam by stereoconversion of compound **(41)** failed, thus instead it may be prepared by following another synthetic route (Figure 5-2). The two hydroxyl groups in both positions 3 and 4 in the

amidine would better mimic the hydroxyl groups in the NAG unit in the peptidoglycan substrate. Accordingly, this molecule might be more active than previous analogues in this study.

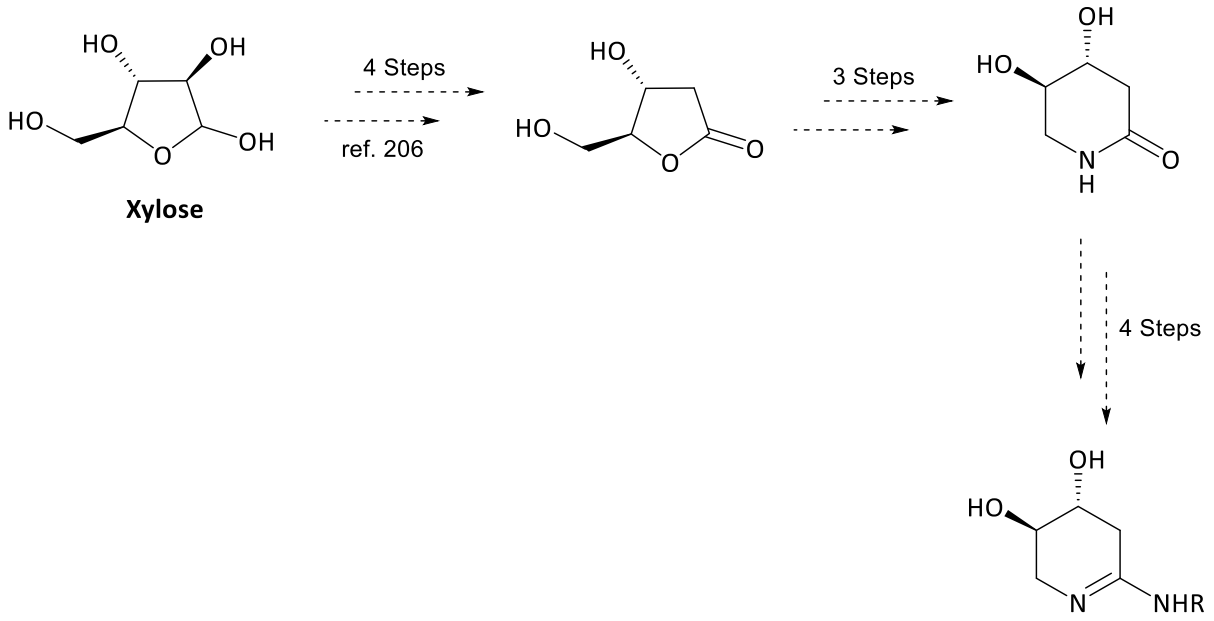

Figure 5-2: *Synthetic route of (3R,4R)-dihydroxy amidine derivatives.*

Moreover, synthesis of gluconoamidine derivatives (Figure 5-3) has been started but not finished in this work, therefore, this synthesis could be completed, and the resulting compounds tested against Slt35 and other LT activity. Such compounds may be good inhibitors for LTs.

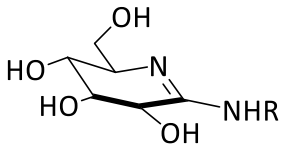

R= various amine moieties

Figure 5-3: *Structure of gluconoamidine derivatives.*

6 Materials and Methods

6.1 Organic synthesis

All chemicals were purchased from Sigma-Aldrich, Fisher Scientific, Carbosynth and Fluorochem unless otherwise stated. Anhydrous MeCN, THF, diethyl ether and toluene were obtained from a MBraun SPS800 solvent purification system.

Compounds are characterised by ^{1}H NMR, ^{13}C NMR, COSY and HSQC NMR experiments. NMR spectra were recorded on a Bruker Avance 500 NMR spectrometer, a Bruker Avance DPX400 NMR spectrometer and a Bruker Fourier 300 NMR spectrometer, and are reported as chemical shifts in parts per million downfield from tetramethylsilane, multiplicity (s = singlet, d = doublet, t = triplet, q = quartet, m = multiplet), coupling constant and assignment, respectively. IR spectra were recorded on a Perkin-Elmer 1600 series FTIR spectrometer. High resolution mass spectra were recorded by the mass spectrometry service in Cardiff University, School of Chemistry. Amidine derivatives were purified by HPLC (Agilent Technologies 1260 infinity series) equipped with a preparative Phenomex Luna C18 column (10 μm C18, 250 × 10 mm). The applied buffers were A: H_2O + formic acid (0.1%) and B: MeCN + formic acid (0.1%). The products that have phenyl rings were detected at 260 and 280 nm while products that have just (C=N) were detected at 230 nm. Melting points were recorded on a Gallenkamp MPD350 apparatus and are quoted uncorrected.

6.1.1 Preparation of (2S,3R,4R,5S,6R)-3-acetamido-6-(acetoxymethyl)tetrahydro-2H-pyran-2,4,5-triacetate (50).[161]

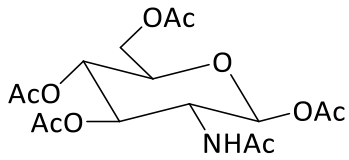

In dry pyridine (60 ml), GlcNAc (5 g, 24 mmol) was treated with acetic anhydride (30 ml) at 0 ^{o}C, and the reaction mixture was stirred at r.t. for three days. After that, the mixture was poured on ice (100 ml) and stirred for 3 hr. The resultant mixture was extracted with DCM (8 × 20 ml). The combined organic layers were acidified with 5 N HCl to pH 1-2, washed with water and then dried over $MgSO_4$. The solvent was removed under reduced pressure followed by high vacuum to give **(50)** as a white solid (6.53 g, 16.8 mmol, 70%), R_F 0.45 (EtOAc:hexane, 10:1). ^{1}H NMR (400 MHz, $CDCl_3$) δ 5.81 (d, 1H, NH), 5.44 (d, *J* = 9.1 Hz, 1H, CHOAc), 4.94-4.81

(m, 2H, 2 CHOAc), 4.14 (ddd, *J* = 10.7, 9.1, 3.7 Hz, 1H, CHOAc), 3.90 (dd, *J*= 12.5, 4.0 Hz, 1H, CH_2OAc), 3.71 (dd, *J*= 12.5, 2.3 Hz, 1H, CH_2OAc), 3.65 (dd, *J*= 9.8, 6.0 Hz, 1H, CHOAc), 1.85 (s, 3H, CH_3CO), 1.74 (s, 3H, CH_3CO), 1.70 (d, 6H, 2 CH_3CO), 1.59 (s, 3H, CH_3CO).^{13}C NMR (100 MHz, $CDCl_3$) δ 171.88 (CO) 170.94 (CO), 170.29 (CO), 169.34 (CO), 168.93 (CO), 90.8 (CHO), 70.79 (CHO), 69.83 (CHO), 67.63 (CHO), 61.69 (CH_2O), 51.15 (CHO), 23.20 (CH_3), 21.13 (CH_3), 20.91 (CH_3), 20.91 (CH_3), 20.76 (CH_3). HRMS *m/z* (M+1) cal. 390.00, measured 390.1500.

6.1.2 Synthesis of (2S,3R,4R,5S,6R)-6-(acetoxymethyl)-3-ethanethioamidotetrahydro-2H-pyran-2,4,5-triacetate (52).[138]

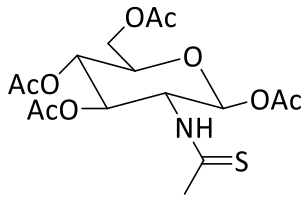

Method A:[138]

To a solution of compound **(50)** (4.05 g, 10 mmol) in 50 ml of dry toluene was added Lawesson's reagent (3.0 g, 9.72 mmol) at 80 ^oC for 1.5 h and / or overnight. The reaction mixture was cooled to room temperature and then concentrated to give a yellow syrup, which was chromatographed on silica with 1:8 ethyl acetate:hexane as the eluent to provide compound **(52)** as a yellow solid (Table 6-1), R_f 0.79 (EtOAc:hexane , 10:1). ^{1}H NMR (400 MHz, $CDCl_3$) δ 6.33 (d, *J* = 3.6 Hz, 1H, NH), 5.35-5.24 (m, 1H, CH), 5.21 (t, *J* = 9.8 Hz, 1H, CH), 5.16-5.01 (m, 1H, CH), 4.22 (dd, *J* = 12.7, 4.2 Hz, 1H, CH), 4.07-3.87 (m, 2H, CH_2O), 2.42 (s, 3H, CH_3), 2.13 (s, 3H, CH_3), 2.04 (s, 3H, CH_3), 2.00 (s, 6H, 2 CH_3); ^{13}C NMR (100 MHz, $CDCl_3$) δ 203.6 (C=S), 172.37 (CO), 171.0 (CO), 169.4 (CO), 168.9 (CO), 89.4 (CH), 70.8 (CH), 69.8 (CH), 67.4 (CH), 61.9 (CH), 57.0 (CH_2), 34.4 (CH_3), 21.2 (CH_3), 21.0 (CH_3), 20.9 (CH_3), 20.8 (CH_3). HRMS (EI) calculated 405.0000, measured 405.1000.

Time	Weight (g)	mmol	%
1.5 h	2.57	6.35	61
Overnight	3.27	8.10	82

Table 6-1: *Different conditions of preparation of compound* ***52.***

Method B:

A solution of compound **(50)** (0.5 g, 1.2 mmol) in 10 ml pyridine was treated with Lawesson's reagent (0.75 g, 1.85 mmol), and the reaction mixture was heated at 100 ^{o}C for 4 hours. After being cooled to room temperature, saturated aqueous sodium hydrogen carbonate solution was added to the reaction mixture, and then extracted with chloroform. The organic layer was washed with water and dried over magnesium sulfate, concentrated and the residue was purified by flash chromatography with ethyl acetate:hexane (8:1) to give brown yellowish product of **(52)** (0.16 g, 0.4 mmol, 44%).

Method C:

A mixture of compound **(50)** (0.16 g, 0.2 mmol) and Lawesson's reagent (0.32 g, 0.4 mmol) in 10 ml dry THF was refluxed overnight and monitored by TLC. The reaction mixture was concentrated under pressure and purified by column chromatography (ethyl acetate: hexane, 8:1) to give compound **(52)** as a yellow solid (0.08 g, 0.2 mmol, 77%).

6.1.3 Preparation of 3,4-dihydroquinoline-2(*1H*)-thione (54).

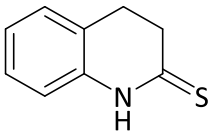

A solution of commercially available 3,4-dihydro-2(1*H*)-quinolinone **(53)** (0.20 g, 1.36 mmol) in 30 ml dry THF was treated with Lawesson's reagent (0.33 g, 0.6 eq., 0.816 mmol) and the reaction mixture was stirred at r.t. overnight. The solvent was evaporated and the residue was purified by flash chromatography (EtOAc:hexane, 1:2, R_f 0.68) to yield a yellow solid (0.2 g, 1.23 mmol, 91%), m.p. 98-100 ^{o}C. ^{1}H NMR (500 MHz, $CDCl_3$) δ 9.87 (s, 1H, NH), 7.17-7.13 (m, 2H, ArCH), 7.12 (d, *J*= 7.5 Hz, 1H, ArCH), 7.01 (t, *J*= 8.1 Hz, 1H, ArCH), 6.81 (dd, *J*= 7.9, 0.7 Hz, 1H, ArCH), 3.04 (t, 2H, *J*= 7.3 Hz, CH_2-C=S), 2.82 (t, 2H, *J*= 7.5 Hz, CH_2-Ar). ^{13}C NMR (125 MHz, $CDCl_3$) δ 200.5 (C=S), 136.2, 128.3, 127.8, 125.2, 115.6 (ArC), 38.9 (CH_2-C=S), 25.3 (CH_2-Ar). HRMS (EI): found 163.0537 C_9H_9NS calculated 163.0534. υ cm^{-1}: 3165.2, 3095.7, 2993.5, 2941.4, 1612.5, 1529.6, 1483.3, 1379.1, 1340.5, 1197.8, 1130.3, 1083.9, 802.4, 619.2, 584.4.

6.1.4 Synthesis of N-propyl-3,4-dihydroquinolin-2-amine (55).

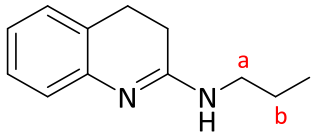

Yellow solid (0.2 mg, 1.06 mmol, 87%), R_f 0.78 (EtOAc:MeOH, 8:2), m.p. 140-142 ^oC. ^1H NMR (400 MHz, MeOD) δ 7.32-7.25 (m, 2H, 2 ArCH), 7.20-7.07 (m, 2H, 2 ArCH), 3.47 (t, 2H, *J*= 6.7 Hz, CH_2-NH), 3.02-2.96 (m, 2H, CH_2-Ar), 2.92-2.87 (m, 2H, CH_2C=N), 1.86 (m, 2H, CH_2-b), 1.09 (t, 3H, *J*= 7.4 Hz, CH_3). ^{13}C NMR (125 MHz, $CDCl_3$) δ 162.2 (C=N), 128.0, 127.7, 125.4, 124.9, 122.7, 117.5 (Ar-C), 44.1 (CH_2-NH), 26.3 (CH_2-Ar), 22.5 (CH_2C=N), 20.8 (CH_2-b), 10.2 (CH_3). HRMS (EI): found 188.1392 $C_{12}H_{16}N_2$, calculated 188.1392. υ cm^{-1}: 3313.7, 2968.4, 2933.7, 1670.4, 1570.1, 1496.8, 1379.1, 1103.3, 1031.9, 983.7, 767.7, 682.8, 518.8.

6.1.5 General method for the preparation of hydroxylactone derivatives[152]

To a solution of sugar (4.0 g) in water (100 ml) was slowly added bromine (8 ml, 2 eq). The red solution was stirred at room temperature for 5 days. After dilution with water (400 ml), Ag_2CO_3 was added until the solution reached pH 7. The suspension was filtered through a Celite pad and the filtrate evaporated and then purified by flash chromatography (EtOAc:MeOH, 10:2).

(4S,5R)-4-hydroxy-5-(hydroxymethyl)dihydrofuran-2(3H)-one (56).

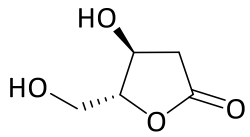

From 2-deoxy-D-ribose. Colourless oil (3.5 g, 26.5 mmol, 89%), R_f 0.67 ($CHCl_3$: MeOH, 1:1). ^1H NMR (300 MHz, D_2O) δ 4.52-4.49 (m, 1H, CHO), 4.49-4.45 (m, 1H, CHOH), 3.80 (dd, *J*= 12.9, 3.2 Hz, 1H, CH_2OH), 3.70 (dd, *J*= 12.9, 4.6 Hz, 1H, CH_2OH), 2.98 (dd, *J*= 18.6, 7.0 Hz, 1H, CH_2CO), 2.51 (dd, *J*= 18.6, 3.0 Hz, 1H, CH_2CO). ^{13}C NMR (75 MHz, D_2O) δ 179.3 (CO), 88.7 (CHO), 68.1 (CHOH), 60.8 (CH_2OH), 37.5 (CH_2CO). HRMS (EI): 101 $[M-31]^+$ $C_5H_8O_4$, calculated 132.0400; found 132.0400.

(4R,5S)-4-hydroxy-5-(hydroxymethyl)dihydrofuran-2(3H)-one (73).

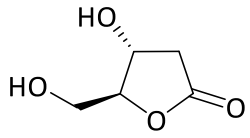

From 2-deoxy-L-ribose. Yellow oil (3.2 g, 24.2 mmol, 81%), R_f 0.51 (EtOAc:MeOH, 10:2). ^{1}H NMR (500 MHz, MeOD) δ 4.46 (ddd, *J*= 5.1, 3.8, 2.9 Hz, 1H, CHOH), 4.37 (ddd, *J*= 6.9, 3.5, 2.9 Hz, 1H, CHO), 3.67 (dd, *J*= 13.5, 3.8 Hz, 1H, CH_2OH), 3.60 (dd, *J*= 13.5, 5.1 Hz, 2H, CH_2OH), 2.96 (dd, *J*= 18.1, 7.0 Hz, 1H, CH_2CO), 2.46 (dd, *J*= 18.1, 3.5 Hz, 1H, CH_2CO). ^{13}C NMR (125 MHz, MeOD) δ 177.3 (CO), 88.9 (CHOH), 68.4 (CHO), 61.14 (CH_2OH), 37.9 (CH_2CO). MS (EI) found: 101 $[M-31]^+$, 102 $[M-30]^+$, 83 $[M-49]^+$ $C_5H_8O_4$, calculated 132.0400.

(3R,4S,5R)-3,4-dihydroxy-5-(hydroxymethyl)dihydrofuran-2(3H)-one (77).

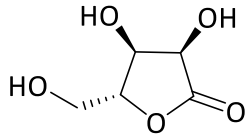

From D-ribose. Green oil (3.6 g, 24.3 mmol, 91%), R_f 0.62 ($CHCl_3$:MeOH, 1:1). ^{1}H NMR (500 MHz, D_2O) δ 4.59 (d, *J*= 5.6 Hz, 1H, CHOH-a), 4.44-4.41 (m, 1H, CHO), 4.28 (d, *J*= 5.5 Hz, 1H, CH_2OH-b), 3.71 (dd, *J*= 13.4, 6.3 Hz, 1H, CH_2OH-c), 3.65 (dd, *J*= 13.1, 4.0 Hz, 1H, CH_2OH-c). ^{13}C NMR (125 MHz, D_2O) δ 178.5 (CO), 86.7 (CHOH-a), 69.6 (CHO), 69.5 (CHOH-b), 60.5 (CH_2OH-c). HRMS (EI): found 91.0000 $[M-57]^+$, 73.0130 $[M-75]^+$, $C_5H_8O_5$, calculated 148.0400.

6.1.6 Synthesis of (6S)-6-(hydroxymethyl)-2,2-dimethyldihydrofuro[3,4-d][1,3]dioxol-4 (*3aH*)-one (79).[177]

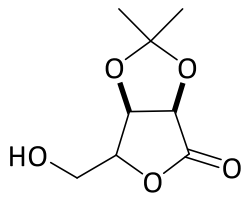

To a suspension of **77** (1.01 g, 6.76 mmol) in acetone (100 ml) was added concentrated sulfuric acid (1 ml) dropwise at 0 °C. The mixture was stirred for 24 h. at r.t. and then neutralized with 35% ammonia solution. The precipitate was dissolved in water and then extracted with EtOAc. The organic layer was evaporated and purified by flash chromatography (Et_2O:MeOH, 10:1, R_f 0.85) to afford **79** as a white solid (516 mg, 2.74 mmol, 40%). ^{1}H NMR (500 MHz, MeOD) δ

4.82-4.81 (m, 2H, CHO-a and CHO-b), 4.64-4.61 (m, 1H, CHO-c), 3.80 (dd, *J*= 12.3, 2.5 Hz, 1H, CH_2OH), 3.76 (dd, *J*= 12.3, 1.9 Hz, 1H, CH_2OH), 1.44 (s, 3H, CH_3), 1.39 (s, 3H, CH_3). ^{13}C NMR (125 MHz, MeOD) δ 175.5 (C=O), 112.4 (quaternary carbon), 83.2 (CHO-a), 78.5 (CHO-b), 75.7 (CHO-c), 60.8 (CH_2OH), 25.9 (CH_3), 24.3 (CH_3). HRMS (EI): found 211.0578 (M+Na), $C_8H_{12}O_5$, calculated 211.0577.

6.1.7 General method for the preparation of (3-hydroxy-5-oxotetrahydrofuran-2-yl)methyl 4-methylbenzenesulfonate derivatives.[152]

Lactone (3.0 g, 22.7 mmol) was dissolved in dry pyridine (100 ml) and cooled to -15 °C for 15 min, and then TsCl (5.0 g, 26.14 mmol, 1.15 eq.) was rapidly added. The mixture was left to stir at -15 °C for 2 h and at 0 °C for 5 h. The solvent was then removed under vacuum and the residue taken up in water (100 ml); the product was extracted with EtOAc (3 × 100 ml) and the combined organic layers washed with 1.0 M HCl and water, then dried with anhydrous Na_2SO_4 and the solvent evaporated to afford crude tosylate, which was purified by flash chromatography (EtOAc:hexane, 7:3) giving pure tosylate.

((2R,3S)-3-hydroxy-5-oxotetrahydrofuran-2-yl)methyl 4-methylbenzensulfonate (57).

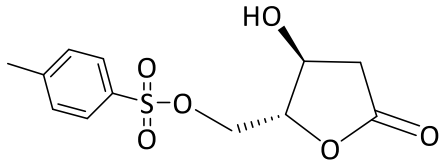

From **56**. Yellow oil (4.43 g, 15.5 mmol, 68%), R_f 0.68 ($CHCl_3$:MeOH, 10:1). ^1H NMR (400 MHz, MeOD) δ 7.82 (d, *J*= 7.6 Hz, 2H, Ar), 7.48 (d, *J*= 8.0 Hz, 2H, Ar), 4.49 (m, 1H,CHO), 4.42-4.32 (m, 1H, CHOH), 4.30-4.20 (m, 2H,CH_2OTs), 2.85 (dd, *J*= 17.9, 6.8 Hz, 1H, CH_2CO), 2.41 (d, *J*= 18.1 Hz, 1H, CH_2CO), 2.48 (s, 3H, CH_3-Ar). ^{13}C NMR (75 MHz, MeOD) δ 175.8 (CO), 145.6 (quaternary aromatic carbon), 132.3 (quaternary aromatic carbon), 129.9 (CH-Ar), 127.7 (CH-Ar), 84.7 (CHO), 68.7 (CH_2OTs), 67.7 (CHOH), 37.2 (CH_2CO), 20.3 (CH_3). HRMS (EI): found 309.0400 (M+Na), $C_{12}H_{14}O_6SNa^+$, calculated 309.0403

((2S,3R)-3-hydroxy-5-oxotetrahydrofuran-2-yl)methyl 4-methylbenzensulfonate (72).

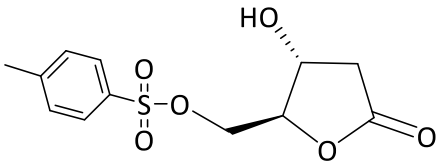

From **73**. Yellow oil, (3.06 g, 10.7 mmol, 47%), R_f 0.62 (EtOAc:hexane, 7:3). ^{1}H NMR (500 MHz, MeOD) δ 7.81 (d, *J*= 8.3 Hz, 2H, ArCH), 7.48 (d, *J*= 8.0 2H, ArCH), 4.51-4.45 (m, 1H, CHO), 4.38-4.33 (m, 1H, CHOH), 4.28 (dd, *J*= 11.4, 3.1 Hz, 1H, CH_2OTs), 4.24 (dd, *J*= 11.4, 4.2 Hz, 1H, CH_2OTs), 2.85 (dd, *J*= 18.1, 7.0 Hz, 1H, CH_2CO), 2.42 (dd, *J*= 18.1, 3.2 Hz, 1H, CH_2CO), 2.48 (s, 3H). ^{13}C NMR (125 MHz, MeOD) δ 175.7 (CO), 148.5 (quaternary aromatic carbon), 132.3 (quaternary aromatic carbon), 129.8 (ArC-CH), 127.7 (ArC-CH), 84.7 (CHO), 67.7 (CHOH), 68.4 (CH_2OTs), 37.1 (CH_2CO), 20.2 (CH_3). HRMS (EI): found 286.0511, $C_{12}H_{14}O_6S$ calculated 286.0500.

6.1.8 Synthesis of (2,2-dimethyl-6-oxotetrahydrofuro[3,4-d][1,3]-dioxol-4-yl)methyl 4-methylbenzenesulfonate (79).[178]

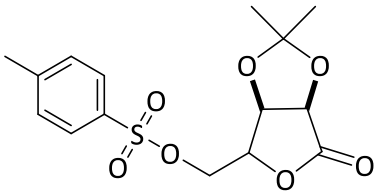

To a solution of compound **78** (231.7 mg, 1.23 mmol) in DCM (50 ml) was added Et_3N (1.1 eq., 0.2 ml, 1.35 mmol). After 5 min., tosyl chloride (1.2 eq., 282 mg, 1.48 mmol) was added at 0 ^{o}C. The resulting mixture was stirred at r.t. for 24 h. The reaction mixture was poured into water and then extracted with DCM. The organic layer was dried over Na_2SO_4 and concentrated and then purified by flash chromatography (Et_2O, R_f 0.77) to give **61** as a white solid (257.4 mg, 0.75 mmol, 61%), m.p. 186-188 ^{o}C. ^{1}H NMR (500 MHz, $CDCl_3$) δ 7.77 (d, *J*= 8.3 Hz, 2H, Ar-H), 7.40 (d, *J*= 8.0 Hz, 2H, Ar-H), 4.80 (d, *J*= 5.6 Hz, 1H, CHO-a), 4.76 (d, *J*= 5.6 Hz, 1H, CHO-b), 4.71-4.69 (m, 1H, CHO-c), 4.35 (dd, *J*= 11.2, 1.9 Hz, 1H, CH_2OTs), 4.19 (dd, *J*= 11.2, 2.4 Hz, 1H, CH_2OTs), 2.48 (s, 3H, CH_3-tosyl), 1.47 (s, 3H, CH_3), 1.40 (s, 3H, CH_3). ^{13}C NMR (125 MHz, MeOD) δ 173.0 (C=O), 145.9 (quaternary aromatic carbon), 131.6 (quaternary aromatic

carbon), 130.3, 127.9 (CH-Ar), 113.9 (quaternary carbon), 79.1 (CHO-c), 77.2 (CHO-b), 75.0 (CHO-c), 68.3 (CH_2OTs), 26.7 (CH_3-Ar), 25.5 (CH_3-C), 21.7 (CH_3-C). HRMS (EI): found 342.0664, $C_{15}H_{18}O_7S$, calculated 342.0800. υ cm^{-1}: 2997.4, 2937.6, 1774.5, 1369.5, 1190.1, 1172.7, 1101.4, 1047.4, 1031.9, 779.2, 702.1, 669.3, 553.6, 536.2.

6.1.9 General method for the preparation of 5-Azidomethyl-4-hydroxydihydrofuran-2-one derivatives.[152]

To a solution of tosylate (1.0 mg, 3.49 mmol) in anhydrous acetonitrile (50 ml) under a nitrogen stream was added 15-crown-5 ether (0.14 ml, 0.7 mmol, 0.2 eq.) and then NaN_3 (0.38 g, 5.93 mmol, 1.7 eq.) was rapidly added. The mixture was heated to reflux for 6 days. After cooling to room temperature, the suspension was filtered through a Celite pad and the filtrate was concentrated under vacuum. The residue was purified by flash chromatography to afford the azide derivative.

(4S,5R)-5-Azidomethyl-4-hydroxydihydrofuran-2-one (40).

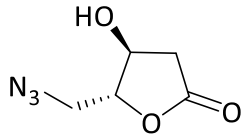

From **57**. Yellow oil (0.462 g, 2.94 mmol, 84%), R_f 0.45 (DCM/MeOH, 10:1), ^{1}H NMR (300 MHz, MeOD) δ 4.50-4.45 (m, 1H, CHO), 4.41-4.34 (m, 1H, CHOH), 3.61 (dd, *J*= 13.5, 3.8 Hz, 1H, CH_2N_3), 3.60 (dd, *J*= 13.5, 5.0 Hz, 1H, CH_2N_3), 2.97 (dd, *J*= 18.1, 6.9 Hz, 1H CH_2CO), 2.47 (dd, *J*= 17.7, 2.9 Hz, 1H, CH_2CO). ^{13}C NMR (75 MHz, MeOD) δ 176.1 (CO), 86.1(CHO), 73.5 (CHOH), 51.7 (CH_2N_3), 37.1 (CH_2CO). HRMS (EI): found 157.0415, $C_5H_8N_3O_3$ calculated 157.0500.

(4R,5S)-5-Azidomethyl-4-hydroxydihydrofuran-2-one (43).

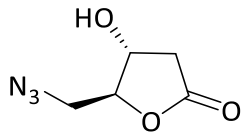

From **74**. Yellow oil (0.456 g, 2.91 mmol, 83%), R_f 0.47 (EtOAc:hexane, 7:3), ^{1}H NMR (400 MHz, MeOD) δ 4.49-4.43 (m, 1H, CHO), 4.39-4.34 (m, 1H, CHOH), 3.63 (ddd, *J*= 18.6, 13.5, 4.5 Hz, 2H, CH_2N_3), 2.96 (dd, *J*= 18.1, 7.0 Hz, 1H, CH_2CO), 2.46 (dd, *J*= 18.1, 3.5 Hz, 1H, CH_2CO). ^{13}C NMR (100 MHz, MeOD) δ 175.9 (CO), 86.1 (CHO), 68.4 (CHOH), 51.7 (CH_2N_3), 37.0 (CH_2CO). HRMS (EI^+): found 157.0573, $C_5H_8N_3O_3$ calculated 157.0500.

6.1.10 Synthesis of 6-(azidomethyl)-2,2-dimethyldihydrofuro-[3,4-d][1,3]dioxol-4(3aH)-one (80).[152]

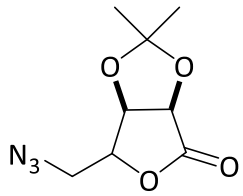

To a solution of compound **79** (280 mg, 0.819 mmol) in anhydrous acetonitrile (30 ml) under a nitrogen stream was added 15-crown-5 ether (33 µl, 0.164 mmol, 0.2 eq.) and then NaN_3 (90.5 mg, 1.392 mmol, 1.7 eq.) was rapidly added. The mixture was heated to reflux for 6 days. After cooling to room temperature, the suspension was filtered through a Celite pad and the filtrate was concentrated under vacuum. The residue was purified by flash chromatography (Et_2O, R_f 0.88). Pure azide was obtained as a colourless oil (155.4 mg, 0.45 mmol, 89%). ^1H NMR (400 MHz, $CDCl_3$) δ 4.86 (d, *J*= 5.7 Hz, 1H, CHO-a)), 4.68 (dd, *J*= 6.0, 3.3 Hz, 1H, CHO-c), 4.65 (d, *J*= 5.7 Hz, 1H, CHO-b), 3.80 (dd, *J*= 13.3, 3.2 Hz, 1H, CH_2N_3), 3.68 (dd, *J*= 13.2, 2.4 Hz, 1H, CH_2N_3), 1.48 (3H, CH_3), 1.39 (3H, CH_3). ^{13}C NMR (100 MHz, MeOD) δ 173.4 (C=O), 113.7 (quaternary carbon), 80.0 (CHO-c), 78.0 (CHO-b), 77.3 (CHO-a), 52.5 (CH_2N_3), 26.5 (CH_3), 25.6 (CH_3). HRMS (EI): found 198.0520 [M-CH_3], 199.06 [M-CH_2], $C_8H_{11}N_3O_4$ calculated 213.0700. υ cm^{-1}: 2484.3, 2077.3, 1647.2, 1456.3, 1116.8, 970.2, 661.6

6.1.11 General method for the preparation of 4,5-dihydroxy-piperidin-2-one.[152]

Azide (750 mg, 4.77 mmol) was dissolved in 30 ml anhydrous MeOH under a nitrogen atmosphere. After that, $Pd(OH)_2$-C (0.10 g, 3 mol%) was added and the reaction was flushed with hydrogen and then left under hydrogen atmosphere at room temperature for 24 h. The suspension was filtered through a Celite Pad and the solvent evaporated to afford pure lactam.

(4S,5R)-4,5-dihydroxypiperidin-2-one (39).

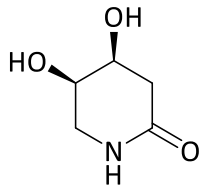

From **40**. White yellowish solid (626 mg, 4.77 mmol, 100%), m.p. 161.1-163.6 °C (lit. 160.9-162.0 °C).[152] ^{1}H NMR (300 MHz, D_2O) δ 4.03-3.88 (m, 2H, $2CH_2OH$), 3.27 (dd, *J*= 13.1, 5.3 Hz, 1H, CH_2NH), 3.17 (dd, *J*= 13.0, 5.3 Hz, 1H, CH_2NH), 2.49 (dd, *J*= 17.9, 4.5 Hz, 1H, CH_2CO), 2.29 (dd, *J*= 17.9, 7.7 Hz, 1H, CH_2CO). ^{13}C NMR (75 MHz, D_2O) δ 173.2 (CO), 65.9 (CHOH), 65.2 (CHOH), 43.6 (CH_2NH), 34.6 (CH_2CO). HRMS (EI): found 131.0600, $C_5H_9NO_3$, calculated 131.0600.

(4R,5S)-4,5-dihydroxypiperidin-2-one (42).

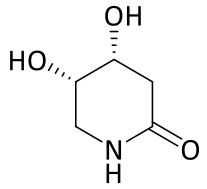

From **43**. Yellow solid product, (388.12 mg, 2.96 mmol, 62%), R_f 0.56 (EtOAc:MeOH, 10:3) ^{1}H NMR (500 MHz, MeOD) δ 4.13-3.88 (m, 2H, 2CHOH), 3.38-3.31 (m, 2H, CH_2NH), 2.55 (dd, *J*= 17.6, 5.2, 1H, CH_2CO), 2.48 (dd, *J*= 17.6, 7.0 Hz). ^{13}C NMR (125 MHz, MeOD) δ 172.1 (CO), 66.6 (CHOH), 65.8 (CHOH), 43.8 (CH_2NH), 35.8 (CH_2CO). HRMS (EI): found 131.0417, $C_5H_9NO_3$, calculated 131.0600.

6.1.12 Synthesis of (3aR,7R,7aR)-7-hydroxy-2,2-dimethyltetra-hydro[1,3]dioxolo[4,5-c]pyridine-4(3aH)-one (81).[152]

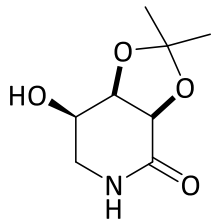

Azide **(80)** (128.6 mg, 0.60 mmol) was dissolved in 10 ml anhydrous MeOH under a nitrogen atmosphere. After that, $Pd(OH)_2$-C (12.7 mg, 3 mol%) was added and the reaction was flushed

with hydrogen and then left under hydrogen atmosphere at room temperature for 24 h. The suspension was filtered through a Celite pad and the solvent evaporated to afford pure lactam as brown-yellowish solid (112.9 mg, 0.60 mmol, 100%), R_f 0.43 (EtOAc:MeOH, 8:2), m.p. 118-120 ^oC. ^1H NMR (400 MHz, MeOD) δ 4.44 (dd, *J*= 6.4, 2.5 Hz, 1H, CH-b), 4.34 (d, *J*= 6.4 Hz, 1H, CH-a), 3.98 (ddd, *J*= 9.2, 4.5, 2.8 Hz, 1H, CH-c), 3.22 (dd, *J*= 11.9, 9.2 Hz, 1H, CH_2NH),3.09 (ddd, *J*= 12.0, 4.4, 0.7 Hz, 1H, CH_2NH), 1.35 (s, 3H, CH_3), 1.31 (s, 3H, CH_3). ^{13}C NMR (100 MHz, MeOD) δ 170.7 (CO), 110.4 (quaternary carbon), 75.75 (CH-b), 73.62 (CH-a), 64.40 (CH-c), 41.5 (CH_2NH), 26.7 (CH_3), 24.3(CH_3). HRMS (EI): found 186.0773, $C_8H_{12}NO_4$ calculated 186.0766. υ cm^{-1}: 3525.9, 3423.6, 3261.6, 2987.7, 2906.7, 1660.7, 1629.8, 1487.1, 1377.2, 1161.2, 1217.1, 1109.1, 1076.3, 1039.6, 790.8, 769.6, 507.3.

6.1.13 General method for the preparation of 2,2-Dimethylterahydro-[1,3]dioxolo[4,5-c]pyridine-6 (*3aH*)-one.[152]

A catalytic amount of p-toluenesulfonic acid (32.3 mg, 0.17 mmol, 0.2 eq.) was added to a solution of lactam (1.09 g, 8.32 mmol) in 5 ml anhydrous MeOH followed by 2,2-dimethoxypropane (18.4 ml, 150 mmol, 18 eq.). The reaction mixture was warmed at 55 ^oC for 5 h. After that, the mixture was diluted with MeOH (5 ml) and neutralized with $NaHCO_3$ and then filtered through a Celite pad. The solvent was evaporated and residue was purified by flash chromatography (DCM:MeOH, 20:1).

(3aR, 7aS)-2,2-Dimethylterahydro-[1,3]dioxolo[4,5-c]pyridine-6 (3aH)-one (58).

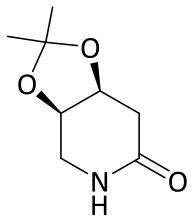

From **39**. White solid (1.24 g, 7.22 mmol, 87%), R_f 0.48 (DCM:MeOH, 20:1), m.p. 118.7- 120.0 ^oC (lit. 118.2-119.2 ^oC).[152] ^1H NMR (400 MHz, MeOD) δ 4.75-4.66 (m, 1H, CHO), 4.51-4.47 (m, 1H, CHO), 3.38-3.21 (m, 2H, CH_2NH), 2.49-2.47 (m, 2H, CH_2CO), 1.39 (s,3H, CH_3), 1.34 (s,3H, CH_3). ^{13}C NMR (125 MHz, MeOD) δ 173.4 (CO), 108.3 (quaternary carbon), 72.7 (CHO), 72.5 (CHO), 42.8 (CH_2NH), 35.5 (CH_2CO), 24.9 (CH_3), 22.6 (CH_3). HRMS (EI): Found 171.1000 $C_8H_{13}NO_3$, calculated 171.0900.

(3aS,7aR)-2,2-Dimethylterahydro-[1,3]dioxolo[4,5-c]pyridine-6 (3aH)-one (73).

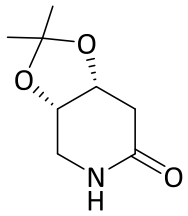

White yellowish solid (1.32 g, 7.72 mmol, 93%), R_f 0.33 (EtOAc:hexane, 10:1), m.p. 110-111 ^oC. ^1H NMR (400 MHz, MeOD) δ 4.74-4.70 (m, 1H, CHO), 4.49 (ddd, *J*= 7.6, 2.4, 1.8 Hz, 1H, CHOH), 3.33 (dd, *J*= 14.4, 1.7 Hz, 1H, CH_2NH), 3.26 (dd, *J*= 14.4, 2.5 Hz, 1H, CH_2NH), 2.49-2.47 (m, 2H, CH_2CO), 1.39 (d, *J*= 0.4 Hz, 3H, CH_3), 1.34 (d, *J*= 0.5 Hz, 3H, CH_3). ^{13}C NMR (125 MHz, MeOD) δ 173.4 (CO), 108.3 (quaternary carbon), 72.7 (CHO), 72.5 (CHO), 42.8 (CH_2NH), 35.5 (CH_2CO), 24.9 (CH_3), 22.8 (CH_3). HRMS (EI): found 171.0980 $C_8H_{13}NO_3$ calculated 171.0974.

6.1.14 Preparation of (4S,5R)-4,5-bis((tert-butyldimethylsilyl)-oxy)-piperidin-2-one (58).[164]

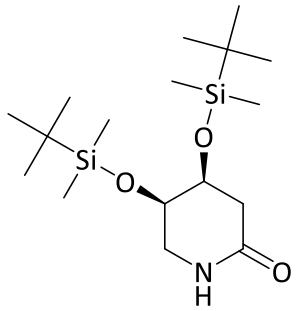

A solution of *tert*-butyldimethylchlorosilane (9.2 g, 60.9 mmol, 2.5 eq.) in DMF (20 ml) was added dropwise to a stirred solution of **39** (3.2 g, 24.4 mmol) and imidazole (4.1 g, 60.9 mmol, 2.5 eq.) in 20 ml DMF at room temperature. The resulting mixture was stirred overnight and then the solvent was evaporated under reduced pressure. The residue was purified by flash chromatography (EtOAc:hexane, 3:2) to afford white solid product (5.44 g, 15.14 mmol, 62%), R_f 0.6 (EtOAc:hexane, 3:2), m.p. 162-163 ^oC. ^1H NMR (500 MHz, $CDCl_3$) δ 5.78 (s, 1H, NH), 3.96-3.77 (m, 2H, 2 CHO), 3.28 (dd, *J* =12.6, 7.4, Hz, 1H, CH_2NH), 3.14 (dd, *J* =12.6, 5.0 Hz, 1H, CH_2NH), 2.49 (dd, *J* = 17.3, 6.7 Hz, 1H, CH_2CO), 2.39 (dd, *J*= 17.3, 4.5 Hz, 1H, CH_2CO), 0.81 (s, 18 H, 6 CH_3), 0.03-(-0.05) (m, 12 H, 4 CH_3). ^{13}C NMR (125 MHz, $CDCl_3$) δ 170.9 (CO), 68.8 (CHO), 68.3 (CHO), 45.1 (CH_2NH), 37.9 (CH_2CO), 25.8 (6 CH_3), 18.2 (2 quaternary carbon), -4.5 (CH_3-

Si), -4.5 (CH_3-Si), -4.7 (CH_3-Si), -4.9 (CH_3-Si). HRMS (EI): found 359.2403 $C_{17}H_{37}N_2O_3Si_2$ calculated 359.2390. υ cm^{-1}: 2927.9, 2856.6, 1674.2, 1616.4, 1247.9, 1091.7, 827.5, 773.5.

6.1.15 Protection of hydroxyl group in (3aR,7R,7aR)-7-hydroxy-2,2-dimethyltetrahydro-[1,3]dioxolo[4,5-c]pyridine-4(3aH)-one.

Three different methods were used to protect the free hydroxyl group in the partially protected lactams:

Preparation of (3aR,7R,7aS)-2,2-dimethyl-7-((trimethylsilyl)oxy)tetrahydro-[1,3]dioxolo[4,5-c]pyridine-4(3aH)-one (83a).[179]

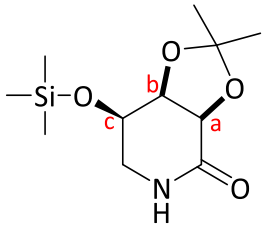

To a solution of lactam **(81)** (200 mg, 1.07 mmol) in dry DCM (10 ml) was added trimethylamine (0.28 ml, 1.3 mmol, 1.2 eq.) and the solution was cooled to -30 °C. Chlorotrimethylsilane (1.2 eq., 1.3 mmol, 0.16 ml) was added dropwise to the cooled solution. After 5 min, the cooling bath was moved, and the reaction mixture was stirred for 2 h at r.t. $KHSO_4$ (5% aq., 6 ml) was added dropwise and after 10 min, the mixture was extracted with DCM (3 x 20 ml). The combined organic layers were dried over anhydrous Na_2SO_4 and the solvent was evaporated under reduced pressure. Crude product was purified by flash chromatography (EtOAc:hexane, 1:1, R_f 0.7), colourless oil (83.7 mg, 0.32 mmol, 30%). ^{1}H NMR (400 MHz, MeOD) δ 4.30 (dd, *J*= 6.4, 2.4 Hz, 1H, CHO-b), 4.26 (d, *J*= 6.4 Hz, 1H, CHO-a), 4.05 (ddd, *J*= 8.7, 4.0, 2.7 Hz, 1H, CHO-c), 3.22 (dd, *J*= 12.0, 8.9 Hz, 1H, CH_2NH), 2.95 (dd, *J*= 12.0, 4.3 Hz, 1H, CH_2NH 1.26 (s, 3H, CH_3-CO), 1.22 (s, 3H, CH_3-CO), -0.0001 (s, 9H, 3 CH_3-Si). ^{13}C NMR (125 MHz, $CDCl_3$) δ 170.7 (C=O), 110.4 (quaternary carbon), 76.0 (CHO), 73.6 (CHO), 65.6 (CHOSi), 41.9 (CH_2NH), 25.7 (CH_3-CO), 24.2 (CH_3-CO), -1.4 (3 CH_3-Si). HRMS (EI): found 259.1200 $C_{11}H_{21}NO_4Si$ calculated 259.1200. υ cm^{-1}: 2357.0, 1683.9, 1217.1, 528.5, 418.6.

Preparation of (3aR,7R,7aS)-7-((tert-butyldimethysilyl)oxy)-2,2-dimethyltetra-hydro[1,3]dioxolo[4,5-c]pyridine-4(3aH)-one (83b).[164]

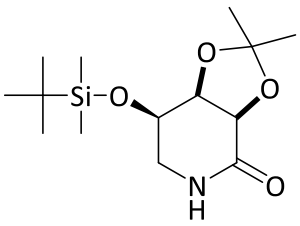

A mixture of partially protected lactam **(81)** (200 mg, 1.07 mmol), tert-butyldimethylsilyl chloride TBDMSCl (1.2 eq., 1.3 mmol, 200 mg) and imidazole (180 mg, 2.68 mmol ,2.5 eq.) was dissolved in DMF (20 ml) and stirred at r.t. for 12 h. The solvent was evaporated under reduced pressure and crude product was purified by flash chromatography (EtOAc:hexane, 1:1, R_f 0.42). White solid product (286 mg, 0.95 mmol, 89%), m.p. 104-106 ^oC. ^1H NMR (500 MHz, $CDCl_3$) δ 5.85 (s, 1H, NH), 4.35 (s, 2H, 2 CHO), 4.06 (dd, *J*= 8.9, 4.1, 1H, CHOSi), 3.51 (d, *J*= 10.6 Hz, 1H, CH_2-NH), 3.09 (dd, *J*= 10.2, 5.8 Hz, 1H, CH_2-NH), 1.43 (s, 3H, CH_3-CO), 1.34 (s, 3H, CH_3-CO), 0.84 (s, 6H, 2 CH_3-Si), -0.0001 (s, 9H, 3 CH_3-CSi). ^{13}C NMR (125 MHz, $CDCl_3$) δ 168.7 (C=O), 110.1 (quaternary carbon), 75.1, 72.5 (2 CHO), 65.4 (CHOSi), 41.9 (CH_2-NH), 25.8 (CH_3-CO), 24.8 (3 CH_3-C-Si), 24.3 (CH_3-CO), 17.2 (C-$(CH_3)_3$), 0.0 (2 CH_3-Si). HRMS (EI): found 301.1786 $C_{14}H_{27}NO_4Si$ calculated 301.1788. υ cm^{-1}: 2929.9, 2895.2, 2856.6, 1666.5, 1473.6, 1379.1, 1246.0, 1209.4, 1166.9, 1134.1, 1043.5, 987.6, 833.3, 775.4, 671.2, 511.1.

Preparation of (3aR,7R,7aS)-5-acetyl-2,2-dimethyl-4-oxohexahydro[1,3]-dioxolo[4,5-c]pyridine-7-yl acetate (85).[180]

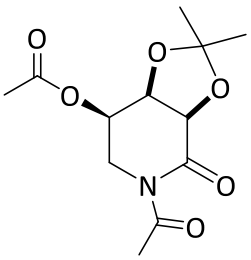

To a solution of partially protected lactam **(81)** (200 mg, 1.07 mmol) in dry pyridine (20 ml) was added acetic anhydride (10 ml) at 0 ^oC. The mixture was stirred at r.t. for 12 h and then was poured on ice. The mixture was extracted with DCM (3 x 20 ml) and the combined organic layers were dried over anhydrous Na_2SO_4. After filtration, the solvent was evaporated under

reduced pressure and crude product was purified by flash chromatography (EtOAc:hexane, 1:1, R_f 0.62). Hygroscopic white solid product (60 mg, 0.22 mmol, 21%). ^{1}H NMR (500 MHz, MeOD) δ 5.23 (ddd, *J*= 6.3, 3.8, 2.3 Hz, 1H, CHO-COCH$_3$), 4.69 (d, *J*= 8.2 Hz, 1H, CHCO), 4.65 (dd, *J*= 8.2, 3.8 Hz, 1H, CHO), 4.06 (dd, *J*= 13.9, 6.7 Hz, 1H, CH$_2$N), 3.62 (dd, *J*= 13.9, 2.2 Hz, 1H, CH$_2$N), 2.39 (s, 3H, CH$_3$COO), 1.95 (s, 3H, CH$_3$CON), 1.36 (s, 3H, CH$_3$), 1.31 (s, 3H, CH$_3$). ^{13}C NMR (125 MHz, MeOD) δ 172.5 (COO), 170.7 (CON), 169.8 (CON), 111.2 (quaternary carbon), 75.5 (CHO), 73.9 (CHO), 64.9 (CHO), 40.7 (CH$_2$N), 25.2 (CH$_3$), 25.1 (CH$_3$), 23.6 (CH$_3$), 19.3 (CH$_3$). HRMS (EI): found 271.1134 $C_{12}H_{17}NO_6$ calculated 271.1134. υ cm^{-1}: 2991.6, 2941.4, 2916.4, 1739.8, 1701.2, 1377.2, 1249.9, 1097.5, 1058.9, 1001.1, 875.7, 829.4, 796.6, 586.4, 511.1.

6.1.16 Deprotection of (3aR,7R,7aR)-7-hydroxy-2,2-dimethyl-tetrahydro[1,3]dioxolo[4,5-c]pyridine-4(3aH)-one (86).

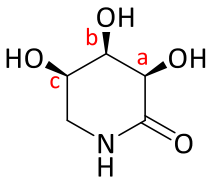

A solution of partially protected lactam **(81)** (0.2 g, 1.07 mmol) in aqueous 2N HCl (10 ml) was heated under stirring for 12 h. at r.t. and then the solvent was removed and the residue was purified by HPLC (detected at 230 nm) to give pure trihydroxylactam as brown oil (0.14 g, 0.95 mmol, 89%), R_f 0.33 (CHCl$_3$:MeOH, 1:1).^{1}H NMR (400 MHz, MeOD) δ 4.67 (d, *J*= 3.9 Hz, 1H, CHOH-a), 4.63 (d, *J*= 5.4 Hz, 1H, CHOH-b), 4.32 (dd, *J*= 5.4, 1.1 Hz, 1H, CHOH-c), 3.39 (dd, *J*= 13.9, 3.1 Hz, 1H, CH$_2$NH), 3.13 (dd, *J*= 13.9, 11.5 Hz, 1H, CH$_2$NH). ^{13}C NMR (125 MHz, MeOD) δ 176.9 (C=O), 81.6 (CHOH-a), 69.1 (CHOH-b), 68.2 (CHOH-c), 40.2 (CH$_2$NH). HRMS (EI): found 147.0608 $C_5H_9NO_4$ calculated 147.0610. υ cm^{-1}: 3546.3, 3416.4, 2890.2, 2524.7, 1645.3, 1450.4, 1203.6, 760.9, 543.1.

6.1.17 Protection of (3R,4R,5R)-3,4,5-trihydroxypiperidin-2-one (87).[164]

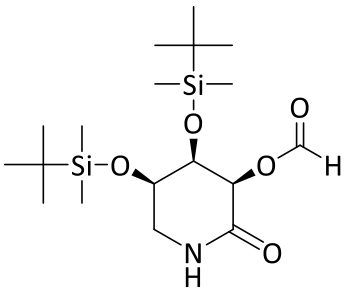

To a solution of trihydroxy lactam **(86)** (224 mg, 1.52 mmol) in DMF (30 ml) was added tert-butyldimethylsilyl chloride TBDMSCl (3.5 eq., 5.33 mmol, 800 mg) and imidazole (3.5 eq., 5.33 mmol, 360 mg). The mixture was stirred at r.t. for 12 h and the solvent was evaporated and then purified by flash chromatography (EtOAc:hexane, 4:6, R_f 0.64) to yield a white solid (272 mg, 0.67 mmol, 44%), m.p. 130-133 ^oC. ^1H NMR (400 MHz, $CDCl_3$) δ 8.14 (s, 1H, HC=O), 6.01 (s, 1H, NH), 4.29 (ddd, *J*= 7.2, 4.6, 2.6 Hz, 1H, CHO), 4.19 (d, *J*= 4.8 Hz, CH-OOH), 4.06 (dd, *J*= 4.8, 2.6 Hz, 1H, CHO), 3.70 (ddd, *J*= 14.5, 6.9, 4.7 Hz, 1H, CH_2NH), 3.27 (ddd, *J*= 14.5, 7.2, 5.5 Hz, 1H, CH_2NH), 0.83 (s, 9H, 3 CH_3), 0.79 (s, 9H, 3 CH_3), 0.078 (s, 3H, CH_3-Si), 0.049 (s, 3H, CH_3-Si), 0.01 (s, 3H, CH_3-Si), -0.0001 (s, 3H, CH_3-Si). ^{13}C NMR (125 MHz, $CDCl_3$) δ 173.9 (CO), 161.6 (HCOO), 83.8 (CH-OCOH), 71.7 (CHO), 70.2 (CHO), 38.6 (CH_2NH), 25.8, 25.7 (6 CH_3), 18.4, 18.1 (2 quaternary carbon), -4.5, -4.7, -4.9, -5.1 (4 CH_3-Si). HRMS (EI): found 404.2300 [M+1], 426.2100 [M+Na], $C_{18}H_{37}NO_5Si_2Na$ calculated 426.2102 υ cm^{-1}: 3319.9, 2927.9, 2856.6, 1774.5, 1678.0, 1535.3, 1165.0, 1109.1, 993.3, 918.1, 839.0, 839.0, 775.4, 677.0.

6.1.18 General procedure for preparation of 2,2-Dimethyltera-hydro-[1,3]dioxolo[4,5-c]pyridine-6 (*3aH*)-thione.[168]

A solution of protected lactam (1.806 g, 10.56 mmol) in 50 ml dry THF was treated with Lawesson's reagent (0.6 eq., 6.34 mmol, 2.56 g) and the reaction mixture was stirred at r.t. overnight. The solvent was evaporated and the residue was purified by flash chromatography.

(3aR, 7aS)-2,2-Dimethylterahydro-[1,3]dioxolo[4,5-c]pyridine-6 (3aH)-thione (60).

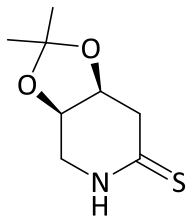

From **58**. White-yellowish oil (1.22 g, 6.53 mmol, 62 %), R_f 0.58 (Et_2O). ^{1}H NMR (500 MHz, MeOD) δ 4.67-4.62 (m,1H, CHO), 4.56-4.51 (m, 1H, CHO), 3.48-3.22 (m, 2H, CH_2NH), 3.21, 2.53 (m, 2H, CH_2CS), 1.38 (s, 3H, CH_3), 1.33 (s, 3H, CH_3). ^{13}C NMR (125 MHz, MeOD) δ 201.5 (C=S), 108.6 (quaternary carbon), 72.3 (CHO), 72.3 (CHO), 45.1 (CH_2NH), 43.6 (CH_2CS), 24.6 (CH_3), 22.9 (CH_3). HRMS (EI): Found 187.0665 $C_8H_{13}NO_2S$, calculated 187.0700. υ cm^{-1}: 3294.4, 2991.6, 2931.8, 2902.9, 1533.4, 1377.2, 1195.9, 1163.1, 1126.4, 1022.3, 995.3, 981.8, 887.3, 833.3, 765.7, 729.1, 594.1, 516.9.

(3aS, 7aR)-2,2-Dimethylterahydro-[1,3]dioxolo[4,5-c]pyridine-6 (3aH)-thione (74).

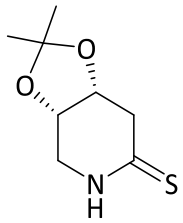

White yellowish oil (1.18 g, 6.32 mmol, 60 %), R_f 0.50 (EtOAc:hexane, 9:1). ^{1}H NMR (500 MHz, MeOD) δ 4.70-4.60 (m, 1H, CHO), 4.57-4.54 (m, 1H, CHOH), 3.47 (dd, *J*= 14.5, 1.4 Hz, 1H, CH_2NH), 3.27 (dd, *J*= 14.5, 2.6 Hz, 1H, CH_2NH), 3.18 (dd, *J*= 15.9, 2.3, 1H, CH_2CO), 2.66 (dd, *J*= 15.9, 4.0 Hz, 1H, CH_2CO), 1.38 (s, 3H, CH_3), 1.33 (s, 3H, CH_3). ^{13}C NMR (125 MHz, MeOD) δ 201.4 (C=S), 108.6 (quaternary carbon), 72.3 (CHOH), 71.9 (CHOH), 54.5 (CH_2NH), 45.2 (CH_2CS), 25.0 (CH_3), 22.8 (CH_3). HRMS (EI): Found 187.0530 $C_8H_{13}NO_2S$, calculated 187.0700. υ cm^{-1}: 2972.3, 2864.3, 1371.4, 1118.5, 1056.9, 972.1.

6.1.19 Preparation of (4S,5R)-4,5-bis((tert-butyldimethylsilyl)-oxy)piperidin-2-thione (61).[168]

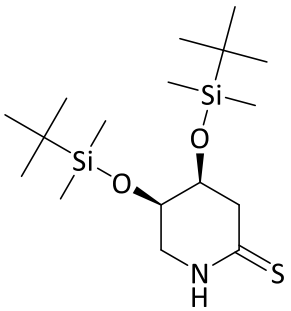

A solution of protected lactam **(59)** (0.337 g, 0.9 mmol) in 30 ml dry THF was treated with Lawesson's reagent (0.6 eq., 0.54 mmol, 0.22 g) and the reaction mixture was stirred at r.t. overnight. The solvent was evaporated and the residue was purified by flash chromatography (EtOAc:hexane, 2:8, R_f 0.43) to yield a white solid (0.34 g, 0.9 mmol, 92%), m.p. 130-132 ^oC. ^1H NMR (500 MHz, $CDCl_3$) δ 8.30 (s, 1H, NH), 3.92-3.87 (m, 1H, CHO), 3.87-3.81 (m, 1H, CHO), 3.35 (dd, *J*= 13.0, 8.7 Hz, 1H, CH_2NH), 3.24 (dd, *J*= 12. 9, 6.8 Hz, 1H, CH_2NH), 3.03 (dd, *J*= 18.5, 6.6 Hz, 1H, CH_2CS), 2.90 (dd, *J*= 18.5, 4.3 Hz, 1H, CH_2CS), 0.88-0.72 (m, 18H, 6 CH_3), 0.05-(-0.05) (m, 12H, 4 CH_3-Si). ^{13}C NMR (125 MHz, $CDCl_3$) δ 200.8 (C=S), 68.1 (CHO), 67.3 (CHO), 48.9 (CH_2NH), 45.6 (CH_2CS), 25.8 (6 CH_3), 18.4 (quaternary carbon), 18.1 (quaternary carbon), -4.5, -4.6, -4.7, -4.8 (4 CH_3-Si). HRMS (EI): found 375.2155, $C_{17}H_{37}NO_2SSi_2$ calculated 375.2162. υ cm^{-1}: 2953.0, 2926.0, 2854.6, 1560.4, 1126.4, 1082.1, 1004.9, 827.5, 777.3, 680.9.

6.1.20 General procedure for preparation of amidine derivatives:

Meerwein's salt (3 eq., 0.36 g, 1.92 mmol) was added under argon to a solution of thiolactam (120 mg, 0.64 mmol) in dry DCM (20 ml) at 0 ^oC. The resulting suspension was stirred at 0 ^oC for 3 h. and then amine (2 eq.) was added. The reaction was allowed to warm to ambient temperature and stirred at the same temperature for three days. The solvent was evaporated and the residue was purified by flash chromatography. For further purification of amidines, HPLC was used.

(3R,4S)-6-(Propylamino)-2,3,4,5-tetrahydropyridine-3,4-diol (35b).

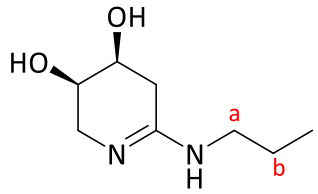

White hygroscopic solid (75.2 mg, 0.44 mmol, 68%), R_f 0.29 (MeCN:H_2O:HOAc 10:2:0.1). ^{1}H NMR (500 MHz, MeOD) δ 4.16-3.99 (m, 2H, 2 CHOH), 3.58-3.44 (m, 2H, CH_2N=C), 3.20-3.15 (m, 2H, CH_2-a), 2.86 (dd, *J*= 17.3, 4.4 Hz, 1H, CH_2C=N), 2.75 (dd, *J*= 17.6, 6.8 Hz, 1H, CH_2C=N), 1.68 (m, 2H, CH_2-b), 1.02 (t, *J*= 7.3 Hz, 3H, CH_3). ^{13}C NMR (125 MHz, MeOD) δ 162.4 (C=N), 64.9 (CHOH), 64.4 (CHOH), 45.2 (CH_2N=C), 43.5 (CH_2-a), 31.3 (CH_2C=N), 20.6 (CH_2-b), 10.2 (CH_3). HRMS (EI): found 172.1209, $C_8H_{16}N_2O_2$, calculated 172.1200. υ cm^{-1}: 3525.9, 1670.4, 1419.6, 1087.8, 520.8.

(3S,4R)-6-(Propylamino)-2,3,4,5-tetrahydropyridine-3,4-diol (36a).

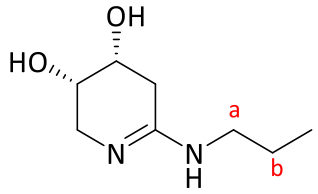

White hygroscopic solid (43.1 mg, 0.25 mmol, 39%), R_f 0.33 (MeCN:H_2O:HOAc, 10:2:0.1). ^{1}H NMR (500 MHz, MeOD) δ 4.02-3.91 (m, 2H, 2CHOH), 3.44 (dd, *J*= 13.2, 4.2 Hz, 1H, CH_2N), 3.35 (dd, *J*= 13.2, 5.8 Hz, 1H, CH_2N), 3.10-3.01 (m, 2H, CH_2-a), 2.75 (dd, *J*= 17.5, 4.9 Hz, 1H, CH_2C=N), 2.63 (dd, *J*= 17.5, 7.2 Hz, 1H, CH_2C=N), 1.65-1.48 (m, 2H, CH_2-b), 0.90 (t, *J*= 7.4 Hz, 3H, CH_3). ^{13}C NMR (125 MHz, MeOD) δ 162.0 (C=N), 65.2 (CHOH), 64.4 (CHOH), 45.2 (CH_2-a), 43.5 (CH_2N=C), 31.3 (CH_2C=N), 20.6 (CH_2-b), 10.2 (CH_3). HRMS (EI): found 172.1200 $C_8H_{16}N_2O_2$, calculated 172.1200. υ cm^{-1}: 3520.3, 1665.1, 1414.8, 1064.2, 522.5.

(3R,4S)-6-(hexylamine)-2,3,4,5-tetrahydropyridine-3,4-diol (35f).

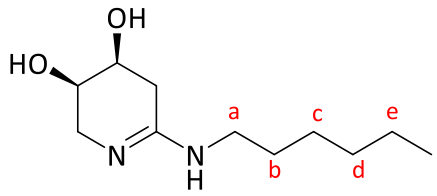

Yellow oil (37.1 mg, 0.17 mmol, 27%), R_f 0.54 (MeCN:H_2O:HOAc, 10:2:0.2). ^{1}H NMR (400 MHz, MeOD) δ 4.06-3.86 (m, 2H, 2 CHOH), 3.44 (dd, *J*= 13.1, 6.3 Hz, 1H, CH_2N=C), 3.35 (dd, *J*= 13.2, 5.7 Hz, 1H, CH_2N=C), 3.09 (dd, *J*= 12.4, 7.1 Hz, 2H, CH_2-a), 2.74 (dd, *J*= 17.4, 4.8 Hz, 1H, CH_2C=N), 2.62 (dd, *J*= 17.5, 7.1 Hz, 1H, CH_2C=N), 1.59-1.47 (m, 2H, CH_2-b), 1.34-1.20 (m, 6H, 3 CH_2(c,d,e)), 0.82 (t, *J*= 6.9 Hz, 3H, CH_3). ^{13}C NMR (125 MHz, MeOD) δ 163.7 (C=N), 64.9 (CHOH), 64.4 (CHOH), 45.1 (CH_2N=C), 41.9 (CH_2NH), 31.3 (CH_2C=N), 27.4, 26.3, 25.9, 22.2 (4 CH_2 (b,c,d,e)), 12.9 (CH_3). HRMS (EI): found 214.1757 $C_{11}H_{22}N_2O_2$, calculated 214.1700. υ cm^{-1}: 3354.2, 2619.3, 1118.7, 972.1, 605.6.

(3aR,7aS)- *N*-Cyclohexyl-2,2-dimethyl-3a,4,7,7a-tetrahydro-[1,3]dioxolo[4,5-c] pyridine-6-amine (63a).

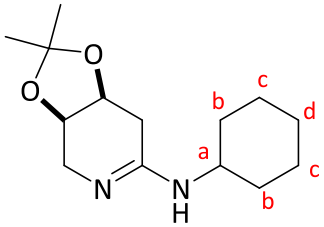

White solid (79.3 mg, 0.31 mmol, 49%), R_f 0.20 (MeCN:H_2O 10:3), m.p. 240-242 ° C. ^{1}H NMR (500 MHz, MeOD) δ 4.78 (ddd, *J*= 7.6, 3.4 Hz, 1H, CHO), 4.63 (dt, *J*= 7.7, 1.9 Hz, 1H, CHO), 3.58 (dd, 2H, *J*= 14.5, 1.5 Hz, 1H, CH_2N=C), 3.52-3.43 (m, 1H, CH-a), 3.33 (dd, 2H, *J*= 14.5, 2.3 Hz, CH_2N=C), 2.83 (dd, *J*= 15.7, 2.4 Hz, 1H, CH_2C=N), 2.70 (dd, *J*= 15.7, 3.5 Hz, 1H, CH_2C=N), 2.06-1.93 (m, 2H, CH_2-b), 1.90-179 (m, 2H, CH_2-b), 1.77-1.64 (m, 1H, CH-d), 1.51-1.20 (m, 5H, CH-d, 2 CH_2-c), 1.37 (s, 3H, CH_3), 1.35 (s, 3H, CH_3). ^{13}C NMR (125 MHz, MeOD) δ 162.3 (C=N), 108.7 (quaternary carbon), 72.2 (CHO), 70.9 (CHO), 51.3 (CH_2-a), 42.7 (CH_2N=C), 31.4 (CH_2C=N), 31.4, 30.5, 24.8, 24.2, 22.5 (5 CH_2-cyclohexyl ring), 24.72, 22.43 (2 CH_3). HRMS (EI): Found 252.1800 $C_{14}H_{24}N_2O_2$, calculated 252.1800. υ cm^{-1}: 2943.4, 2858.5, 1660.7, 1446.6, 1211.3, 1087.8, 1035.8, 1008.8, 956.7, 707.9.

(3aS,7aR)-*N*-Cyclohexyl-2,2-dimethyl-3a,4,7,7a-tetrahydro-[1,3]dioxolo[4,5-c] pyridine-6-amine (76b).

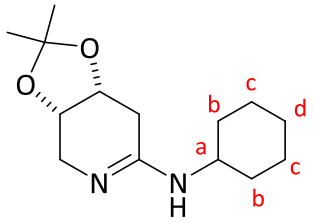

White hygroscopic solid (37.2 mg, 0.15 mmol, 23%), R_f 0.2 (MeCN:H_2O:HOAc, 10:2:0.5). ^{1}H NMR (400 MHz, MeOD) δ 4.77 (ddd, *J*= 7.6, 3.4, 2.4 Hz, 1H, CHO), 4,65-4.61 (m, 1H, CHO), 3.59 (dd, *J*= 15.9, 1.5 Hz, 1H, CH_2N=C), 3.57-3.54 (m, 1H, CH-a), 3.48 (dd, *J*= 15.7, 2.7 Hz, 1H, CH_2N=C), 2.83 (dd, *J*= 15.3, 4.6 Hz, 1H, CH_2C=N), 2.70 (dd, *J*= 15.7, 3.4 Hz, 1H, CH_2C=N), 2.03-1.90 (m, 2H, CH_2-b), 1.88-1.77 (m, 2H, CH_2-b), 1.76-1.64 (m, 1H, CH_2-d), 1.56-1.16 (m, 5H, CH-d, 2 CH_2-c), 1.37 (s, 3H, CH_3), 1.35 (s, 3H, CH_3). ^{13}C NMR (125 MHz, MeOD) δ 162.3 (C=N), 108.7 (quaternary carbon), 72.2 (CHO), 70.9 (CHO), 51.3 (CHNH), 42.7 (CH_2N=C), 31.4 (CH_2C=N), 31.4, 31.1, 24.7, 24.2, 24.0 (5 CH_2-cyclohexyl ring), 24.9, 22.5 (2 CH_3). HRMS (EI): found 252.1916 $C_{14}H_{24}N_2O_2$, calculated 252.1800. υ cm^{-1}: 2821.3, 2655.9, 1613.5, 1512.9, 1080.4, 1023.8, 864.1, 623.5.

(3aR,7aS)-*N*-(2-Fluorobenzyl)-2,2-dimethyl-3a,4,7,7a-tetrahydro-[1,3]dioxolo [4,5-c]pyridine-6-amine (63b).

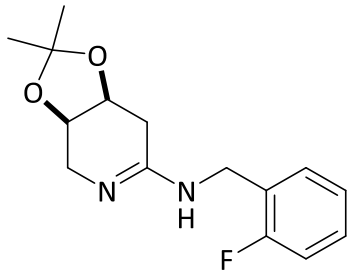

Yellow oil (86.7 mg, 0.31 mmol, 49%), R_f 0.62 ($CHCl_3$:MeOH:NH_3, 7:3:0.3). ^{1}H NMR (500 MHz, MeOD) δ 7.47-7.42 (m, 2H, 2 ArCH), 7.28-7.16 (m, 2H, 2 ArCH), 4.82 (m, 1H, CHO), 4.68 (m, 1H, CHO), 4.61 (d, *J*= 15.2 Hz, 1H, CH_2NH), 4,53 (d, *J*= 15.3 Hz , 1H, CH_2NH), 3.61 (d, *J*= 14.5 Hz, 1H, CH_2N=C), 3.39 (d, *J*= 14.7 Hz, 1H, CH_2N=C), 2.92 (d, *J*= 15.8 Hz, 1H, CH_2C=N), 2.80 (d, *J*= 15.9 Hz, 1H, CH_2C=N), 1.36 (s, 6H, 2 CH_3). ^{13}C NMR (125 MHz, MeOD) δ 164.0 (C=N), 161.9, 160.0 (CF), 130.5 (ArCH), 130.5 (ArCH), 124.5 (ArCH), 121.3 (quaternary carbon-Ar), 115.4

(ArCH), 108.8 (quaternary carbon), 73.9 (CHO), 72.1 (CHO), 42.9 (CH_2N=C), 39.8 (CH_2NH), 31.3 (CH_2C=N), 24.7, 24.5 (2 CH_3). HRMS (EI): found 278.1500 $C_{15}H_{19}FN_2O_2$, calculated 278.1400. υ cm^{-1}: 1647.2, 1124.5, 972.1, 842.9.

(3aS,7aR)-N-(2-Fluorobenzyl)-2,2-dimethyl-3a,4,7,7a-tetrahydro-[1,3]dioxolo [4,5-c]pyridine-6-amine (76c).

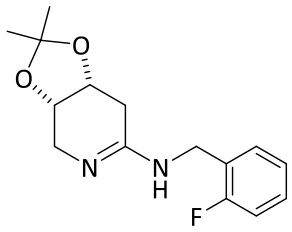

White-yellowish hygroscopic solid (32.15 mg, 0.12 mmol, 18%), R_f 0.41 (MeCN:H_2O:HOAc, 10:2:0.1). ^{1}H NMR (500 MHz, MeOD) δ 7.48-7.40 (m, 2H, ArCH), 7.27-7.16 (m, 2H, ArCH), 4.81-4.77 (m, 1H, CHO), 4.66-4.63 (m, 1H, CHO), 4.61-4.52 (m, 2H, CH_2-NH), 3.63 (dd, *J*= 14.5, 1.4 Hz, 1H, CH_2N=C), 3.37 (dd, *J*= 14.5, 2.3 Hz, 1H, CH_2N=C), 2.95 (dd, *J*= 15.8, 2.3 Hz, 1H, CH_2C=N), 2.78 (dd, *J*= 15.8 Hz, 1H, CH_2C=N), 1.36 (s, 3H, 2 CH_3). ^{13}C NMR (125 MHz, MeOD) δ 164.0 (CO), 161.9 (ArC-F), 130.0 (ArCH), 129.7 (ArCH), 124.4 (ArCH), 121.5 (CF), 115.4 (ArCH), 108.8 (quaternary carbon), 72.1 (CHO), 70.9 (CHO), 42.9 (CH_2NH), 39.8 (CH_2N=C), 31.3 (CH_2C=N), 24.8 (CH_3), 22.5 (CH_3). HRMS (EI): found 278.1500 $C_{15}H_{20}FN_2O_2$, calculated 278.1400. υ cm^{-1}: 1620.3, 1265.1, 894.4, 712.8.

(3aR,7aS)-*N*-(3-Fluorobenzyl)-2,2-dimethyl-3a,4,7,7a-tetrahydro-[1,3]dioxolo [4,5-c]pyridine-6-amine (63c).

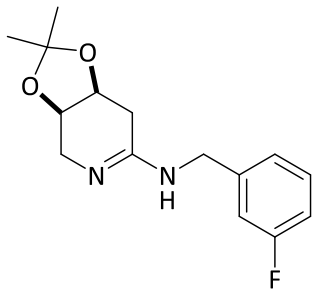

White-yellowish hygroscopic solid (26.7 mg, 0.096 mmol, 15%), R_f 0.37 (MeCN:H_2O:HOAc, 10:2:0.1). ^{1}H NMR (500 MHz, MeOD) δ 7.23 (dd, *J*= 14.3, 7.1 Hz, 1H, ArCH), 6.99 (d, *J*= 7.7 Hz, 1H, ArCH), 6.94-6.88 (m, 2H, ArCH), 4.59 (d, *J*= 6.0 Hz, 1H, CHO), 4.43 (d, *J*= 7.5 Hz, 1H, CHO), 4.39-4.30 (m, 2H, CH_2NH), 3.38 (d, *J*= 14.5 Hz, 1H, CH_2N=C), 3.14 (d, *J*= 14.6 Hz, 1H, CH_2N=C),

2.75 (d, *J*= 15.8 Hz, 1H, CH_2C=N), 2.60 (d, *J*= 15.8 Hz, 1H, CH_2C=N), 1.14 (s, 3H, CH_3), 1.12 (s, 3H, CH_3). ^{13}C NMR (125 MHz, MeOD) δ 164.1 (C=N), 162.1 (CF), 137.2 (quaternary carbon-Ar), 130.6 (ArCH), 123.1 (ArCH), 114.8 (ArCH), 114.1 (ArCH), 108.9 (quaternary carbon), 72.1 (CHO), 70.7 (CHO), 44.7 (CH_2NH), 43.1 (CH_2N=C), 31.7 (CH_2C=N), 24.7 (CH_3), 22.4 (CH_3). HRMS (EI): found 278.1484 $C_{15}H_{20}FN_2O_2$, calculated 278.1400. υ cm^{-1}: 3360.0, 2605.8, 1647.2, 1593.2, 1379.1, 1118.7, 983.7, 877.6, 690.5.

2-((((3aR,7aS)-2,2-dimethyl-3a4,7,7a-tetrahydro-[1,3]dioxolo[4,5-c]pyridine-6-yl)amino)methyl)phenol (63d).

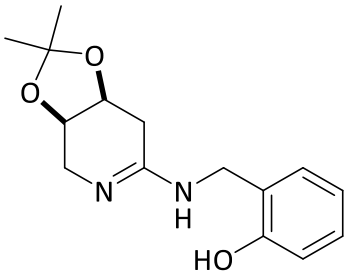

Colourless oil (53.1 mg, 0.19 mmol, 30%), R_f 0.40 (MeCN:H_2O:HOAc, 10:2:0.1). ^{1}H NMR (500 MHz, MeOD) δ 7.34-7.19 (m, 2H, ArCH), 6.93-6.85 (m, 2H, ArCH), 4.78-4.73 (m, 1H, CHO), 4.66-4.59 (m, 1H, CHO), 4.49 (d, *J*= 14.5 Hz, H, CH_2NH), 3.39 (d *J*= 14.6 Hz, 1H, CH_2NH), 3.60 (d, *J*= 14.5 Hz, 1H, CH_2N=C), 3.37 (d, *J*= 14.5 Hz, 1H, CH_2N=C), 2.89 (d, *J*= 15.8 Hz, 1H, CH_2C=N), 2.73 (d, 15.7 Hz, 1H, CH_2C=N), 1.34 (s, 3H, CH_3), 1.25 (s, 3H, CH_3). ^{13}C NMR (125 MHz, MeOD) δ 163.5 (C=N), 155.3 (CF), 129.7 (quaternary carbon-Ar), 120.5 (ArCH), 119.8 (2 ArCH), 114.8 (2 ArCH), 108.8 (quaternary carbon), 72.2 (CHO), 70.8 (CHO), 42.8 (CH_2NH), 40.9 (CH_2N=C), 31.9 (CH_2C=N), 24.6 (CH_3), 22.6 (CH_3). HRMS (EI): found 276.1554 $C_{15}H_{20}N_2O_3$, calculated 276.1500. υ cm^{-1}: 3361.3, 3135.7, 2429.1, 1635.2, 1436.9, 1210.2, 923.5, 654.8.

(3aR,7aS)-2,2-Dimethyl-*N*-(morpholinoethyl)-3a,4,7,7a-tetrahydro-[1,3] dioxolo[4,5-c]pyridine-6-amine (63e).

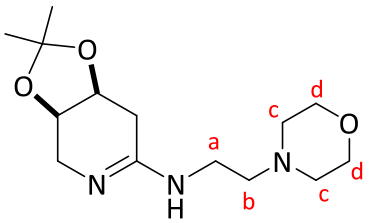

Colourless oil (45.5 mg, 0.16 mmol, 25%), R_f 0.9 (MeCN:H_2O, 10:2). ^{1}H NMR (400 MHz, MeOD) δ 4.78 (ddd, *J*= 7.6, 3.5 Hz, 1H, CHO), 4.70-4.58 (m, 1H, CHO), 3.75-3.71 (m, 4H, 2 CH_2-d), 3.63 (dd, *J*= 14.6, 1.5 Hz, 1H, CH_2N=C), 3.44 (t, *J*= 5.4 Hz, 2H, CH_2NH-a), 3.37-3.35 (m, 1H, CH_2N=C), 2.91 (dd, *J*= 15.8, 2.3 Hz, 1H, CH_2C=N), 2.72 (dd, *J*= 15.7, 3.5 Hz, 1H, CH_2C=N), 2.66 (t, *J*= 5.9 Hz, 2H, CH_2N-b), 2.59-2.50 (m, 4H, 2 CH_2N-c), 1.37 (s, 3H, CH_3), 1.35 (s, 3H, CH_3). ^{13}C NMR (125 MHz, MeOD) δ 164.5 (C=N), 108.7 (quaternary carbon), 72.2 (CHO), 70.8 (CHO), 66.4 (2 CH_2-d), 55.78 (CH_2NH-a), 53.4 (CH_2N-c), 42.4 (CH_2N=C), 39.3 (CH_2N-b), 31.2 (CH_2C=N), 24.9, 22.5 (2 CH_3). HRMS (EI): found 284.1969 $C_{14}H_{25}N_3O_3$, calculated 284.1900. υ cm^{-1}: 2267.4, 1647.2, 1124.5, 1062.8, 972.1.

(3aS,7aR)-2,2-Dimethyl-*N*-(morpholinoethyl)-3a,4,7,7a-tetrahydro-[1,3] dioxolo[4,5-c]pyridine-6-amine (76d).

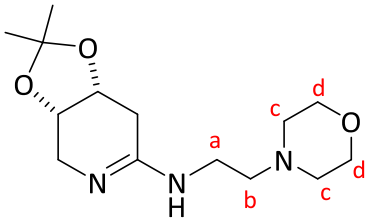

Yellow oil (21.8 mg, 0.077 mmol, 12%), R_f 0.73 (EtOAc:MeOH:NH_3, 10:3:0.5). ^{1}H NMR (500 MHz, MeOD) δ 4.83-4.77 (m, 1H, CHO), 4.69-4.64 (m, 1H, CHO), 3.90-3.86 (m, 4H, 2CH_2-d), 3.78-3.65 (m, 2H, CH_2-a), 3.63 (d, *J*= 14.6 Hz, 2H, CH_2N=C), 3.39 (dd, *J*= 14.5, 2.2 Hz, 1H, CH_2N=C), 3.22 (dd, *J*= 14.9, 6.3 Hz, 1H, CH_2-b), 3.17-3.08 (m, 4H, 2CH_2-c), 2.88 (dd, *J*= 15.9, 2.0 Hz, 1H, CH_2C=N), 2.78 (dd, *J*= 15.9, 3.3 Hz, 1H, CH_2C=N), 1.38 (s, 3H, CH_3), 1.35 (s, 3H, CH_3). ^{13}C NMR (125 MHz, MeOD) δ 165.0 (C=N), 108.9 (quaternary carbon), 72.1 (CHO), 70.9 (CHO), 64.5 (2CH_2-d), 54.4 (CH_2-a), 52.9 (2CH_2-c), 43.0 (CH_2-N=C), 37.2 (CH_2-b), 31.6 (CH_2-C=N), 24.9

(CH_3), 22.5 (CH_3). HRMS (EI): found 283.1969 $C_{14}H_{25}N_3O_3$, calculated 283.1900. υ cm^{-1}: 2618.4, 1631.1, 1321.3, 1034.5, 1010.3, 978.4, 734.5.

6.1.21 Synthesis of *N*-((3aR,7aS)-2,2-dimethyl-3a,4,7,7a-tetra-hydro-[1,3]dioxolo[4,5-c]pyridin-6-yl)hydroxylamine (66).

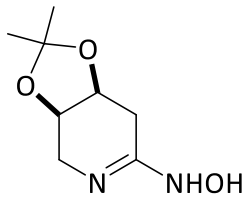

To a solution of thiolactam (100 mg, 0.53 mmol) in dry methanol (20 ml) were added hydroxylamine hydrochloride (2.53 eq., 1.34 mmol, 0.093 g) and sodium hydrogen carbonate (1.53 eq., 1.34 mmol, 0.142 g). The mixture was heated under reflux for 3 h and then filtered. The solvent was evaporated and the crude product was purified by flash chromatography (32.2 mg, 0.17 mmol, 27%), R_f 0.15 (MeCN:H_2O, 10:3). ^{1}H NMR (400 MHz, MeOD) δ 4.53-4.47 (m, 1H, CHO), 3.36-4.32 (m, 1H, CHO), 3.22-3.18 (m, 2H, CH_2N=C), 2.29-2.26 (m, 2H, CH_2C=N), 1.27 (s, 3H, CH_3), 1.21 (s, 3H, CH_3). ^{13}C NMR (100 MHz, MeOD) δ 152.5 (C=N), 108.4 (quaternary carbon), 73.4 (CHO), 71.5 (CHO), 41.4 (CH_2N=C), 28.9 (CH_2C=N), 25.1 (CH_3), 23.0 (CH_3). HRMS (EI): found 186.1000 $C_8H_{14}N_2O_3$, calculated 186.1000. υ cm^{-1}: 2610.2, 2465.7, 1198.6, 1025.5, 978.6, 884.2, 674.1.

6.1.22 General method for deprotection of acetonide protected group in amidine derivatives:

A solution of protected amidine in aqueous 2 N HCl (10 ml) was heated with stirring for 12 h at r.t. and then the solvent was removed and the residue was triturated with diethyl ether and then dried under vacuum to give an amidine derivative.

(3R,4S)-6-(Hydroxyamino)-2,3,4,5-tetrahydropyridine-3,4-diol (35a).

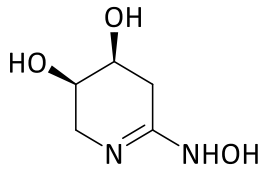

Brown hygroscopic solid (6.7 mg, 0.046 mmol, 29%), R_f 0.12 (MeCN:H_2O:HOAc, 10:2:0.2). ^{1}H NMR (400 MHz, MeOD) δ 4.15-4.10 (m, 1H, CHOH), 4.10-4.05 (m, 1H, CHOH), 3.54 (dd, 2H, *J*=

13.3, 4.0 Hz, 1H, CH_2N=C), 3.45 (dd, *J*= 13.2, 5.9 Hz, 1H, CH_2N=C), 2.78 (dd, 2H, *J*= 16.9, 4.1Hz, 1H, CH_2C=N), 2.67 (dd, *J*= 17.0, 7.0 Hz, 1H, CH_2C=N). ^{13}C NMR (100 MHz, MeOD) δ 159.1 (C=N), 65.3 (CHOH), 64.2 (CHOH), 44.3 (CH_2N=C), 27.6 (CH_2C=N). HRMS (EI): found 146.0800 $C_5H_{10}N_2O_3$, calculated 146.0700. υ cm^{-1}: 3369.6, 2613.6, 2333.9, 1388.7, 1220.9, 1116.8, 968.3, 879.5, 644.2.

(3R,4S)-6-(cyclohexylamino)-2,3,4,5-tetrahydropyridine-3,4-diol (35c).

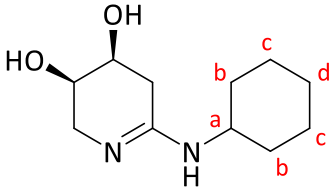

Hygroscopic white solid (60.03 mg, 0.15 mmol, 90%), R_f 0.22 (MeCN:H_2O:HOAc, 10:2:0.2). ^{1}H NMR (500 MHz, MeOD) δ 4.02-3.87 (m, 2H, 2 CHOH), 3.44 (dd, *J*= 13.1, 3.4 Hz, 2H, CH_2N=C), 3.39-3.32 (m, 2H, 1H CH_2N=C, 1H CH-a), 2.74 (dd, *J*= 17.5, 4.2 Hz, 1H, CH_2C=N), 2.63 (dd, *J*= 17.5, 6.9 Hz, 1H, CH_2C=N), 1.88-1.80 (m, 2H, CH_2-b), 1.74-1.68 (m, 2H, CH_2-b), 1.60-1.54 (m, 1H, CH-d), 1.38-1.08 (m, 5H, CH-d, 2 CH_2-c). ^{13}C NMR (125 MHz, MeOD) δ 160.6 (C=N), 67.5 (CHOH), 64.5 (CHOH), 51.1 (CH-a), 45.2 (CH_2N=C), 32.6 (CH_2C=N), 31.3, 30.5, 25.1, 24.7, 24.2 and 23.9 (cyclohexyl ring). HRMS (EI): Found 212.1603 $C_{11}H_{20}N_2O_2$, calculated 212.1500. υ cm^{-1}: 3361.9, 2628.9, 1384.8, 1114.9, 1028.1, 964.4, 584.4.

(3S,4R)-6-(cyclohexylamino)-2,3,4,5-tetrahydropyridine-3,4-diol (36b).

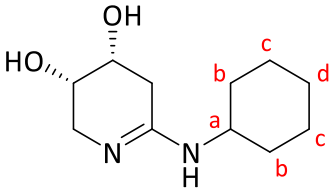

White hygroscopic solid (19.1 mg, 0.19 mmol, 61%), R_f 0.24 (MeCN:H_2O:HOAc, 10:2:0.1). ^{1}H NMR (400 MHz, MeOD) δ 4.15-4.0 (m, 2H, 2 CHOH), 3.57-3.40 (m, 3H, 2 CH_2N=C, CH-a), 2.83 (d, *J*= 16.4 Hz, 1H, CH_2C=N), 2.73 (dd, *J*= 16.8, 5.9 Hz, 1H, CH_2C=N), 2.0-1.90 (m, 2H, CH_2-b), 1.86-1.79 (m, 2H, , CH_2-b), 1.72-1.67 (m, 1H, CH-d), 1.45-1.20 (m, 5H, CH-d, 2 CH_2-c). ^{13}C NMR (125 MHz, MeOD) δ 167.2 (C=N), 64.9 (CHOH), 64.5 (CHOH), 51.0 (CH-a), 45.1 (CH_2-N=C), 31.3 (CH_2C=N), 31.3 (CH_2-d), 24.8 ($2CH_2$-b), 24.2 ($2CH_2$-c). HRMS (EI): found 212.1525 $C_{11}H_{20}N_2O_2$, calculated 212.1500. υ cm^{-1}: 3441.0, 2918.3, 2848.9, 1668.4, 1010.7, 950.9, 542.0.

(3R,4S)-6-((2-Fluorobenzyl)amino)-2,3,4,5-tetrahydropyridine-3,4-diol (35d).

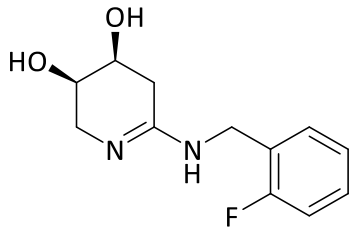

Hygroscopic white solid (31.4 mg, 0.09 mmol, 29%), R_f 0.31 (MeCN:H_2O:HOAc, 10:2:0.1). ^{1}H NMR (500 MHz, MeOD) δ 7.36-7.28 (m, 2H, 2 Ar-CH), 7.16-7.04 (m, 2H, 2 Ar-CH), 4.45-4.40 (m, 2H, 2 CHOH), 4.04-3.97 (m, 2H, CH_2NH), 3.49 (d, *J*= 12.9 Hz, 1H, CH_2N=C), 3.41 (d, *J*= 12.5 Hz, 1H, CH_2N=C), 2.82 (d, *J*= 17.0 Hz, 1H, CH_2C=N), 2.70 (dd, *J*= 17.2, 6.0 Hz, 1H, CH_2C=N). ^{13}C NMR (125 MHz, MeOD) δ 162.0 (C=N), 161.9 (ArC-F), 131.4, 131.6, 124.8, 121.5, 117.2 (Ar-C), 65.5 (CHOH), 65.1 (CHOH), 47.2 (CH_2-NH), 40.4 (CH_2N=C), 31.7 (CH_2C=N). HRMS (EI): Found 238.1151 $C_{12}H_{15}FN_2O_2$ calculated 238.1100. υ cm^{-1}: 3375.3, 2557.6, 2366.7, 1456.3, 1217.1, 615.3.

(3S,4R)-6-((2-Fluorobenzyl)amino)-2,3,4,5-tetrahydropyridine-3,4-diol (36c).

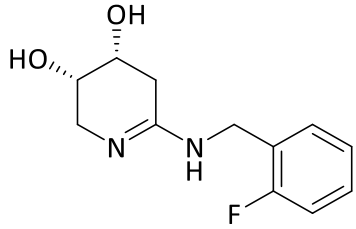

White hygroscopic solid (27.5 mg, 0.12 mmol, 68%), R_f 0.29 (MeCN:H_2O:HOAc, 10:2:0.1). ^{1}H NMR (400 MHz, MeOD) δ 7.49-7.39 (m, 2H, 2 ArCH), 7.29-7.14 (m, 2H, 2 ArCH), 4.55- 4.52(m, 2H, 2 CHOH), 4.17-4.07 (m, 2H, CH_2NH), 3.60 (d, *J*= 13.5 Hz, 1H, CH_2N=C), 3.53 (dd, *J*= 13.2, 5.2 Hz, 1H, CH_2N=C), 2.94 (dd, *J*=17.6, 3.6 Hz, 1H, CH_2C=N), 2.82 (dd, *J*=17.5, 6.6 Hz, 1H, CH_2C=N). ^{13}C NMR (125 MHz, MeOD) δ 162.3 (C=N), 160.0 (ArC-F), 130.5, 130.4, 124.7, 121.4, 115.4 (ArC), 64.9 (CHOH), 64.4 (CHOH), 45.4 (CH_2NH), 39.9 (CH_2N=C), 31.6 (CH_2C=N). HRMS (EI): found 238.1120 $C_{12}H_{15}FN_2O_2$, calculated 238.1100. υ cm^{-1}: 3118.9, 1662.6, 1398.4, 1056.9, 794.7, 545.8.

(3R,4S)-6-((3-Fluorobenzyl)amino)-2,3,4,5-tetrahydropyridine-3,4-diol (35e).

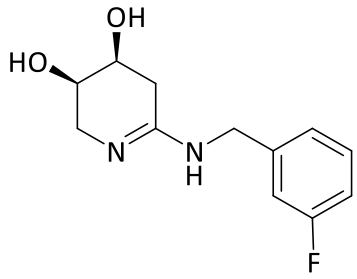

White yellowish oil (18.5 mg, 0.08 mmol, 74%), R_f 0.26 (MeCN:H_2O:HOAc, 10:2:0.1). ^{1}H NMR (500 MHz, MeOD) δ 7.34 (dd, *J*= 13.7, 7.4 Hz, 1H, ArCH-F), 7.11 (m, 3H, ArCH), 4.40 (s, 2H,CHO), 4.10-3.90 (m, 2H, CH_2NH), 3.47 (d, *J*= 12.4 Hz, 1H, CH_2N=C), 3.42-3.38 (m, 1H, CH_2N=C), 2.85 (d, *J*=17.0 Hz, 1H, CH_2C=N), 2.73 (dd, *J*=16.9, 5.0 Hz, 1H, CH_2C=N). ^{13}C NMR (125 MHz, MeOD) δ 164.0 (C=N), 162.1 (ArC-F), 137.2 (quaternary carbon-Ar), 130.8, 125.5, 114.8, 114.6 (4 ArCH) 65.5 (CHOH), 64.9 (CHOH), 45.3 (CH_2NH), 44.9 (CH_2N=C), 31.7 (CH_2C=N). HRMS (EI): Found 238.1122 $C_{12}H_{15}FN_2O_2$ Cal. 238.1100. υ cm^{-1}: 3360.0, 2605.8, 1647.2, 1593.2, 1379.1, 1219.01, 1118.7, 983.7, 877.6, 632.6.

(3R,4S)-6-((2-Hydroxybenzyl)amino)-2,3,4,5-tetrahydropyridine-3,4-diol (35g).

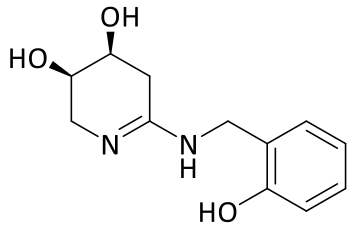

White hygroscopic solid (22 mg, 0.093 mmol, 49%), R_f 0.23 (MeCN:H_2O:HOAc, 10:2:0.1). ^{1}H NMR (500 MHz, MeOD) δ 7.14-7.0 (m, 2H, 2 ArCH), 6.78-6.74 (m, 2H, 2 ArCH), 4.28 (s, 2H, 2 CHO), 3.97 (s, 2H, CH_2NH), 3.47 (d, *J*= 12.3 Hz, 1H, CH_2N=C), 3.40 (dd, *J*= 12.8, 4.7 Hz, 1H, CH_2N=C), 2.76 (d, *J*= 15.0 Hz, 1H, CH_2C=N), 2.66 (dd, *J*= 17.6, 6.4 Hz, 1H, CH_2C=N). ^{13}C NMR (125 MHz, MeOD) δ 161.7 (C=N), 155.4 (ArC-OH), 129.8, 129.7, 120.5, 119.5, 114.8 (5 ArC), 65.0 (CHOH), 64.5 (CHOH), 45.1 (CH_2NH), 41.1 (CH_2N=C), 31.4 (CH_2C=N). HRMS (EI): Found 236.1100 $C_{12}H_{16}N_2O_3$, calculated 236.1200. υ cm^{-1}: 3566.4, 3030.2, 2929.9, 1670.4, 1436.9, 1010.7, 950.9, 709.8.

(3S,4R)-6-((2-Morpholinoethyl)amino)-2,3,4,5-tetrahydropyridine-3,4-diol (36d).

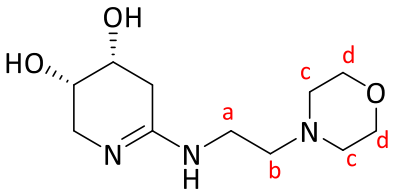

Yellow oil (18.7 mg, 0.077 mmol, 47%), R_f 0.16 (MeCN:H_2O:HOAc, 10:2:0.1). ^{1}H NMR (500 MHz, MeOD) δ 4.14-4.01 (m, 2H, 2 CHOH), 3.76-3.68 (m, 4H, 2 CH_2-d), 3.56 (dd, *J*= 13.1, 4.1 Hz, 1H, CH_2N=C), 3.49 (dd, *J*= 13.2, 5.4 Hz, 1H, CH_2N=C), 3.39 (t, *J*= 5.6 Hz, 2H, CH_2-a), 2.87 (dd, *J*= 17.6, 4.9 Hz, 1H, CH_2C=N), 2.77 (dd, *J*= 17.6, 7.1 Hz, 1H, CH_2C=N), 2.66 (t, *J*= 5.6 Hz, 2H, CH_2-b), 2.60-2.53 (m, 4H, 2CH_2-c). ^{13}C NMR (125 MHz, MeOD) δ 162.7 (C=N), 66.5 (2 CH_2-d), 65.9 (CHOH), 64.5 (CHOH), 55.8 (CH_2-b), 53.0 (2 CH_2-c), 45.0 (CH_2N=C), 39.2 (CH_2-a), 31.3 (CH_2-C=N). HRMS (EI): found 243.1665 $C_{11}H_{21}N_3O_3$, calculated 243.1600. υ cm^{-1}: 3489.2, 3016.7, 2924.1, 1676.1, 1577.8, 1436.9, 1201.7, 1010.7, 950.9, 709.8.

(3R,4S)-6-((2-Morpholinoethyl)amino)-2,3,4,5-tetrahydropyridine-3,4-diol (35h).

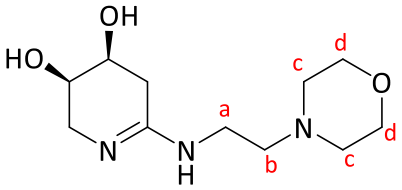

White hygroscopic solid (20 mg, 0.008 mmol, 44%), R_f 0.13 (MeCN:H_2O:HOAc, 7:3:1). ^{1}H NMR (500 MHz, MeOD) δ 4.13-4.02 (m, 2H, 2 CHOH), 3.74-3.70 (m, 4H, 2 CH_2-d), 3.57 (dd, *J*= 13.2, 4.3 Hz, 1H, CH_2N=C), 3.50 (dd, *J*= 13.2, 5.7 Hz, 1H, CH_2N=C), 3.39 (dd, *J*= 10.7, 4.8Hz, 2H, CH_2N-a), 2.88 (dd, 17.5, 4.9 Hz, 1H, CH_2C=N), 2.78 (dd, 17.6, 7.1 Hz, 1H, CH_2C=N), 2.65 (dd, 10.9, 5.2 Hz, 2H, CH_2N-b), 2.60-2.54 (m, 4H, 2 CH_2-c. ^{13}C NMR (125 MHz, MeOD) δ 161.2 (C=N), 64.9 (CHOH), 64.7 (2 CH_2-d), 64.3 (CHOH), 54.6 (CH_2N-a), 52.4 (2 CH_2-c), 45.3 (CH_2N=C), 37.2 (CH_2N-b), 31.5 (CH_2C=N). HRMS (EI): found 243.1661 $C_{11}H_{21}N_3O_3$, calculated 243.1661. υ cm^{-1}: 3360.0, 3174.8, 3093.8, 2935.7, 2563.4, 2465.0, 1668.4, 1446.6, 1348.2, 1193.9, 1064.7, 995.3, 725.2.

6.1.23 General procedure for preparation of amidine derivatives from thiolactam:

Meerwein's salt (3 eq., 0.30 g, 1.6 mmol) was added under argon to a solution of thiolactam (200 mg, 0.53 mmol) in dry DCM (20 ml) at 0 ^{o}C. The resulting suspension was stirred at 0 ^{o}C for 3 h. and then amine (2 eq.) was added. The reaction was allowed to warm to ambient temperature and stirred at the same temperature for three days. The solvent was evaporated and the residue was purified by flash chromatography and HPLC for further purification.

N-((4S,5R)-4,5-Bis((tert-butyldimethylsilyl)oxy)-3,4,5,6-tetrahydropyridin-2-yl)hydroxylamine (67).

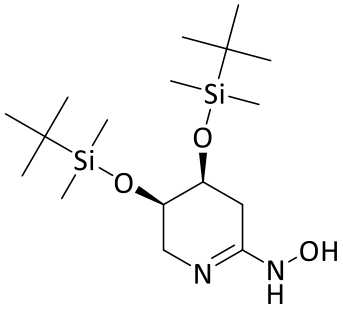

White-yellowish solid (199 mg, 0.53 mmol, 100%), R_f 0.88 (EtOAc:MeOH, 8:2), m.p. 104-106 ^{o}C . ^{1}H NMR (500 MHz, MeOD) δ 3.96-3.93 (m, 1H, CHO), 3.94 (ddd, *J*= 6.0, 3.8 Hz, 1H, CHO), 3.90-3.87 (m, 1H, CHO), 3.16 (dd, *J*= 11.0, 7.4 Hz, 2H, CH_2N=C), 3.08 (dd, *J*= 11.0, 4.5 Hz, 1H, CH_2N=C), 2.31 (dd, *J*= 15.6, 6.2 Hz, 1H, CH_2C=N), 2.25 (dd, *J*= 15.6, 6.2 Hz, 1H, CH_2C=N) 0.81-0.79 (m, 18H, 6 CH_3), 0.021-(-0.005) (m, 12H, 4 CH_3-Si). ^{13}C NMR (125 MHz, MeOD) δ 152.1 (C=N), 69.4 (CHO), 68.9 (CHO), 44.4 (CH_2N=C), 31.6 (CH_2C=N), 25.0, 24.9 (6 CH_3), 17.6, 17.6 (2 C-Si), -5.6, -5.7, -5.9, -6.1 (4 CH_3-Si). HRMS (EI): found 374.2502 $C_{17}H_{38}N_2O_3Si_2$, calculated 374.2400. υ cm^{-1} 2927.9, 2856.6, 1666.5, 1641.4, 1471.7, 1249.9, 1141.8, 1095.6, 1004.9, 939.3, 877.6, 827.5, 771.4.

(4S,5R)-4,5-Bis((tert-butyldimethylsilyl)oxy)-*N*-propyl-3,4,5,6-tetrahydropyridin-2-amine (65a).

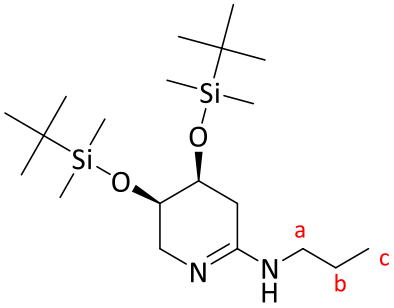

White solid (183 mg, 0.46 mmol, 86%), R_f 0.66 (EtOAc:MeOH, 8:2), m.p. 176-178 °C. ^{1}H NMR (500 MHz, MeOD) δ 4.06-3.99 (m, 2H, CHO), 3.34(dd, *J*= 13.0, 3.4 Hz, 1H, CH_2N=C), 3.24 (dd, *J*= 12.7, 6.0 Hz, 1H, CH_2N=C), 3.01 (t, *J*= 7.9 Hz, 2H, CH_2NH), 2.70 (dd, *J*= 17.0, 3.6 Hz, 1H, CH_2C=N), 2.55 (dd, *J*= 17.4, 6.7 Hz, 1H, CH_2C=N), 1.57-1.44 (m, 2H, CH_2-b), 0.85 (t, *J*= 7.3 Hz, 3H, CH_3), 0.77 (s, 18H, 6 CH_3), 0.0001 (s, 12H, 4 CH_3). ^{13}C NMR (125 MHz, MeOD) δ 162.0 (C=N), 67.2 (CHO), 66.7 (CHO), 45.9 (CH_2-a), 43.3 (CH_2N=C), 32.9 (CH_2C=N), 24.9 (6 CH_3), 20.7 (CH_2-b), 17.5 (CH_3-c), 10.1 (2 C-Si), -5.7, -5.8, -6.1, -6.2 (4 CH_3-Si). HRMS (EI): found 401.3017 $C_{20}H_{45}N_2O_2Si_2$, calculated 401.3020. υ cm^{-1}: 3327.2, 2617.4, 2075.4, 1647.2, 1394.5, 1118.7, 972.1, 873.7, 651.9.

(4S,5R)-4,5-Bis((tert-butyldimethylsilyl)oxy)-N-cyclohexyl-3,4,5,6-tetrahydropyridin-2-amine (65b).

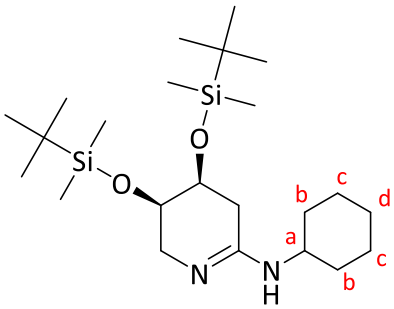

White solid (218.6 mg, 0.50 mmol, 93%), R_f 0.81 (EtOAc:MeOH, 8:2), m.p. 175-178 °C. ^{1}H NMR (500 MHz, MeOD) δ 4.05-3.96 (m, 2H, 2 CHO), 3.35 (dd, *J*= 12.8, 4.1 Hz, 1H, CH_2N=C), 3.23 (dd, *J*= 12.9, 6.1 Hz, 1H, CH_2N=C), 3.31-3.26 (m, 1H, CH-a), 2.69 (dd, *J*= 17.2, 4.4 Hz, CH_2C=N), 2.52 (dd, *J*= 17.3, 6.9 Hz, CH_2C=N), 1.85-1.72 (m, 2H, CH_2-b), 1.71-1.60 (m, 2H, CH_2-b), 1.54 (m, 1H, CH-d), 1.35-1.01 (m, 5H, 2 CH_2-c, CH-d), 0.77 (s, 18H, 6 CH_3), 0.0075 (s, 6H, 2 CH_3-Si), 0.0001

(s, 6H, 2 CH_3-Si). ^{13}C NMR (125 MHz, MeOD) δ 160.7 (C=N), 67.1 (CHO), 66.7 (CHO), 50.6 (CHNH), 45.9 (CH_2N=C), 33.2 (CH_2C=N), 31.4, 31.2, 24.7, 24.2, 24.1 (5 CH_2), 24.8 (6 CH_3), 17.5, 17.5 (2 C-Si), -5.7, -5.8, -6.1, -6.2 (4 CH_3-Si). HRMS (EI): found 440.3349 $C_{23}H_{48}N_2O_2Si_2$, calculated 440.3333. υ cm^{-1} 2929.9, 2856.6, 1662.6, 1585.5, 1462.0, 1251.8, 1097.5, 1053.13, 1018.4, 829.4, 775.4, 669.3.

tert-Butyl (2-((4S,5R)-4,5-bis((tert-butyldimethylsilyl)oxy)-3,4,5,6-tetrahydro-pyridin-2-yl)amino)ethyl)carbamate (65c).

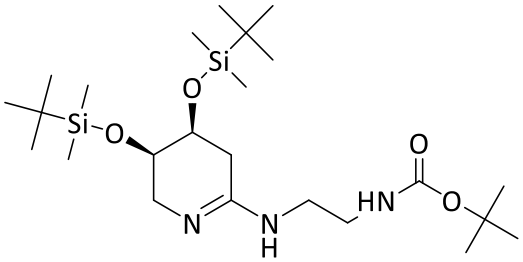

Colourless oil (211 mg, 0.42 mmol, 79%), R_f 0.76 (EtOAc:MeOH, 10:1). ^{1}H NMR (400 MHz, MeOD) δ 4.11-3.91 (m, 2H, 2 CHO), 3.39 (dd, *J*= 12.9, 3.9 Hz, 1H, CH_2N=C), 3.26 (dd, *J*= 13.0, 5.9 Hz, 1H, CH_2N=C), 3.16 (br, 2H, CH_2NH), 3.18-3.15 (m, 2H, CH_2NHCOO), 3.13-3.10 (m, 2H, CH_2NH), 2.70 (dd, *J*= 17.0, 4.0 Hz, 1H, CH_2C=N), 2.55 (dd, *J*= 17.3, 7.0 Hz, 1H, CH_2C=N), 1.30 (s, 9H, 3 CH_3), 0.77 (s, 18H, 6 CH_3C-Si), 0.0001 (m, 12H, 4 CH_3-Si). ^{13}C NMR (125 MHz, MeOD) δ 162.6 (C=O), 157.4 (C=N), 79.8 (C-O), 67.1 (CHO), 66.6 (CHO), 46.0 (CH_2NHCOO), 41.6 (CH_2NH), 37.7 (CH_2N=C), 32.9 (CH_2C=N), 27.4 (3 CH_3-CO), 25.2 (6 CH_3-C-Si), 17.6 (C-Si), 17.6 (C-Si), -5.6, -5.6, -5.9, -6.0 (4 CH_3-Si). HRMS (EI): found 501.3497 $C_{24}H_{51}N_3O_4Si_2$, calculated 501.3400. υ cm^{-1}: 3311.8, 2929.8, 2856.6, 1668.4, 1014.6.

(4S,5R)-4,5-Bis((tert-butyldimethylsilyl)oxy)-*N*-(2-fluorobenzyl)-3,4,5,6-tetra-hydropyridin-2-amine (65d).

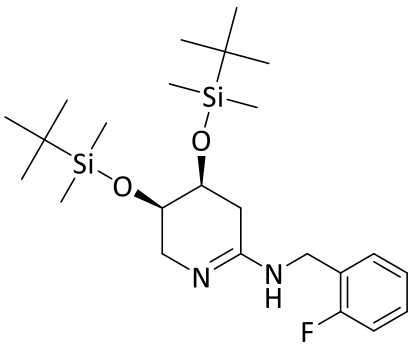

Yellow solid (181 mg, 0.39 mmol, 73%), R_f 0.72 (EtOAc:MeOH, 8:2), m.p. 152-155 ^oC. ^1H NMR (500 MHz, MeOD) δ 7.32-7.17 (m, 2H, 2 ArCH), 7.11-6.98 (m, 2H, 2 ArCH), 4.39 (d, *J*= 15.1 Hz, 1H, CH_2NH), 4.31 (d, *J*= 15.1 Hz, 1H, CH_2NH), 4.09-4.01 (m, 2H, 2 CHO), 3.38 (dd, *J*= 12.9, 4.0 Hz, CH_2N=C), 3.26 (dd, *J*= 12.9, 6.2 Hz, 1H, CH_2N=C), 2.75 (dd, *J*= 17.4, 4.2 Hz, 1H, CH_2C=N), 2.59 (dd, *J*= 17.4, 6.9 Hz, 1H, CH_2C=N), 0.78 (s, 18H, 6 CH_3), 0.014-0.0001 (m, 12H, 4 CH_3-Si). ^{13}C NMR (125 MHz, MeOD) δ 162.2 (C=N), 160.0 (CF), 130.5, 129.5, 124.5, 115.3 (Ar-CH), 121.7 (C-Ar), 67.1 (CHO), 66.6 (CHO), 46.3 (CH_2NH), 39.7 (CH_2N=C), 33.0 (CH_2C=N), 24.9 (6 CH_3), 17.5 (2 C-Si), -5.7, -5.8, -6.1, -6.2 (4 CH_3-Si). HRMS (EI): found 467.2913 $C_{24}H_{44}N_2O_2FSi_2$, calculated 467.2925. υ cm^{-1}: 3375.4, 2557.6, 2366.7, 1456.3, 1217.1, 615.3.

(**4S,5R)-4,5-Bis((tert-butyldimethylsilyl)oxy)-*N*-(3-fluorobenzyl)-3,4,5,6-tetra-hydropyridin-2-amine (65e).**

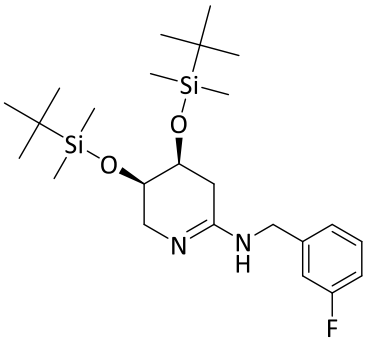

White-yellowish solid (129 mg, 0.28 mmol, 52%), R_f 0.8 (EtOAc:MeOH, 8:2), m.p. 144-146 ^oC. ^1H NMR (500 MHz, MeOD) δ 7.28-7.23 (m, 1H, ArCH), 7.00-6.91 (m, 3H, ArCH), 4.32 (s, 2H, 2 CH_2NH), 4.08-4.05 (m, 1H, CHO), 4.03 (ddd, *J*= 6.0, 4.1 Hz, 1H, CHO), 3.36 (dd, *J*= 13.0, 4.0 Hz, 1H, CH_2N=C), 3.23 (dd, *J*= 13.0, 6.1 Hz, 1H, CH_2C=N), 2.78 (dd, *J*= 17.4, 4.4 Hz,1H, CH_2C=N), 2.61

(dd, *J*= 17.4, 7.0 Hz, 1H, CH_2C=N), 0.77 (d, 18H, 6 CH_3), 0.0062 (d, 12 H, 4 CH_3-Si). ^{13}C NMR (125 MHz, MeOD) δ 164.1 (C=N), 162.5 (CF-Ar), 137.2 (Ar-C), 130.6, 123.0, 114.8, 113.9 (4 ArCH), 67.1 (CHO), 66.6 (CHO), 46.1 (CH_2NH), 44.5 (CH_2N=C), 33.1 (CH_2C=N), 24.9, 24.9 (6 CH_3), -5.7, -5.8, -6.1, -6.2 (4 CH_3-Si). HRMS (EI): found 467.2925 $C_{24}H_{44}N_2O_2FSi_2$, calculated 467.2925. υ cm^{-1}: 2929.8, 2858.5, 1672.3, 1595.1, 1253.7, 1097.5, 1002.9, 827.5, 777.3, 684.7, 518.8.

(4S,5R)-4,5-Bis((tert-butyldimethylsilyl)oxy)-*N*-(2-morpholinoethyl)-3,4,5,6-tetrahydropyridin-2-amine (65f).

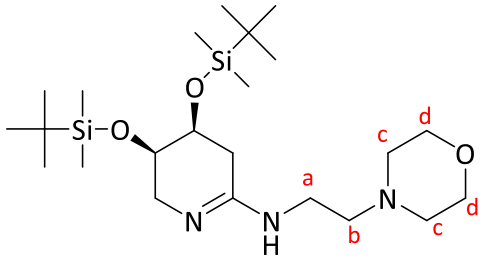

White hygroscopic solid (245 mg, 0.52 mmol, 98%), R_f 0.6 (EtOAc:MeOH:NH_3, 10:2:0.1).^{1}H NMR (500 MHz, MeOD) δ 4.08-3.98 (m, 2H, 2 CHO), 3.55 (t, 4H, 4.6 Hz, 4H, 2 CH_2-d), 3.37 (dd, *J*= 12.9, 4.0 Hz, 1H, CH_2N=C), 3.25 (dd, *J*= 13.0, 6.0 Hz, 1H, CH_2N=C), 3.22-3.19 (m, 2H, CH_2NH-a), 2.71 (dd, *J*= 17.3, 4.4 Hz, 1H, CH_2C=N), 2.57 (dd, *J*= 17.4, 7.1 Hz, 1H, CH_2C=N), 2.49-2.44 (m, 2H, CH_2N-b), 2.2.43-2.30 (m, 4H, 2 CH_2-c), 0.78 (s, 18H, 6 CH_3), 0.0063, -0.0001 (s, 12H, 4 CH_3-Si). ^{13}C NMR (125 MHz, MeOD) δ 162.7 (C=N), 67.1 (CHO), 66.7 (CHO), 66.4 (2 CH_2-d), 55.7 (CH_2NH-a), 53.0 (2 CH_2-c), 45.9 (CH_2N=C), 39.0 (CH_2N-b), 32.7 (CH_2C=N), 24.9, 24.8 (6 CH_3), 17.6 (C-Si), -5.7, -5.8, -6.1, -6.2 (4 CH_3-Si). HRMS (EI): found 471.3393 $C_{23}H_{49}N_3O_3Si_2$, calculated 471.3391. υ cm^{-1}: 2929.9, 2858.5, 1672.3, 1251.8, 1153.4, 1089.8, 1055.1, 1010.7, 977.9, 777.3, 835.2, 671.2, 520.8.

(4S,5R)-4,5-Bis((tert-butyldimethylsilyl)oxy)-*N*-(2-(4-ethylpiperazine-1-yl)-ethyl)-3,4,5,6-tetrahydropyridin-2-amine (65g).

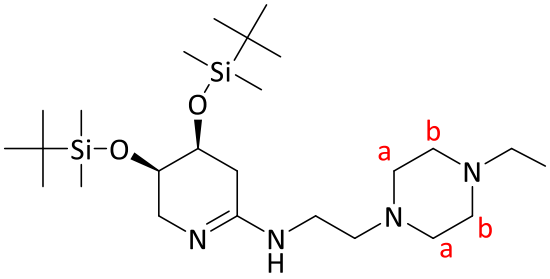

Yellow oil (137.8 mg, 0.28 mmol, 52%), R_f 0.73 (EtOAc:MeOH, 15:1). ^{1}H NMR (500 MHz, MeOD) δ 4.10-3.84 (m, 2H, 2 CHO), 3.38 (dd, *J*= 12.9, 4.0 Hz, 1H, CH_2N=C), 3.26 (dd, *J*= 12.9, 6.1 Hz, 1H, CH_2N=C), 3.22-3.16 (m, 2H, CH_2NH), 3.18-3.14 (m, 4H, 2 CH_2-a), 3.10 (t, *J*= 5.1 Hz, 2H, CH_2-Et), 2.74 (dd, *J*= 17.4, 4.4 Hz, 1H, CH_2C=N), 2.63-2.50 (m, 3H, 1H CH_2C=N, 2H CH_2N), 2.60-2.52 (m, 4H, 2 CH_2-b), 1.17 (t, *J*= 7.2 Hz, CH_3), 0.77 (s, 18H, 6 CH_3), -0.0001 (d, 12H, 4 CH_3-Si). ^{13}C NMR (125 MHz, MeOD) δ 162.4 (C=N), 67.1 (CHO), 66.6 (CHO), 54.3 (CH_2NH), 51.4 (CH_2N), 49.2 (CH_2N-a), 45.9 (CH_2N=C), 43.5 (CH_2N-b), 38.9 (CH_2C=N), 32.8 (CH_2-Et), 24.9, 24.9 (6 CH_3), 17.5 (C-Si), -5.7, -5.7, -6.1, -6.2 (4 CH_3-Si). HRMS (EI): found 498.3865 $C_{25}H_{55}N_4O_2Si_2$, calculated 498.3864. υ cm^{-1}: 1620.2, 1255.7, 839.0, 779.2.

(4S,5R)-*N*-(2,3-Bis((tert-butyldimethylsilyl)oxy)propyl)-4,5,-bis((tetrabutyl-dimethylsilyl)oxy)-3,4,5,6-tetrahydropyridin-2-amine (65h).

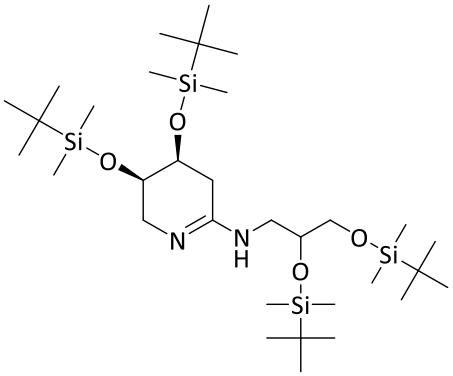

Yellow oil (80.96 mg, 0.12 mmol, 23%), R_f 0.66 (EtOAc:MeOH, 10:1). ^{1}H NMR (500 MHz, MeOD) δ 4.05 (ddd, *J*= 6.5, 4.4, 1.7, 1H, CHO), 4.01 (ddd, *J*= 5.8, 4.1, 1.7 Hz, 1H, CHO), 3.83-3.74 (m, 1H, CH-OTBS), 3.53 (dd, *J*= 10.7, 4.8 Hz, 1H, CH_2OTBS), 3.47 (dd, *J*= 10.5, 6.1 Hz, 1H, CH_2OTBS), 3.35 (dd, *J*= 13.0, 4.0 Hz, 1H, CH_2N=C), 3.29-3.22 (m, 3H, 1H CH_2N=C, 2H CH_2NH), 2.72 (dd, *J*= 17.4, 4.4 Hz, 1H, CH_2C=N), 2.60 (dd, *J*= 17.4, 7.1 Hz, 1H, CH_2C=N), 0.79-0.75 (m, 36H, 12 CH_3),

0.02-(-0.08) (m, 24H, 12 CH_3). ^{13}C NMR (125 MHz, MeOD) δ 162.8 (C=N), 71.1 (CHOTBS), 67.2 (CHO), 67.1 (CHO), 64.7 (CH_2NH), 45.9 (CH_2N=C), 45.1 (CH_2OTBS), 33.0 (CH_2C=N), 25.1, 25.0, 24.9 (12 CH_3), -5.6, -5.7, -5.7, -5.9, -6.0, -6.1, -6.5, -6.6 (8 CH_3-Si). HRMS (EI): found 660.4651 $C_{32}H_{73}N_2O_4Si_4$, calculated 660.4647. υ cm^{-1}: 2956.8, 2931.8, 2860.4, 1473.6, 1257.6, 977.9, 835.2, 777.3.

6.1.24 General method for deprotection of silyl protected group in amidine derivatives:

A solution of protected amidine in aqueous 2N HCl (10 ml) was heated with stirring for 12 h and then the solvent was removed and the residue was triturated with diethyl ether and then dried under vacuum to give an amidine derivative.

(4S,5R,E)-4,5-Dihydroxy-2-(hydroxyl-λ^4-azaneylidene)piperidin-1-ium chloride (68a).

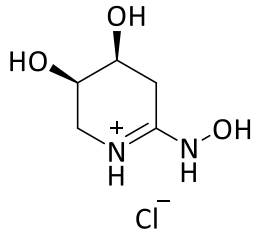

White yellowish solid (79.6 mg, 0.44 mmol, 82%), R_f 0.15 (MeCN:H_2O: HOAc, 10:2:0.2), m.p. 176-177 °C. ^1H NMR (500 MHz, MeOD) δ 4.12 (ddd, *J*= 6.9, 4.7 Hz, 1H, CHOH), 4.07 (ddd, *J*= 6.4, 4.6 Hz, 1H, CHOH), 3.54 (dd, *J*= 13.2, 4.5 Hz, 1H, CH_2N=C), 3.45 (dd, *J*= 13.2, 6.1 Hz, 1H, CH_2N=C), 2.77 (dd, *J*= 17.2, 4.7 Hz, 1H, CH_2C=N), 2.66 (dd, *J*= 17.2, 7.0 Hz, 1H, CH_2C=N). ^{13}C NMR (125 MHz, MeOD) δ 159.1 (C=N), 65.3 (CHOH), 64.3 (CHOH), 44.3 (CH_2N=C), 27.6 (CH_2C=N). HRMS (EI): found 146.0765 $C_5H_{10}N_2O_3$, calculated 146.0700. υ cm^{-1}: υ cm^{-1}: 3064.8, 1558.5, 1431.2, 1305.8, 1064.7.

(4S,5R,E)-4,5-Dihydroxy-2-(propylimino)piperidin-1-ium chloride (68b).

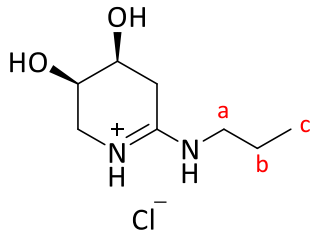

White hygroscopic solid (95.3 mg, 0.46 mmol, 100%), R_f 0.19 (MeCN:H_2O:HOAc, 10:2:0.2). ^{1}H NMR (500 MHz, MeOD) δ 4.11-4.05 (m, 2H, 2 CHOH), 3.55 (dd, *J*= 13.2, 4.3 Hz, 1H, CH_2N=C), 3.47 (dd, *J*= 13.2, 5.8 Hz, 1H, CH_2N=C) 3.19 (t, *J*= 7.2 Hz, 2H, CH_2-a), 2.87 (dd, *J*= 17.5, 4.8 Hz, 1H, CH_2C=N), 2.76 (dd, *J*= 17.5, 7.1 Hz, 1H, CH_2C=N), 1.74-1.59 (m, 2H, CH_2-b), 1.02 (t, *J*= 7.4 Hz, 3H, CH_3). ^{13}C NMR (125 MHz, MeOD) δ 161.8 (C=N), 65.0 (CHOH), 64.8 (CHOH), 45.0 (CH_2N=C), 43.5 (CH_2-a), 31.3 (CH_2C=N), 20.6 (CH_2-b), 10.2 (CH_3). HRMS (EI): found 172.1296 $C_8H_{16}N_2O_2$, calculated 172.1290. υ cm^{-1}: 3450.6, 3070.7, 2920.2, 1672.3, 1454.3, 1083.9, 507.3.

(4S,5R,E)-4,5-Dihydroxy-2-(cyclohexylimino)piperidin-1-ium chloride (68c).

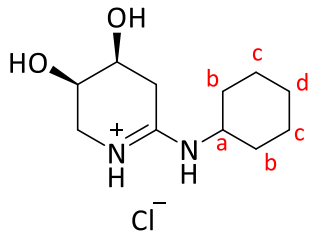

White solid (80 mg, 0.32 mmol, 65%), R_f 0.26 (MeCN:H_2O:HOAc, 10:2:0.2). ^{1}H NMR (500 MHz, MeOD) δ 4.15-4.00 (m, 2H, 2 CHOH), 3.63-3.44 (m, 3H, CH_2N=C, CHNH), 2.86 (d, *J*= 16.5 Hz, 1H, CH_2C=N), 2.75 (d, *J*= 16.2 Hz, 1H, CH_2C=N), 2.00-1.90 (m, 2H, CH_2-b), 1.88-1.76 (m, 2H, CH_2-b), 1.73-1.63 (m, 2H, CH_2-d), 1.51-1.19 (m, 4H, 2 CH_2-c). ^{13}C NMR (125 MHz, MeOD) δ 160.6 (C=N), 65.0 (CHOH), 64.5 (CHOH), 51.2 (CHNH), 45.2 (CH_2N=C), 31.7 (CH_2C=N), 31.4 (CH_2-b), 24.8 (CH_2-d), 24.2 (CH_2-c). HRMS (EI): found 212.1525 $C_{11}H_{20}N_2O_2$, calculated 212.1500. υ cm^{-1}: 3350.4-3228.8, 2933.7, 2858.5, 1654.9, 1066.6.

(4S,5R,E)-2-((2-Fluorobenzyl)imino)-4,5-dihydroxypiperidin-1-ium chloride (68d).

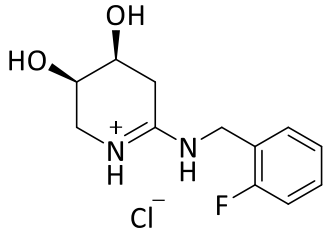

White yellowish solid (71 mg, 0.26 mmol, 67%), R_f 0.31 (MeCN:H_2O:HOAc, 10:2:0.2), m.p. 129-130 ^oC . ^1H NMR (400 MHz, MeOD) δ 7.39-7.22 (m, 2H, 2 ArCH), 7.18-7.03 (m, 2H, 2 ArCH), 4.39 (s, 2H, CH_2NH), 4.03-3.89 (m, 2H, 2 CHOH), 3.47 (dd, 2H, *J*= 13.3, 4.2 Hz, 1H, CH_2N=C), 3.40 (dd, 2H, *J*= 13.3, 4.2 Hz, 1H, CH_2N=C), 2.67 (dd, *J*= 17.4, 4.2 Hz, 1H, CH_2C=N), 2.56 (dd, *J*= 17.4, 6.9 Hz, 1H, CH_2C=N). ^{13}C NMR (125 MHz, MeOD) δ 162.2 (C=N), 160.1 (C-F), 130.5, 130.5, 124.5, 121.4, 115.2 (5 ArCH), 64.9 (CHOH), 64.3 (CHOH), 45.3 (CH_2N=C), 39.7 (CH_2NH), 39.0 (CH_2C=N). HRMS (EI): found 238.1120 $C_{12}H_{15}N_2O_2F$, calculated 238.1118. υ cm^{-1}: 3212.3, 1650.7, 1465.1, 1122.6, 881.4, 720.3.

(4S,5R,E)-2-((3-Fluorobenzyl)imino)-4,5-dihydroxypiperidin-1-ium chloride (68e).

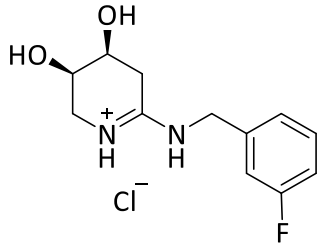

Yellow oil (50 mg, 0.18 mmol, 47%), R_f 0.28 (MeCN:H_2O:HOAc, 10:2:0.2).^1H NMR (500 MHz, MeOD) δ 7.27 (dd, *J*= 13.9 Hz, 1H, ArCH), 7.06-6.93 (m, 3H, 3 ArCH), 4.36 (s, 2H, CH_2NH), 4.00-3.87 (m, 2H, 2 CHOH), 3.41 (d, *J*= 11.7 Hz, 1H, CH_2N=C), 3.34 (dd, *J*= 12.1, 4.3 Hz, 1H, CH_2N=C), 2.74 (dd, 2H, *J*= 38.83, 18.93 Hz, CH_2C=N). ^{13}C NMR (125 MHz, MeOD) δ 164.1 (C=N), 162.1 (C-F), 137.3, 130.8, 123.5, 114.8, 114.6 (5 ArC), 65.0 (CHOH), 64.5 (CHOH), 45.4 (CH_2N=C), 44.9 (CH_2NH), 31.7 (CH_2C=N). HRMS (EI): found 238.1195 $C_{12}H_{15}N_2O_2F$, calculated 238.1196. υ cm^{-1}: 3201.8, 3059.1, 1662.6, 1591.3, 1450.5, 1249.9, 1192.0, 1068.6, 729.1, 680.9, 545.8.

(4S,5R,E)-4,5-Dihydroxy-2-((2-morpholinoethyl)imino)-pipyeridin-1-ium chloride (68f).

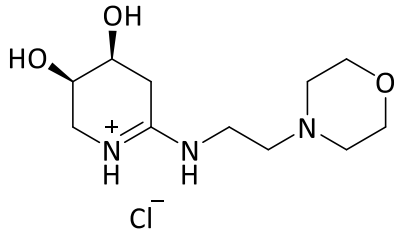

White hygroscopic solid (125 mg, 0.45 mmol, 99%), R_f 0.17 (MeCN:H_2O:HOAc, 10:2:0.2). ^{1}H NMR (400 MHz, MeOD) δ 4.15-4.02 (m, 2H, 2 CHOH), 3.75-3.68 (m, 4H, 2 CH_2-d), 3.57 (dd, *J*= 13.2, 4.3 Hz, 1H, CH_2N=C), 3.50 (dd, *J*= 13.2, 5.7 Hz, 1H, CH_2N=C), 3.42-3.36 (m, 2H, CH_2-a), 2.88 (dd, *J*= 17.5, 4.9 Hz, 1H, CH_2C=N), 2.78 (dd, *J*= 17.6, 7.1 Hz, 1H, CH_2C=N), 2.66 (t, 2H, *J*= 5.70 Hz, CH_2-b), 2.59-2.54 (m, 4H, 2 CH_2-c). ^{13}C NMR (125 MHz, MeOD) δ 162.8 (C=N), 66.4 (2 CH_2-d), 65.0 (CHOH), 64.5 (CHOH), 55.8 (CH_2-a), 53.0 (2 CH_2-c), 45.0 (CH_2N=C), 39.2 (CH_2-b), 31.3 (CH_2C=N). HRMS (EI): found 243.1663 $C_{11}H_{21}N_3O_3$, calculated 243.1600. υ cm^{-1}: 3365.8, 2598.1, 1595.1, 1118.7, 970.2, 534.3.

(4S,5R,E)-2-((2-(4-Ethylpiperazin-1-yl)ethyl)imino)-4,5-dihydroxypiperidin-1-ium chloride (68g).

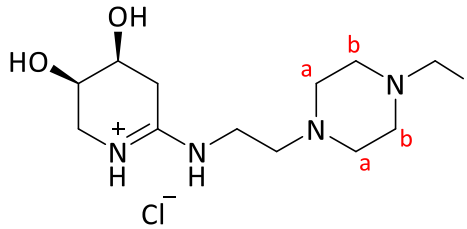

Yellow oil (63.2 mg, 0.21 mmol, 75%), R_f 0.41 (MeCN:H_2O:HOAc, 10:2:0.2).^{1}H NMR (500 MHz, MeOD) δ 4.15-4.05 (m, 2H, 2 CHOH), 3.61-3.48 (m, 2H, CH_2N=C), 3.41-3.37 (m, 2H, CH_2NH), 3.33 (s, 4H, 2 CH_2-a), 3.26-3.19 (m, 4 H, CH_2-N, CH_2-Et), 2.93 (d, *J*= 17.4 Hz, 1H, CH_2C=N), 2.82 (dd, *J*= 17.2, 6.5 Hz, 1H, CH_2C=N), 2.75 (s, 4H, 2 CH_2-b), 1.38 (t, *J*= 6.8 Hz, 3H, CH_3-Et). ^{13}C NMR (125 MHz, MeOD) δ 162.4 (C=N), 65.0 (CHOH), 64.4 (CHOH), 54.7 (CH_2NH), 51.6 (CH_2-N), 51.2, 49.4 (CH_2-a, CH_2-b), 45.2 (CH_2N=C), 39.2 (CH_2-Et), 8.2 (CH_3). HRMS (EI): found 270.2100 $C_{13}H_{26}N_4O_2$, calculated 270.2100. υ cm^{-1}: 3344.6, 1654.9, 1593.2, 1354.0, 1118.7, 972.1, 879.5, 765.7, 636.5.

(4S,5R,E)-2-((2-Aminoethyl)imino)-4,5-dihydroxypipyeridin-1-ium chloride (68h).

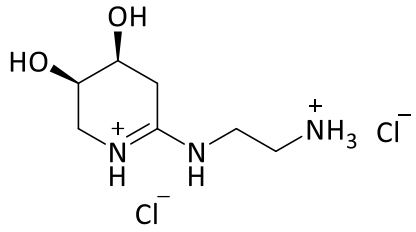

Colourless oil (73.6 mg, 0.3 mmol, 71%), R_f 0.19 (MeCN:H_2O:HOAc, 10:3:0.3). ^{1}H NMR (500 MHz, MeOD) δ 4.14-4.03 (m, 2H, 2 CHOH), 3.65 (t, *J*= 5.6 Hz, 2H, CH_2NH), 3.58 (dd, *J*= 13.4, 4.1 Hz, 1H, CH_2N=C), 3.52 (dd, *J*= 13.4, 5.6 Hz, 1H, CH_2N=C), 3.26-3.20(m, 2H, CH_2NH_3), 2.91 (dd, *J*= 17.6, 5.0 Hz, 1H, CH_2C=N), 2.81 (dd, *J*= 17.8, 7.1 Hz, 1H, CH_2C=N). ^{13}C NMR (125 MHz, MeOD) δ 163.0 (C=N), 64.9 (CHOH), 64.4 (CHOH), 45.3 (CH_2NH), 44.2 (CH_2C=N), 39.2 (CH_2NH_3), 31.5 (CH_2C=N). HRMS (EI): found 173.1250 $C_7H_{15}N_3O_2$, calculated 173.1200. υ cm^{-1}: 3313.7, 2945.3, 2831.5, 1593.2, 1018.4.

6.1.25 Protection of 3-aminopropan-1,2-diol (70).

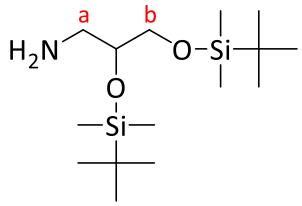

A solution of *tert*-butyldimethylchlorosilane (2.0 eq., 3.0 g, 20 mmol) in DMF (20 ml) was added dropwise to a stirred solution of (s)-3-amino-1,2-propanediol (0.911 g, 10 mmol) and imidazole (2.0 eq., 1.36 g, 20 mmol) in 50 ml DMF at room temperature. The resulting mixture was stirred overnight and then the solvent was evaporated under reduced pressure. The residue was purified by flash chromatography (EtOAc:MeOH:NH_3, 15:2:0.1, R_f 0.57), Yellow oil product (1.49 g, 4.7 mmol, 47%). ^{1}H NMR (500 MHz, MeOD) δ 3.68-3.59 (m, 1H, CHOTBS), 3.53 (dd, *J*= 10.3, 5.1 Hz, 1H, CH_2OTBS), 3.46 (dd, *J*= 10.3, 6.4 Hz, 1H, CH_2OTBS), 2.70 (dd, *J*= 13.0, 4.4 Hz, 1H, CH_2NH_2), 2.57 (dd, *J*= 13.0, 5.9 Hz, 1H, CH_2NH_2), 0.85-0.81 (m, 18H, 6 CH_3), 0.06-0.03 (m, 12H, 4 CH_3). ^{13}C NMR (125 MHz, MeOD) δ 73.6 (CHOTBS), 65.3 (CH_2OTBS), 44.4 (CH_2NH_2), 25.1 (3 CH_3), 25.0 (3 CH_3), -5.5, -5.8, -6.5, -6.6 (4 CH_3-Si). HRMS (EI): found 319.2439

$C_{15}H_{37}NO_2Si_2$, calculated 319.2400. υ cm^{-1}: 2953.0, 2927.9, 2856.6, 1462.0, 1251.8, 1107.1, 831.3, 773.5, 667.4.

6.1.26 Synthesis of 5-(azidomethyl)furan-2(5H)-one (89).[181]

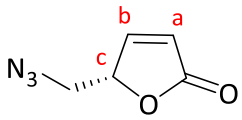

Triflic anhydride (0.28 ml, 1.65 mmol, 1.3 eq.) was added to a solution of a mixture of **(41)** (0.2 g, 1.27 mmol) and 2,6-lutidine (0.21 ml, 1.78 mmol, 1.4 eq.) in 10 ml DCM at -16 °C. After the mixture was stirred for 2.5 h at the same temperature, 1 ml water and 10 ml DMF were added to the mixture and it was warmed up to room temperature. Following, the reaction vessel was equipped with a reflux condenser and a Dean-Stark apparatus to remove DCM and the mixture was heated up to 100 °C (oil bath) with stirring for 2 h. After cooling to room temperature, 5 ml methanol and triethylamine (0.9 ml, 6.4 mmol, 5 eq.) were added to the mixture at the same temperature. The mixture was stirred for 30 min followed by addition of 7 ml HCl (1 M) and extracted with DCM (10 ml x 3). The combined organic layers were washed with brine and dried over anhydrous Na_2SO_4. The filtrate was concentrated under reduced pressure and the residue was purified by flash chromatography (EtOAc:hexane, 3:2, R_f 0.45) to produce compound (**89**) as brown oil (230 mg, 1.65 mmol, 38%). ^{1}H NMR (400 MHz, MeOD) δ 7.68 (dd, *J*= 5.8, 1.6 Hz, 1H, CH-a), 6.28 (dd, *J*= 5.8, 2.1 Hz, 1H, CH-b), *5*.34 (ddd, *J*= 7.2, 3.6, 1.8 Hz, 1H, CH-c), 3.82 (dd, *J*= 13.5, 3.6 Hz, 1H, CH_2-N_3), 3.55 (dd, *J*= 13.5, 5.2 Hz, 1H, CH_2-N_3). ^{13}C NMR (100 MHz, MeOD) δ 170.1 (C=O), 154.9 (CH-a), 121.9 (CH-b), 82.7 (CH-c), 51.7 (CH_2-N_3). HRMS (EI): found 84.0197 [M-55], 83.0131 [M-54] $C_5H_5N_3O_2$, calculated 139.0400. υ cm^{-1}: 2935.7, 2098.6, 1770.7, 1276.9, 1159.2, 1049.3, 937.4, 651.9, 553.6.

6.1.27 Synthesis of tetrakis(benzyloxy)-5-hydroxyhexanamide (92).

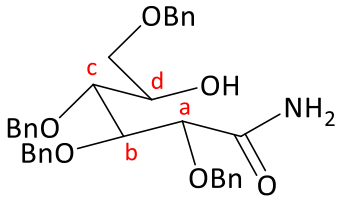

Benzylated gluconolactone derivative (0.3 g, 0.56 mmol) was dissolved in 10 ml methanolic ammonia and the mixture was stirred overnight at room temperature. The solvent was evaporated under reduced pressure and the crude product was purified by flash chromatography (EtOAc:hexane, 7:3, R_f 0.48) to afford brown yellowish oil product (0.245 g, 0.44 mmol, 79%). ^{1}H NMR (500 MHz, MeOD) δ 7.24-7.05 (m, 20 H, ArCH), 4.61-4.56 (m, 2 H, CH_2-Bn), 4.55-4.49 (m, 2H, CH_2-Bn), 4.41 (d, *J*= 11.2 Hz, 1H, CH_2-Bn), 4.37-4.28 (m, 2H, CH_2-Bn), 4.07 (d, *J*= 4.4 Hz, 1H, CH-a), 4.00-3.94 (m, 1H, CH-b), 3.80-3.69 (m, 2H, CH_2OBn), 3.52 (dd, 2H, *J*= 10.0, 3.2 Hz, CH-c), 3.43 (dd, *J*= 10.0, 5.0 Hz, CH-d). ^{13}C NMR (125 MHz, MeOD) δ 175.0 (C=O), 138.6, 138.3, 138.2, 137.2 (4 quaternary carbon-Ar), 128.2-127.2 (Ar-CH), 80.7, 80.6, 78.9, 70.9 (4 CH), 75.3, 74.1, 73.2, 71.1 (5 CH_2). HRMS (EI): found 555.2600 $C_{34}H_{37}NO_6$, calculated 555.2600.

6.2 Protein production

6.2.1 Materials and buffers

All chemicals used in this work were purchased from Sigma Aldrich or Fisher Scientific, unless otherwise stated. All restriction enzymes were purchased from New England Biolabs. The gene encoding Slt35 was purchased from Epoch Gene Synthesis (USA).

Media

Luria-Bertani medium (LB)

10 g Tryptone, 5 g yeast extract and 10 g NaCl were dissolved in 1 L of deionised water. The solution was sterilised in an autoclave at 121 ^{o}C, 15 lb in^{-2} for 20 minutes.

LB agar medium

5.0 g Tryptone, 5.0 g NaCl, 2.5 g yeast extract and 7.5 g agar were dissolved in 500 ml deionised water for preparation of culture plates. The solution was sterilised in an autoclave at 121 ^{o}C, 15 lb in^{-2} for 20 minutes.

Sterile Solutions

Antibiotic

Kanamycin was dissolved in deionised water to a concentration of 50 mg/ml and used in working concentration of 0.1 mg/ml.

Isopropyl-β-D-1-thiogalactopyranoside (IPTG)

IPTG (360 mg) was dissolved in 1 ml of deionised water and used at working concentration of 0.12 mg/ml.

Competent cell solutions

The following buffers were used to prepare competent cells:

Rubidium chloride solution 1 (Rb1) (30 mM KOAc, 100 mM RbCl, 10 mM $CaCl_2$, 50 mM $MnCl_2$, 15% (v/v) glycerol, pH 5.8)

Potassium acetate (294 mg), rubidium chloride (1.21 g), calcium chloride (111 mg), manganese chloride (692 mg) and glycerol (15 ml) were dissolved in 80 ml deionised water. The pH of the solution was adjusted to 5.8 with dilute acetic acid (0.1 M). The total volume was taken to 100 ml with deionised water and then the solution was sterilised utilising a 0.2 μm syringe filter and stored at 4 ^{o}C.

Rubidium chloride solution 2 (Rb2) (10 mM MOPS, 75 Mm $CaCl_2$, 10 mM RbCl, 15% (v/v) glycerol, pH 6.5)

3-(*N*-morpholino)propanesulfonic acid (MOPS) (209 mg), calcium chloride (832 mg), rubidium chloride (121 mg) and glycerol (15 ml) were dissolved in 100 ml deionised water. The pH was adjusted with dilute NaOH (0.1 M) and the solution was sterilised utilising a 0.2 μm syringe filter and then stored at 4 ^{o}C.

Calcium chloride solution

100 mM Calcium chloride (1.11g) and 15% (v/v) glycerol (15 ml) were dissolved in 100 ml deionised water. The solution was sterilised *via* autoclave at 121 ^{o}C (15 1b in^{-2}) for 20 minutes and was stored at 4 ^{o}C.

Non- sterile Solutions

Ethidium bromide

A stock solution of ethidium bromide (25 mM) was prepared by dissolving 8.1 g of the solid in 100 ml deionised water and stored in the dark at 4 ^{o}C. The solution was used at working concentration of 6 μM, by adding 48 μl to 200 ml deionised water immediately prior to gel staining.

10x DNA loading dye

0.5% (w/v) Bromophenol blue (2 μl) and glycerol (300 ml) were dissolved in 0.7 ml of deionised water yielding concentrations of 0.001 (w/v) bromophenol blue and 30% (v/v) glycerol and the solution was stored at room temperature. Immediately prior to use, the dye was diluted 1:9 with each DNA sample.

TAE buffer stock (50x) for agarose gels

Tris base (242 mg) was dissolved in 800 ml deionised water containing 57.1 ml glacial acetic acid and 100 ml of 0.5 M EDTA solution pH 8. EDTA solution was prepared immediately prior to use by dissolving 14.61 g EDTA in 50 ml deionised water, adjusting the pH with 5 M NaOH, and then taking the volume to 100 ml with deionised water. The solution was stored at room temperature. The working solution (1x) was made by diluting the stock solution 1:49 with deionised water immediately prior to used.

Agarose gel

Agarose (1-2 g) was added to 100 ml 1x TAE buffer. The mixture was heated in the microwave until fully dissolved and then poured into a casting block and allow to set. Gels were run at constant amplitude of 80 V for 45 minutes followed by staining with 200 ml of dilute ethidium bromide solution and visualised using a Syngene GeneFlash UV light box (Syngene, Cambridge, UK).

SDS stacking buffer

Tris base (6.0 g) was dissolved in 100 ml deionised water to give a concentration of 0.5 M. The pH was adjusted to 6.8 with 6 M HCl and the solution was stored at room temperature.

SDS resolving buffer

Tris base (27.73 g) was dissolved in 150 ml deionised water to give a concentration of 1.5 M. The pH was adjusted to 8.8 with 6 M HCl and the solution was stored at room temperature.

Sodium Dodecyl Sulfate (SDS) (10% w/v)

SDS (10.0 g) was dissolved in 100 ml deionised water and the solution was stored at room temperature.

Ammonium persulfate (APS) (10% w/v)

Ammonium persulfate (100 mg) was dissolved in 1.0 ml deionised water. The solution was freshly made prior to use.

SDS electrode running buffer (10x)

0.25 M Tris base (30.3 g), 1.92 M glycine (144.0 g), 1% SDS (10.0 g) were dissolved in 1 L deionised water. The pH (~8.3) was not adjusted and was the solution was stored at room temperature. Prior to use the solution was diluted 1:9 with deionised water.

Protein loading dye

0.5 M Tris-HCl (1.25 ml, pH 6.8) (SDS stacking buffer), 30% glycerol (3 ml), 0.6% (w/v) bromophenol blue (1 ml) and 10% SDS (2 ml) were mixed and the total volume taken to 10 ml with deionised water. β-Mercaptoethanol (β-ME) was added to a final concentration of 10% (v/v) prior to use.

Buffers used for protein purification

Buffer A (20 mM HEPES, 0.5 M NaCl, 10% glycerol, 0.05% Tween-20 pH 7)

HEPES (4.77 g), NaCl (29.22 g), glycerol (50 ml) and Tween-20 (0.5 ml) were dissolved in 899.5 ml deionised water. The pH of the solution was adjusted to 7 by using 5 M NaOH. The solution was filtered and stored at room temperature.

Buffer B (50 mM Tris-HCl, 0.5 M NaCl, 10% glycerol, 0.05% Tween-20, pH 7)

Tris-HCl (7.90 g), NaCl (29.22 g), glycerol (100 ml) and Tween-20 (0.5 ml) were dissolved in 899.5 ml deionised water and the pH was adjusted to 7 using 5 M NaOH. The solution was filtrated and stored at room temperature.

Buffer C (50 mM potassium phosphate, 0.5 M NaCl, 10% glycerol and 0.05% Tween-20)

Sodium phosphate dibasic Na_2HPO_4 (2.05 g), sodium phosphate monobasic NaH_2PO_4 (1.26 g), NaCl (14.61 g), glycerol (50 ml) and Tween-20 (0.25 ml) were dissolved in 450 ml deionised water and the solution was adjusted to the desired pH (7.0, 6.5, 6.0, 5.5, 5.0, 4.5, 4.0). The solutions were filtered and stored at room temperature.

Dialysis buffers

Buffer A (20 mM HEPES, 300 mM NaCl, 0.05% Tween-20 pH 7)

HEPES (23.83 g), NaCl (87.7 g) and Tween20 (2.5 ml) were dissolved in 5 L deionised water and the pH was adjusted to 7 by using 5 M NaOH. The buffer was prepared fresh each time and the dialysis was performed at 4 ^oC.

Buffer B (50 mM Tris-HCl, 300 mM NaCl, 0.05% Tween 20, pH 7)

Tris-HCl (50 mM, 39.4 g), NaCl (300 mM, 87.7 g) and Tween 20 (0.05%, 2.5 ml) were dissolved in 5 L deionised water. The pH of the solution was adjusted to 7 and used immediately and dialysis was performed at 4 ^oC.

Plasmid DNA purification buffers

The following buffers were prepared and stored at room temperature except P1.

Buffer P1 (suspension buffer)

50 mM Tris-HCl (157.6 mg), 10 mM EDTA (58.5 mg) and RNase A (50 μg/ml final concentration) were dissolved in 15 ml deionised water. The pH was adjusted to 8.0 and the total volume taken to 20 ml with deionised water and stored at 4 ^oC.

Buffer P2 (lysis buffer)

0.2 M NaOH (4 g) and 1% (w/v) SDS (5 g) were dissolved separately in 250 ml deionised water. The solutions were mixed 1:1 and then stored at room temperature.

Buffer N3 (neutralisation and binding buffer)

4 M Guanidine hydrochloride (7.6 g) and 0.5 M potassium acetate (0.98 g) were dissolved in 20 ml deionised water. The pH was adjusted to 4.2 with 6.0 M HCl and then stored at room temperature.

Buffer PB (wash buffer)

5 M Guanidine hydrochloride (9.5 g) and 20 mM Tris-HCl (63.0 mg) were dissolved 7.4 ml deionised water. Ethanol (7.6 ml) (38% v/v) was added and the total volume was taken to 20 ml with deionised water. The pH was adjusted to 6.6 and the solution was stored at room temperature.

Buffer PE (wash buffer)

2 mM Tris-HCl (6.3 mg) and 20 mM NaCl (23.4 mg) were dissolved in 2 ml deionised water. Ethanol (16 ml, 80%, v/v) was added, the pH was adjusted to 7.5 and the total volume taken to 20 ml deionised water. The solution was stored at room temperature.

Buffer EB (elution buffer)

20 mM Tris-HCl (32 mg) was dissolved in 20 ml deionised water. The pH was adjusted to 8.5 and the solution was stored at room temperature.

CD Spectroscopy buffer (10 mM Tris-HCl, 250 mM NaF, pH 7)

10 mM Tris-HCl (0.39 g) and 250 mM NaF (2.1 g) were dissolved in 250 ml deionised water. The was adjusted to pH 7, sterilised using a 0.2 μm syringe filter, and degassed under reduced pressure.

6.2.2 Enzymatic assay buffers

Buffer A for lysozyme assay (25 mM Tris-maleate, 100 mM KCl, pH 6.0)

Tris-maleate (1.19 g) and KCl (1.50 g) were dissolved in 200 ml deionised water. The pH of the solution was adjusted to 6.0 by using 5 M NaOH, filtrated and then stored at 4 ^{o}C.

Buffer B for Slt35 assay (25 mM Tris-maleate, 10 mM $CaCl_2$, pH 5.8)

Tris-maleate (1.19 g) and $CaCl_2$ (0.22 g) were dissolved in 200 ml deionised water. The solution was adjusted to pH 5.8 by using 5 M NaOH, filtered and then stored at 4 ^{o}C.

6.2.3 Methods

SDS-PAGE protocol

The gel was composed of two parts. The resolving and stacking solutions were prepared as following (Table 6.1):

Component	Resolving solution / (ml)	Stacking solution / (ml)
H_2O	1.7	2.85
Gel buffer	1.25	1.25
30% Acrylamide solution (with bis-acrylamide)	2.0	0.85
10% SDS solution	0.05	0.05
10% APS	0.05	0.05
TEMED	0.01	0.015

Table 6- 2: *Components in the resolving and stacking solutions for SDS-PAGE gel preparation.*

Prior to pouring the resolving solution freshly prepared ammonium persulfate solution (APS) and TEMED were added to the resolving solution and poured carefully between the casting plates following by covering with an isopropanol layer to remove air bubbles. The gel was left for 20 minutes to polymerise. After polymerisation was completed, the isopropanol was removed and the stacking solution was prepared, gently mixed and then added to the top of resolving gel layer. The comb was added, and the gel was left for an additional 20 minutes for complete polymerisation. The gel was either used immediately or wrapped in wet tissue and foil and then stored at 4 ^{o}C.

Protein preparation

Preparation of competent cells

Competent cells were prepared by streaking a glycerol stock of the cells on non-selective agar plates and incubating at 37 ^{o}C overnight. A single colony from the agar plate was inoculated in non-selective LB medium (10 ml) and incubated at 37 ^{o}C until the optical density reached 0.6 at 600 nm and then the cells were chilled on ice for at least 20 min. The cells were harvested by centrifugation (Eppendorf centrifuge 5810R) at RCF 3220 *g* for 10 min at 4 ^{o}C and the supernatant solution was discarded. Cells were resuspended in 5 ml Rb1 solution and incubated on ice for 20 min, centrifugation step was repeated, and the supernatant solution discarded once more. The pellets were resuspended in calcium chloride solution then aliquoted (100 μl) into sterile Eppendorf tubes and flash frozen in liquid nitrogen for storage at -80 ^{o}C.

Transformation protocol

The appropriate competent cells and DNA solution were allowed to thaw on ice. The DNA solution (1 μl) was transferred into the cell suspension and mixed with the pipette tip under sterile conditions. The mixture (DNA/cell) was incubated on ice for 30 minutes, and then heat shocked at 40 ^{o}C for 40 second and returned to the ice for 2 minutes. To this mixture was added 250 ml from non-selective LB medium and incubated for 1 hour at 37 ^{o} C. The cells were harvested by centrifugation in (Eppendorf centrifuge 5415R) at RCF 16100 *g* for 1 minute. The supernatant solution was discarded, and the pellet was resuspended in 100 μl of LB medium and plated onto agar plates that contained the appropriate antibiotic. The plated cells were incubated at 37 ^{o}C overnight.

Plasmid purification

After transforming cells (XL1-blue or DH5α *E. coli* cloning strain) with the desired plasmid, one colony was extracted from the kanamycin selective plate and placed into 10 ml LB medium containing kanamycin (25 μg/ml). The culture was incubated overnight at 37 ^{o}C with shaking at 150 rpm in an Innova® 43 shaker (New Brunswick Scientific, Hertfordshire, UK). The cells were then harvested *via* centrifugation (Eppendorf centrifuge 5810R) for 10 minutes at RCF 3220*g*, and the supernatant solution was discarded. The pure plasmid was isolated using a QIAprep spin miniprep kit (QIAGEN, Crawley, UK) *via* alkaline lysis of the bacterial cells. The pellet initially resuspended in buffer P1 (250 μl). Cells underwent lysis *via* the alkaline lysis

buffer P2 (250 µl) followed by buffer N3 (350 µl). The solution was mixed then cells were harvested by centrifugation (Eppendorf centrifuge 5810R) for 10 min 13000 rpm. The supernatant solution was collected and added to a spin column where the plasmid then binds to the filter. The centrifugation step was then repeated for 1 minute at 13000 rpm and the flow through solution was discarded. To the spin column PE buffer (750 µl) was added for washing step, the centrifugation step was repeated, the flow through solution was discarded and to ensure all buffer was removed the centrifugation step was repeated once more. The miniprep filter was then placed in a clean Eppendorf tube. Water (50 µl) was added and then centrifugation was repeated, during this final step the plasmid DNA was washed from the column and collected in an Eppendorf tube. The purified DNA solution was then stored at -20 ^{o}C.

DNA Sequencing

The concentration of pure plasmid DNA isolated from the appropriate cloning strain of competent cells was measured by Nanodrop spectrophotometer. A concentration of 50-100 ng / µl was sent to the School of Bioscience, Cardiff University, for sequencing.

Expression

A single colony was extracted from a kanamycin selective plate of a freshly transformed cells (BL21(DE3) *E. coli* strain) and inoculated in 100 ml LB medium containing kanamycin (50 µg / ml) overnight at 37 ^{o}C and 180 rpm. This overnight culture (10 ml) was used to inoculate 500 ml fresh LB medium containing 50 µg / ml kanamycin, and then the growth was continued with agitation (190 rpm) at 37^{o}C until the culture reached an OD_{600} of 0.6-0.8. At this stage, 60 mg of isopropyl-β-D-thiogalactopyranoside (IPTG) was added to the cultures, which were incubated at the appropriate temperature (18 ^{o}C) overnight. The cells were harvested *via* centrifugation in a Sorvall RC 6 Plus Centrifuge (Thermo Fisher Scientific, Inc, MA, USA) using an SLA-3000 rotor at RCF 6080*g* for 30 minutes and the pellets were stored at -20 ^{o}C.

Protein purification

Cells were harvested by centrifugation, re-suspended in a minimal volume of buffer A, B or C. The suspension was sonicated three times for 5 minutes on ice and re-centrifuged at RCF 17065*g* for 30 minutes in a Sorvall RC 6 Plus Centrifuge (Thermo Fisher Scientific, Inc, MA, USA) using an F21S-8x50 rotor to pellet cell debris. The supernatant solution was used for subsequent purification.

Affinity chromatography

Protein purification with buffer A or B

The supernatant was loaded onto a HiTrap Chelating column. The column was washed with buffer A (20 mM HEPES buffer pH 7.0 containing 0.5 M NaCl, 10% glycerol, 0.05% Tween 20) or buffer B (50 mM Tris-HCl pH 7.0 containing 0.5 M NaCl, 10% glycerol, 0.05% Tween 20). Elution of protein was performed by using a gradient from 0-100% of 500 mM of imidazole supplemented to the washing buffer (buffer A or B) (0 mM, 20 mM, 50 mM, 200 mM, 500 mM). The fractions were collected and then analysed by SDS-PAGE gel. Fractions containing the desired protein were collected together, dialysed overnight with the appropriate dialysed buffer A or B and then concentrated by Amicon to about 10 ml.

Protein purification by buffer C

The supernatant solution was applied to a HiTrap Chelating column after it was equilibrated with buffer C (50 mM potassium phosphate pH 7.0 containing 0.5 M NaCl, 10% glycerol, 0.05% Tween 20). Flow through was collected and the column was washed with buffer C pH 7.0 and the bound enzyme was eluted by decreasing pH ranging 7.0-4.0 (7.0, 6.5, 6.0, 5.5, 5.0, 4.5, 4.0). Fractions were collected and then analysed by SDS-PAGE.

Size exclusion chromatography (Superdex 75)

Protein eluted from the HiTrap Chelating column was concentrated to 10 ml by Amicon and injected into Superdex 75 size exclusion column with column volume of 320 ml, equilibrated with buffer B. The protein was eluted 1.5 column volume of buffer B (at 2.5 ml / min). The fractions were collected and analysed by SDS-PAGE.

Protein concentration determination

The concentration of pure protein was determined using Bradford assay with BSA serving as the standard.

Preparation of Bradford reagent.

Bradford reagent was prepared by dissolving 100 mg Coomassie Brilliant Blue G-250 in 50 ml 95% ethanol followed by addition of 100 ml 85% (w/v) phosphoric acid and then the solution was diluted to 1 L with deionised water. The solution was wrapped with foil and stored at 4 ^{o}C.

Preparation of standard curve and samples.

Bradford reagent was mixed and filtrated before use. A series of dilutions (0.002-0.02 mg/ml) from BSA standard stock solution (1 mg/ml) was prepared. A fixed volume (800 μl) of Bradford

reagent was added to standard concentrations of BSA and unknown samples in a total volume of 1 ml. Once the samples were prepared, they were gently mixed and the absorbance of protein-dye complex was measured at wavelengths 595-450 nm after the samples were transferred to the cuvette. From the series of dilutions of BSA and their absorbance at 450 and 595 nm, a standard curve was plotted and the concentration of pure enzyme (mg/ml) was determined from the equation of the curve. To express the concentration into μM, the concentration in mg/ml was divided by the molecular weight of enzyme and multiplied by 10^6 (equation 6.1)

$$\text{Concentration } (\mu M) = \frac{\text{Conc.}_{\text{mg/ml}}}{\text{M. wt.}} \times 10^6 \qquad \textbf{(6.1)}$$

Circular Dichroism Spectroscopy

All circular dichroism spectroscopy was carried out using a Chirascan™ spectrometer (Applied Photophysics Limited, UK).

CD Spectroscopy buffer

Tris-HCl (10 mM) pH 7.0 containing 250 mM NaF was used for denaturation experiments. Prior to the experiment, a blank measurement was taken of the buffer alone.

Calculation of the Mean Residue Ellipticity (MRE)

The signal obtained from CD experiments was converted into mean residue ellipticity (Θ_{MRE}) using following equation:

$$\Theta_{MRE} = \Theta / 10.n.c.l \qquad (6.2)$$

Where: Θ = CD signal in millidegrees, n = number of backbone peptide bonds (i.e. number of amino acid residue -1), c = molar concentration of sample, and l = pathlength of cuvette used in cm.

The cuvette that was used has a pathlength of 0.1 cm and the total volume of 350 μl. The CD spectra of Slt35 were collected at 200-350 nm at 20 ^oC and the total concentration of protein was ~10 μM. Thermal melting temperature was monitored at 220 nm and 5-85 ^oC.

6.2.4 Testing of inhibitors

Glycosidase assay

Assay buffers

50 mM Tris-HCl pH 6.0: 15.8 g Tris-HCl was dissolved in 200 ml deionised water and the pH of the solution was adjusted to 6.0.

1 M Na_2CO_3: 21.2 g Na_2CO_3 was dissolved in 200 ml deionised water.

Assay

A stock solution of p-nitrophenyl-β-D-glucopyranoside (pNPG-βGlc) (1 M) was prepared by dissolving in deionised water. Different concentrations of pNPG-βGlc were mixed with enzyme (1 mg/ml) in 50 mM Tris-HCl pH 6.0 and incubated at different temperatures (40 ^oC and r.t.) for 1 h. The reactions were terminated by adding two volumes of 1 M Na_2CO_3. The absorbance was then read at 405 nm *via* UV spectroscopy (UV-2600, Shimadzu).

Turbidometry assay

Assay buffers

For Slt35, 25 mM Tris-maleate and 10 mM $CaCl_2$ were dissolved in deionized water and then adjusted to pH 5.8. For lysozyme, 25 mM Tris-maleate and 100 mM KCl were dissolved in deionized water followed by adjustment to pH 6.0. The solutions were stored at room temperature.

Assay

Lytic activity of lytic transglycosylase (Slt35) and lysozyme and their inhibition were measured by using the turbidometric assay of Hash (1967)[191] with *Micrococcus lysodeikticus* cells (ATCC 4698, Sigma-Aldrich) as a substrate. The whole cells were suspended in assay buffer at a final concentration of 0.3 mg/ml for Slt35 and 0.6 mg/ml for lysozyme. The desired concentration of lysozyme or purified Slt35 was added to 500 μl of cell suspension and the decrease of turbidity was monitored at 600 nm and 37 ^oC over 1 min.

Enzyme inhibition

Inhibition of Slt35 and lysozyme was assessed by using the turbidometry assay described above. Slt35 or lysozyme was pre-incubated with the potential inhibitors (different concentrations were used) for 10 min at 0 ^oC before being added to the assay mixture. Negative controls were performed by mixing 500 μl cells with 500 μl buffer in the absence of enzyme. For a positive control, 500 μl cells were mixed with 0.1 μM lysozyme (HEWL, Sigma-

Aldrich) and made to a final volume 1 ml with assay buffer. The Slt35 concentration in the assay mixture was 7 μM. The decrease of turbidity was monitored at 600 nm and 37 ^{o}C for 1 minute. The data were normalised between the rate in the absence of inhibitor and the rate in the absence of enzyme, and then reported as a percent inhibition (where normalised rate in the absence of inhibitor = 0% inhibition and normalised rate in the absence of enzyme = 100% inhibition). The data were fitted by nonlinear regression using Sigma Plot 10 (Ligand Binding, sigmoidal dose-response (variable slope) equation 6.2):

F= min + (max-min)/(1+10^((logEC50-x)*Hillslope)) (6.2)

Fluorometric titration

The fluorescence spectra were obtained with the use of LS-22 Luminescence Spectrometer (Perkin-Elmer, Buckinghamshire, UK), which was attached to a Julabo, F25 water bath (Julabo, Seelbach, Germany). A total volume of 2 ml of 3.0 μM enzyme (lysozyme or Slt35) in buffer A or B (Section 6.6.2) was titrated by increasing the concentration of inhibitors in a fluorometric cuvette. Fluorescence spectra of protein and protein-inhibitor solution was recorded after each titration. The excitation wavelength and slit were 280 and 10 nm respectively, and the emission wavelength and slit were 290-450 and 5 nm respectively. The maximum emission spectrum of lysozyme presented at an excitation wavelength of 348 nm while that of Slt35 was at 344 nm. The fluorescence intensity at maximum wavelength was corrected for dilution and analysed using equation (6.3):

$$\Delta I_f = - (I_{f\ final} - I_{f\ initial}) \quad (6.3)$$

The analysed titration data were then fitted by nonlinear regression using SigmaPlot 10 (Ligand Binding, one site saturation equation 6.4):

F= Bmax*abs(x)/(kd + abs(x)) (6.4)

Mass spectrometer method

Liquid chromatography mass spectrometry (LC-MS) was performed on a Waters Synapt G2-Si quadrupole time of flight mass spectrometer coupled to a Waters Acquity H-Class UPLC system. The column was an Acquity UPLC protein BEH C4 (300 Å 1.7 μm × 2.1 mm × 100 mm) operated in reverse phase and held at 60 °C. The gradient employed was 95% A to 35% A over 50 minutes, where A is H_2O with 0.1% HCO_2H and B is acetonitrile (ACN) with 0.1% HCO_2H. Data was collected in positive ionisation mode and analyzed using the *Waters*

MassLynx software version 4.1. Deconvolution of protein charged states was obtained using the maximum entropy 1 processing software.

7 References

1. M. Rai, K.K., A. Gade, A. Ingle, D. Nagaonkar, P. Paralikar and S.S. da Silva, *Antibiotic Resistance: Can Nanoparticles Tackle The Problem?*, in *Antibiotic Resistance: Mechanisms and New Antimicrobial Approaches*, M.R. Kateryna Kon, Editor. 2016.
2. Kishore R. Sakharkar, M.K.S., and Vincent T. K. Chow, *Biocomputational Strategies for Microbial Drug Target Identification*, in *New Antibiotic Targets*, W.S. Champney, Editor. 2008.
3. Li, F., J.G. Collins, and F.R. Keene, *Ruthenium complexes as antimicrobial agents.* Chem Soc Rev, 2015. **44**(8): p. 2529-2542.
4. Tipper, D.J. and J.L. Strominger, *Mechanism of action of penicillins; a proposal based on their structural similarity to acyl-D-alanyl-D-alanine.* Proc. Natl. Acad. Sci. U. S. A., 1965. **54**(4): p. 1133-1141.
5. Azami, H., et al., *Synthesis and antibacterial activity of novel 4-pyrrolidinylthio carbapenems. I. 2-Alkoxymethyl derivatives.* Bioorg. Med. Chem., 1997. **5**(11): p. 2069-2087.
6. Dunn, G.L., *Ceftizoxime and other third-generation cephalosporins: structure-activity relationships.* J. Antimicrob. Chemother., 1982. **10**(Suppl. C): p. 1-10.
7. Fuchs, P.C., et al., *In vitro antimicrobial activity of tigemonam, a new orally administered monobactam.* Antimicrob. Agents Chemother., 1988. **32**(3): p. 346-349.
8. Worthington, R.J. and C. Melander, *Overcoming Resistance to β-Lactam Antibiotics.* J. Org. Chem., 2013. **78**(9): p. 4207-4213.
9. Arthur, M. and P. Courvalin, *Genetics and mechanisms of glycopeptide resistance in enterococci.* Antimicrob. Agents Chemother., 1993. **37**(8): p. 1563-1571.
10. Meziane-Cherif, D., et al., *Structural basis for the evolution of vancomycin resistance D,D-peptidases.* Proc. Natl. Acad. Sci. U. S. A., 2014. **111**(16): p. 5872-5877.
11. in *Antibiotics: Challenges, Mechanisms, Opportunities*, T.W. Christopher Walsh, Editor. 2016 Washington, District of Columbia : ASM Press.
12. Taylor, R., et al., *Daptomycin Pore Formation Is Restricted by Lipid Acyl Chain Composition.* ACS Infect. Dis., 2017. **3**(11): p. 797-801.
13. Falagas, M.E., P.I. Rafailidis, and D.K. Matthaiou, *Resistance to polymyxins: Mechanisms, frequency and treatment options.* Drug Resist. Updates, 2010. **13**(4-5): p. 132-138.

14. Arenz, S. and D.N. Wilson, *Bacterial protein synthesis as a target for antibiotic inhibition.* Cold Spring Harbor Perspect. Med., 2016. **6**(9): p. a025361/1-a025361/15.
15. Cocito, C., et al., *Inhibition of protein synthesis by streptogramins and related antibiotics.* J. Antimicrob. Chemother., 1997. **39**(Suppl. A): p. 7-13.
16. Berkov-Zrihen, Y., et al., *Synthesis and Evaluation of Hetero- and Homodimers of Ribosome-Targeting Antibiotics: Antimicrobial Activity, in Vitro Inhibition of Translation, and Drug Resistance.* J. Med. Chem., 2013. **56**(13): p. 5613-5625.
17. Katz, L. and G.W. Ashley, *Translation and Protein Synthesis: Macrolides.* Chem. Rev. (Washington, DC, U. S.), 2005. **105**(2): p. 499-527.
18. Parajuli, P., et al., *Enzymatic glycosylation of the topical antibiotic mupirocin.* Glycoconjugate J., 2014. **31**(8): p. 563-572.
19. Capobianco, J.O., C.C. Doran, and R.C. Goldman, *Mechanism of mupirocin transport into sensitive and resistant bacteria.* Antimicrob. Agents Chemother., 1989. **33**(2): p. 156-163.
20. Vioque, A., *Protein synthesis inhibitors and catalytic RNA. Effect of puromycin on tRNA precursor processing by the RNA component of Escherichia coli RNase P.* FEBS Lett., 1989. **246**(1-2): p. 137-139.
21. Hooper, D.C., *Mechanisms of fluoroquinolone resistance.* Drug Resist. Updates, 1999. **2**(1): p. 38-55.
22. Aivasashvilli, V.A. and R.S. Bebelashvilli, *Sequence-specific inhibition of RNA elongation by actinomycin D.* FEBS Lett., 1983. **160**(1-2): p. 124-128.
23. Yun, M.-K., et al., *Catalysis and sulfa drug resistance in dihydropteroate synthase.* Science, 2012. **335**(6072): p. 1110-1114.
24. Rothstein, D.M., *Rifamycins, alone and in combination.* Cold Spring Harbor Perspect. Med., 2016. **6**(7): p. a027011/1-a027011/20.
25. Li, L.H., et al., *Effects of streptovaricins and their degradation products on RNA-directed DNA polymerase of Rauscher leukemia virus.* J. Natl. Cancer Inst., 1977. **58**(2): p. 239-243.
26. Abraham, E.P. and E. Chain, *An enzyme from bacteria able to destroy penicillin.* Nature, 1940. **146**: p. 837.
27. Walsh, C., *Molecular mechanisms that confer antibacterial drug resistance.* Nature, 2000. **406**(6797): p. 775-781.

28. Tenover, F.C., *Mechanisms of antimicrobial resistance in bacteria.* Am. J. Med., 2006. **119**(6A): p. S3-S10.

29. Munita, J.M.A., Cesar A., *Mechanisms of antibiotic resistance*, in *Virulence Mechanisms of Bacterial Pathogens, Fifth Edition*, N.A.C. Indira T. Kudva, Paul J. Plummer, Qijing Zhang, Tracy L. Nicholson, John P. Bannantine, Bryan H. Bellaire, Editor. 2016, American Society for Microbiology.

30. Pontes, D.S., et al., *Genetic Mechanisms of Antibiotic Resistance and the Role of Antibiotic Adjuvants.* Curr. Top. Med. Chem., 2018. **18**(1): p. 42-74.

31. McManus, M.C., *Mechanisms of bacterial resistance to antimicrobial agents.* Am J Health Syst Pharm, 1997. **54**(12): p. 1420-1433.

32. Ramirez, M.S. and M.E. Tolmasky, *Aminoglycoside modifying enzymes.* Drug Resist. Updates, 2010. **13**(6): p. 151-171.

33. Li, X.-Z. and H. Nikaido, *Efflux-mediated drug resistance in bacteria: an update.* Drugs, 2009. **69**(12): p. 1555-1623.

34. Poole, K., *Efflux-mediated antimicrobial resistance.* J. Antimicrob. Chemother., 2005. **56**(1): p. 20-51.

35. Vollmer, W., D. Blanot, and M.A. de Pedro, *Peptidoglycan structure and architecture.* FEMS Microbiol. Rev., 2008. **32**(2): p. 149-167.

36. Schleifer, K.H. and O. Kandler, *Peptidoglycan types of bacterial cell walls and their taxonomic implications.* Bacteriol. Rev., 1972. **36**(4): p. 407-477.

37. Lee, M., et al., *Catalytic Spectrum of the Penicillin-Binding Protein 4 of Pseudomonas aeruginosa, a Nexus for the Induction of β-Lactam Antibiotic Resistance.* J. Am. Chem. Soc., 2015. **137**(1): p. 190-200.

38. Vollmer, W., *Structural variation in the glycan strands of bacterial peptidoglycan.* FEMS Microbiol. Rev., 2008. **32**(2): p. 287-306.

39. Typas, A., et al., *From the regulation of peptidoglycan synthesis to bacterial growth and morphology.* Nat. Rev. Microbiol., 2012. **10**(2): p. 123-136.

40. Barreteau, H., et al., *Cytoplasmic steps of peptidoglycan biosynthesis.* FEMS Microbiol. Rev., 2008. **32**(2): p. 168-207.

41. Mengin-Lecreulx, D. and J. van Heijenoort, *Identification of the glmU gene encoding N-acetylglucosamine-1-phosphate uridyltransferase in Escherichia coli.* J. Bacteriol., 1993. **175**(19): p. 6150-6157.

42. Mengin-Lecreulx, D. and J. van Heijenoort, *Copurification of glucosamine-1-phosphate acetyltransferase and N-acetylglucosamine-1-phosphate uridyltransferase activities of Escherichia coli: characterization of the glmU gene product as a bifunctional enzyme catalyzing two subsequent steps in the pathway for UDP-N-acetylglucosamine synthesis.* J. Bacteriol., 1994. **176**(18): p. 5788-5795.

43. Marquardt, J.L., et al., *Cloning and sequencing of Escherichia coli murZ and purification of its product, a UDP-N-acetylglucosamine enolpyruvyl transferase.* J. Bacteriol., 1992. **174**(17): p. 5748-5752.

44. Brown, E.D., et al., *MurA (MurZ), the enzyme that catalyzes the first committed step in peptidoglycan biosynthesis, is essential in Escherichia coli.* J. Bacteriol., 1995. **177**(14): p. 4194-4197.

45. Pucci, M.J., L.F. Discotto, and T.J. Dougherty, *Cloning and identification of the Escherichia coli murB DNA sequence, which encodes UDP-N-acetylenolpyruvoylglucosamine reductase.* J. Bacteriol., 1992. **174**(5): p. 1690-1693.

46. Healy, V.L., et al., *Vancomycin resistance in enterococci: reprogramming of the D-Ala-D-Ala ligases in bacterial peptidoglycan biosynthesis.* Chem. Biol., 2000. **7**(5): p. R109-R119.

47. Teo, A.C.K. and D.I. Roper, *Core steps of membrane-bound peptidoglycan biosynthesis:recent advances, insight and opportunities.* Antibiotics (Basel, Switz.), 2015. **4**(4): p. 495-520.

48. Bouhss, A., et al., *The biosynthesis of peptidoglycan lipid-linked intermediates.* FEMS Microbiol. Rev., 2008. **32**(2): p. 208-233.

49. Muench, D., et al., *Identification and in vitro analysis of the GatD/MurT enzyme-complex catalyzing lipid II amidation in Staphylococcus aureus.* PLoS Pathog., 2012. **8**(1): p. e1002509.

50. Shepherd, J. and M. Ibba, *Direction of aminoacylated transfer RNAs into antibiotic synthesis and peptidoglycan-mediated antibiotic resistance.* FEBS Lett., 2013. **587**(18): p. 2895-2904.

51. Zapun, A., et al., *In vitro Reconstitution of Peptidoglycan Assembly from the Gram-Positive Pathogen Streptococcus pneumoniae.* ACS Chem. Biol., 2013. **8**(12): p. 2688-2696.

52. Ikeda, M., et al., *Structural similarity among Escherichia coli FtsW and RodA proteins and Bacillus subtilis SpoVE protein, which function in cell division, cell elongation, and spore formation, respectively.* J. Bacteriol., 1989. **171**(11): p. 6375-6378.

53. Mohammadi, T., et al., *Identification of FtsW as a transporter of lipid-linked cell wall precursors across the membrane.* EMBO J., 2011. **30**(8): p. 1425-1432.

54. Hvorup, R.N., et al., *The multidrug/oligosaccharidyl-lipid/polysaccharide (MOP) exporter superfamily.* Eur. J. Biochem., 2003. **270**(5): p. 799-813.

55. Ruiz, N., *Bioinformatics identification of MurJ (MviN) as the peptidoglycan lipid II flippase in Escherichia coli.* Proc. Natl. Acad. Sci. U. S. A., 2008. **105**(40): p. 15553-15557.

56. Mohamed, Y.F. and M.A. Valvano, *A Burkholderia cenocepacia MurJ (MviN) homolog is essential for cell wall peptidoglycan synthesis and bacterial viability.* Glycobiology, 2014. **24**(6): p. 564-576.

57. Lovering, A.L., M. Gretes, and N.C.J. Strynadka, *Structural details of the glycosyltransferase step of peptidoglycan assembly.* Curr. Opin. Struct. Biol., 2008. **18**(5): p. 534-543.

58. Sauvage, E., et al., *The penicillin-binding proteins: structure and role in peptidoglycan biosynthesis. [Erratum to document cited in CA148:278370].* FEMS Microbiol. Rev., 2008. **32**(3): p. 556.

59. Hameed P, S., et al., *Pyrazolopyrimidines establish MurC as a vulnerable target in Pseudomonas aeruginosa and Escherichia coli.* ACS Chem. Biol., 2014. **9**(10): p. 2274-2282.

60. Goodell, E.W., *Recycling of murein by Escherichia coli.* J. Bacteriol., 1985. **163**(1): p. 305-310.

61. Sharma, A.K., et al., *Prediction of peptidoglycan hydrolases- a new class of antibacterial proteins.* BMC Genomics, 2016. **17**: p. 411/1-411/12.

62. Hoeltje, J.-V., *From growth to autolysis: the murein hydrolases in Escherichia coli.* Arch. Microbiol., 1995. **164**(4): p. 243-254.

63. Vollmer, W., et al., *Bacterial peptidoglycan (murein) hydrolases.* FEMS Microbiol. Rev., 2008. **32**(2): p. 259-286.

64. Lipski, A., et al., *Structural and biochemical characterization of the β-N-acetylglucosaminidase from Thermotoga maritima: toward rationalization of mechanistic knowledge in the GH73 family.* Glycobiology, 2015. **25**(3): p. 319-330.

65. Zhang, R., et al., *Enzymatic properties of β-N-acetylglucosaminidases.* Appl. Microbiol. Biotechnol., 2018. **102**(1): p. 93-103.

66. Zechel, D.L. and S.G. Withers, *Glycosidase Mechanisms: Anatomy of a Finely Tuned Catalyst.* Acc. Chem. Res., 2000. **33**(1): p. 11-18.

67. Gloster, T.M. and G.J. Davies, *Glycosidase inhibition: assessing mimicry of the transition state.* Org. Biomol. Chem., 2010. **8**(2): p. 305-320.

68. Vuong, T.V. and D.B. Wilson, *Glycoside hydrolases: Catalytic base/nucleophile diversity.* Biotechnol. Bioeng., 2010. **107**(2): p. 195-205.

69. Lairson, L.L., et al., *Glycosyltransferases: structures, functions, and mechanisms.* Annu. Rev. Biochem., 2008. **77**: p. 521-555.

70. Ho, L.A., et al., *A mechanism-based GlcNAc-inspired cyclophellitol inactivator of the peptidoglycan recycling enzyme NagZ reverses resistance to β-lactams in Pseudomonas aeruginosa.* Chem. Commun., 2018. **54**(75): p. 10630-10633.

71. Acebron, I., et al., *Catalytic cycle of the N-acetylglucosaminidase NagZ from Pseudomonas aeruginosa.* J. Am. Chem. Soc., 2017. **139**(20): p. 6795-6798.

72. Stubbs, K.A., et al., *The Development of Selective Inhibitors of NagZ: Increased Susceptibility of Gram-Negative Bacteria to β-Lactams.* ChemBioChem, 2013. **14**(15): p. 1973-1981.

73. Mondon, M., et al., *Selective trihydroxyazepane NagZ inhibitors increase sensitivity of Pseudomonas aeruginosa to β-lactams.* Chem. Commun. (Cambridge, U. K.), 2013. **49**(93): p. 10983-10985.

74. Vadlamani, G., et al., *Conformational flexibility of the glycosidase NagZ allows it to bind structurally diverse inhibitors to suppress β-lactam antibiotic resistance.* Protein Sci., 2017. **26**(6): p. 1161-1170.

75. Stubbs, K.A., et al., *Small Molecule Inhibitors of a Glycoside Hydrolase Attenuate Inducible AmpC-mediated β-Lactam Resistance.* J. Biol. Chem., 2007. **282**(29): p. 21382-21391.

76. Wohlkonig, A., et al., *Structural relationships in the lysozyme superfamily: significant evidence for glycoside hydrolase signature motifs.* PLoS One, 2010. **5**(11): p. 1-10.

77. Vocadlo, D.J., et al., *Catalysis by hen egg-white lysozyme proceeds via a covalent intermediate.* Nature, 2001. **412**(6849): p. 835-839.

78. Callewaert, L. and C.W. Michiels, *Lysozymes in the animal kingdom.* J. Biosci., 2010. **35**(1): p. 127-160.

79. Abergel, C., et al., *Structure and evolution of the Ivy protein family, unexpected lysozyme inhibitors in Gram-negative bacteria.* Proc. Natl. Acad. Sci. U. S. A., 2007. **104**(15): p. 6394-6399.

80. Liu, Z., et al., *Protecting Gram-negative bacterial cell envelopes from human lysozyme: Interactions with Ivy inhibitor proteins from Escherichia coli and Pseudomonas aeruginosa.* Biochim. Biophys. Acta, Biomembr., 2015. **1848**(11_Part_B): p. 3032-3046.

81. Yum, S., et al., *Structural basis for the recognition of lysozyme by MliC, a periplasmic lysozyme inhibitor in Gram-negative bacteria.* Biochem. Biophys. Res. Commun., 2009. **378**(2): p. 244-248.

82. Um, S.-H., et al., *Structural Basis for the Inhibition of Human Lysozyme by PliC from Brucella abortus.* Biochemistry, 2013. **52**(51): p. 9385-9393.

83. Ogata, M., et al., *A Novel Transition-state Analogue for Lysozyme, 4-O-β-Tri-N-acetylchitotriosyl Moranoline, Provided Evidence Supporting the Covalent Glycosyl-enzyme Intermediate.* J. Biol. Chem., 2013. **288**(9): p. 6072-6082.

84. Shanmugaraj, K., S. Anandakumar, and M. Ilanchelian, *Probing the binding interaction of thionine with lysozyme: A spectroscopic and molecular docking investigation.* Dyes Pigm., 2015. **112**: p. 210-219.

85. Scheurwater, E., C.W. Reid, and A.J. Clarke, *Lytic transglycosylases: Bacterial space-making autolysins.* Int. J. Biochem. Cell Biol., 2008. **40**(4): p. 586-591.

86. Lee, M., et al., *From Genome to Proteome to Elucidation of Reactions for All Eleven Known Lytic Transglycosylases from Pseudomonas aeruginosa.* Angew. Chem., Int. Ed., 2017. **56**(10): p. 2735-2739.

87. Mijoon Lee, D.H., Leticia I. Llarrull, Elena Lastochkin, Hualiang Pi, Bill Boggess, and Shahriar Mobashery, *Reactions of All Escherichia coli Lytic Transglycosylases with Bacterial Cell Wall* J. Am. Chem. Soc. , 2013. **2135**.

88. Artola-Recolons, C., et al., *Structure and cell wall cleavage by modular lytic transglycosylase MltC of Escherichia coli.* ACS Chem. Biol., 2014. **9**(9): p. 2058-2066.

89. Blackburn, N.T. and A.J. Clarke, *Identification of Four Families of Peptidoglycan Lytic Transglycosylases.* J. Mol. Evol., 2001. **52**(1): p. 78-84.

90. Herlihey, F.A. and A. J. Clarke, *Controlling Autolysis During Flagella Insertion in Gram-Negative Bacteria*, in *Protein Reviews*, M. Zouhair Atassi, Editor. Springer Nature Singapore Pte Ltd. 2017.

91. Scheurwater, E.M. and A.J. Clarke, *The C-terminal Domain of Escherichia coli YfhD Functions as a Lytic Transglycosylase.* J. Biol. Chem., 2008. **283**(13): p. 8363-8373.

92. Herlihey, F.A., et al., *Modulation of the lytic activity of the dedicated autolysin for flagellum formation SltF by flagellar rod proteins FlgB and FlgF.* J. Bacteriol., 2016. **198**(13): p. 1847-1856.

93. Jorgenson, M.A., et al., *The bacterial septal ring protein RlpA is a lytic transglycosylase that contributes to rod shape and daughter cell separation in Pseudomonas aeruginosa.* Mol. Microbiol., 2014. **93**(1): p. 113-128.

94. van Asselt, E.J., A.-M.W.H. Thunnissen, and B.W. Dijkstra, *High Resolution Crystal Structures of the Escherichia coli Lytic Transglycosylase Slt70 and its Complex with a Peptidoglycan Fragment.* J. Mol. Biol., 1999. **291**(4): p. 877-898.

95. Fibriansah, G., F.I. Gliubich, and A.-M.W.H. Thunnissen, *On the mechanism of peptidoglycan binding and cleavage by the endo-specific lytic transglycosylase MltE from Escherichia coli.* Biochemistry, 2012. **51**(45): p. 9164-9177.

96. Powell, A.J., et al., *Crystal Structures of the Lytic Transglycosylase MltA from N.gonorrhoeae and E.coli: Insights into Interdomain Movements and Substrate Binding.* J. Mol. Biol., 2006. **359**(1): p. 122-136.

97. van Straaten, K.E., et al., *Structure of Escherichia coli Lytic Transglycosylase MltA with Bound Chitohexaose: Implications for peptidoglycan binding and cleavage.* J. Biol. Chem., 2007. **282**(29): p. 21197-21205.

98. Van Asselt, E.J., et al., *Crystal structure of Escherichia coli lytic transglycosylase Slt35 reveals a lysozyme-like catalytic domain with an EF-hand.* Structure (London), 1999. **7**(10): p. 1167-1180.

99. Ioulia Nikolaidis, T.I., Viviana Job, Nicole Thielens, Eefjan Breukink, and Andre´a Dessen, *Calcium-Dependent Complex Formation Between PBP2 and Lytic Transglycosylase SltB1 of Pseudomonas aeruginosa.* Microbial Drug Resistance 2012. **18**(3): p. 298-305.

100. Lee, M., et al., *Turnover of bacterial cell wall by SltB3, a multidomain lytic transglycosylase of Pseudomonas aeruginosa.* ACS Chem. Biol., 2016. **11**(6): p. 1525-1531.

101. Leung, A.K.W., et al., *Crystal Structure of the Lytic Transglycosylase from Bacteriophage Lambda in Complex with Hexa-N-acetylchitohexaose.* Biochemistry, 2001. **40**(19): p. 5665-5673.

102. Thunnissen, A.-M.W.H., N.W. Isaacs, and B.W. Dijkstra, *The catalytic domain of a bacterial lytic transglycosylase defines a novel class of lysozymes.* Proteins: Struct., Funct., Genet., 1995. **22**(3): p. 245-258.

103. Thunnissen, A.-M.W.H., et al., *Structure of the 70-kDa Soluble Lytic Transglycosylase Complexed with Bulgecin A. Implications for the Enzymic Mechanism.* Biochemistry, 1995. **34**(39): p. 12729-12737.

104. Yunck, R., H. Cho, and T.G. Bernhardt, *Identification of MltG as a potential terminase for peptidoglycan polymerization in bacteria.* Mol Microbiol, 2016. **99**(4): p. 700-718.

105. Heffron, J.D., B. Orsburn, and D.L. Popham, *Roles of germination-specific lytic enzymes CwlJ and SleB in Bacillus anthracis.* J. Bacteriol., 2009. **191**(7): p. 2237-2247.

106. Moynihan, P.J. and A.J. Clarke, *O-Acetylated peptidoglycan: Controlling the activity of bacterial autolysins and lytic enzymes of innate immune systems.* Int. J. Biochem. Cell Biol., 2011. **43**(12): p. 1655-1659.

107. Weadge, J.T. and A.J. Clarke, *Identification and Characterization of O-Acetylpeptidoglycan Esterase: A Novel Enzyme Discovered in Neisseria gonorrhoeae.* Biochemistry, 2006. **45**(3): p. 839-851.

108. Weadge, J.T., J.M. Pfeffer, and A.J. Clarke, *Identification of a new family of enzymes with potential O-acetylpeptidoglycan esterase activity in both gram-positive and gram-negative bacteria.* BMC Microbiol., 2005. **5**: doi:10.1186/1471-2180-5-49.

109. Legaree, B.A. and A.J. Clarke, *Interaction of penicillin-binding protein 2 with soluble lytic transglycosylase B1 in Pseudomonas aeruginosa.* J. Bacteriol., 2008. **190**(20): p. 6922-6926.

110. Holtje, J.-V., *Growth of the stress-bearing and shape-maintaining murein sacculus of Escherichia coli.* Microbiol. Mol. Biol. Rev., 1998. **62**(1): p. 181-203.

111. Dominguez-Gil, T., et al., *Activation by Allostery in Cell-Wall Remodeling by a Modular Membrane-Bound Lytic Transglycosylase from Pseudomonas aeruginosa.* Structure, 2016. **24**(10): p. 1729-1741.

112. Dijkstra, A.J., F. Hermann, and W. Keck, *Cloning and controlled overexpression of the gene encoding the 35 kDa soluble lytic transglycosylase from Escherichia coli.* FEBS Lett., 1995. **366**(2,3): p. 115-118.

113. Lewit-Bentley, A. and S. Rety, *EF-hand calcium-binding proteins.* Curr. Opin. Struct. Biol., 2000. **10**(6): p. 637-643.

114. Gifford, J.L, M.P. Walsh and H.J. Vogel, *Structures and metal-ion-binding properties of the Ca^{2+}-binding helix–loop–helix EF-hand motifs* Biochem.J., 2007. 405: p. 199-229.

115. Van Asselt, E.J. and B.W. Dijkstra, *Binding of calcium in the EF-hand of Escherichia coli lytic transglycosylase Slt35 is important for stability.* FEBS Lett., 1999. **458**(3): p. 429-435.

116. Van Asselt, E.J., K.H. Kalk, and B.W. Dijkstra, *Crystallographic Studies of the Interactions of Escherichia coli Lytic Transglycosylase Slt35 with Peptidoglycan.* Biochemistry, 2000. **39**(8): p. 1924-1934.

117. Reid, C.W., et al., *Inhibition of membrane-bound lytic transglycosylase B by NAG-thiazoline.* FEBS Lett., 2004. **574**(1-3): p. 73-79.

118. Reid, C.W., N.T. Blackburn, and A.J. Clarke, *Role of Arginine Residues in the Active Site of the Membrane-Bound Lytic Transglycosylase B from Pseudomonas aeruginosa.* Biochemistry, 2006. **45**(7): p. 2129-2138.

119. Reid, C.W., D. Brewer, and A.J. Clarke, *Substrate Binding Affinity of Pseudomonas aeruginosa Membrane-Bound Lytic Transglycosylase B by Hydrogen-Deuterium Exchange MALDI MS.* Biochemistry, 2004. **43**(35): p. 11275-11282.

120. Lovering, A.L., et al., *Structural Insight into the Transglycosylation Step of Bacterial Cell-Wall Biosynthesis.* Science, 2007. **315**(5817): p. 1402-1405.

121. Sauvage, E., et al., *The penicillin-binding proteins: structure and role in peptidoglycan biosynthesis.* FEMS Microbiol. Rev., 2008. **32**(2): p. 234-258.

122. Jacoby, G.A., *AmpC β-lactamases.* Clin. Microbiol. Rev., 2009. **22**(1): p. 161-182.

123. Park, J.T., *Identification of a dedicated recycling pathway for anhydro-N-acetylmuramic acid and N-acetylglucosamine derived from Escherichia coli cell wall murein.* J. Bacteriol., 2001. **183**(13): p. 3842-3847.

124. Kraft, A.R., et al., *Interference with murein turnover has no effect on growth but reduces β-lactamase induction in Escherichia coli.* J. Bacteriol., 1999. **181**(23): p. 7192-7198.

125. Tomoshige, S., et al., *Total Syntheses of Bulgecins A, B, and C and Their Bactericidal Potentiation of the β-Lactam Antibiotics.* ACS Infect. Dis., 2018. **4**(6): p. 860-867.

126. Loveridge, E.J., et al., *Reclassification of the specialized metabolite producer Pseudomonas mesoacidophila ATCC 31433 as a member of the Burkholderia cepacia complex.* J. Bacteriol., 2017. **199**(13): p. e00125-17/1-e00125-17/12.

127. Shinagawa, S., et al., *Structures of bulgecins, bacterial metabolites with bulge-inducing activity.* Tetrahedron, 1984. **40**(18): p. 3465-3470.

128. Shinagawa, S., et al., *Isolation and characterization of bulgecins, new bacterial metabolites with bulge-inducing activity.* J. Antibiot., 1985. **38**(1): p. 17-23.

129. Templin, M.F., D.H. Edwards, and J.V. Hoeltje, *A murein hydrolase is the specific target of bulgecin in Escherichia coli.* J. Biol. Chem., 1992. **267**(28): p. 20039-20043.

130. Williams, A.H., et al., *Bulgecin A: the key to a broad-spectrum inhibitor that targets lytic transglycosylases.* Antibiotics (Basel, Switz.), 2017. **6**(1): doi:10.3390/antibiotics6010008.

131. Reid, C.W., N.T. Blackburn, and A.J. Clarke, *The effect of NAG-thiazoline on morphology and surface hydrophobicity of Escherichia coli.* FEMS Microbiol. Lett., 2004. **234**(2): p. 343-348.

132. Clarke, C.A., E.M. Scheurwater, and A.J. Clarke, *The Vertebrate Lysozyme Inhibitor Ivy Functions to Inhibit the Activity of Lytic Transglycosylase.* J. Biol. Chem., 2010. **285**(20): p. 14843-14847.

133. Yamaguchi, T., et al., *Inhibitors for bacterial cell wall recycling.* ACS Med. Chem. Lett., 2012. **3**(3): p. 238-242.

134. Johnson, J.W., J.F. Fisher, and S. Mobashery, *Bacterial cell-wall recycling.* Ann. N. Y. Acad. Sci., 2013. **1277**(Antimicrobial Therapeutics Reviews): p. 54-75.

135. Langley, D.B., et al., *Structure of N-acetyl-β-D-glucosaminidase (GcnA) from the Endocarditis Pathogen Streptococcus gordonii and its Complex with the Mechanism-based Inhibitor NAG-thiazoline.* J. Mol. Biol., 2008. **377**(1): p. 104-116.

136. Whitworth, G.E., et al., *Analysis of PUGNAc and NAG-thiazoline as Transition State Analogues for Human O-GlcNAcase: Mechanistic and Structural Insights into Inhibitor Selectivity and Transition State Poise.* J. Am. Chem. Soc., 2007. **129**(3): p. 635-644.

137. Lemieux, M.J., et al., *Crystallographic Structure of Human β-Hexosaminidase A: Interpretation of Tay-Sachs Mutations and Loss of GM2 Ganglioside Hydrolysis.* J. Mol. Biol., 2006. **359**(4): p. 913-929.

138. Knapp, S., et al., *NAG-thiazoline, An N-Acetyl-β-hexosaminidase Inhibitor That Implicates Acetamido Participation.* J. Am. Chem. Soc., 1996. **118**(28): p. 6804-6805.

139. Liu, T., et al., *Exploring NAG-thiazoline and its derivatives as inhibitors of chitinolytic β-acetyl glucosaminidases.* FEBS Lett., 2015. **589**(1): p. 110-116.

140. Krejzova, J., et al., *Inhibition of microbial β-N-acetylhexosaminidases by 4-deoxy- and galacto-analogues of NAG-thiazoline.* Bioorg. Med. Chem. Lett., 2014. **24**(22): p. 5321-5323.

141. Kong, H., et al., *Synthesis of NAG-thiazoline-derived inhibitors for β-N-acetyl-D-hexosaminidases.* Carbohydr. Res., 2015. **413**: p. 135-144.

142. Papandreou, G., M.K. Tong, and B. Ganem, *Amidine, amidrazone, and amidoxime derivatives of monosaccharide aldonolactams: synthesis and evaluation as glycosidase inhibitors.* J. Am. Chem. Soc., 1993. **115**(25): p. 11682-11690.

143. Hafelinger, G., *General and theoretical aspects of amidines and imidic acid derivatives* in *The chemistry of amidines and imidates*, S. PATAI, Editor. 1975, John Wiley & Sons, Ltd.

144. in *Superbases for Organic Synthesis: Guanidines, Amidines, Phosphazenes and Related Organocatalysts*, T. Ishikawa, Editor. 2009, John Wiley & Sons, Ltd.

145. Tong, M.K., G. Papandreou, and B. Ganem, *Potent, broad-spectrum inhibition of glycosidases by an amidine derivative of D-glucose.* J. Am. Chem. Soc., 1990. **112**(16): p. 6137-6139.

146. Kanso, R. and S. Striegler, *Multi gram-scale synthesis of galactothionolactam and its transformation into a galactonoamidine.* Carbohydr. Res., 2011. **346**(7): p. 897-904.

147. Bleriot, Y., A. Genre-Grandpierre, and C. Tellier, *Synthesis of a benzylamidine derived from D-mannose. A potent mannosidase inhibitor.* Tetrahedron Lett., 1994. **35**(12): p. 1867-1870.

148. Fan, Q.-H., K.A. Claunch, and S. Striegler, *Structure-Activity Relationship of Highly Potent Galactonoamidine Inhibitors toward β-Galactosidase (Aspergillus oryzae).* J. Med. Chem., 2014. **57**(21): p. 8999-9009.

149. Heck, M.-P., et al., *Cyclic Amidine Sugars as Transition-State Analogue Inhibitors of Glycosidases: Potent Competitive Inhibitors of Mannosidases.* J. Am. Chem. Soc., 2004. **126**(7): p. 1971-1979.

150. Bleriot, Y., et al., *Synthesis of an amidine pseudo-(1→6)-dimannoside and evaluation as a glycosidase inhibitor.* Tetrahedron Lett., 1995. **36**(29): p. 5175-5178.

151. Sousa, S.F., P.A. Fernandes, and M.J. Ramos, *Protein-ligand docking: current status and future challenges.* Proteins: Struct., Funct., Bioinf., 2006. **65**(1): p. 15-26.

152. Scarpi, D., et al., *Complementary and stereodivergent approaches to the synthesis of 5-hydroxy- and 4,5-dihydroxypipecolic acids from enantiopure hydroxylated lactams.* Eur. J. Org. Chem., 2013. **2013**(7): p. 1306-1317.

153. Rothman, J.H., *Direct and Facile Syntheses of Heterocyclic Vinyl-C-Nucleosides for Recognition of Inverted Base Pairs by DNA Triple Helix Formation: First Report by Direct Wittig Route.* J. Org. Chem., 2007. **72**(10): p. 3945-3948.

154. Song, J. and R.I. Hollingsworth, *Homochiral 4-hydroxy-5-hexenoic acids and their derivatives and homologs from carbohydrates.* Tetrahedron: Asymmetry, 2001. **12**(3): p. 387-391.

155. Wang, D. and W.A. Nugent, *2-Deoxyribose as a Rich Source of Chiral 5-Carbon Building Blocks.* J. Org. Chem., 2007. **72**(19): p. 7307-7312.

156. Tran, V.T. and K.A. Woerpel, *Nucleophilic Addition to Silyl-Protected Five-Membered Ring Oxocarbenium Ions Governed by Stereoelectronic Effects.* J. Org. Chem., 2013. **78**(13): p. 6609-6621.

157. Olsen, R.K., et al., *Syntheses of (S)-(-)-3-piperidinol from L-glutamic acid and (S)-malic acid.* J. Org. Chem., 1985. **50**(6): p. 896-899.

158. Dey, S., P.U. Karabal, and A. Sudalai, *Concise Enantioselective Synthesis of Naturally Active (S)-3-Hydroxypiperidine.* Synth. Commun., 2015. **45**(13): p. 1559-1565.

159. Huh, N. and C.M. Thompson, *Enantioenriched N-(2-chloroalkyl)-3-acetoxypiperidines as potential cholinotoxic agents. Synthesis and preliminary evidence for spirocyclic aziridinium formation.* Tetrahedron, 1995. **51**(21): p. 5935-5950.

160. Herdeis, C. and E. Heller, *Synthesis of (2S,4S,5S)-5-hydroxy-4-methylpipecolic acid via amide methylenation of 5-hydroxy-4-methyl-2-piperidinone with dimethyltitanocene.* Tetrahedron: Asymmetry, 1997. **8**(7): p. 1115-1121.

161. Horton, D., *The anomeric 1,3,4,6-tetra-O-acetyl-2-deoxy-2-(2,4-dinitro-anilino)-D-glucopyranoses.* J. Org. Chem., 1964. **29**(7): p. 1776-1782.

162. Singleton, J., K. Sahteli, and J.O. Hoberg, *Synthesis of 2,3-dihydroxyhex-4-enoates by palladium-catalyzed allylic alkylations of carbohydrate derived vinyl lactones.* Synthesis, 2008(22): p. 3682-3686.

163. Tarrade-Matha, A., et al., *Enantiospecific synthesis of a protected equivalent of APTO, the β-amino acid fragment of microsclerodermins C and D, by aziridino-γ-lactone methodology.* Eur. J. Org. Chem., 2009(5): p. 673-686.

164. Fenster, M.D.B. and G.R. Dake, *A Formal Construction of Fasicularin.* Org. Lett., 2003. **5**(23): p. 4313-4316.

165. Lennartz, M., M. Sadakane, and E. Steckhan, *Electrochemical oxidation of (R)-4-hydroxy-2-pyrrolidone: a key building block for stereoselective N-acyliminium ion coupling reactions.* Tetrahedron, 1999. **55**(50): p. 14407-14420.

166. Imamura, H., et al., *Stereoselective Synthesis of a Broad Spectrum 1β-Methylcarbapenem, J-114,870.* Tetrahedron, 2000. **56**(39): p. 7705-7713.

167. Liu, R.-C., et al., *Concise asymmetric synthesis of (-)-deoxoprosophylline.* Tetrahedron: Asymmetry, 2008. **19**(23): p. 2731-2734.

168. Gerasyuto, A.I. and R.P. Hsung, *Stereodivergent Total Syntheses of Precoccinelline, Hippodamine, Coccinelline, and Convergine.* Org. Lett., 2006. **8**(21): p. 4899-4902.

169. Devel, L., et al., *Synthesis of protected 2-amino-2-deoxy-D-xylothionolactam derivatives and some aspects of their reactivity.* Carbohydr. Res., 2003. **338**(15): p. 1591-1601.

170. Kanso, R., E.A. Yancey, and S. Striegler, *N-Benzylgalactonoamidines as potent β-galactosidase inhibitors.* Tetrahedron, 2012. **68**(1): p. 47-52.

171. Fan, Q.-H., et al., *Illuminating the binding interactions of galactonoamidines during the inhibition of β-galactosidase (E. coli).* Bioorg. Med. Chem., 2016. **24**(4): p. 661-671.

172. Vonhoff, S., T.D. Heightman, and A. Vasella, *Inhibition of glycosidases by lactam oximes. Influence of the aglycon in disaccharide analogs.* Helv. Chim. Acta, 1998. **81**(9): p. 1710-1725.

173. Graczyk, P.P., et al., *The neuroprotective action of JNK3 inhibitors based on the 6,7-dihydro-5H-pyrrolo[1,2-a]imidazole scaffold.* Bioorg. Med. Chem. Lett., 2005. **15**(21): p. 4666-4670.

174. Collin, M.-P. and A. Vasella, *Towards the Synthesis of 1-Deoxy-1-nitropiperidinoses.* Helv. Chim. Acta, 2010. **93**(12): p. 2297-2317.

175. Vonhoff, S., et al., *Inhibition of cellobiohydrolases from Trichoderma reesei. Synthesis and evaluation of some glucose-, cellobiose-, and cellotriose-derived hydroximolactams and imidazoles.* Helv. Chim. Acta, 1999. **82**(7): p. 963-980.

176. Wang, J., et al., *Synthesis and biological evaluation of D-gluconhydroximo-1,5-lactam and its oxime-substituted derivatives as pharmacological chaperones for the treatment of Gaucher disease.* MedChemComm, 2016. **7**(2): p. 365-370.

177. Oh, H.-S. and H.-Y. Kang, *Total synthesis of neomethymycin and novamethymycin.* Tetrahedron, 2010. **66**(24): p. 4307-4317.

178. Chen, W., et al., *Synthesis of analogues of salacinol containing a carboxylate inner salt and their inhibitory activities against human maltase glucoamylase.* Carbohydr Res, 2007. **342**(12-13): p. 1661-1667.

179. Scarpi, D., et al., *Gold-Catalysed Synthesis of Exocyclic Vinylogous Amides and β-Amino Ketones: A Detailed Study on the 5-exo/6-endo-dig Selectivity, Methodology and Scope.* Eur. J. Org. Chem., 2015. **2015**(15): p. 3251-3265.

180. Fringuelli, R., et al., *Synthesis and evaluation of anti-apoptotic activity of L-carnitine cyclic analogues and amino acid derivatives.* Farmaco, 2004. **59**(4): p. 271-277.

181. Patschinski, P., C. Zhang, and H. Zipse, *The Lewis base-catalyzed silylation of alcohols--a mechanistic analysis.* J Org Chem, 2014. **79**(17): p. 8348-8357.

182. Ochiai, H., T. Niwa, and T. Hosoya, *Stereo-inversion of Stereo-congested Carbocyclic Alcohols via Triflation and Subsequent Treatment with Aqueous N,N-Dimethylformamide.* Org. Lett., 2016. **18**(23): p. 5982-5985.

183. Julia Lodge, P.L.S.M., in *Gene cloning : principles and applications* E. Owen, Editor. 2007.

184. Pelton, J.T. and L.R. McLean, *Spectroscopic Methods for Analysis of Protein Secondary Structure.* Anal. Biochem., 2000. **277**(2): p. 167-176.

185. Bayley, S.R.M.a.P.M., *Absorption and Circular Dichroism Spectroscopy*, in *Calcium-Binding Protein Protocols* H.J. Vogel, Editor. 2002.

186. Greenfield, N.J. and G.D. Fasman, *Computed circular dichroism spectra for the evaluation of protein conformation.* Biochemistry, 1969. **8**(10): p. 4108-4116.

187. Engel, H., et al., *Murein-metabolizing enzymes from Escherichia coli: existence of a second lytic transglycosylase.* J. Bacteriol., 1992. **174**(20): p. 6394-6403.

188. Blackburn, N.T. and A.J. Clarke, *Characterization of soluble and membrane-bound family 3 lytic transglycosylases from Pseudomonas aeruginosa.* Biochemistry, 2002. **41**(3): p. 1001-1013.

189. Blackburn, N.T. and A.J. Clarke, *Assay for Lytic Transglycosylases: A Family of Peptidoglycan Lyases.* Anal. Biochem., 2000. **284**(2): p. 388-393.

190. Ben-Bassat, A., et al., *Processing of the initiation methionine from proteins: properties of the Escherichia coli methionine aminopeptidase and its gene structure.* J. Bacteriol., 1987. **169**(2): p. 751-757.

191. Lee, J.M., et al., *Characterization of salt-tolerant β-glucosidase with increased thermostability under high salinity conditions from Bacillus sp. SJ-10 isolated from jeotgal, a traditional Korean fermented seafood.* Bioprocess Biosyst. Eng., 2015. **38**(7): p. 1335-1346.

192. Tipton, K.F., *Principles of enzyme assays and kinetic studies*, in *Enzyme assays* R.Eisenthal.and M.J. Danson, Editor. 2002, Oxford University Press Inc., New York.

193. Hash, J.H., *Measurement of bacteriolytic enzymes.* J. Bacteriol., 1967. **93**(3): p. 1201-2.

194. Harris, T.K. and G.J. Turner, *Structural basis of perturbed pKa values of catalytic groups in enzyme active sites.* IUBMB Life, 2002. **53**(2): p. 85-98.

195. Shen, P. and R. Larter, *Role of substrate inhibition kinetics in enzymatic chemical oscillations.* Biophys J, 1994. **67**(4): p. 1414-1428.

196. Bugg, T.D.H., in *Introduction to enzyme and coenzyme chemistry*. 2012, John Wiley & Sons, Ltd.

197. Voet, D.J., in *Principles of Biochemistry*. 2013, John Wiley & Sons, Inc.

198. D. Hames and N. Hooper, in *Biochemistry*. 2011, Garland Science, Taylor & Francis Group, LLC.

199. Copeland, R.A., in *Evaluation of enzyme inhibitors in drug discovery*. 2005.

200. de la Fuente, A., et al., *Stereoselective Synthesis of 2-Acetamido-1,2-dideoxyallonojirimycin (DAJNAc), a New Potent Hexosaminidase Inhibitor.* Org. Lett., 2013. **15**(14): p. 3638-3641.

201. Borges de Melo, E., A.d.S. Gomes, and I. Carvalho, *α- and β-Glucosidase inhibitors: chemical structure and biological activity.* Tetrahedron, 2006. **62**(44): p. 10277-10302.

202. Scofield, A.M., et al., *Castanospermine and other polyhydroxy alkaloids as inhibitors of insect glycosidases.* Comp. Biochem. Physiol., A: Physiol., 1995. **112A**(1): p. 187-196.

203. Hayashi, K., et al., *The position of the active tryptophan residue in lysozyme.* J. Biochem., 1965. **58**(3): p. 227-235.

204. Jash, C., et al., *Binding of the Iminium and Alkanolamine Forms of Sanguinarine to Lysozyme: Spectroscopic Analysis, Thermodynamics, and Molecular Modeling Studies.* J. Phys. Chem. B, 2014. **118**(46): p. 13077-13091.

205. Wang, J., et al., *Triclinic lysozyme at 0.65 Å resolution.* Acta Crystallogr., Sect. D: Biol. Crystallogr., 2007. **63**(12): p. 1254-1268.

206. Chaudhuri, N., et al., *Development of a Novel Synthetic Process for 2-Deoxy-3,5-di-O-p-toluoyl-α-l-ribofuranosyl Chloride: A Versatile Intermediate in the Synthesis of 2'-Deoxy-l-ribonucleosides.* Organic Process Research & Development, 2005. **9**(4): p. 457-465.

8 Appendix

Table 1. Crystal data and structure refinement for compound 86h.

Identification code	**68h**
Empirical formula	$C_5 H_{11} Cl N_2 O_3$
Formula weight	182.61
Temperature	296(2) K
Wavelength	1.54184 Å
Crystal system	Monoclinic
Space group	P 21
Unit cell dimensions Volume	a = 6.9955(4) Å α= 90°.
	b = 6.5732(3) Å β= 111.923(6)°.
	c = 9.1718(5) Å γ = 90°.
Z	2
Density (calculated)	1.550 Mg/m^3
Absorption coefficient	4.066 mm^{-1}
F(000)	192
Crystal size	0.259 x 0.158 x 0.121 mm^3
Theta range for data collection	5.198 to 73.623°.
Index ranges	-8<=h<=7, -7<=k<=8, -11<=l<=8
Reflections collected	2427
Independent reflections	1514 [R(int) = 0.0217]
Completeness to theta = 67.	684° 99.7 %
Refinement method	Full-matrix least-squares on F2
Data / restraints / parameters	1514 / 1 / 103
Goodness-of-fit on F2	1.047
Final R indices [I>2sigma(I)]	R1 = 0.0323, wR2 = 0.0873
R indices (all data)	R1 = 0.0329, wR2 = 0.0888
Absolute structure parameter	0.023(12)
Extinction coefficient	n/a
Largest diff. peak and hole	0.190 and -0.285 $e.Å^{-3}$

Table 2. Atomic coordinates (x 10^4) and equivalent isotropic displacement parameters ($Å^2$x 10^3) for rka1801b. U(eq) is defined as one third of the trace of the orthogonalized U^{ij} tensor.

	x	y	z	U(eq)
C(1)	13573(4)	7878(4)	7677(3)	30(1)
C(2)	12932(4)	8426(4)	9036(3)	28(1)
C(3)	11083(4)	7154(4)	8947(3)	28(1)
C(4)	9280(4)	7522(5)	7428(3)	29(1)
C(5)	9891(4)	7745(4)	6032(3)	25(1)
N(1)	11819(3)	7959(3)	6175(2)	28(1)
N(2)	8393(3)	7794(4)	4664(2)	32(1)
O(1)	12470(3)	10553(3)	8947(2)	30(1)
O(2)	10371(3)	7666(4)	10172(2)	33(1)
O(3)	8849(3)	8284(3)	3360(2)	35(1)
Cl(1)	6303(1)	12510(1)	6556(1)	45(1)

Table 3. Bond lengths [Å] and angles [°] for rka1801b.

C(1)-N(1)	1.464(3)
C(1)-C(2)	1.517(4)
C(1)-H(1A)	0.9700
C(1)-H(1B)	0.9700
C(2)-O(1)	1.431(3)
C(2)-C(3)	1.517(4)
C(2)-H(2)	0.9800
C(3)-O(2)	1.429(3)
C(3)-C(4)	1.509(4)
C(3)-H(3)	0.9800
C(4)-C(5)	1.501(3)
C(4)-H(4A)	0.9700
C(4)-H(4B)	0.9700
C(5)-N(2)	1.301(3)
C(5)-N(1)	1.313(3)
N(1)-H(1)	0.8600
N(2)-O(3)	1.386(3)
N(2)-H(2A)	0.8600
O(1)-H(1)	0.8200

O(2)-C(3)-C(4)	105.74(19)
O(2)-C(3)-C(2)	111.6(2)
C(4)-C(3)-C(2)	111.3(2)
O(2)-C(3)-H(3)	109.4
C(4)-C(3)-H(3)	109.4
C(2)-C(3)-H(3)	109.4
C(5)-C(4)-C(3)	113.37(19)
C(5)-C(4)-H(4A)	108.9
C(3)-C(4)-H(4A)	108.9
C(5)-C(4)-H(4B)	108.9
C(3)-C(4)-H(4B)	108.9
H(4A)-C(4)-H(4B)	107.7
N(2)-C(5)-N(1)	121.4(2)
N(2)-C(5)-C(4)	116.2(2)
N(1)-C(5)-C(4)	122.3(2)
C(5)-N(1)-C(1)	123.9(2)
C(5)-N(1)-H(1)	118.0
C(1)-N(1)-H(1)	118.0
C(5)-N(2)-O(3)	118.4(2)
C(5)-N(2)-H(2A)	120.8
O(3)-N(2)-H(2A)	120.8
C(2)-O(1)-H(1)	109.5
C(3)-O(2)-H(2)	109.5
N(2)-O(3)-H(3)	109.5

Symmetry transformations used to generate equivalent atoms: